Summer 2015

Measurement of the physical properties of ultrafine particles in the rural continental US

Ashish Singh
University of Iowa

MEASUREMENT OF THE PHYSICAL PROPERTIES OF ULTRAFINE PARTICLES IN THE RURAL CONTINENTAL US

by

Ashish Singh

A thesis submitted in partial fulfillment
of the requirements for the Doctor of
Philosophy degree in Chemical and Biochemical Engineering in the
Graduate College of
The University of Iowa

August 2015

Thesis Supervisor: Associate Professor Charles O. Stanier

Graduate College
The University of Iowa
Iowa City, Iowa

CERTIFICATE OF APPROVAL

_____

PH.D. THESIS

_____

This is to certify that the Ph.D. thesis of

Ashish Singh

has been approved by the Examining Committee for
the thesis requirement for the Doctor of Philosophy degree
in Chemical and Biochemical Engineering at the August 2015 graduation.

Thesis Committee: _____
Charles O. Stanier, Thesis Supervisor

_____
Gregory R. Carmichael

_____
Elizabeth A. Stone

_____
Vicki H. Grassian

_____
Jennifer Fiegel

To my mom

For the love of learning, for caring about the place we call the earth and for the people who are fighting each day to make a meaningful living, spreading hope and are a source of inspiration.

Unknown

ACKNOWLEDGEMENTS

The work I have shown in the thesis is a work of collaborations. I have had the chance to learn from many people in and outside of campus. First, I would like to express sincere acknowledgement to my thesis adviser Prof. Charles Stanier for taking me as his student and for his patience, encouragement, guidance and support from the day one to last. I am also in-debt to the guidance, and mentorship of Prof. Stone. Thanks to Prof. Carmichael who has been a guardian figure for me in CGRER. Special thanks to Prof. Grassian and her graduate students for wonderful advice, and collaboration. Thanks to Prof. Fiegel for being part of the thesis committee. Outside the committee, I appreciate the collaboration and discussions with Dr. Scott Spak, and Dr. Thomas Peters and would like to extend my gratitude to them.

My colleagues at CGRER were a crucial part of this journey. I would like to thank Pablo and his wife Paula for their crucial support personally and professionally. Special thanks to Robert Bullard and his wonderful family for listening and sharing new life in Iowa. I am equally obliged that I got to know Yu (*Man*), Mong, Negin, Nathan, Chan, Maryam and Ester and hope to continue this friendship wherever we may be. Thanks to Jaemeen and Sang-Rin for their meaningful advice during early phase of my study. Thanks to CGRER staff Jeremie Moen and Jane Frank for all their help.

I would also like to sincerely acknowledge friends I get to know in Iowa City whose company and conversations have helped me understand American culture, and made me feel at home.

ABSTRACT

The drivers of human health and changing climate are important areas of environmental and atmospheric studies. Among many environmental factors present in our biosphere, small particles, also known as ultrafine particles or UFPs, have direct and indirect pathways to affect human health and climatic processes. The rapid change in their properties makes UFPs dynamic and often challenging to quantify their effect on health and radiative forcing. To reduce uncertainty in the climate effects of UFPs and to strengthen the evidence on health effects, accurate characterizations of physical and chemical properties of UFPs are needed.

In this thesis, two broad aspects of UFPs were investigated: (1) the development of particle instrumentation to study particle properties; and (2) measurement of physical and chemical properties of UFPs relevant to human health and climate. These two broad aspects are divided into four specific aims in this thesis.

The measurement of UFP concentration at different locations in an urban location, from roadside to various residential areas, can be improved by using a mobile particle counter. A TSI 3786 Condensation Particle Counter (CPC) was modified for mobile battery-power operation. This design provided high-frequency, one second time resolution measurements of particle number and carbon dioxide (CO_2). An independent electric power system, a central controller and robust data acquisition system, and a GPS system are the major components of this mobile unit. These capabilities make the system remotely deployable, and also offer flexibility to integrate other analog and digital sensors.

A Volatility Tandem Differential Mobility Analyzer (V-TDMA) system was designed and built to characterize the volatility behavior of UFPs. The physical and chemical properties of UFPs are often challenging to measure due to limited availability of instruments, detection limit in terms of particle size and concentration, and sampling frequency. Indirect methods such as V-TDMA are useful, for small mass (<1 $\mu g/m^3$), and nuclei mode particles (<30 nm). Another advantage of V-TDMA is its fast response in terms of sampling frequency. A secondary motivation for building a V-TDMA system was to improve instrumentation capability of our group, thus enabling study of kinetic and thermodynamic properties of novel aerosols.

Chapter four describes the design detail of the built V-TDMA system, which measures the change in UFP size and concentration during heated and non-heated (or ambient) condition. The V-TDMA system has an acceptable penetration efficiency of 85% for 10 nm and maintains a uniform temperature profile in the heating system. Calibration of V-TDMA using ammonium sulfate particles indicated that the system produces comparable evaporation curves (in terms of volatilization temperature) or volatility profiles to other published V-TDMA designs. Additionally the system is fully programmable with respect to particle size, temperature and sampling frequency and can be run autonomously after initial set up.

The thesis describes a part of yearlong study to provide a complete perspective on particle formation and growth in a rural and agricultural Midwestern site. Volatility characterizations of UFPs were conducted to enable inference about particle chemistry, and formation of low volatile core or evaporation resistant residue in the UFP in the Midwest. This study addresses identification of the volatility signature of particles in the

UFP size range, quantification of physical differences of UFPs between NPF[1] and non-NPF events and relation of evaporation resistant residue with particle size, seasonality and mixing state. K-means clustering was applied to determine three unique volatility clusters in 15, 30, 50 and 80 nm particle sizes. Based on the proposed *average volatility*, the identified volatility clusters were classified into high volatile, intermediate volatile and least volatile group. Although VFR alone is insufficient to establish chemical composition definitively, least volatile cluster based on *average volatility* may be characteristically similar to the pure ammonium sulfate. The amount of evaporation residue at 200 ^{o}C was positively correlated with particle size and showed significant correlation with ozone, sulfur dioxide and solar radiation. Residue also indicated the presence of external mixture, often during morning and night time.

Air quality science and management of an accidental urban tire fire occurring in Iowa City in May and June of 2012 were investigated. Urban air quality emergencies near populated areas are difficult to evaluate without a proper air quality management and response system. To support the development of an appropriate air quality system, this thesis identified and created a rank for health-related acute and chronic compounds in the tire smoke. For health risk assessment, the study proposed an empirical equation for estimating multi-pollutant air quality index. Using mobile measurements and a dispersion model in conjunction with the proposed air quality index, smoke concentrations and likely health impact were evaluated for Iowa City and surrounding areas. It was concluded that the smoke levels reached unhealthy outdoor levels for sensitive groups out to distances of 3.1 km and 18 km at 24 h and 1h average times. Tire smoke characterization was another important aspect of this study which provided important and

[1] New particle formation (NPF)

new information about tire smoke. Revised emission factors for coarse particle mass and aerosol-PAH and new emission factors and enhancement ratios values for a wide range of fine particulate mass, particle size (0.001-2.5 μm), and trace gas were estimated.

Overall the thesis added new instrumentation in our research group to measure various physical properties such as size, concentration, and volatility UFP. The built instruments, data processing algorithm and visualization tools will be useful in estimation of accurate concentration and emission factors of UFP for health exposure studies, and generate a fast response measurement of kinetic and thermodynamics properties of ambient particles. This thesis also makes a strong case for the development of an air quality emergency system for accidental fires for urban location. It provides useful evaluation and estimation of many aspects of such system such as smoke characterization, method of air quality monitoring and impact assessment, and develops communicable method of exposure risk assessment.

PUBLIC ABSTRACT

The drivers of human health and changing climate are important areas of environmental and atmospheric studies. Among many environmental factors present in our biosphere, small particles, defined in this thesis as particles less than 100 nm in diameter, have been shown to affect human health and climatic processes. The sources of these small particles, also referred as ultrafine particles or UFP, are mainly exhaust emission from vehicles and industries in the urban areas, and also from aggregation of favorable gas molecules in the atmosphere.

This thesis describes (1) the development of instrumentation; and (2) measurement of physical properties of these particles in the ambient air. In the instrumentation development, a mobile particle counter was built which provides a concentration map of the UFP concentration in an area. Another major design work involved a thermal treatment system for the measurement of physical properties of ambient aerosol. Application of such thermal treatment in Bondville, IL revealed that UFPs in the Midwest have three distinct evaporation profiles, each of which are related to particle chemical composition. The study also identified ammonium sulfate as a major contributor to the UFP composition and that all particle sizes have an evaporation resistant residue at 200 ^{0}C.

The thesis also made significant contribution by providing realistic exposure and health risk assessment during a toxic tire fire. This included characterization of tire smoke, identification of hazardous compounds in the smoke, and estimation of health risk by proposing a multi-pollutant quality index. In this respect, this thesis can serve as an important scientific and policy document for air quality management during fires.

TABLE OF CONTENTS

LIST OF TABLES

LIST OF FIGURES

CHAPTER 1: GENERAL INTRODUCTION

1.1 Background

The size of atmospheric particles is strongly linked to health and climate effects. The size, concentration and other properties of atmospheric particles are influenced by different sources and atmospheric processes (IPCC, 2014). Based on their depositional behavior in the lung and their potential translocation in the body, particles less than 100 nm are considered more harmful than larger size particles (HEI, 2013). In this thesis, ultrafine particles (UFPs) are defined as particles with less than 100 nm in diameter. UFP constitute a significant fraction, in the range of 84 to 90% of the total particle concentration in urban environment (Kumar et al., 2014; Morawska et al., 2008; Stanier et al., 2004). Along with size, UFPs have higher surface area than larger particles. These properties allow UFPs to have high deposition efficiencies in the respiratory tract, higher absorptivity, and surface reactivity. Consequently UFPs have higher toxicity and causes oxidative stress on a cellular level, and inflammatory response on tissues, and organs (Oberdörster et al., 2005). As a result of large surface area, significant (~50% by mass) aerosol poly-aromatic hydrocarbon (PAH) are observed in the UFP size in urban locations (Lin et al., 2008).

UFPs contribute to changing climate by acting as cloud condensation nuclei (CCN). CCN affect the climate directly by reflecting or absorbing solar radiation (Ramanathan et al., 2001). This change in solar radiation flux reaching the earth surface is also defined as radiative forcing. Among radiative forcers in the atmosphere, IPCC estimates that the anthropogenic aerosol contributes to a significant radiative forcing, close to -0.35 Wm^{-2}. This estimation of aerosol-related radiative flux has a large

uncertainty from -0.85 to 0.15 (IPCC 2013). This uncertainty hinders accurate assessments of the climate sensitivity due to radiative forcing (Andreae et al., 2005). The reduction of uncertainties in aerosol radiative forcing is linked better characterization of different source of particles, how they grow from clusters of a few molecules to CCN sizes (>100 nm), and how they form cloud droplets. This also includes better characterization of physical and chemical properties of particles such as their composition, their hygroscopic and optical properties, and the variation of these properties with time and space (IPCC 2013). Lack of a UFPs routine monitoring network in the US compounds the state of understanding on UFPs, as physical and chemical properties have large spatial and temporal variation (Eeftens et al., 2015; Sabaliauskas et al., 2013; Sioutas et al., 2005; Zwack et al., 2011).

1.2 Sources of UFPs

UFPs originate from a wide variety of natural and anthropogenic sources. Primary particles are directly emitted as liquids or solids from sources such as biomass burning, incomplete combustion of fossil fuels, and volcanic eruptions. Secondary particles, on the other hand, are formed by gas-to-particle conversion and growth in the atmosphere.

Primary sources of UFP are mainly road transport related, followed by non-road transport (e.g., aircraft and ship related) and household fuel combustion (González et al., 2011; Just et al., 2013; Kumar et al., 2014; Morawska et al., 2002; Westerdahl et al., 2008). Other sporadic sources of UFPs include large-scale fires such as forest fires, landfill fires, and tire fires, commonly reported in both urban and rural areas (Akagi et al., 2012; Hays et al., 2005; Stockwell et al., 2015; Urbanski, 2013; USFA, 1998; Yokelson et al., 2011).

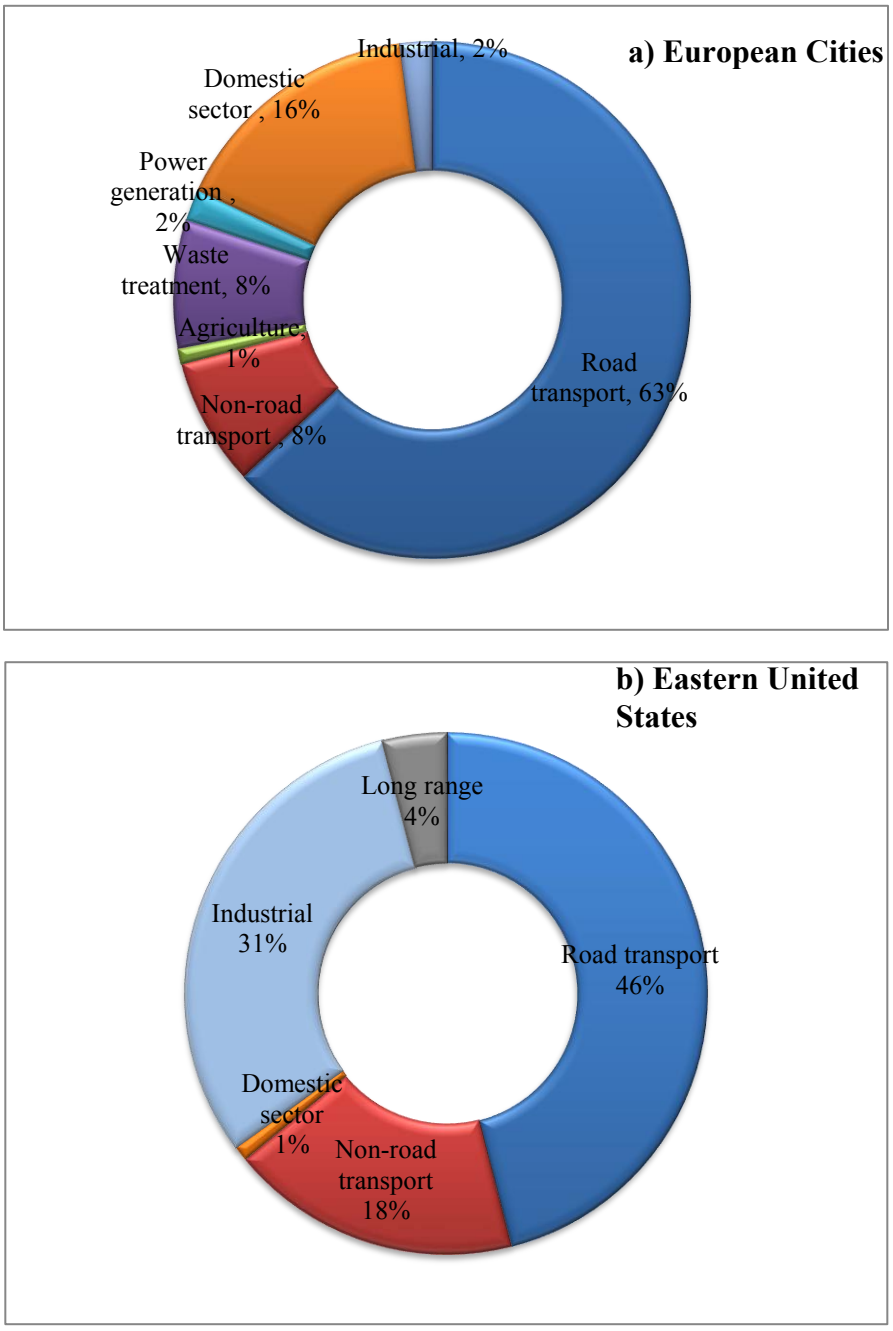

Figure 1.1 Sources of primary particles across different regions. Panel a shows measured source apportionment of primary particles averaged for 28 European cities for the year 2010 by Kumar et al. (2013). Panel b is the modeled source apportionment prediction by Posner and Pandis (2015) for the Eastern United States regions for the year 2001.

Figure 1.1 illustrates source contributions of primary particles in two different regions of the world. Although the classification of the sources in these two studies are

not consistent, it is evident that road transport is the dominant source, followed by domestic and industrial sources. Sporadic fire such as forest and tire fire were not accounted in these studies, but emit a large amount of UFPs. Comparison of source strength of forest and tire fire by Janhall et al. (2010) and Downard et al. (2015) found that the emission factor of UFPs were in the range of $3x10^{15}$-$5x10^{16}$ #/cm^3, similar in range with a gasoline vehicle whose emission factor could be found in the range of $1x10^{14}$-$6x10^{16}$ #/cm^3 (Kittelson et al., 2004).

Primary sources of UFP such as biomass and tire fires, though sporadic in nature, are important sources of UFPs which poses a unique challenge to public health (Downard et al., 2015; Lemieux et al., 2004; Singh et al., 2015). Tire fires studies have reported the presence and concentration of the known carcinogens such as benzo[a]pyrene (BaP) in the particulate phase as well as high emission of UFPs similar to the emission profile from a vehicular exhaust (Downard et al., 2015; EPA, 1997). Over the last two decades, dozen major tire fires have been recorded in the United States (Singh et al., 2015). However many tire fires, particularly those that are small in scale, are not well documented in terms of emission profile from a toxic smoke, and exposure risk to the public. Most tire fire emission characterizations are limited to controlled-burning in a laboratory condition (Lemieux and Ryan, 1993; Stockwell et al., 2014; Wang et al., 2007). Laboratory controlled studies of tire fire do not reflect the open burn conditions which is influenced by combustion and atmospheric conditions (Downard et al., 2015). Detailed literature review of the tire emission is provided in Chapter six.

In this thesis, a field-based approach was employed to estimate ambient concentration and emission characterization of particulate and gaseous pollutant during

the Iowa City landfill tire fire. The field-based approach used in this study provides a real-world perspective on the open burning of tires (Lemieux and Ryan, 1993; Stockwell et al., 2014). This thesis provides, for the first time, smoke characterization of tire smoke in a ambient condition for UFPs including total particle number, fine particulate mass ($PM_{2.5}$ mass), and $PM_{2.5}$ PAH, which are important to understanding the population exposure and potential health impacts of this source. Furthermore, the emission factors determined in this study were also critical to formulate recommendations on air monitoring needs in response to large-scale tire fires (Singh et al., 2015). From public health and air quality perspectives, the response to a large scale tire fire also includes many decisions which may include specific monitoring plan, interpreting and assessing population risk and public health messaging. Existing reports from past fires have major shortcomings as a guide to the public health response (JCPHD, 2012). This thesis provides a framework to better the air quality response through a hierarchy of monitoring priorities for large scale tire fires, a tire fire irritant Air Quality Index (AQI) for interpretation of the measured values, and a ranking of tire fire components by acute and cancer hazard ratios. The details about the tire fire study are provided in Chapter six in this thesis.

Concentration of particle number varies by many orders of magnitude with distance from the source (Chan and Yao, 2008). Accurate estimation of concentration of total particle concentration across time and space during sporadic events, such as tire fire, or in high population density area is challenging without a mobile sampler. The motivation for determining accurate concentration of pollutants, such as particle number, is primarily for improving exposure estimates for health impact analysis (Sioutas et al.,

2005). This is crucial for total particle number and specifically for particle less than 100 nm (or UFP). Lack of routine monitoring for UFP in urban locations in the US has hindered the building of UFP exposure estimates in many urban locations (Kumar et al., 2014). Available exposure estimates are usually based on a short term campaign measurements of UFPs which may not be a representative sample. Mobile measurement are also better equipped to provide temporal and spatial variability in pollutants in areas such as a city area which usually have densely packed high-rise buildings and diverse micrometeorology leading to substantial variation in concentration temporal and spatially (Kumar et al., 2011).

Temporally and spatially-resolved concentration are also critical in many decision support systems and emission control measures such as identification of pollution hotspots, changing vehicle and fuel type, and avoiding traffic congestion (Singh et al., 2015). Chapter four describes the design, construction details and application of a mobile particle counter for ground and aerial sampling. Mobile measurements of pollutants, particularly online measurements, are one of the efficient techniques to produce high resolution time and space concentration map of UFPs, and aid in the development of exposure models. The mobile unit for measuring total particle concentration, described in chapter three, will help in providing accurate estimation of concentration at finer spatial and temporal resolution.

1.3 UFPs studies in the Midwest

The sources of the UFPs in the Midwest are primary and secondary. The secondary source of UFPs is mainly particle formation via nucleation. In nucleation, gaseous molecules combine with each other forming a cluster of 1-3 nm in size. These

clusters grow via condensation, and coagulation (Kulmala et al., 2004). Nucleation is found to be ubiquitous in the troposphere and has been reported in many different locations such as urban centres, forest areas, rural continental areas and even in Southern ocean near Antarctica (Dal Maso et al., 2005; Kulmala et al., 2004; Nallathamby et al., 2014; Pryor et al., 2014; Yu et al., 2014;Koponen et al., 2003). The most recent theory of nucleation includes three gaseous molecules responsible for cluster formation and growth. They are sulfuric acid, water and an organic or inorganic molecule present as a fraction that not only stabilizes the cluster, but also contributes to its growth (Almeida et al., 2013; Kulmala and Kerminen, 2008b; Schobesberger et al., 2013). Nucleation also depends on many factors such as concentration of trace inorganic and organic gases, and other physical parameters such as solar radiation and condensation sinks[2] (Kulmala and Kerminen, 2008b).

In the Midwest, UFP from particle formation may dominate over primary sources (Posner and Pandis, 2015; Pryor et al., 2010). The increasing contribution of secondary sources to the UFP concentration in the Midwest can have significant influence in health, and cause local changes in cloud nuclei concentration, and aerosol-related radiative forcing in the Midwest. Therefore in this thesis, a primary goal is to examine the properties of UFPs from primary and secondary sources including nucleation in the Midwest and thus help develop a detailed parameterization of how these particles are forming, determine the role of precursors gases and meteorology. At present, parameterization of particle formation and the nature of growth of clusters to larger sizes is weakly understood in the Midwest (Pryor et al., 2010).

[2] It is a measure of particle population's ability to remove vapor by condensation

The rural continental Midwest US is an interesting atmospheric regime compared to other prominent nucleation study sites (South Eastern US, Hytiaala Finland, Po Valley Italy, Melpitz, Germany) due to relatively high concentrations of SO_2 (1-10 ppb) and excess ammonia (NH_3) concentrations (Pryor et al., 2011; Stanier et al., 2012) and diverse land use (Crippa et al., 2013). SO_2 is oxidized to sulfuric acid which is a key gas for the cluster formation whereas ammonia is an inorganic gas which is reported to stabilize and grow the cluster to larger size (Schobesberger et al., 2013).

Long term total particle number concentration record in the Midwest over the last twenty years as the concentration shows a declining concentration trend (Bullard et al., 2013). This reflects the likely influence of federal and state regulation on emissions from primary sources such as industries and vehicles. However for the same time period, summer time total particle concentrations is increasing (Pryor et al., 2011), likely due to increased frequency of particle formation via nucleation (see Figure 1.2 for a summertime nucleation in the Midwest from Bullard et al. (2015)). The implication of increasing frequency of nucleation on UFP concentration was also shown by Posner and Pandis (2015) who reported that nucleation contributed 96% of the total UFP concentration during summer season. Similarly particle size distribution (PSD) characterization in the Midwest by Pryor et al. (2011) and Crippa et al. (2013) showed that nucleation intensities (in terms of particle concentration) and growth rate of particles were also higher in summer and spring season at multiple sites in Indiana.

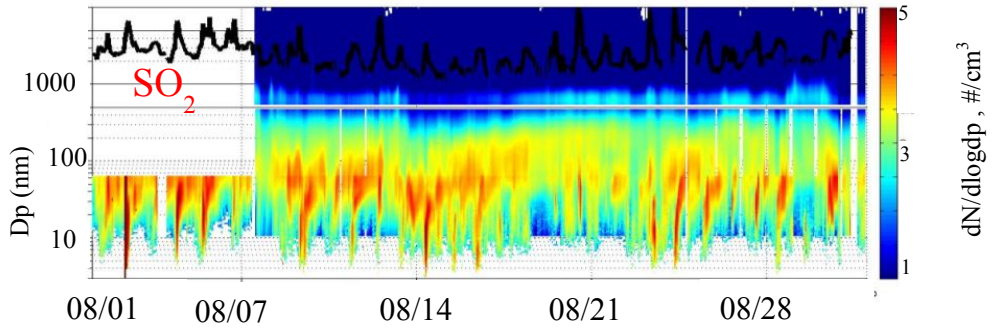

Figure 1.2 Time series of particle size distribution measurement in Bondville showing frequent new particle formation events during the month of August in 2013. The left y-axis shows the particle diameter and right y-axis shows the particle concentration. The corresponding concentration of SO_2 is shown in the figure by the black bold line (Bullard et al., 2015).

The mechanism for particle formation in the Midwest is likely to be ternary, involving sulfuric acid, water and ammonia (Crippa et al., 2013). Direct measurements of aerosol composition in freshly formed particles and growth thereafter have not been conducted in the Midwest which hinders quantification of the participating precursors. Studies elsewhere showed that composition of ultrafine particles from particle formation are dominated by sulfate, ammonium, and organic carbon, and nitrate (Bzdek et al., 2012, Park et al., 2009). The presence of other compounds such as amine, silicon, elemental carbon, organo-sulfates, organo-nitrates, carboxylic and hydroxyl carboxylic organic acid, aldehydes, and alcohols have also been reported in the freshly nucleated particle (Smith et al., 2008; Bzdek et al., 2014; Fanizza et al., 2010; Zhang et al., 2012). Low saturation vapor pressure organics, resulting in low volatile core or evaporation resistant residue in particles, have also been associated with the growth of the freshly nucleated particles in many locations (Ehn et al., 2014; Ristovski et al., 2010; Laaksonen et al., 2008)

In the Midwest, particle number concentration has shown sensitivity to trace gas concentrations including sulfur dioxide, nitrogen oxides and ammonia (Crippa et al., 2013). There is some evidence about the likely contribution (23 to 85% of particle mass) of ambient sulfuric acid concentration in 6-30 nm particle size range during particle formation (Pryor et al. 2010; Pryor et al. 2011). The contribution of sulfuric acid contribution (as sulfate in particulate phase) is in contrast with 100% contributions in the Southeastern US (Stolzenburg et al., 2005) and 4-10% contribution in the Boreal forest in Europe (Almeida et al., 2013; Riipinen et al., 2011; Wehner et al., 2005). Pryor et al. estimated that during a nucleation event in Indiana the total particle mass below ≤30 nm was accounted by NH_4^+ and SO_4^{2-} and for particle larger than 30 nm, the mass of these ion were insufficient to account for the total particle mass. This indicates that ammonia is playing an important role in neutralizing the sulfuric acid in the nuclei mode (<30 nm) and limited for larger sizes because of the limited availability of sulfuric acid (Zhang et al., 2009). The mass discrepancy increases for particles > 30 nm (chemically not quantified) is likely due to organic (Pryor et al., 2011; Yu et al., 2014).

The extent of organic vapor condensation and the size dependence organic vapor partition is still not examined (Pryor et al., 2011). Few studies have shown the likely associations of biogenic organics to the particle formation and growth in the Midwest. In a forested site in Indiana, weakening of the growth rate of freshly formed particle was found sensitive to the severity in the drought in this region. This provides a causal evidence of semi-volatile partition of biogenic VOC (Pryor et al., 2014). This was also supported by observations from Ozark forest in Missouri, where stronger positive correlation was observed between the growth of the nucleated particle with biogenic

VOC, O_3 than SO_2 indicating O_3 led oxidation of the biogenic VOC (Yu et al., 2014). Similarly measurements from CABINEX campaign in forest areas in Michigan found that air mass coming from North which is rich in biogenic VOC was associated with particle formation. Hygroscopic measurements of these freshly formed particles were lower compared to the freshly formed particle the impact of anthropogenic air mass from south and east. Particle formed during the anthropogenic mass showed > 60% mass fraction (in particle less than 100 nm) to be dominated by ammonium and sulfate (VanReken et al., 2015).

Based on the studies conducted so far, ammonia could be a likely to dominate the composition for particle below 30 nm, via neutralization reaction in forested and urban location. Other precursors may dominate the growth of particle > 30 nm, which could be site specific. The concentration of the biogenic VOC (0.1-0.2 ppb) reported by these studies are at least one order of magnitude lower than SO_2 (1-1.5 ppb). It is likely that the concentration of these trace gases are not a strong indicator of nucleation rate and growth, rather specific oxidation products and meteorology such as ultra-violet radiation (UV) may be significant.

Thus a detailed region specific characterization of physical and chemical properties of particles is required in the Midwest to answer questions related to nucleation, its intensity, timing and growth (Pryor et al., 2010a; Yu et al., 2014). In this context, region around Bondville IL, differs substantially in its land use than previously studied sites. Bondville, IL is a perturbed rural continental site with intensive agriculture, complementary to other site which have taken place in urban-industrial and deciduous forest locations.

To improve the physical and chemical characterization of UFPs in the Midwest, this thesis provides design and development of instrumentation related to particle volatility and field measurements of atmospheric UFP in a rural and agricultural Midwestern site. Chapter four, in this thesis, presents a detailed design and construction description of a Volatility Tandem Differential Mobility Analyzer (V-TDMA).

The Tandem Differential Mobility Analyzer (TDMA) is often used to provide insight into the particle composition by adding a conditioning system such as heating[3] (An et al., 2007; Frey et al., 2008a; Huffman et al., 2008; Lee et al., 2010; Orsini et al., 1999; Villani et al., 2007b; Wehner et al., 2002), and humidification[4] (Ehn et al., 2007a; Johnson et al., 2004d; Swietlicki et al., 2008) and organic vapor[5] (Joutsensaari et al., 2001). Advanced instrumentation such a TD-CIMS[6], and NAMS[7] offer direct bulk compositional and elemental information about the particle. But the constraint on their availability and their working particle size range, TDMA technique is often a preferred method for small mass (<1 $\mu g/m^3$) associated with the nuclei mode particle (<30 nm) and fast sampling frequency or response time for the particle size resolved information.

A V-TDMA measures the change in particle size and number concentration before and after heating at a certain temperature. The heat treatment system in the V-TDMA is also referred as a "thermodenuder". The change in size of aerosol population is measured using condensation particle counters (CPC)[8] and scanning mobility particle

[3] TDMA with heating system are generally abbreviated as V-TDMA and will be used for the rest of the thesis
[4] TDMA with humidification system are generally abbreviated as RH or H-TDMA.
[5] Organic TDMA is abbreviated as O-TDMA
[6] Thermal Desorption Chemical Ionization Mass Spectrometry
[7] Nano Aerosol Mass Spectrometer
[8] Condensation particle counters, TSI Inc.

counters (SMPS)[9]. The change in size and concentration at different temperature can be used to estimate volatile, semi-volatile and low volatile volume fraction (An et al., 2007; Johnson et al., 2004a; Jonsson et al., 2007; Ristovski et al., 2010a; Tritscher et al., 2011). V-TDMA also provides an almost direct measurement of the combination of physical properties related to particle volatility (vapor pressure, surface tension, accommodation coefficient, enthalpy of vaporization) (Huffman et al., 2009; Pierce et al., 2011; Riipinen et al., 2010).

Comparison of particle volatility signatures[10] measured in the field with those of laboratory aerosols of known chemical composition has been used to identify the contribution of sulfate, nitrate, and oxidized organics in the particle (Huffman et al., 2009; Lee et al., 2010; Raatikainen et al., 2010). Likewise volatility signature often provides a strong indication of chemical composition from volatility measurements of particles. For example, particle below 15 nm were nonvolatile at 100 ^{o}C which indicated conversion of sulfuric acid into ammonium sulfate (Sakurai et al., 2003). Also heating > 150 ^{o}C can reveal the presence of nonvolatile organics (Smith et al., 2010; Sakurai et al., 2005). Similarly, heating to 280-300 ^{o}C has been used to determine the nonvolatile core, presumably polymerized organic. The nonvolatile core may account for 20-40% of volume in 3-25 nm particles (Wehner et al., 2005; Hakkinen et al., 2012).

The main importance of V-TDMA for the study of UFPs lies in its fast response of particle volatility within 2 minutes or less compared to TD-CIMs which takes more than 15 minutes to provide a response. Detailed design including laboratory test and calibration of the V-TDMA is also provided in chapter four.

[9] Scanning mobility particle spectrometer, TSI Inc.
[10] Volatility signature usually refer to volume thermograph plot (2D) where the x-axis is the temperature and y-axis is a ratio of particle volume at temperature T to volume at 25 C.

Chapter six provides an overview of the first volatility measurement of UFP at the Bondville Environment and Atmospheric Research Site (BEARS) site in Bondville IL. The goal of the study is to enable indirect inference about particle chemistry, and formation of evaporation resistant residue in the UFP in the Midwest. This study addresses few specific objectives which include identification of the volatility signature of particles, quantification of physical differences of UFPs between new particle formation and non-events, and association of evaporation resistant residue with size, and seasonality.

1.4 References

Akagi, S.K., Craven, J.S., Taylor, J.W., McMeeking, G.R., Yokelson, R.J., Burling, I.R., Urbanski, S.P., Wold, C.E., Seinfeld, J.H., Coe, H., Alvarado, M.J., Weise, D.R., 2012. Evolution of trace gases and particles emitted by a chaparral fire in California. Atmospheric Chemistry and Physics 12, 1397-1421.

Almeida, J., Schobesberger, S., Kuerten, A., Ortega, I.K., Kupiainen-Maatta, O., Praplan, A.P., Adamov, A., Amorim, A., Bianchi, F., Breitenlechner, M., David, A., Dommen, J., Donahue, N.M., Downard, A., Dunne, E., Duplissy, J., Ehrhart, S., Flagan, R.C., Franchin, A., Guida, R., Hakala, J., Hansel, A., Heinritzi, M., Henschel, H., Jokinen, T., Junninen, H., Kajos, M., Kangasluoma, J., Keskinen, H., Kupc, A., Kurten, T., Kvashin, A.N., Laaksonen, A., Lehtipalo, K., Leiminger, M., Leppa, J., Loukonen, V., Makhmutov, V., Mathot, S., McGrath, M.J., Nieminen, T., Olenius, T., Onnela, A., Petaja, T., Riccobono, F., Riipinen, I., Rissanen, M., Rondo, L., Ruuskanen, T., Santos, F.D., Sarnela, N., Schallhart, S., Schnitzhofer, R., Seinfeld, J.H., Simon, M., Sipila, M., Stozhkov, Y., Stratmann, F., Tome, A., Troestl, J., Tsagkogeorgas, G., Vaattovaara, P., Viisanen, Y., Virtanen, A., Vrtala, A., Wagner, P.E., Weingartner, E., Wex, H., Williamson, C., Wimmer, D., Ye, P., Yli-Juuti, T., Carslaw, K.S., Kulmala, M., Curtius, J., Baltensperger, U., Worsnop, D.R., Vehkamaki, H., Kirkby, J., 2013. Molecular understanding of sulphuric acid-amine particle nucleation in the atmosphere. Nature 502, 359-+.

Austin, C., 2008. Wildland firefighter health risks and respiratory protection, Montreal, Canada, pp. 1-52.

Bianchi, F., Junninen, H., Troestl, J., Duplissy, J., Rondo, L., Simon, M., Kuerten, A., Adamov, A., Curtius, J., Dommen, J., Weingartner, E., Worsnop, D.R., Kulmala, M., Baltensperger, U., 2013. Particle nucleation events at the high alpine station

Jungfraujoch, 19th International Conference on Nucleation and Atmospheric Aerosols (ICNAA), Colorado State Univ, Ctr Arts, Fort Collins, CO, pp. 222-225.

Birmili, W., Wiedensohler, A., 2000. New particle formation in the continental boundary layer: Meteorological and gas phase parameter influence. Geophysical Research Letters 27, 3325-3328.

Bullard, R.L., Stanier, C.O., Ogren, J.A., Sheridan, P.J., 2013. Determination of Seasonal, Diurnal, and Height Resolved Average Number Concentration in a Pollution Impacted Rural Continental Location, 19th International Conference on Nucleation and Atmospheric Aerosols (ICNAA), Colorado State Univ, Ctr Arts, Fort Collins, CO, pp. 583-586.

Bzdek, B.R., Zordan, C.A., Pennington, M.R., Luther, G.W., Johnston, M.V., 2012. Quantitative Assessment of the Sulfuric Acid Contribution to New Particle Growth. Environmental Science & Technology 46, 4365-4373.

Crippa, P., Pryor, S.C., 2013. Spatial and temporal scales of new particle formation events in eastern North America. Atmospheric Environment 75, 257-264.

Dal Maso, M., Kulmala, M., Riipinen, I., Wagner, R., Hussein, T., Aalto, P.P., Lehtinen, K.E., 2005. Formation and growth of fresh atmospheric aerosols: eight years of aerosol size distribution data from SMEAR II, Hyytiala, Finland. Boreal Environment Research 10, 323.

Downard, J., Singh, A., Bullard, R., Jayarathne, T., Rathnayake, C.M., Simmons, D.L., Wels, B.R., Spak, S.N., Peters, T., Beardsley, D., Stanier, C.O., Stone, E.A., 2015. Uncontrolled combustion of shredded tires in a landfill - Part 1: Characterization of gaseous and particulate emissions. Atmospheric Environment 104, 195-204.

Eeftens, M., Phuleria, H.C., Meier, R., Aguilera, I., Corradi, E., Davey, M., Ducret-Stich, R., Fierz, M., Gehrig, R., Ineichen, A., Keidel, D., Probst-Hensch, N., Ragettli, M.S., Schindler, C., Künzli, N., Tsai, M.-Y., 2015. Spatial and temporal variability of ultrafine particles, NO2, PM2.5, PM2.5 absorbance, PM10 and PMcoarse in Swiss study areas. Atmospheric Environment 111, 60-70.

EPA, 1997. Air emissions from scrap tire combustion. Environment Protection Agency, Washington, D.C.

González, Y., Rodríguez, S., García, J.C.G., Trujillo, J.L., García, R., 2011. Ultrafine particles pollution in urban coastal air due to ship emissions. Atmospheric Environment 45, 4907-4914.

Hays, M.D., Fine, P.M., Geron, C.D., Kleeman, M.J., Gullett, B.K., 2005. Open burning of agricultural biomass: physical and chemical properties of particle-phase emissions. Atmospheric Environment 39, 6747-6764.

Huffman, J.A., Docherty, K.S., Aiken, A.C., Cubison, M.J., Ulbrich, I.M., DeCarlo, P.F., Sueper, D., Jayne, J.T., Worsnop, D.R., Ziemann, P.J., Jimenez, J.L., 2009. Chemically-resolved aerosol volatility measurements from two megacity field studies. Atmospheric Chemistry and Physics 9, 7161-7182.

IPCC, 2014. Climate Change 2013: The Physical Science Basis: Working Group I Contribution to the Fifth Assessment Report of the Intergovernmental Panel on Climate Change. Cambridge University Press.

Jacobson, M.Z., 2005. Fundamentals of atmospheric modeling. Cambridge university press.

Just, B., Rogak, S., Kandlikar, M., 2013. Characterization of ultrafine particulate matter from traditional and improved biomass cookstoves. Environmental science & technology 47, 3506-3512.

Kittelson, D.B., Watts, W.F., Johnson, J.P., 2004. Nanoparticle emissions on Minnesota highways. Atmospheric Environment 38, 9-19.

Koponen, I.K., Virkkula, A., Hillamo, R., Kerminen, V.M., Kulmala, M., 2003. Number size distributions and concentrations of the continental summer aerosols in Queen Maud Land, Antarctica. Journal of Geophysical Research-Atmospheres 108.

Kulmala, M., Kerminen, V.-M., 2008a. On the formation and growth of atmospheric nanoparticles. Atmospheric Research 90, 132-150.

Kulmala, M., Vehkamäki, H., Petäjä, T., Dal Maso, M., Lauri, a., Kerminen, V.M., Birmili, W., McMurry, P.H., 2004. Formation and growth rates of ultrafine atmospheric particles: a review of observations. Journal of Aerosol Science 35, 143-176.

Kumar, P., Morawska, L., Birmili, W., Paasonen, P., Hu, M., Kulmala, M., Harrison, R.M., Norford, L., Britter, R., 2014. Ultrafine particles in cities. Environment International 66, 1-10.

Lee, B.H., Kostenidou, E., Hildebrandt, L., Riipinen, I., Engelhart, G.J., Mohr, C., DeCarlo, P.F., Mihalopoulos, N., Prevot, A.S.H., Baltensperger, U., Pandis, S.N., 2010. Measurement of the ambient organic aerosol volatility distribution: application during the Finokalia Aerosol Measurement Experiment (FAME-2008). Atmospheric Chemistry and Physics 10, 12149-12160.

Lemieux, P.M., Lutes, C.C., Santoianni, D.A., 2004. Emissions of organic air toxics from open burning: a comprehensive review. Progress in Energy and Combustion Science 30, 1-32.

Lin, C.-C., Chen, S.-J., Huang, K.-L., Lee, W.-J., Lin, W.-Y., Tsai, J.-H., Chaung, H.-C., 2008. PAHs, PAH-induced carcinogenic potency, and particle-extract-induced

cytotoxicity of traffic-related nano/ultrafine particles. Environmental science & technology 42, 4229-4235.

Morawska, L., Jayaratne, E., Mengersen, K., Jamriska, M., Thomas, S., 2002. Differences in airborne particle and gaseous concentrations in urban air between weekdays and weekends. Atmospheric Environment 36, 4375-4383.

Morawska, L., Ristovski, Z., Jayaratne, E.R., Keogh, D.U., Ling, X., 2008. Ambient nano and ultrafine particles from motor vehicle emissions: Characteristics, ambient processing and implications on human exposure. Atmospheric Environment 42, 8113-8138.

Nallathamby, P.D., Hopke, P.K., Rossner, A., Dhaniyala, S., Marzocca, P., Petaja, T., Barthelmie, R.J., Pryor, S.C., 2014. Particle nucleation in a forested environment. Atmospheric Pollution Research 5, 805-810.

Nieminena, T., Kontkanena, J., Krejcia, R., Hoffmand, P., 2013. New particle formation events observed at a high altitude site Pico Espejo, Venezuela, NUCLEATION AND ATMOSPHERIC AEROSOLS: 19th International Conference. AIP Publishing, pp. 413-416.

Oberdörster, G., Oberdörster, E., Oberdörster, J., 2005. Nanotoxicology: an emerging discipline evolving from studies of ultrafine particles. Environmental health perspectives, 823-839.

Orville, R.E., Huffines, G., Nielsen-Gammon, J., Zhang, R., Ely, B., Steiger, S., Phillips, S., Allen, S., Read, W., 2001. Enhancement of cloud-to-ground lightning over Houston, Texas. Geophysical Research Letters 28, 2597-2600.

Pierce, J.R., Riipinen, I., Kulmala, M., Ehn, M., Petaja, T., Junninen, H., Worsnop, D.R., Donahue, N.M., 2011. Quantification of the volatility of secondary organic compounds in ultrafine particles during nucleation events. Atmospheric Chemistry and Physics 11, 9019-9036.

Pryor, S., Barthelmie, R., Sørensen, L.L., McGrath, J., Hopke, P., Petäjä, T., 2011. Spatial and vertical extent of nucleation events in the Midwestern USA: insights from the Nucleation In ForesTs (NIFTy) experiment. Atmospheric Chemistry and Physics 11, 1641-1657.

Pryor, S., Spaulding, A., Barthelmie, R., 2010a. New particle formation in the Midwestern USA: Event characteristics, meteorological context and vertical profiles. Atmospheric Environment 44, 4413-4425.

Pryor, S.C., Hornsby, K.E., Novick, K.A., 2014. Forest canopy interactions with nucleation mode particles. Atmospheric Chemistry and Physics 14, 11985-11996.

Raatikainen, T., Vaattovaara, P., Tiitta, P., Miettinen, P., Rautiainen, J., Ehn, M., Kulmala, M., Laaksonen, A., Worsnop, D.R., 2010. Physicochemical properties and origin of organic groups detected in boreal forest using an aerosol mass spectrometer. Atmospheric Chemistry and Physics 10, 2063-2077.

Ramanathan, V., Crutzen, P., Kiehl, J., Rosenfeld, D., 2001. Aerosols, climate, and the hydrological cycle. science 294, 2119-2124.

Riipinen, I., Pierce, J.R., Donahue, N.M., Pandis, S.N., 2010. Equilibration time scales of organic aerosol inside thermodenuders: Evaporation kinetics versus thermodynamics. Atmospheric Environment 44, 597-607.

Riipinen, I., Pierce, J.R., Yli-Juuti, T., Nieminen, T., Hakkinen, S., Ehn, M., Junninen, H., Lehtipalo, K., Petaja, T., Slowik, J., Chang, R., Shantz, N.C., Abbatt, J., Leaitch, W.R., Kerminen, V.M., Worsnop, D.R., Pandis, S.N., Donahue, N.M., Kulmala, M., 2011. Organic condensation: a vital link connecting aerosol formation to cloud condensation nuclei (CCN) concentrations. Atmospheric Chemistry and Physics 11, 3865-3878.

Rivera, M., Basagaña, X., Aguilera, I., Agis, D., Bouso, L., Foraster, M., Medina-Ramón, M., Pey, J., Künzli, N., Hoek, G., 2012. Spatial distribution of ultrafine particles in urban settings: A land use regression model. Atmospheric Environment 54, 657-666.

Sabaliauskas, K., Jeong, C.-H., Yao, X., Jun, Y.-S., Evans, G., 2013. Cluster analysis of roadside ultrafine particle size distributions. Atmospheric Environment 70, 64-74.

Sakurai, H., Fink, M.a., McMurry, P.H., Mauldin, L., Moore, K.F., Smith, J.N., Eisele, F.L., 2005. Hygroscopicity and volatility of 4–10 nm particles during summertime atmospheric nucleation events in urban Atlanta. Journal of Geophysical Research 110, D22S04-D22S04.

Schobesberger, S., Junninen, H., Bianchi, F., Lonn, G., Ehn, M., Lehtipalo, K., Dommen, J., Ehrhart, S., Ortega, I.K., Franchin, A., Nieminen, T., Riccobono, F., Hutterli, M., Duplissy, J., Almeida, J., Amorim, A., Breitenlechner, M., Downard, A.J., Dunne, E.M., Flagan, R.C., Kajos, M., Keskinen, H., Kirkby, J., Kupc, A., Kuerten, A., Kurten, T., Laaksonen, A., Mathot, S., Onnela, A., Praplan, A.P., Rondo, L., Santos, F.D., Schallhart, S., Schnitzhofer, R., Sipila, M., Tome, A., Tsagkogeorgas, G., Vehkamaki, H., Wimmer, D., Baltensperger, U., Carslaw, K.S., Curtius, J., Hansel, A., Petaja, T., Kulmala, M., Donahue, N.M., Worsnop, D.R., 2013. Molecular understanding of atmospheric particle formation from sulfuric acid and large oxidized organic molecules. Proceedings of the National Academy of Sciences of the United States of America 110, 17223-17228.

Shantz, N.C., Pierce, J.R., Chang, R.Y.W., Vlasenko, A., Riipinen, I., Sjostedt, S., Slowik, J.G., Wiebe, A., Liggio, J., Abbatt, J.P.D., Leaitch, W.R., 2012. Cloud condensation nuclei droplet growth kinetics of ultrafine particles during anthropogenic nucleation events. Atmospheric Environment 47, 389-398.

Singh, A., Spak, S.N., Stone, E.A., Downard, J., Bullard, R.L., Pooley, M., Kostle, P.A., Mainprize, M.W., Wichman, M.D., Peters, T.M., Beardsley, D., Stanier, C.O., 2015. Uncontrolled combustion of shredded tires in a landfill - Part 2: Population exposure, public health response, and an air quality index for urban fires. Atmospheric Environment 104, 273-283.

Sioutas, C., Delfino, R.J., Singh, M., 2005. Exposure Assessment for Atmospheric Ultrafine Particles (UFPs) and Implications in Epidemiologic Research. Environmental Health Perspectives 113, 947-955.

Smith, J., Moore, K., McMurry, P., Eisele, F., 2004. Atmospheric measurements of sub-20 nm diameter particle chemical composition by thermal desorption chemical ionization mass spectrometry. Aerosol Science and Technology 38, 100-110.

Smith, J.N., Moore, K.F., Eisele, F.L., Voisin, D., Ghimire, A.K., Sakurai, H., McMurry, P.H., 2005. Chemical composition of atmospheric nanoparticles during nucleation events in Atlanta. Journal of Geophysical Research-Atmospheres 110.

Stanier, C., Singh, A., Adamski, W., Baek, J., Caughey, M., Carmichael, G., Edgerton, E., Kenski, D., Koerber, M., Oleson, J., 2012. Overview of the LADCO winter nitrate study: hourly ammonia, nitric acid and PM 2.5 composition at an urban and rural site pair during PM 2.5 episodes in the US Great Lakes region. Atmospheric Chemistry and Physics 12, 11037-11056.

Stanier, C.O., Khlystov, A.Y., Pandis, S.N., 2004. Nucleation events during the Pittsburgh air quality study: Description and relation to key meteorological, gas phase, and aerosol parameters. Aerosol Science and Technology 38, 253-264.

Stockwell, C.E., Veres, P.R., Williams, J., Yokelson, R.J., 2015. Characterization of biomass burning emissions from cooking fires, peat, crop residue, and other fuels with high-resolution proton-transfer-reaction time-of-flight mass spectrometry. Atmospheric Chemistry and Physics 15, 845-865.

Stolzenburg, M.R., McMurry, P.H., Sakurai, H., Smith, J.N., Mauldin, R.L., Eisele, F.L., Clement, C.F., 2005. Growth rates of freshly nucleated atmospheric particles in Atlanta. Journal of Geophysical Research-Atmospheres 110.

Urbanski, S., 2013. Wildland fire emissions, carbon, and climate: Emission factors. Forest Ecology and Management 2.

USFA, 1998. Special Report : Scrap and Shredded Tire Fires, Technical Report Series. United States Fire Administration, Maryland.

Venzac, H., Sellegri, K., Laj, P., Villani, P., Bonasoni, P., Marinoni, A., Cristofanelli, P., Calzolari, F., Fuzzi, S., Decesari, S., 2008. High frequency new particle formation in the Himalayas. Proceedings of the National Academy of Sciences 105, 15666-15671.

Virtanen, A., Ronkko, T., Kannosto, J., Ristimaki, J., Makela, J.M., Keskinen, J., Pakkanen, T., Hillamo, R., Pirjola, L., Hameri, K., 2006. Winter and summer time size distributions and densities of traffic-related aerosol particles at a busy highway in Helsinki. Atmospheric Chemistry and Physics 6, 2411-2421.

Wang, Z., Li, K., Lambert, P., Yang, C., 2007. Identification, characterization and quantitation of pyrogenic polycylic aromatic hydrocarbons and other organic compounds in tire fire products. Journal of chromatography. A 1139, 14-26.

Wehner, B., Petäjä, T., Boy, M., Engler, C., Birmili, W., Tuch, T., Wiedensohler, A., Kulmala, M., 2005. The contribution of sulfuric acid and non-volatile compounds on the growth of freshly formed atmospheric aerosols. Geophysical research letters 32.

Westerdahl, D., Fruin, S.A., Fine, P.L., Sioutas, C., 2008. The Los Angeles International Airport as a source of ultrafine particles and other pollutants to nearby communities. Atmospheric Environment 42, 3143-3155.

Westervelt, D.M., Pierce, J.R., Riipinen, I., Trivitayanurak, W., Hamed, A., Kulmala, M., Laaksonen, A., Decesari, S., Adams, P.J., 2013. Formation and growth of nucleated particles into cloud condensation nuclei: model-measurement comparison. Atmospheric Chemistry and Physics 13, 7645-7663.

Woo, K.S., Chen, D.R., Pui, D.Y.H., McMurry, P.H., 2001. Measurement of Atlanta aerosol size distributions: Observations of ultrafine particle events. Aerosol Science and Technology 34, 75-87.

Wu, Z., Birmili, W., Poulain, L., Wang, Z., Merkel, M., Fahlbusch, B., Pinxteren, D.v., Herrmann, H., Wiedensohler, A., 2013. Particle hygroscopicity during atmospheric new particle formation events: implications for the chemical species contributing to particle growth. Atmospheric Chemistry and Physics 13, 6637-6646.

Yokelson, R.J., Burling, I., Urbanski, S., Atlas, E., Adachi, K., Buseck, P., Wiedinmyer, C., Akagi, S., Toohey, D., Wold, C., 2011. Trace gas and particle emissions from open biomass burning in Mexico. Atmospheric Chemistry and Physics 11, 6787-6808.

Yu, H., Ortega, J., Smith, J.N., Guenther, A.B., Kanawade, V.P., You, Y., Liu, Y., Hosman, K., Karl, T., Seco, R., Geron, C., Pallardy, S.G., Gu, L., Mikkila, J., Lee, S.-H., 2014. New Particle Formation and Growth in an Isoprene-Dominated Ozark Forest: From Sub-5 nm to CCN-Active Sizes. Aerosol Science and Technology 48, 1285-1298.

Yue, D.L., Hu, M., Zhang, R.Y., Wang, Z.B., Zheng, J., Wu, Z.J., Wiedensohler, A., He, L.Y., Huang, X.F., Zhu, T., 2010. The roles of sulfuric acid in new particle formation and growth in the mega-city of Beijing. Atmospheric Chemistry and Physics 10, 4953-4960.

Yue, D.L., Hu, M., Zhang, R.Y., Wu, Z.J., Su, H., Wang, Z.B., Peng, J.F., He, L.Y., Huang, X.F., Gong, Y.G., Wiedensohler, A., 2011. Potential contribution of new particle formation to cloud condensation nuclei in Beijing. Atmospheric Environment 45, 6070-6077.

Zhang, R., Khalizov, A., Wang, L., Hu, M., Xu, W., 2012. Nucleation and growth of nanoparticles in the atmosphere. Chemical reviews 112, 1957-2011.

Zhang, R., Tie, X., Bond, D.W., 2003. Impacts of anthropogenic and natural NOx sources over the US on tropospheric chemistry. Proceedings of the National Academy of Sciences 100, 1505-1509.

Zordan, C.A., Pennington, M.R., Johnston, M.V., 2010. Elemental composition of nanoparticles with the nano aerosol mass spectrometer†. Analytical chemistry 82, 8034-8038.

Zwack, L.M., Hanna, S.R., Spengler, J.D., Levy, J.I., 2011. Using advanced dispersion models and mobile monitoring to characterize spatial patterns of ultrafine particles in an urban area. Atmospheric Environment 45, 4822-4829.

CHAPTER 2: SPECIFIC AIM OF THE THESIS

The thesis has four specific aims. The first three aims are relevant to measurement of physical properties of ultrafine particles or UFPs. This includes number and size distribution, estimation of volatile, semi-volatile and low volatile fraction and identification of volatility clusters among different particle size. The fourth aim explores the link between primary emission sources, air quality measurements tools, and human health by adding providing new emission factors estimation of pollutant in the smoke, and improved method of health impact assessment and air quality response. The four specific aims are as follows.

2.1 Specific Aim 1

Mapping particle concentrations with a mobile CPC

Application of a mobile platform provides a better spatial estimation of concentration of UFP. In this aim, we evaluated the feasibility of a particle sensor as a mobile platform to generate a map of ultrafine particle concentration.

2.2 Specific Aim 2

Design, construction, and testing of a V-TDMA

Volatility signature of the atmospheric particle is often dependent on the design configuration of the tandem differential mobility analyzers system. In this aim, a volatility tandem differential mobility analyzer (V-TDMA) was designed to characterize the volatility of atmospheric UFP. The relation between TDMA design parameters and volatility response of UFP were also determined.

2.3 Specific Aim 3

Volatility measurement of primary and secondary UFP in the rural continental Midwest

Volatility characterizations enable indirect inference about particle chemistry, and formation of residue in the UFP in the Midwest. This aim examined the relation between the nature of volatility response and its association with particle size, chemistry and trace gas in the Midwest. Association of volatility response with particle formation (NPF) and non-NPF were established. The relation between the residue with size, trace gas and particle formation event were quantified.

2.4 Specific Aim 4

Population exposure, public health response, and an air quality index for urban fires

This aim evaluated various aspects of an emergency air quality response system for an urban fire. The nature of linkage between accidental fire, smoke characterization, potential impact and nature of emergency response were established in the study. A multi-pollutant air quality index was proposed as an appropriate measure of population risk during a toxic fire.

CHAPTER 3: MAPPING PARTICLE CONCENTRATIONS WITH A MOBILE CPC

3.1 Abstract

Ground measurements of air pollutants are essential to understanding the change in their concentration across space and time. Typical ground measurements are usually obtained from stationary monitoring stations. These monitoring stations provide data that is spatially limited and can have difficulty in accurate concentration values, especially for pollutants such as particle number concentration that can vary by several orders of magnitude between the source and the monitoring site. A portable mobile particle counter is built to generate a high-resolution spatial map of total particle concentration encompassing the UFP size range. The portable counter is equipped to provide high-frequency, continuous, on-road synchronous measurements of particle number and CO_2. The mobile platform is integrated with an independent power supply system, a robust controller and data acquisition, and a GPS system. These capabilities make the mobile particle counter deployable remotely, used for both ground and aerial measurements and offer the flexibility to integrate other analog and digital sensors in the existing configuration. For data visualization, the Matlab-google earth tool kit is used to display the data graphically.

3.2 Introduction

Mobile measurements are commonly deployed to measure local to regional scale pollutants (Pirjola et al., 2004). The existing routine monitoring network[11] such as SLAMS[12], CASNET[13], and NCore[14] mainly focuses on the measurement of criteria pollutants, which does not include total particle number concentration, of which ultrafine particle make up more than 50% of the total number concentration (Kumar et al., 2014). UFPs in the ambient air are associated with adverse health effects in humans. For e.g. UFPs have higher penetration efficiency into the human lungs than larger particles reaching the alveolar part of the human lung, and also deposits efficiently due to diffusion (Phalen et al., 2006; Frampton, 2007). Due to their content of reactive oxygen species (ROS) and large combined surface area, UFPs also have the potential to damage pulmonary cells (Delfino et al., 2005). Stationary monitors are limited in their accuracy to provide high resolution spatial concentration data for exposure studies and often difficult to identify sources, evolution and fate of urban air pollution.

Changes in the concentration of air pollutants, with respect to time and space, can be critical for urban area which are usually associated with elevated pollutant concentrations, high population density and multitude of sources (Chan and Yao, 2008). Our ability to determine or predict the concentration of pollutants can also help in various decision support systems and emission control measures such as identification of

[11] These are all EPA routine monitoring network managed for different objectives (population exposure, area attainment and have sampling methodology.
[12] SLAMS: State or Local Air Monitoring Stations Network, SLAMS include NCore, PAMs and other EPA network, http://www.epa.gov/ttn/amtic/slams.html
[13] CASTNET: The Clean Air Status and Trends Network is a national air quality monitoring network designed to provide data to assess trends in air quality, atmospheric deposition, and ecological effects due to changes in air pollutant emissions, http://epa.gov/castnet/javaweb/index.html
[14] NCore or National Core Network is a multi-pollutant network that integrates several advanced measurement systems for particles, pollutant gases and meteorology, http://www.epa.gov/ttnamti1/ncore/index.html

pollution hotspots, changing vehicle and fuel type, and avoiding traffic congestion (Singh et al., 2015). It also assists in estimation of realistic exposure levels, thus reducing the large uncertainties associated with the stationary monitors (Sioutas et al., 2005). This is crucial for a pollutant such as total particle number and specifically for particle less than 100 nm (or UFP). The absence of routine monitoring for UFP in urban locations in the US makes it difficult to provide an accurate estimate of UFP exposure. Available exposure estimates are usually based on a short term campaign measurements.

The sources of UFP in a urban location can be contributed by variety of sources: traffic (Nickel et al., 2013), industrial and power plant plume (Saarnio et al., 2014), airports (Hudda et al., 2014), tire and road surface wear (Panko et al., 2013), natural formation (Ma and Birmili, 2015), biomass burning (Akagi et al., 2011) and other emerging sources such as manufactured nano-materials (Mueller and Nowack, 2008). Among other air pollutants, the concentration of UFP in an urban area can vary strongly due to, among others, street canyon effects, urban micrometeorology, and atmospheric stability (Kumar et al., 2011).

To improve UFP spatial coverage, many different ground and aerial measurements have been conducted using mobile platforms, as shown in Figure 3.1. Often measurements are also "gap-filled" in time and space using land-use regression and dispersion models (Stanier and Lee, 2014; Zwack et al., 2011). Mobile measurements of pollutants, particularly online measurements, are one of the efficient techniques to produce high resolution time and space concentration profile of UFP, develop spatial distribution maps and eventually aid in the development of exposure models. Mobile platforms are also used to establish the vertical profile of UFP in the atmosphere to

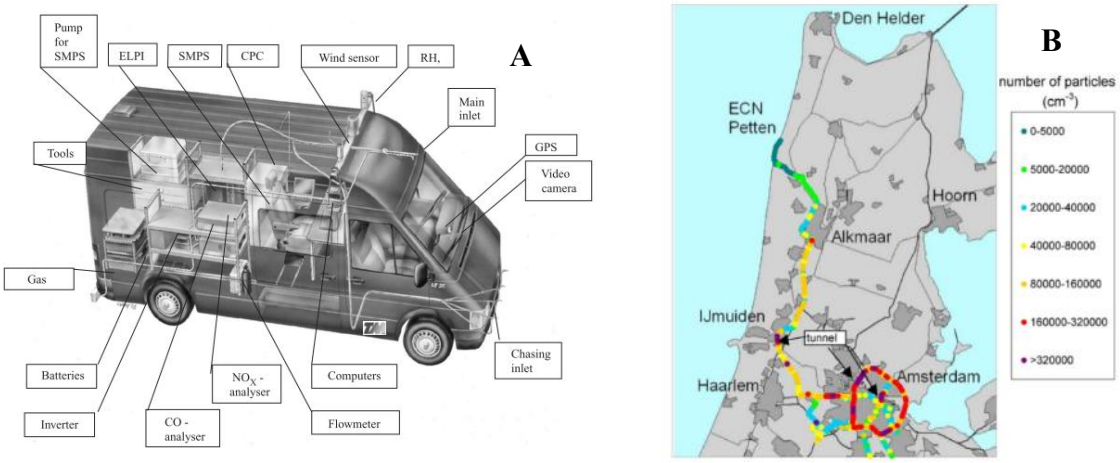

Figure 3.1 An example of the mobile laboratory designed for an urban measurement in Europe. 3.1A shows the various component of the mobile laboratory. 3.1B shows the high resolution particle count along the road network (Pirjola et al., 2004).

provide evidence for particle movement in and out of the continental boundary layer (Bullard et al., 2013; Sheridan et al., 2012).

Many multi-pollutants mobile stations have been developed, housed in a large mobile unit such as trailer or van (Peters et al., 2013; Peters et al., 2006; Pirjola et al., 2006; Weijers et al., 2004). These set-ups have also been used in conjunction with aerosol mapping techniques for better visualization of UFP concentration in open spaces to work place environment (**Fig.3.1**). Large mobile stations such as the one shown in **Figure 3.1** can measure many pollutants and local meteorology, but requires a large independent power supply, and can have difficulty in its mobility in narrow roads and alleys. The presence of a small mobile measurement system could greatly complement larger mobile stations due to its better portability, lower power requirements and minimal logistic challenges. At the same time, they can be operated independently and remotely through a data logging systems which can also act as a controller to initiate and control different components of the mobile unit. Also, they can offer higher spatial resolution of UFP

concentration and thus would be a useful tool for hotspot identification and aerial sampling.

The hurdle in developing a mobile UFP counter is that most commercially available particle counters including TSI's water and butanol based CPC's are stationary counter and requires an AC[15] power supply. Water based CPCs are one of the few instruments capable of fast response and real time measurement of UFP.

In this thesis, a mobile CPC counter was designed and assembled. The current design is motivated to help estimate spatial and temporal distributions of UFP concentrations in urban locations and provide a dispersion map of UFP from road to surrounding location. The portability of the counter will also help aerial deployment for examining the vertical profile of UFP to evaluate the extent of UFP entrainment prior to and during particle formation in the atmosphere.

To accomplish this goal, the study explored the possibility of using water based CPC 3786 as a portable mobile counter. Water based CPC offers some advantages over the butanol based CPC 3022. The CPC 3786 has a lower D_{50} of 2.5 nm and is one of the fastest responding CPC's (counting speed < 2 s for water based CPC 3786 compared to 15 s for butanol based CPC 3022). These two features make water based CPC 3786 a better unit for detecting particles down to the nuclei mode (< 30 nm) and are sensitive to detect sudden changes in UFP concentration during mobile sampling. This can help in providing an accurate measurement of UFP.

[15] Alternative current (AC)

3.3 Methodology

3.3.1 Description of the mobile CPC

The basic design for the mobile UFP sampler includes a CPC, a data acquisition unit, GPS unit, independent power supply and a casing for the sampler. Programmatically it required a system that can communicate with the various sensors such as CPC, GPS and other instruments in the unit and collect, process and stores the data.

3.3.2 Experimental and data analysis methods

3.3.1.1 Inlet system of the mobile unit

The design of the inlet system for the mobile station was simple. The inlet system uses CPC's internal pump to pull in the particles from the ambient air. The inlet of the CPC was connected with an external transport tube (¼ inch internal diameter (ID) non-conducting tube, 1 m length) via a Swagelok fitting at the posterior wall of the Pelican case (See **Appendix** section 9.2 simple diagram of the inlet**)**. The loss of UFP in the inlet line was calculated using the Particle Loss Calculator (PCL)[16] developed by Weiden et al., 2009. The loss calculator uses the IGOR programming platform, and accounts for loss due to diffusion, sedimentation, inertial deposition, the effect of changing tube diameter and tube bend. The loss calculation shown in **Figure 3.2** is a penetration loss[17] via the inlet tube of 1 m long and ¼ inches of ID, at a flow rate of 0.6 lpm without considering any bend that is likely in the tube. The penetration efficiency of the simple inlet is

[16] The loss calculator can be found at http://www.mpch-mainz.mpg.de/~drewnick/PLC, Weiden, S.-L., Drewnick, F., Borrmann, S., 2009. Particle Loss Calculator–a new software tool for the assessment of the performance of aerosol inlet systems. Atmospheric Measurement Techniques 2, 479-494.

[17] Ratio of the number concentration of particles leaving a tube to the number concentration of particles entering the tube

approximately 80% for 10 nm which confirms no significant loss of UFP in the inlet sampling line.

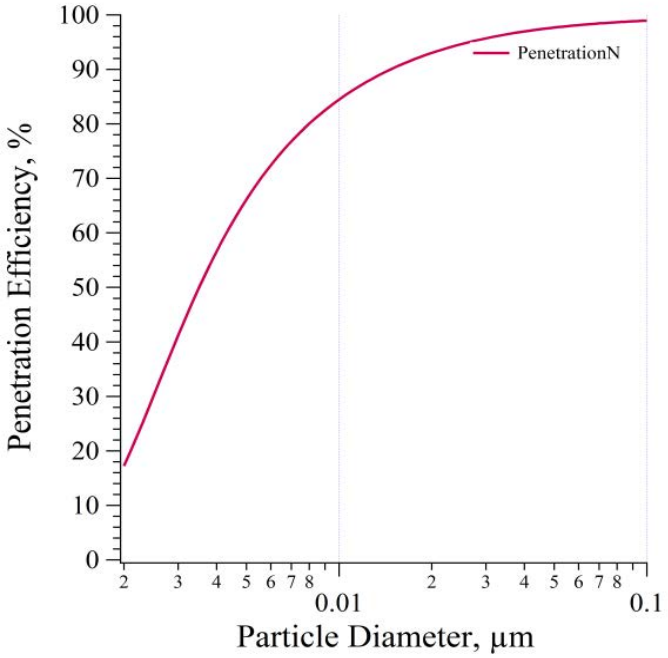

Figure 3.2 Estimated penetration loss for a 1 m long sampling tube (1/4 inch internal diameter) used in the mobile unit. The estimation was performed using the particle loss counter (PCL) in IGOR.

3.3.1.2. Portable CPC

The major focus of the mobile device is to measure ambient UFP. TSI's CPC 3786 particle monitor was used for the measurement of UFP concentration. The instrumental details of CPC 3786 are provided in Table 3.1. It is a fast responding CPC and can measure particles as small as 2.5 nm. The power requirement for the CPC is 12 VDC, and it can be controlled independently using serial communication via hyper terminal, CR basic or Matlab.

3.3.1.3. CO_2 monitor

The CO_2 monitor was an experimental "add on" to the initial design of the mobile unit. The Vaisala GMP 343[18] is ideally suited for a low powered mobile applications (Poppa et al., 2013). The GMP 343 can work for a wide range of temperatures and humidity and features an accuracy of 3 ppm (+ 1% of reading) and a noise of 3 ppm within the measurement range of 0-1000 ppm. The fastest response time of the sensor is 2 s (without filter attachment and internal filtering). It requires 12 VDC and 4-24 mA to operate. The CO_2 monitor shares a common power source with the data logger.

Table 3.1 Summary of the components of mobile CPC platform

Measurements Instruments	Measurement quantity	Flow rate	Sampling frequency	Lower detection limit
TSI CPC 3786	Total particle number	0.6 lpm	1 s	D_{50}: 2.5 nm
Vaisala GMP 343	CO_2, 0-1000 ppm	1.2 lpm[19]	5 s	0 ppm, (2%)
Garmin 16 HVS	WAAS/RTCM GPS coordinates	NA	1 s	< 15 meters,
CR 850	Main Controller & data acquisition	NA	1 s	NA
Power supply	12 V, 2.5 Ah, 10 cell NiMh (1.5V each)	NA	NA	NA
Pelican 0350[20]	Mobile Case	18" x 18" x 18"		

[18] http://www.vaisala.com/en/products/carbondioxide/Pages/gmp343.aspx
[19] lpm: liters per minute
[20] http://www.pelican.com/cases_detail/Case/0350/

3.3.1.4. VDC power source

The independent power supply for the mobile sampler uses a Nickel metal hydride cell (NiMH, 1.2 VDC, and 2.5 Ah each). The minimum power requirement was 12 VDC, so two 5 cell packs were connected in parallel to generate 12 VDC and 5 Ah. Details of the VDC power supply is provided in the **Appendix** (Section 9.1: Power supply design for the mobile CPC)**.** This power source can operate the CPC for approximately 1- 1.3 h.

3.3.1.5. Data acquisition and operation of the mobile unit

A central data acquisition system was used to collect all the data from particle, CO_2, and GPS unit. Campbell Scientific[21] (Camp. Sci) commercial data loggers are rugged, reliable data logger and micro-computer system used in many environmental monitoring applications (Andrews et al., 2014; Dietz and Abraham, 2012). The model CR 850 offers 12 MB memory inbuilt, 3 serial ports, and 5 analog inputs for communication and data acquisition. CR 850 model is used in the current mobile system, which communicates with the CPC's, and GPS unit using RS 232 serial output. This data acquisition system also acts as a central controller thus avoids the use of central PC or laptop. The logger is also capable of synchronization of data stream and the collected data can be monitored in real time

The CR 850 uses a CR basic (C++) programming language for communication and controls. The software communicates with the individual instruments using RS 232 serial communication protocol. For the mobile operation, a CR-basic program was

[21] https://www.campbellsci.com/cr800

written/developed which can store particle concentration, and GPS data. The details of the CR program can be found in the **Appendix** (Section 9.1. CR BASIC PROGRAM).

3.3.1.6. GPS system

GPS system is a common, but critical part of the mobile unit. Garmin model HVS16x[22] is a portable device which works on a WAAS[23] navigation system. It offers high accuracy (<15 m), fast time resolution (1 s), and possesses an inbuilt antenna for better reception. This model offers serial communication (RS 232) and is compatible with CR 850 data logger, making it a good choice for mobile applications (Adams et al., 2012; Yu et al., 2014). In the current mobile configuration, the GPS unit is powered using the CR 850's power source.

3.3.1.7. Data visualization tool

The Matlab toolbox by Scott L. Davis[24] was used as the main data visualization tool. This tools box was modified to integrate the concentration and GPS data and produce a Google Earth kml[25] file. The kml file can either be opened with Matlab or Google Earth application. Particle concentration associated with each GPS point every second will be plotted. A 64 color scale was developed for visualization of the particle concentrations, which uses the co-ordinate data from the GPS to geo-localize the particle concentration.

[22] https://buy.garmin.com/en-US/US/oem/sensors-and-boards/gps-16x-/prod13194.html
[23] Wide Area Augmentation System (WAAS)
[24] http://www.mathworks.com/matlabcentral/fileexchange/12954-google-earth-toolbox
[25] KML stands for Keyhole Markup Language. The KML file format is used in google maps.

3.4 Results

3.4.1 System configuration

Design configuration of the mobile platform is shown in **Figure 3.3 (A).** The pink solid lines are the power connections, whereas the blue dotted lines indicate the data cable connections. **Figure 3.3 (B)** shows the assembled mobile unit encased in a Pelican case. **Figure 3.3 (C)** is a picture of VDC powered CPC 3786 in operational condition.

3.4.2 Laboratory test

The water and butanol based CPC are originally designed by TSI Inc. as stationary instruments running on a steady analog current (AC) power supply. Changes from AC to VDC power supply for the CPC is usually not expected to influence its functioning. However the effects of VDC supply on CPC functioning needs verification. For use in a mobile unit, it was critical that the movement of CPC (as a mobile unit) and VDC power supply did not influence CPC counting efficiency. A series of tests were conducted to check these concerns.

3.4.2.1. Effect of power supply on CPC counting efficiency

To test how the choice of power supply may affect the counting efficiency of the CPC, a simple experiment was set up, as shown in **Figure 3.4**. A 0.1 molar ammonium sulfate (AS)[26] solution was fed to atomizer[27] to generate poly-disperse AS particles.

The poly-disperse AS particles were dried, charged[28] and size-selected using TSI SMPS to get a sharp peak of 100 nm. The resulting mono-disperse AS particles was then fed into CPC 3785 and 3786 **(Fig. 3.4)**. Tests was conducted at both low concentration (<

[26] Ammonium sulfate will be abbreviated as "AS" for the rest of the thesis.
[27] TSI Atomizer model 3076, http://www.tsi.com/aerosol-generators-and-dispersers/
[28] Charging was conducted using TSI 3077 Neutralizer, Kr-85 gamma radiation

$1x10^3$ #/cm^3) and high concentration (>$1x10^3$ #/cm^3) by varying the flow rate of aqueous AS solution to the atomizer from 0.7 to 1.5 ml/h.

During the test, the relative humidity (RH) of the particle stream exiting the dryer was maintained below 20%. In this experiment, CPC 3786 is connected to VDC power supply and CPC 3875 is connected to AC power supply.

The result of the comparison between AC and VDC run is depicted in **Figure 3.5**. In general, particle counts are close between the two CPCs at both concentration ranges. This is indicated by a strong correlation (R^2~1) for a wide range of concentration range. The test was limited to particle concentration between $1x10^3$ and $2x10^4$ #/cm^3, close to the reported ambient concentrations of the accumulation mode particle (>80 nm) (Bullard et al., 2013; Downard et al., 2015).

Overall, the near R^2~1 correlation coefficient observed in **Figure 3.5 (A** and **B)** suggests that the battery operated CPC 3785 gives roughly the same readings as the AC operated CPC 3786. However this correlation appears to diverge at high concentrations as can be observed in **Figure 3.5 (B).**

The slope of the line is also close to 0.9 which indicate that the concentration reported by these CPC, one with battery operated and the other on an AC power, were similar. These results were expected from a robust device such as TSI CPC. The strength of the results validates the use of CPC with battery and it is shown from these tests that operation of CPC in a battery power should not hamper its counting efficiency.

Figure 3.3 Overview of the configuration, assembly, and testing of the mobile CPC. 3.3 A is a schematic configuration in the mobile CPC showing electrical (magenta) and data lines(blue).3.3 B shows the assembly of the mobile unit in a Pelican case showing integrated GPS, data logger and NiMh battery pack; 3.3 C illustrates the design of the external VDC supply to the CPC 3786.

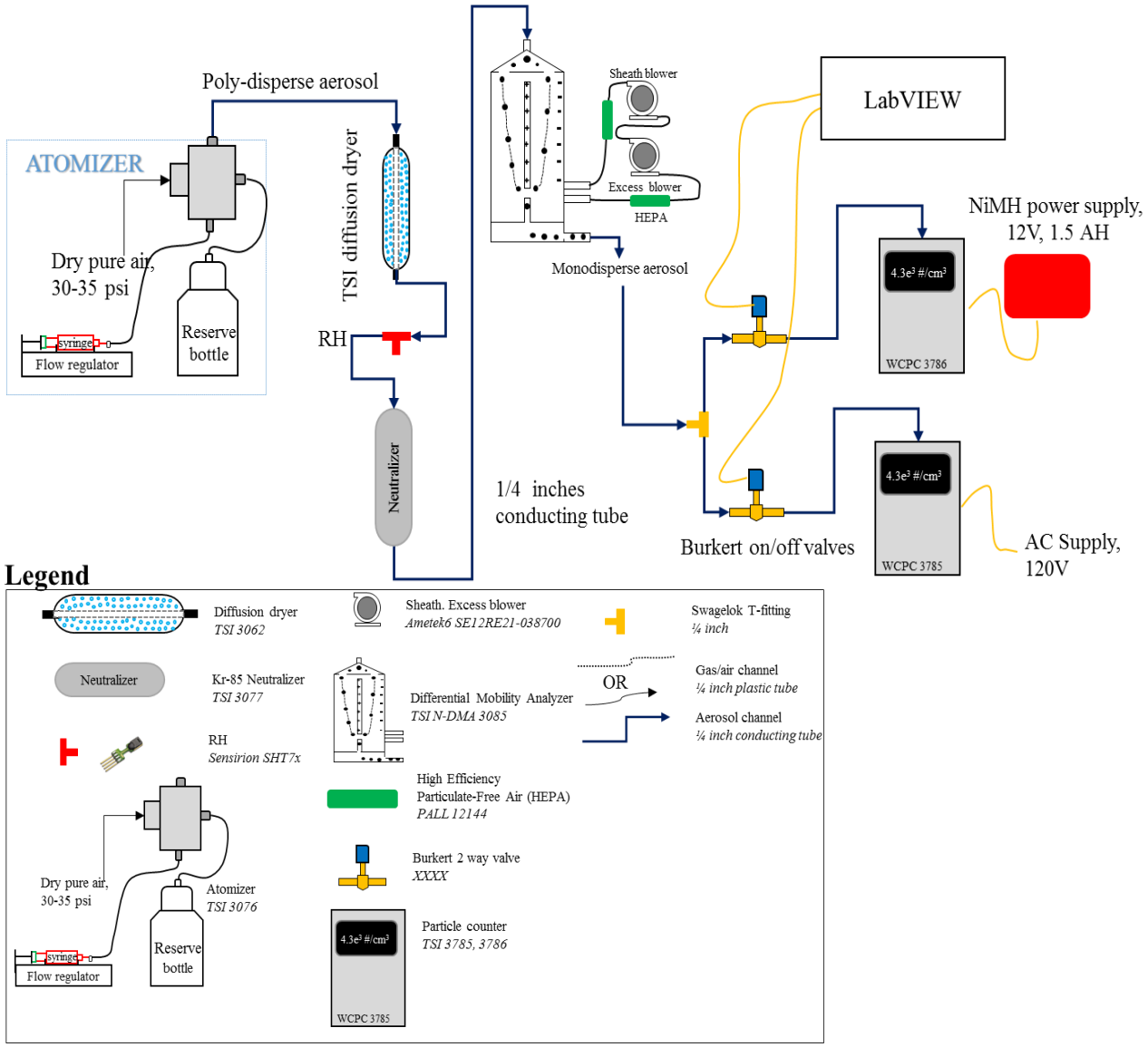

Figure 3.4 Laboratory testing of the CPC using a laboratory generated ammonium sulfate and sized to 100 nm. The figure shows the comparative test conducted between 3786 (connected to the battery pack, 12 VDC, 5.5 Ah) and CPC 3785 (connected to the normal AC supply).

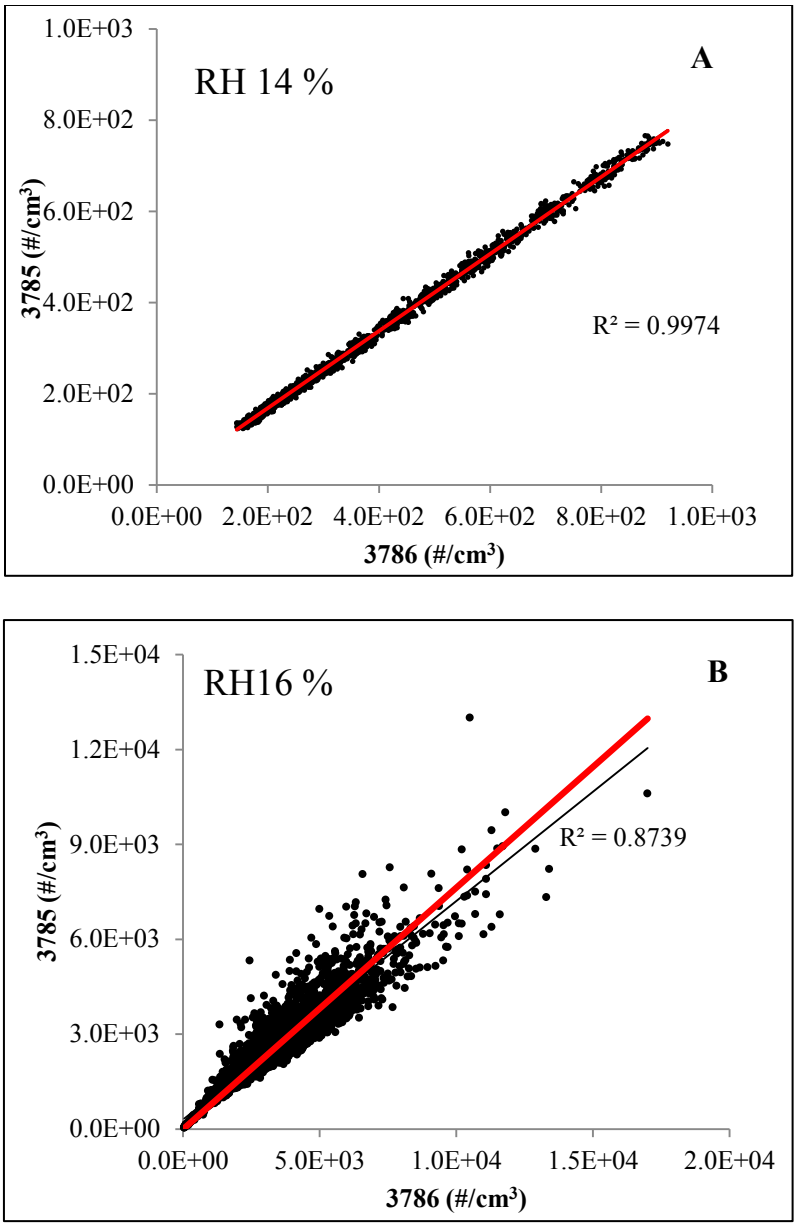

Figure 3.5 Comparison between CPC run with AC (CPC 3785) and battery power (CPC 3786). Panel A shows the test run conducted at particle concentration range of $0.5x10^3$-$1x10^3$ #/cm^3. Panel B shows the test run conducted at particle concentration range of $>1x10^3$-$20x10^3$ #/cm^3.

3.4.2.2. Effect of mobile CPC on count efficiency

The motion of the vehicle carrying the mobile CPC was tested by comparing by simultaneously taking the measurement from the mobile counter mounted at the back of

an electric van. The mobile measurement from the mobile CPC was taken by driving the electric van in a circle for 5 mins and the stationary measurement was taken by parking the vehicle at the center of the circle and the engine of the electric turned off.

The results of these outdoor tests are shown in **Figure 3.6 (A) and (B).** The mean count of the mobile CPC during the stationary condition was ~$1.2x10^4$ #/cm^3 compared to ~$1.1x10^4$ #/cm^3 during the mobile condition. The inherent variation in particle concentration reported in the TSI operation manual[29] for CPC 3786 is 12% of particle concentration (for a particle concentration of $1x10^5$ #/cm^3), and thus the mean differences between the mobile and stationary mode CPC was within the range of variability. In conclusion, vehicle motion at the examined speeds and concentrations does not appear to affect the measured particle concentration.

3.4.3 Summary of the testing

Battery operation doesn't seem to affect CPC performance. The comparison between AC and battery operated CPC are in good agreement. AC and battery run CPC correlated well (R^2 =0.99) at low concentrations (<1 $x10^3$ #/cm^3). The correlation decreases (R^2 = 0.87) at higher particle concentrations (>1 to 1.5 $x10^3$ #/cm^3). Likewise, motion and stationary sampling test shows variation with them, but the test do not show any significant difference between the compared cases. The current power supply can provide one hour of stable data collection.

[29] TSI CPC 3786 operation manual

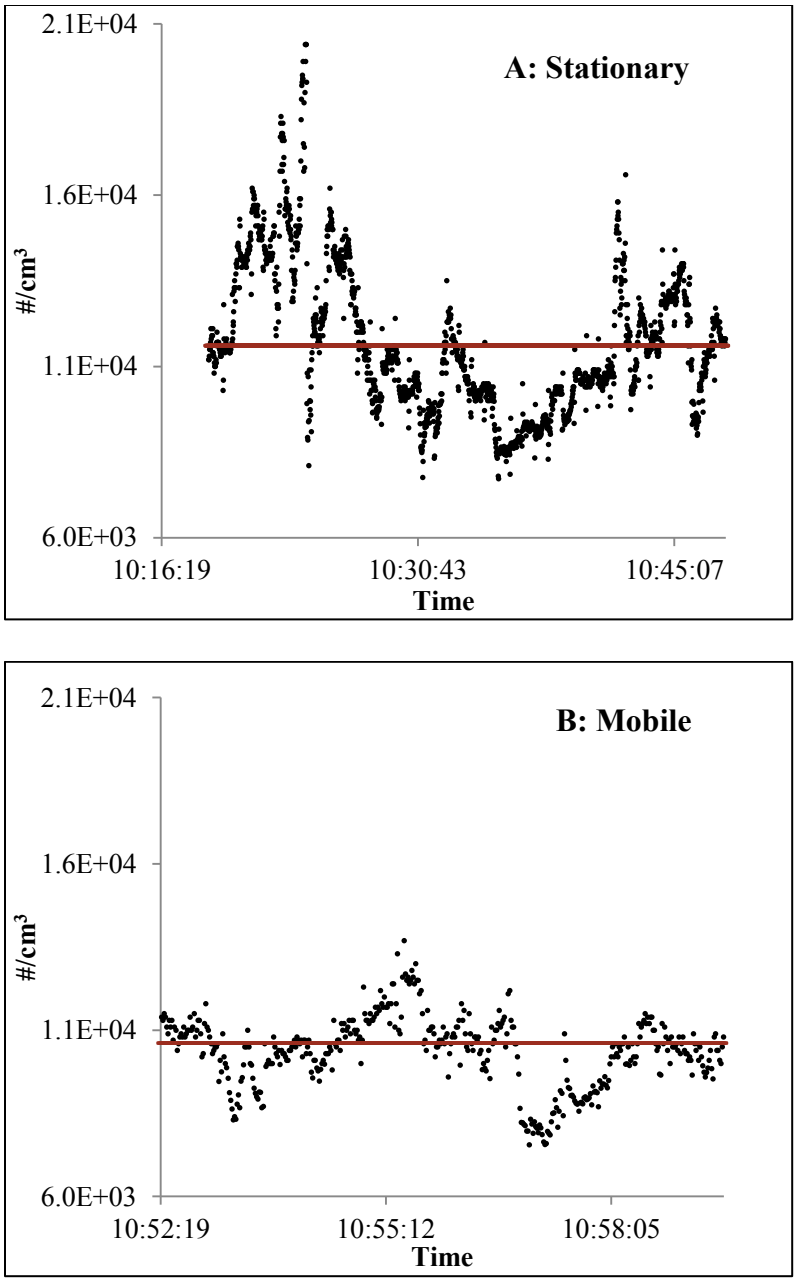

Figure 3.6 Performance of the mobile CPC unit in a stationary and mobile position. Top panel (A) show the concentration time series during stationary condition and bottom panel (B) shows the concentration time series during mobile condition.

3.4.4 Field trial using mobile CPC

Trial runs using mobile CPC system were conducted in Iowa City to test the applicability of the system. **Figure 3.7** depicts an example of one of the trial run conducted in Iowa City on Sept. 14th 2012 which included many areas near the downtown

areas of the university and I-80 freeway. Google Earth was used to generate a useful background for the plot. In the figure colored circular dots indicate the total particle concentration in various streets across Iowa City. Each dot in the figure represents a 1 s average of particle concentration data. The data logger also stores speed and altitude, along with GPS coordinates. This could help relate the relation between vehicle speed and particle concentration.

The spatial visualization of particle concentrations, such as **Figure 3.7**, provides detailed information on how particle concentrations vary between different roads. Based on a repeated trials conducted in Iowa City using the mobile CPC, a major road networks are characterized, as shown in **Figure 3.8**. Mean concentration of particle show comparable concentration range in repeated trials indicating similar sources and atmospheric conditions. Elevated concentrations at South Riverside may indicate larger traffic volume. The sampling on 18th November 2012 was close to evening rush hours and could be related to slowing in the speed. Field trial on the 11th November 2012 sampling was performed during mid-day with strong winds, comparatively warmer.

Spatial visualization also help shows how bends in roads and traffic lights affect UFP concentrations, which may help in developing new methods for estimating exposures. A simple illustration of the role of bend and de-acceleration is shown in **Figure 3.9.** As an illustration point S1 and S2 are highlighted in the figure to show the effect of bend on particle concentration.

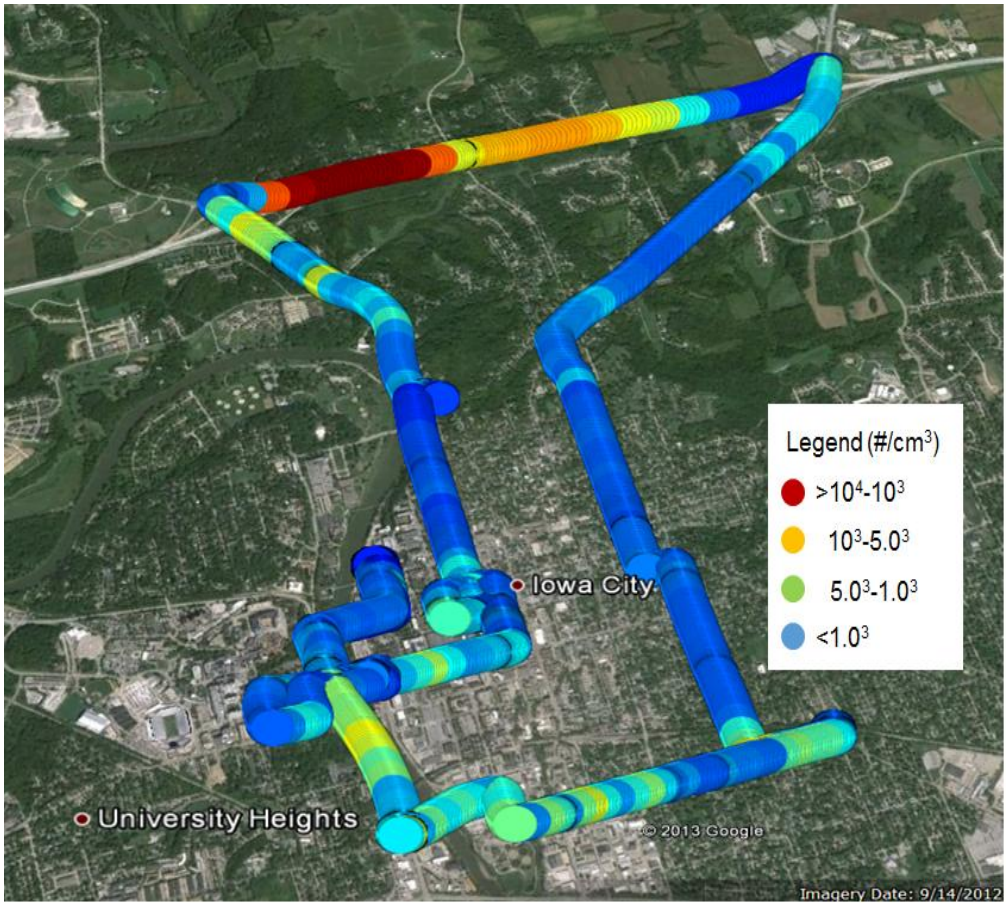

Figure 3.7 A trial mobile sampling conducted with the newly built mobile CPC in various road networks (inner city, free-way, residential and commercial areas) in Iowa City on September 12 2012. Each circle indicates 1 s data collected for 1.2 hr during the trial.

3.4.5 Potential limitation of the mobile CPC

The mobile CPC system was designed primarily to measure total particle concentrations in the UFP range and aimed for a short duration of sampling in the order of 1-2 h. The system can be easily modified to run for longer durations by adding larger battery cell in the system.

This system is limited to measuring total particle concentrations, and does not provide size distribution information which can be crucial in identifying possible sources. Mobile CPC monitoring such as the one developed in this thesis can be further improved

by integrating with systems such as Arduino[30] which provides a miniature version of a traditional microcontroller, easily programmable and can be connected to the recently developed low cost digital and analog sensors.

These low cost sensors can allow the measurement of local meteorological parameters such as temperature, RH, pressure, as well as miniature GPS module and electrochemical gas sensors for NO_x, CO, O_3 and VOCs (Mead et al., 2013). Additionally, possible integration of a mobile unit with a Quadcopter is another exciting novelty, which has the potential to collect spatial vertical profiles of many pollutants.

The data retrieval and graphical interface used in the current mobile CPC can be made more efficient by automatizing the data retrieval, processing, and visualization step. Replacing the GPS module with a *Wifi-GPS shield* will enable the capability to collect and transmit the data into a server while sampling. This can also be useful when working with more than one mobile unit. Actively processing the data while sampling are also useful to find any likely errors with the device, identify any bug in the mobile system and also to view the data real time.

Overall the mobile unit needs further integration of other available low cost sensors to make the current system effective in determining not only concentration, but possibly identify sources, and hotspot in an area. The system can also be made more portable by using new CPC which are much smaller than the one currently used. Lastly, the mobile system needs improvements in the data retrieval, processing and transfer to better suit the mobile sensor as a real time system.

[30] Hagler, G.S., Solomon, P.A., Hunt, S.W., 2014. Real-Time Air Monitoring.

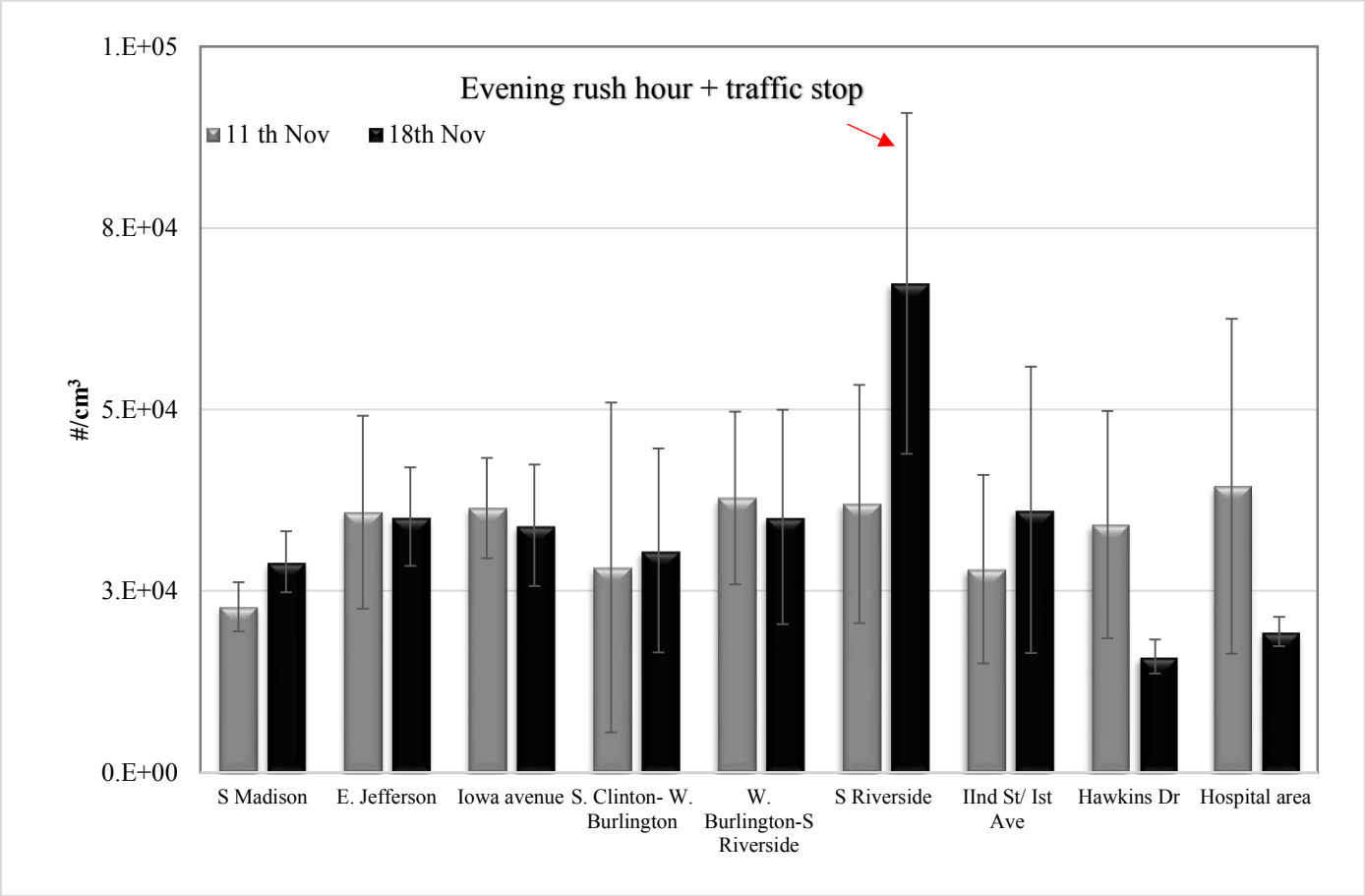

Figure 3.8 Average total particle concentrations at different road networks in Iowa City generated using field trials of the mobile CPC on two different days. Distinct variance in the #/cm^3 especially at the intersection and rush hour period (18th November) are typically associated with higher concentration than day time (11th November)

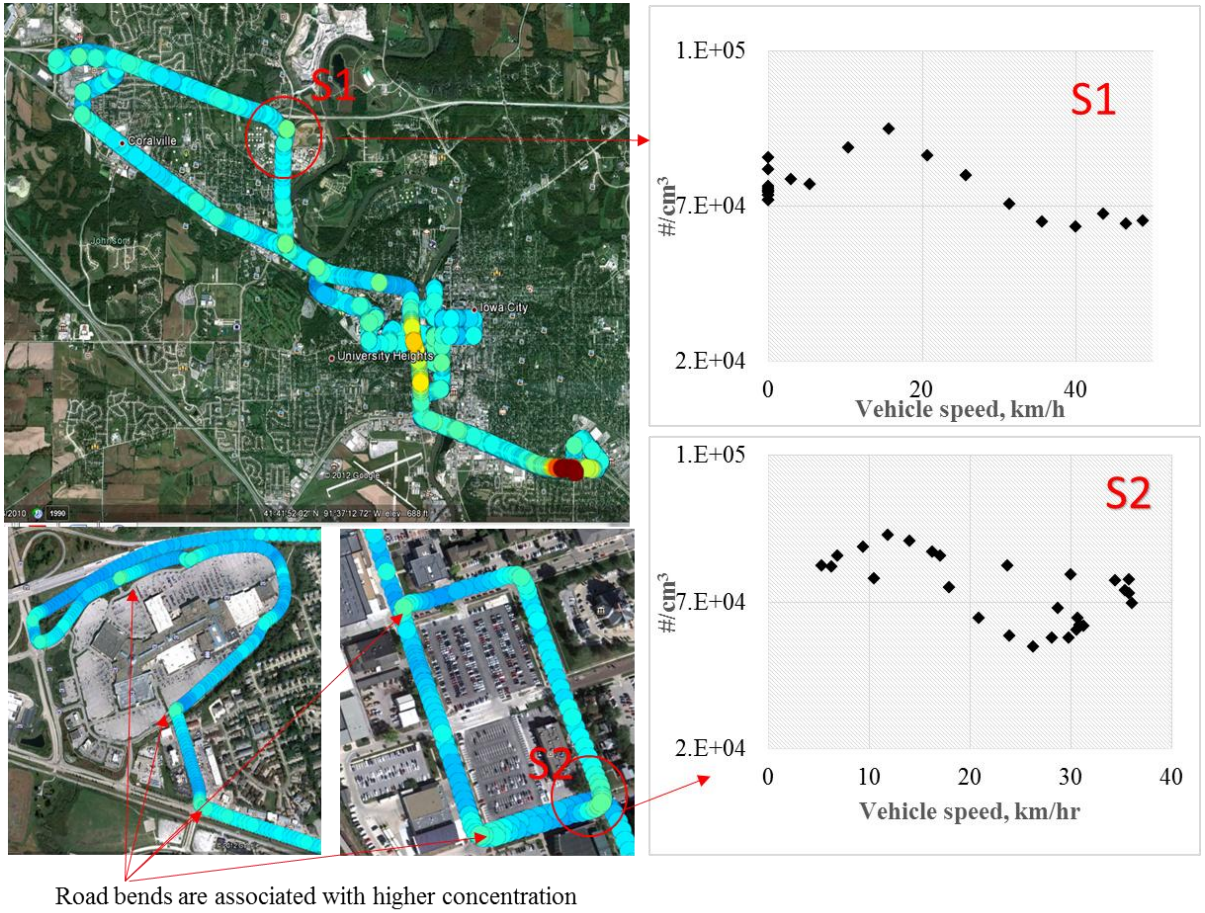

Figure 3.9 A trial sampling conducted with the Mobile CPC in various road networks in Iowa City and Coralville area. Right panels indicate changes in particle concentration with vehicular speed at sampling point S1 (top) and S2 (bottom)

3.5 Conclusion and future direction

Mobile measurements provide accurate concentration of air pollutants across space and time. Stationary monitoring may have limited spatial representation to provide accurate concentration values, especially particle number concentration which may vary significantly from source.

A mobile CPC was built to generate spatial map of total particle concentration encompassing the UFP size range. This design is equipped to provide high-frequency, continuous, on-road synchronous measurements of particle number and carbon dioxide (CO_2). The mobile platform is integrated with an independent electric power system, a central controller and robust data acquisition, and GPS system. These capabilities make the system suitable for remote deployment, capable of ground and aerial measurement and offers flexibility to integrate other analog and digital sensors. For data visualization, Matlab-Google Earth tool kit was used.

In the context of providing complete information about particle source, diurnal variation and trace gas measurement, the next phase of the mobile particle counter should be multiplatform, and utilize recent technological developments in low cost sensors. The newly developed low cost electrochemical gas sensors such as NO_x, CO, O_3, SO_2, and VOCs as well as portable meteorology sensors, provide a wonderful opportunity in this direction. The choice of these sensors will be dependent on the research objectives however integrating all these sensors in a microprocessor such as Arduino will not only be economic, but provides a lot of flexibility in the adding more functionality in the mobile device. One such functionality is the automatic data retrieval while sampling, transferring into a web server and data processing algorithm for continually reading and

plotting the data for real time application. This could be achieved by a *Wifi-GPS shield* which will enable the capability to collect and transmit the data into a server while sampling. The next generation of mobile unit should also need to explore the application of quadcopters and building an integrated system that involves these drone based application with the air quality sensors. The vertical resolution of many air pollutants including particle number are still estimated indirectly via satellite retrieval techniques. The uncertainty in satellite based retrieval can also be improved in the presence of accurate measurement of vertical profile.

3.6 Acknowledgements

The author would like to acknowledge the support of the undergraduates (Allaa Hassanein and Andrew Hesselink) at the Stanier research laboratory for aiding the mobile testing. I would also like to thank Bridget Hall, data logger engineer at the Campbell Scientific, for guiding me through the finicky nature of date logger program and its operation in the beginning.

Funding was provided by the National Science Foundation under Grant No. ATM-0748602.

3.7 References

Adams, M.D., DeLuca, P.F., Corr, D., Kanaroglou, P.S., 2012. Mobile air monitoring: Measuring change in air quality in the city of Hamilton, 2005–2010. Social indicators research 108, 351-364.

Akagi, S.K., Yokelson, R.J., Wiedinmyer, C., Alvarado, M.J., Reid, J.S., Karl, T., Crounse, J.D., Wennberg, P.O., 2011. Emission factors for open and domestic biomass burning for use in atmospheric models. Atmospheric Chemistry and Physics 11, 4039-4072.

Andrews, A., Kofler, J., Trudeau, M., Williams, J., Neff, D., Masarie, K., Chao, D., Kitzis, D., Novelli, P., Zhao, C., 2014. CO 2, CO, and CH 4 measurements from tall towers in the NOAA Earth System Research Laboratory's Global Greenhouse Gas Reference Network: Instrumentation, uncertainty analysis, and recommendations for future high-accuracy greenhouse gas monitoring efforts. Atmospheric Measurement Techniques 7, 647-687.

Bullard, R.L., Stanier, C.O., Ogren, J.A., Sheridan, P.J., 2013. Determination of Seasonal, Diurnal, and Height Resolved Average Number Concentration in a Pollution Impacted Rural Continental Location, 19th International Conference on Nucleation and Atmospheric Aerosols (ICNAA), Colorado State Univ, Ctr Arts, Fort Collins, CO, pp. 583-586.

Chan, C.K., Yao, X., 2008. Air pollution in mega cities in China. Atmospheric environment 42, 1-42.

Dietz, M.E., Abraham, J., 2012. Stormwater monitoring and resident behavior in a semi-arid region. J. Ext 49, 3.

Downard, J., Singh, A., Bullard, R., Jayarathne, T., Rathnayake, C.M., Simmons, D.L., Wels, B.R., Spak, S.N., Peters, T., Beardsley, D., Stanier, C.O., Stone, E.A., 2015. Uncontrolled combustion of shredded tires in a landfill - Part 1: Characterization of gaseous and particulate emissions. Atmospheric Environment 104, 195-204.

Hagler, G.S., Solomon, P.A., Hunt, S.W., 2014. Real-Time Air Monitoring.
Hudda, N., Gould, T., Hartin, K., Larson, T.V., Fruin, S.A., 2014. Emissions from an international airport increase particle number concentrations 4-fold at 10 km downwind. Environmental science & technology 48, 6628-6635.

Kumar, P., Ketzel, M., Vardoulakis, S., Pirjola, L., Britter, R., 2011. Dynamics and dispersion modelling of nanoparticles from road traffic in the urban atmospheric environment—a review. Journal of Aerosol Science 42, 580-603.

Ma, N., Birmili, W., 2015. Estimating the contribution of photochemical particle formation to ultrafine particle number averages in an urban atmosphere. Science of The Total Environment 512, 154-166.

Mead, M., Popoola, O., Stewart, G., Landshoff, P., Calleja, M., Hayes, M., Baldovi, J., McLeod, M., Hodgson, T., Dicks, J., 2013. The use of electrochemical sensors for monitoring urban air quality in low-cost, high-density networks. Atmospheric Environment 70, 186-203.

Mueller, N.C., Nowack, B., 2008. Exposure modeling of engineered nanoparticles in the environment. Environmental Science & Technology 42, 4447-4453.

Nickel, C., Kaminski, H., Hellack, B., Quass, U., John, A., Klemm, O., Kuhlbusch, T.A., 2013. Size resolved particle number emission factors of motorway traffic differentiated between heavy and light duty vehicles. Aerosol and Air Quality Research 13, 450-461.

Panko, J.M., Chu, J., Kreider, M.L., Unice, K.M., 2013. Measurement of airborne concentrations of tire and road wear particles in urban and rural areas of France, Japan, and the United States. Atmospheric Environment 72, 192-199.

Peters, J., Theunis, J., Van Poppel, M., Berghmans, P., 2013. Monitoring PM10 and ultrafine particles in urban environments using mobile measurements. Aerosol and Air Quality Research 13, 509-522.

Peters, T.M., Heitbrink, W.A., Evans, D.E., Slavin, T.J., Maynard, A.D., 2006. The mapping of fine and ultrafine particle concentrations in an engine machining and assembly facility. Annals of Occupational Hygiene 50, 249-257.

Pirjola, L., Paasonen, P., Pfeiffer, D., Hussein, T., Hameri, K., Koskentalo, T., Virtanen, a., Ronkko, T., Keskinen, J., Pakkanen, T., 2006. Dispersion of particles and trace gases nearby a city highway: Mobile laboratory measurements in Finland. Atmospheric Environment 40, 867-879.

Poppa, F., Zimmer, U., Feitz, A., Berko, H., 2013. Development of a carbon dioxide monitoring rotorcraft unmanned aerial vehicle, Robotics: Science and Systems (RSS) Workshop on Robotics for Environmental Monitoring (WREM), pp. 24-28.

Saarnio, K., Frey, A., Niemi, J.V., Timonen, H., Rönkkö, T., Karjalainen, P., Vestenius, M., Teinilä, K., Pirjola, L., Niemelä, V., 2014. Chemical composition and size of particles in emissions of a coal-fired power plant with flue gas desulfurization. Journal of Aerosol Science 73, 14-26.

Sheridan, P., Andrews, E., Ogren, J.A., Tackett, J., Winker, D., 2012. Vertical profiles of aerosol optical properties over central Illinois and comparison with surface and satellite measurements.

Singh, A., Spak, S.N., Stone, E.A., Downard, J., Bullard, R.L., Pooley, M., Kostle, P.A., Mainprize, M.W., Wichman, M.D., Peters, T.M., Beardsley, D., Stanier, C.O., 2015. Uncontrolled combustion of shredded tires in a landfill - Part 2: Population exposure, public health response, and an air quality index for urban fires. Atmospheric Environment 104, 273-283.

Sioutas, C., Delfino, R.J., Singh, M., 2005. Exposure Assessment for Atmospheric Ultrafine Particles (UFPs) and Implications in Epidemiologic Research. Environmental Health Perspectives 113, 947-955.

Stanier, C.O., Lee, S.-R., 2014. Development and application of an aerosol screening model for size-resolved urban aerosols. Research report (Health Effects Institute), 3-79.

Weiden, S.-L., Drewnick, F., Borrmann, S., 2009. Particle Loss Calculator–a new software tool for the assessment of the performance of aerosol inlet systems. Atmospheric Measurement Techniques 2, 479-494.

Weijers, E., Khlystov, A., Kos, G., Erisman, J., 2004. Variability of particulate matter concentrations along roads and motorways determined by a moving measurement unit. Atmospheric Environment 38, 2993-3002.

Yu, Q., Li, T., Wu, M., Chen, Q., 2014. Influence of Operating Characteristics of On-Road Gasoline Passenger Car on Emissions in Nanjing, China. Bridges 10, 9780784412442.9780784412285.

Zwack, L.M., Hanna, S.R., Spengler, J.D., Levy, J.I., 2011. Using advanced dispersion models and mobile monitoring to characterize spatial patterns of ultrafine particles in an urban area. Atmospheric Environment 45, 4822-4829.

CHAPTER 4: DESIGN, CONSTRUCTION, AND TESTING OF A V-TDMA

4.1 Abstract

Volatility characterization provides information related to the thermodynamics, kinetics and composition of atmospheric particles. Often particle volatility is analyzed using thermal treatment in a TDMA system. In this work, the development, fabrication and characterization of a Volatility Tandem Differential Mobility Analyzer (V-TDMA) is described. The design of the V-TDMA mainly focused on the design of thermodenuder (TD) for the study of UFP volatilities. The TD in the current V-TDMA system consists of a heated tube (0.305 inch~0.75 mm ID, 1 m length) and wrapped by a pair of rope heaters and temperature controllers. The centerline residence time in the TD for a flow rate of 1 lpm is 2 s and aerosol flow is laminar. Estimated penetration efficiency is close to 85% for 10 nm and a uniform temperature profile is maintained across the length of the TD. Laboratory tests showed that for UFP particle and their atmospheric concentration, the presence of denuder does not change the volatility profile. Comparison of volatility profile of pure ammonium sulfate at various across different TD designs indicated that the volatilization temperature[31], observed in the current design, is similar to TD designs with residence time below 10 s.

Operationally the overall V-TDMA system can be programmable with respect to temperature, diameter of interest and sampling frequency. This was achieved by a LabVIEW program built for V-TDMA operation.

[31] Temperature at which AS completely volatilizes or vaporizes

4.2 Introduction

A comprehensive understanding of the life cycle of UFP is crucial to estimate its direct and indirect climate and health impact. Direct measurement of chemical and physical properties of UFP is limited to few recent inventions such as the Thermal Desorption Chemical Ionization Mass Spectrometry (TD-CIMS)[32], High-resolution chemical ionization mass spectrometry (ToF-CIMS)[33] and Nano Aerosol Mass Spectrometer (NAMS)[34]. Indirect measurements techniques for UFP studies have been a useful method to extract various physical and chemical properties of UFP which could be associated with the chemistry of the particles. Indirect techniques are used to estimate the properties of particles in the nuclei mode size range or larger. These techniques include physicochemical techniques using different CPC (Kulmala et al., 2007), TD-CIMS, range 5–20 nm (Smith et al., 2004; Smith et al., 2005); Aerosol Mass Spectrometry (AMS), >20 nm (Allan et al., 2006; Zhang et al., 2004) and TDMA technique to measure volatility and hygroscopicity (Huffman et al., 2008; Johnson et al., 2004a; Sakurai et al., 2005).

Measurement of aerosol volatility by thermal treatment in a TDMA also referred as "V-TDMA" has been employed to infer various physical and chemical properties of the particles. The heat treatment system coupled with TDMA is referred as a "thermodenuder (TD)". A V-TDMA measures the change in particle size and number concentration before and after heating at a certain temperature. This information is used to estimate volatile, semi-volatile and low volatile volume fraction (An et al., 2007;

[32] Smith, J., Moore, K., McMurry, P., Eisele, F., 2004. Atmospheric measurements of sub-20 nm diameter particle chemical composition by thermal desorption chemical ionization mass spectrometry. Aerosol Science and Technology 38, 100-110.
[33] Zhao, J., F. L. Eisele, M. Titcombe, C. Kuang, and P. H. McMurry, 2010), Chemical ionization mass spectrometric measurements of atmospheric neutral clusters using the cluster-CIMS, J. Geophys. Res., 115, D08205, doi:10.1029/2009JD012606.
[34] Zordan, C.A., Pennington, M.R., Johnston, M.V., 2010. Elemental composition of nanoparticles with the nano aerosol mass spectrometer†. Analytical chemistry 82, 8034-8038.

Johnson et al., 2004a; Jonsson et al., 2007; Ristovski et al., 2010a; Tritscher et al., 2011). The change in size of aerosol can be measured using condensation particle counters (CPC)[35] and scanning mobility particle counters (SMPS)[36].

The Tandem Differential Mobility Analyzer (TDMA) is often used to provide insight into the particle composition by adding a conditioning system such as heating[37] (An et al., 2007; Frey et al., 2008a; Huffman et al., 2008; Lee et al., 2010; Orsini et al., 1999; Villani et al., 2007b; Wehner et al., 2002), and humidification[38] (Ehn et al., 2007a; Johnson et al., 2004d; Swietlicki et al., 2008) and organic vapor[39] (Joutsensaari et al., 2001). Advanced instrumentations such as TD-CIMS and NAMS offer direct measurements of functional group and elemental information about particle composition. But their limited availability and working particle size range, TDMA technique is often a preferred method especially for small mass (<1 $\mu g/m^3$) associated with nuclei mode particle *(*<30 nm). TDMA are fast responding and can analyze multiple particle size within few minutes. In addition, TDMAs provide information about the compositional homogeneity or heterogeneity of particles by studying their mixing state[40] at >200 ^oC or higher (Frey et al., 2008b; Wehner et al., 2009; Wehner et al., 2005). Likewise, TDMA is often used to estimate low volatile compounds[41] in the particles and thus trace possible particle source, condensing gases and meteorology (Ehn et al., 2007c; Häkkinen et al., 2012).

---

[35] Condensation particle counters, TSI Inc.
[36] Scanning mobility particle spectrometer, TSI Inc.
[37] TDMA with heating system are generally abbreviated as V-TDMA and will be used for the rest of the thesis
[38] TDMA with humidification system are generally abbreviated as RH or H-TDMA.
[39] Organic TDMA is abbreviated as O-TDMA
[40] Mixing state is a measure of distribution of chemical in the aerosol population. Mixing state is also referred to the distribution of chemical compounds within a particle. In this study the mixing state refers distribution of chemical in the aerosol population.
[41] These are physically defined as the un-evaporated volume at 200 or higher temperature.

Different volatile fraction could be binned into volatility basis [42]set for empirically solving the mass transfer during evaporation (Cappa, 2010; Riipinen et al., 2010). Volatility basis set classify or lumps compounds together based on the similarity of their vapor pressure or saturation concentration, so that numerous species in a particle could be classified in a small number of class. On their own, measurements of particle volatility can be a relatively weak constraint on the actual composition of UFPs because different chemical species can display similar volatile profiles within a TDMA system (Karnezi et al., 2014). V-TDMA systems are complemented by a Hygroscopicity-TDMA ("RH-TDMA") or Organic-TDMA (O-TDMA) system which measures the tendency of particles to grow in the saturated water and organics vapor (Joutsensaari et al., 2001; Ristovski et al., 2006; Tiitta et al., 2010).

In this thesis, a V-TDMA system was designed and constructed. The goal of this design is to characterize atmospheric UFPs in the Midwest. Particle formation is a major source of UFP in the Midwest (Bullard et al., 2013; Pryor et al., 2010). Size resolved measurement of particle volatility are useful to characterize particle growth and formation mechanisms (Meyer and Ristovski, 2007; Ristovski et al., 2010b; Sakurai et al., 2005). Chemical and physical characterization of particle from the Midwest is still scarce (Pryor et al., 2010). The built V-TDMA will be a useful tool for Stanier research group to measure particle volatility, and estimate other important properties such as evaporation resistant residue, and mixing state.

Several V-TDMA designs exist (An et al., 2007; Engler et al., 2007; Huffman et al., 2008; Park et al., 2008; Saleh et al., 2011) and are distinguished mainly by some key

[42] (Donahue, N.M., Robinson, A.L., Stanier, C.O., Pandis, S.N., 2006. Coupled partitioning, dilution, and chemical aging of semivolatile organics. Environmental Science & Technology 40, 2635-2643.

design features of the thermodenuder. The key differences in design include the heating method, residence time in the TD, and presence/absence of the absorbing system in the TD.

4.3 Methodology

4.3.1 Experimental design

4.3.1.1. Process flow of the V-TDMA

The schematic of the process flow in the current V-TDMA is shown in **Figure 4.1**. The V-TDMA consists of three main components (indicated by bold fonts, **Fig. 4.1**): particle size selection, particle heating treatment, and size measurement of exiting particles. The V-TDMA was designed to analyze particles in the UFP range. For this reason, tube lengths and bends were minimized to avoid particle loss. The aerosol line uses a tubing of ¼ inch internal diameter, shown in **Figure 4.1** by dark solid blue lines.

For the laboratory operation of the V-TDMA, the particles are either generated using an Atomizer (TSI 3076) or drawn from ambient air during field deployments (as shown by bold fonts). Either of the particle source will be poly-disperse in their size distribution. This stream of poly-disperse particles are dried to RH<20% using a diffusion dryer (TSI 3062) and then charged using a radioactive neutralizer (TSI 3077). The particles are then size filtered using an N-DMA (TSI 3085) one controlled by Classifier one. The particle stream is then either sent through the heated or bypass (non-heated) tubes using an automated three-way solenoid valve (see valve one in **Fig. 4.1**). The switching of the solenoid valve is synchronized with the sample routine of SMPS (N-DMA two and CPC 3785 in **Fig. 4.1**). The heated line or TD has two additional solenoid valves (valve two and three) which allow the use of a purge clean air stream to cool the

line in between runs. At the end of each temperature cycle[43] while the bypass is being sampled by the SMPS, the dry air runs through the heated line to cool it down to the initial set temperature. The initiation and operation of cooling system is tied to the set point temperature of the heated tube and is also synchronized with the SMPS sampling time. The third section of the V-TDMA consists of a SMPS system which will measure the size and number concentration of particles from either heated or bypass line.

The aerosol flow in the V-TDMA is maintained by the CPC sample flow rate of 1 lpm. The flow regime in the V-TDMA is laminar for two types of sampling lines in the V-TDMA (heated/bypass tube with 0.75 mm and non-conducting tubes with 6.5 mm ID). The Reynolds number for these two configurations is in the range of 150-200, which indicate laminar flow in the V-TDMA system.

4.3.1.2. Design of thermodenuder in V-TDMA

A standard TD consists of a heating section, where particles are heated to defined temperature and an adsorbing section[44] where the vapor evaporated during the heating section is adsorbed (see **Appendix** Section 9.2. Typical design of a thermodenuder). Normally adsorbing section uses granular activated charcoal as an adsorbing material. Controlled heating is performed using a combination of commercial temperature controllers and rope/tape heaters. The heating section is covered with glass wool insulation to prevent heat loss and help maintain a uniform temperature. Either fan or water cooling system is also added in the heating section to either prevent overheating during the operation (An et al., 2007; Huffman et al., 2008; Villani et al., 2007). The

[43] The temperature cycle starts at 80 or 100 and goes to 200 or 250. After capturing the heated sample the highest temperature, the sampling switches to bypass at the lowest temperature. During that period the cooling system is trigged on and while the system samples via bypass, the heating tube is getting cooled to the starting temperature.

[44] The adsorbing section works as the denuder to remove all the gases

adsorbing section, however, is perforated to provide contact with the activated charcoal. The gap between metal case and wall of perforated tube is filled with granular activated charcoal.

Important design parameters of a TD include residence time of aerosol in the heating section; influence of adsorbing section; minimization of loss; data treatment via equilibrium or kinetic model; effect of heating on the particles.

Residence time

A wide range of residence time of particle exists in the published TD designs. The residence time ranges from < 1 to 20 s (An et al., 2007; Frey et al., 2008; Huffman et al., 2008; Tritscher et al., 2011). The relation between residence time and particle evaporation is complicated, as the actual equilibrium time for aerosol is difficult to ascertain. Equilibration time scales could be influenced by particle phase, bulk-core chemical composition, volatilities of condensed materials, particle size, and concentration, among other variables (Riipinen et al., 2010; Shiraiwa and Seinfeld, 2012). Equilibration time scales thus vary from a few seconds (for e.g. highly volatile organics with large mass loading~ >> 10 $\mu g/m^3$) to a few hours (for e.g. low volatile organics, low mass loading). Differences in residence times between TD's complicate comparisons between different volatility studies. In addition, many TD designs may be operating in the non-equilibrium condition which may results in underestimation of the aerosol volatility.

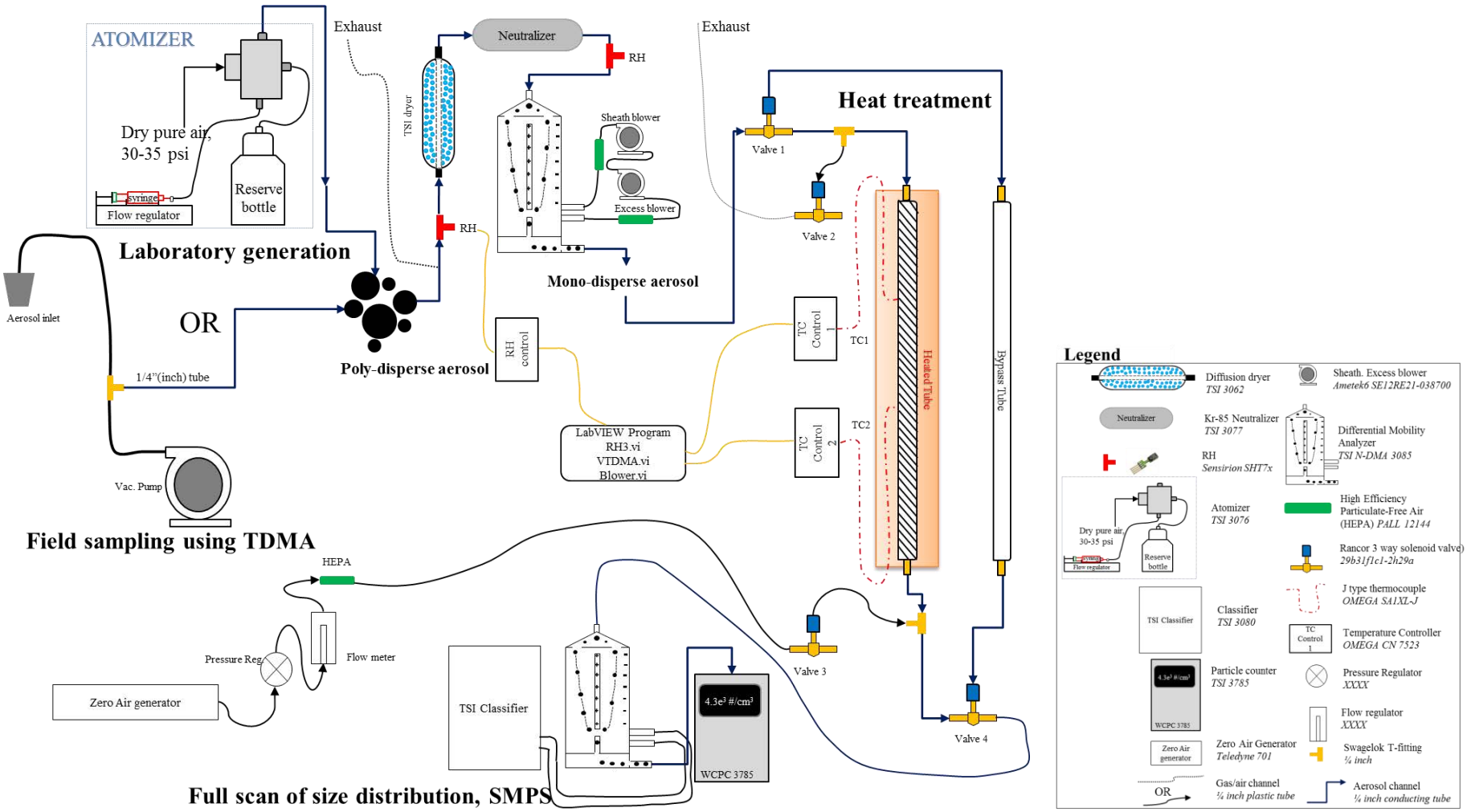

Figure 4.1 A detail of the current volatility-tandem differential mobility analyzer (V-TDMA) design used for laboratory and field deployment in the Stanier Research Group.

The empirical equilibration equation provided by Saleh et al. (2011) was used to characterize the relationship between the size, concentration and residence time. However this equation has limited application since factors such as particle phase, and inhomogeneity of mixing are not considered (Shiraiwa and Seinfeld, 2012; Vaden et al., 2010).

The empirical equation by Saleh et al. (2011) for the TD design is,

$$\frac{Tr}{\tau} = 2\pi^2 D \times N_{tot} \times dp_i \times F \times L \times \frac{{d_t}^2}{Q} \qquad (4.1)$$

where, Tr is the residence time, τ is time constant, D is particle diffusivity, N_{tot} is total particle concentration, F is the fuch correction[45], L is length of the tube, d_t is the tube internal diameter, and Q is volumetric flow in the tube.

Adsorbing system

The adsorbing system in a TD is used to remove evaporated gas phase species to minimize re-condensation onto particles. Many previous TD designs (An et al., 2007; Faulhaber et al., 2009; Fierz et al., 2007; Huffman et al., 2008; Madl et al., 2003; Wehner et al., 2002b) have employed an activated charcoal denuder as an adsorbing system. Condensation of evaporated vapor on the aerosol particle surface is likely when evaporated vapor cools below the heated temperature. Evaporation at different particle loading using adsorbing system indicate that unless high aerosol loading (>100 μg/m^3) is used, low aerosol loading (<10 μg/m^3) do not show any significant difference in evaporation (Cappa, 2010; Saleh et al., 2011).

[45] Fuch correction is calculated from equation 12.34 in Seinfeld and Pandis, (2012). This is a simply a correction factor used to adjust for the diffusion of gas molecules into particles when the particle size equals the mean free path of the gas molecule.

The role of adsorbing system is also experimentally tested. In order to show this experimentally an aerosol mixture (inorganic/organic) was examined using the TD with (AC) and without (NAC) the activated charcoal denuder. The design for the activated charcoal denuder was based on the simple 1 D radial diffusivity shown by Fierz et al. (2007). Diffusion coefficient of adipic acid of 0.2 cm^2/s was used during the calculation. A minimum length of denuder is ~ 40 cm at a flow rate of 1 lpm was estimated. In order to improve absorption, Activated Carbon Cloth (ACC)[46] was used as a denuder material, which has larger surface area (1000-2000 m^2/g) than granular activated charcoal. The constructed adsorber section is shown in **Figure 4.2**.

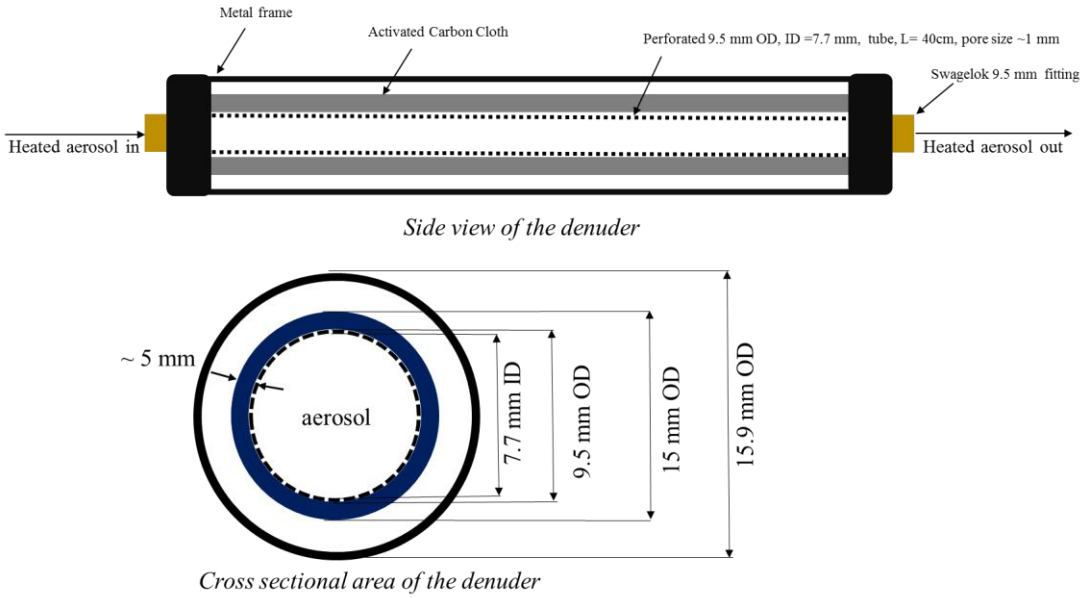

Figure 4.2 Schematics of the constructed denuder system for the experiment; The top section shows the side view of the denuder and bottom section of the figure shows the cross section of the denuder.

[46] http://www.buyactivatedcharcoal.com/activated_carbon_fiber_cloth

Calibration of TD with ammonium sulfate

The performance of the completed TD was tested using pure ammonium sulfate (AS) particles. AS particles have been used for calibrating many TD designs (An et al., 2007; Frey et al., 2008). AS particles are easy to produce consistently in different laboratories and thus provide an easy means to compare different TD systems.

Mono-disperse AS particles at different sizes between 15 to 80 nm were sampled using the TD. The heating tube temperatures used in these tests were at 100, 130 150 and 200 $^{\circ}$C. Thermograph was generated from the results and compared with the published thermographs of AS produced by other TD's.

Calculation of residence time in the TD

The residence time reported for the current TD is a centerline residence time. The inclusion of a radial velocity profile in an evaporation model by Cappa et al. (2010) showed no difference in the volatility response of a test aerosol compared to the center line velocity profile case. Therefore using a centerline residence time to characterize the TD is acceptable. This is also supported by the fact that maximum particle concentration in the TD is likely to be at the center (Orsini et al., 1999; Fuentes and McFiggans et al., 2012).

The centerline residence time is calculated from the mean residence time which is the ratio of volume of the TD to flow rate. For the parabolic flow profile in the TD, the centerline velocity is double the mean velocity, and the centerline residence time is approximately half of the mean residence time. A center line residence time is therefore reported in this thesis hereafter.

Particle loss in the TD

For the UFP size range, many factors can cause particle loss in the TD. Maintaining laminar flow within the TD helps avoid turbulence related losses. Other important loss mechanism include diffusional, thermophoretic and inertial losses (Seinfeld and Pandis, 2012). Two types of loss calculations were examined for the TD which include transmission (at ambient condition) and relative transmission of particles between the heated and bypass tube.

Transmission loss were performed a particle loss calculators (Weiden et al., 2009) and the relative transmission was experimentally verified. For experimental verification, pure ammonium sulfate particles from 10 to 80 nm were sampled alternating between the heated and bypass tubes. The end of each tube is connected to CPC for the measurement of particle concentration. The temperature of the heated tube was maintained at 25 ^{o}C and rapid switching between the heated and bypass tube was performed.

The number concentration ratio between the heated and bypass tube is the relative transmission ratio. The uncertainty in the relative transmission ratio was calculated using the following equation,

$$E_{dpi} = \frac{1}{\sqrt{(n-1)}}\left(\frac{{\alpha_h}^2}{N_b^2} + \frac{{\alpha_b}^2 N_h^2}{N_b^4}\right)^{0.5} \qquad (4.2)$$

where, n is number of sample in heated or bypass sample, α_h is std. deviation of avg. heated conc., α_b is standard deviation of avg. bypass concentration, N_h and N_b are average concentration in heated and bypass for particle size dp_i.

V-TDMA data analysis

The first step in V-TDMA data analysis involves the calculation of the volume fraction remaining (VFR) for a particle size at different temperature. The VFR calculated at different temperature is used to produce a VFR curve (as shown in **Fig. 4.4**).

The VFR curve shows how the particle volume evaporates when heated which is strongly related to the volatility of the particle. As shown in Equation 4.3 VFR is the ratio of the particle volume (V_{td}) heated to temperature > 25 ^{o}C (in the TD) to particle volume ($V_{25\ ^{o}C}$) in ambient or non-heated condition (see **Equation 4.3**).

In the current V-TDMA system, volume measurement in bypass tube (~25 ^{o}C) is also referred as the bypass volume. The conversion of number concentration and particle size, measured by SMPS in the V-TDMA, to volume assumes spherical particle.

$$VFR_{Ti}=\frac{V_{td}}{V_{25^{o}c}} \qquad (4.3)$$

4.4 Results

A threshold residence time at which particles can be expected to reach equilibrium at different particle concentrations was determined using **Equation 4.1**. This relationship between the residence time vs particle concentration is shown in **Figure 4.3** (panel (a) and (b) characterizes adipic acid (AA) and ambient organics (OA)).

Saleh et al. (2010) suggests that equilibrium is achieved in a TD when $Tr/\tau \geq 9$. The red band in the Figure 4.3 is the residence time in the current TD. **Equation 4.1** was solved for $Tr/\tau=9$ to calculate the equilibrium residence time (in s) for a wide range of particle concentration ($1x10^{3}$ -$1x10^{7}$ #/cm^{3}) and also for a range of particle sizes.

Ambient concentrations of UFPs are observed in the $1x10^{3}$ to $1x10^{4}$ #/cm^{3}, and at this concentration, the TD needs at least >100 s of residence times for attaining equilibrium (**Fig. 4.3,** log-log plot). Only concentration as high as $\geq 10^{6}$ #/cm^{3} are likely to achieve equilibrium residence time.

These concentrations are only feasible either in a laboratory conditions or near a particle sources such as engine exhaust and road-side measurement. UFP concentrations

in the atmosphere very rarely reach such high concentrations. Ambient organic aerosols require slightly longer equilibrium residence time because of its low evaporation coefficient of 0.1 compared to 0.5 used for adipic acid.

Longer residence times (>5 s) in TD are not feasible due to design and likelihood of loss, particularly for particle <100 nm. Diffusional losses restrict the use of longer residence time TDs. Longer TD tubes are also required, which can be challenging to manage in already elaborate V-TDMA set ups.

The effectiveness of activated charcoal as an adsorbing system in the TD is illustrated in **Figure 4.4**. The figure shows two VFR profiles of a laboratory generated aerosol mixture, one generated using denuder (blue diamond marker) and another without denuder (orange box marker).

The aerosol mixture contains ammonium sulfate, adipic acid and sodium chloride in 3:6:1 mass ratio. VFR profiles in both of these cases look similar at all temperatures, indicating that the use of a denuder does not affect the VFR profile.

Similar experimental conclusions were drawn from Saleh et al. (2010) and Tritscher et al. (2011). Experiments were run with 20 nm particle size and at $1x10^3$-1 $x10^4$ #/cm^3.

The comparative results indicate that the volatility profile is similar for with activated charcoal and without activated charcoal case. TD experiments by Saleh et al. (2011) and simulations by Rippinen et al. (2010), Fuentes and Mcfiggans (2012) and Faulhaber (2009) have also shown that adsorbing systems are typically not necessary and sometimes may induce further evaporation.

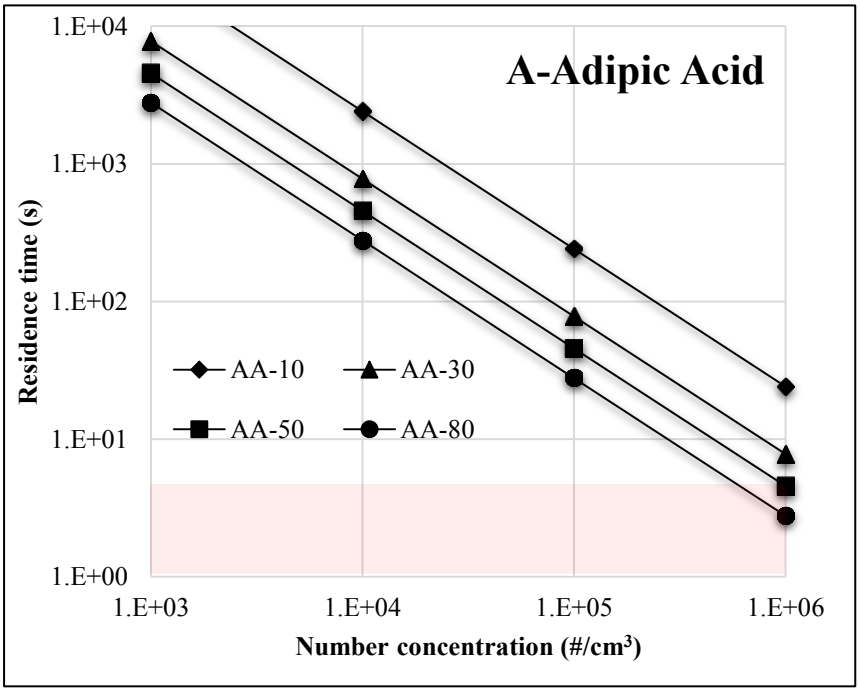

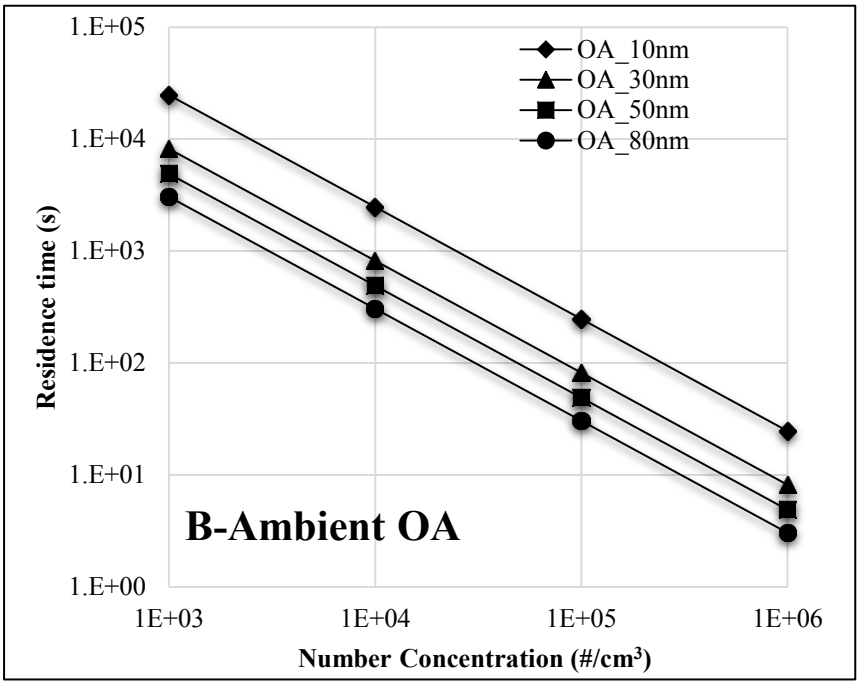

Figure 4.3 Time required for equilibrium in a V-TDMA according to the Equation 4.1. Equilibrium time (y-axis) is graphed vs. particle number concentration (x-axis) for a particle sizes from 10 to 80 nm. Adipic acid (panel A) equilibrates slightly faster than organic aerosol (panel B) due to higher evaporation coefficient. See text for assumptions on organic aerosol. (Both axes are in log scale).

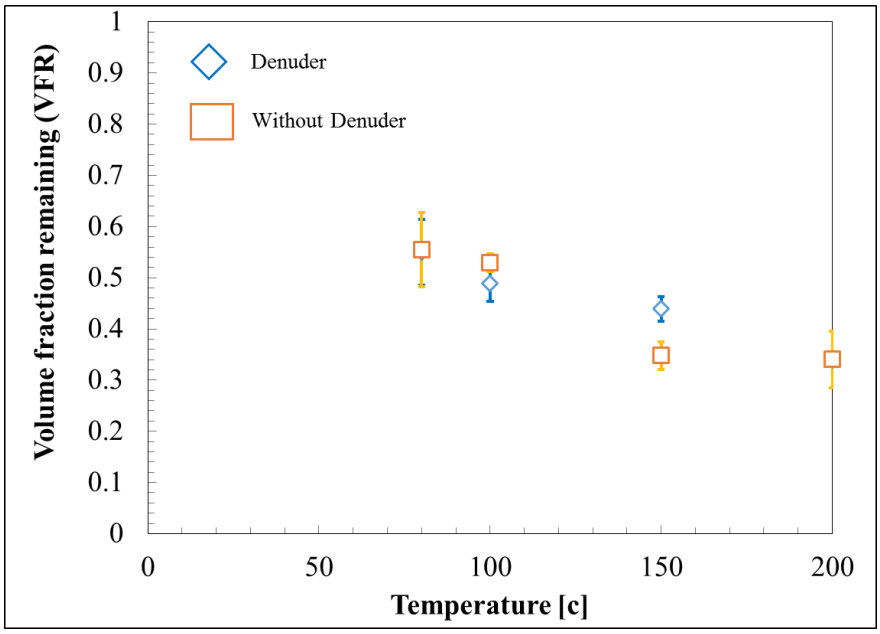

Figure 4.4 Characterization of volatility profile with activated carbon denuder (blue diamond) and without denuder (orange box) using an aerosol mixture of ammonium sulfate, adipic acid and sodium chloride (3:6:1 mass fraction).

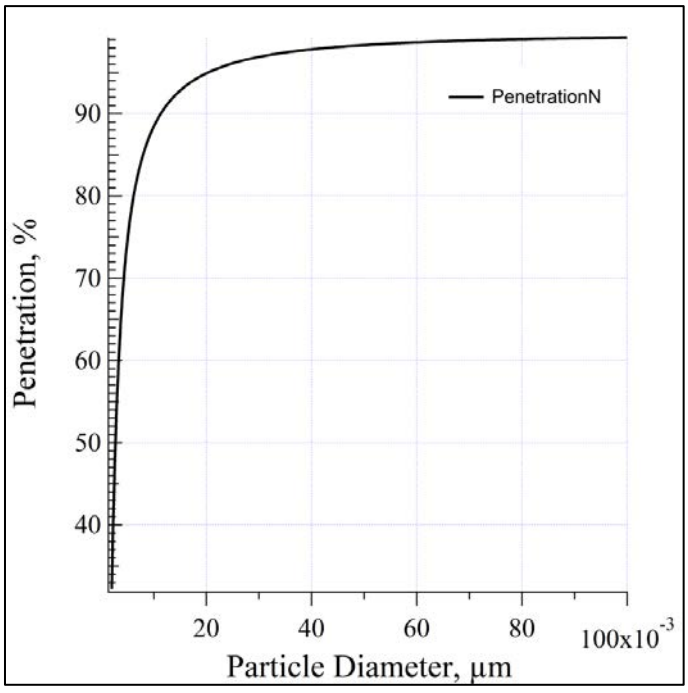

Figure 4.5 Estimation of transmission loss in the current TD for the center line residence time of 2 s at 25 ^{o}C using particle loss calculator (PCL) from Weiden et al. (2009).

Figure 4.5 shows the transmission efficiency of particles in the heated tube, which is the ratio of number concentrations at the entry and exit of the tube. More than 85% transmission efficiency is estimated for 10 nm particles for a residence time of 2 s (laminar flow condition with CPC flow rate of 1 lpm) in the heated tube. This is promising for the TD designed to study particles in the UFP size range.

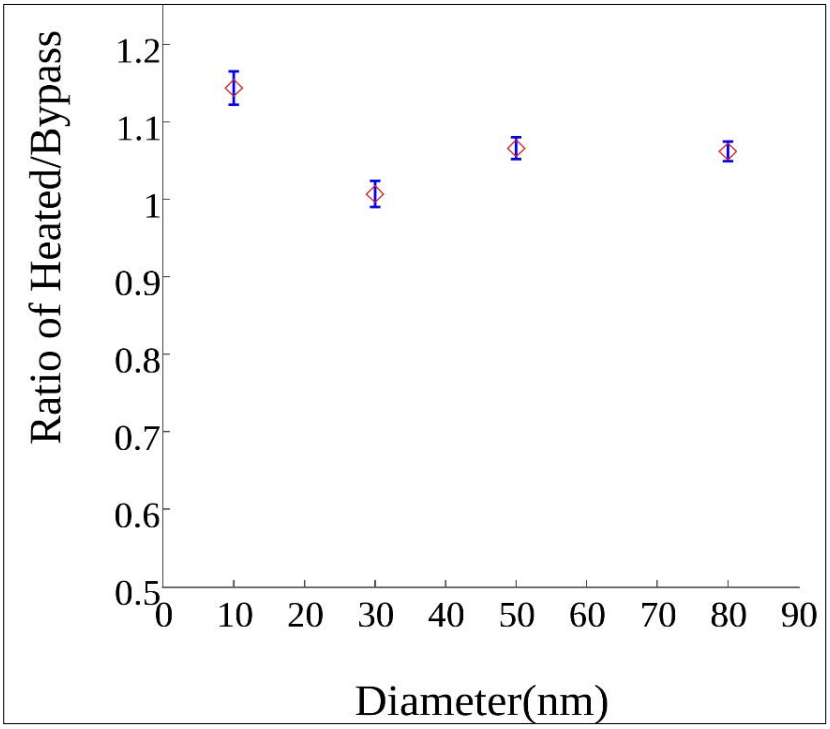

Figure 4.6 Transmission ratio between the heated and bypass tube of TD at an average residence time of 2 s and 25 ^{o}C using pure ammonium sulfate particles. The uncertainty in the ratio (y-axis) was calculated from Equation 4.2.

The other transport loss of interest to the TD design is the ratio between the particle concentrations exiting the heated tube and those exiting the bypass tube. Already described in the methods section, the objective of this ratio is to evaluate any particle concentration differences in these flow paths at 25 ^{o}C. Both heated and bypass tube have the same dimension, so ideally the ratio should be close to 1. Most uncertainty is

expected to be due to the bend encountered when passing through the solenoid valves, but this is expected to be small for particles in the UFP size range. **Figure 4.6** shows the experimentally calculated transmission ratio for four different sizes. The error bar is the uncertainty calculated using the **Equation 4.2**.

The transmission ratio indicates that the ratio is close to 1 for particles >10 nm, within 5% of each other. At 10 nm, the difference is close to 15% implying that the heated tube count is marginally higher than bypass tube. This results in a 2-5% difference in the total volume of all exiting particles between the heated and bypass tubes.

4.4.1 Physical characterization of TD

4.4.1.1 Temperature profile

Temperature profile is another important design parameter for TDs. **Figure 4.7** shows the TD measured wall (panel a) and gas temperature (panel b). The measurement of gas temperature inside the TD was conducted by inserting a special tailored (24 inches, 0.01 inches ID) temperature probe from OMEGA.[47] Measurement of wall temperature was conducted using placing adhesive type thermocouple (SA1XL-J OMEGA) at multiple points along the wall of the TD.

Temperature gradient along the wall is smooth and uniform across the length of the TD. Heat loss is expected to be significant at the entrance and exit of the TD (Wehner et al., 2002) which is evident in the figure. Avoiding cold-spot and maintaining uniformity in the gas temperature is important to achieve accurate volatilization of the aerosol. This method of gas temperature measurement is disruptive to gas flow. Likely errors in the gas temperature measurement include positioning of probe inside the tube,

[47] TJ36-ICIN-18G-6, https://www.omega.com/subsection/transition-joint-probes-probes.html

and sensitivity of temperature probe to movement. Nonetheless it was the most feasible method available for measuring the temperature inside the TD.

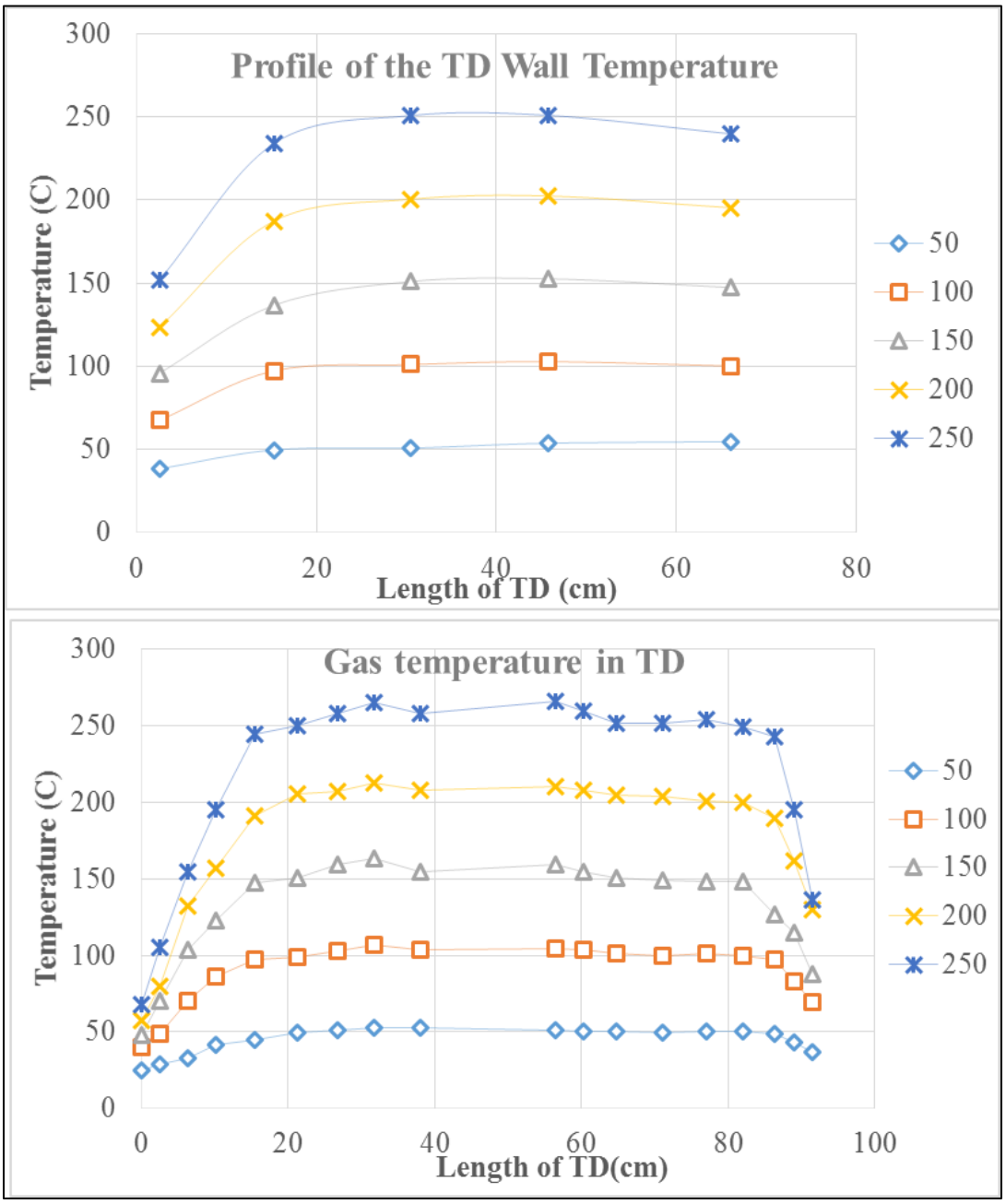

Figure 4.7 Wall and gas temperature measurement in the TD. Top panel shows the wall temperature measurements at multiple points along the wall of TD. Bottom panel shows the gas temperature inside the TD for various set temperature.

The uniformity of the TD temperature (wall and gas temperature) is influenced by wrapping of the heating rope/cables and placement of the thermocouple sensor for the temperature controller. After repeated measurement of wall and gas temperature and also adjusting the heating rope/cables and thermocouple sensor, it was decide that using two heater cables would provide better uniformity to the temperature profile, one at least at the entry and another at the end region of the TD **(**see **Fig. 4.10 and 4.11** for details**)**. **Figure 4.7** shows the final two profile of final temperature profile of the TD for wall and gas temperature, with two rope heaters in operation. The final configuration uses two 64 W, 120V OMEGA HTC-030 cable heaters (1 m in length each), and connected to two separate OMEGA CN 7523 temperature controllers. Each controller manages one of the heater cables based on readings from the corresponding SA1XL-J OMEGA thermocouple.

Heat loss is a very important consideration in TD design. The heating tube in the design considered in this thesis was insulated using 3 inches thick commercial glass wool as is standard for insulating hot pipes in industry.

4.4.1.2 Characterizing the volatility profile of TD using ammonium sulfate

TD is commonly characterized by volatility profile of commonly used laboratory aerosol such as ammonium sulfate (AS). The volatility profile is useful in comparing with other TD designs and also provides a volatility response of AS which is one of the major component of atmospheric aerosols. In order to determine the AS volatility profile produced by the TD, AS was generated in the laboratory and test in TD were conducted for particle sizes between 15 and 80 nm and temperature between 100 and 200 ^{o}C. Based

on **Equation 4.3**, the volatile fraction remaining (VFR) was calculated for different temperatures and sizes and a plot of temperature and VFR was produced. This is also referred to as a "thermogram" in literature (Hakkinen et al., 2012; Hong et al., 2014).

The VFR thermograms of pure ammonium sulfate are shown in **Figure 4.8**. For comparison, thermograms of AS from other TD designs are also plotted in the **Figure 4.9**. From thermgram, the temperature at which the volume of the heated sample is less than less than five percent of the bypass volume is also referred as *volatilization temperature*. This is also referred as *complete volatilization*. Similarly the term *no evaporation* is used in this thesis to describe either no change or less than five percent change in VFR at that temperature. Volatilization temperature of AS has a wide range of values, which is likely due to the variations in TD designs. Generally, it was observed that TD operating at >10 s residence time have the volatilization temperature in the range of 140-160 ^{o}C (An et al., 2007; Burtscher et al., 2001; Huffman et al., 2008; Tritscher et al., 2011). Volatilization temperatures for TD operating at < 10 s fall in the range of 180-235 ^{o}C (Johnson et al., 2004a; Philippin et al., 2004; Villani et al., 2007a; Wu et al., 2009). TD residence times play a significant role in determining the volatilization temperature of an aerosol (An et al., 2007; Burtscher et al., 2001). However there are a number of other factors that can influence volatilization temperature such as the consistency of the temperature profile, and purity of the AS.

Figure 4.8 showed that the complete volatilization of AS for the current TD design is in the range 170-200 ^{o}C depending on the size. AS below 15 nm has VFR less than 5% at 170 ^{o}C. The VFR for particle 30 nm or higher resulted in a VFR of less than 3% at 200 ^{o}C. For comparison with other design, pure AS VFR at 30, 50 and 80 nm from

our design is plotted, in Figure 4.9, with AS VFR from existing designs. Volatilization temperature also reflects the effect of size (i.e. Kelvin effect) which is significant for small sizes (see **Figure 4.8**). Pure AS particle generally do not evaporate until 140-150 ^{o}C as indicted by the VFR close to 0.9 to 1 for most sizes, but the change is VFR is more than 50% in the temperature range of 150-180 ^{o}C region. Nuclei size AS (<30 nm) show complete evaporation (or VFR less than 5%) near 170 ^{o}C compared to Aitken sizes that do not completely evaporate until 190-200 ^{o}C.

Our observation in **Figure 4.9** is indicated by the line plots whereas the AS VFR from other designs are shown as scatter plots. From the volatilization temperature for the sizes between 30 to 100 nm AS experiment, the volatility response from our TD falls in the TD designs having the aerosol residence time of <10 s.

The size distributions of the exiting AS particles are displayed in **Figure 4.10**. The size distribution reflects two important characteristics of the TD volatilization. The

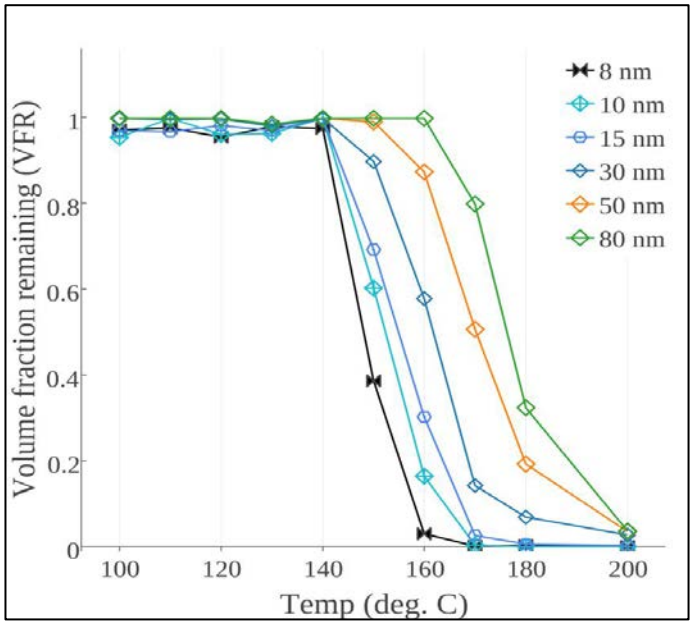

Figure 4.8 Volatility profile of pure ammonium sulfate at 8, 10, 15, 30, 50 and 80 nm generated from the current TD.

mode of size distribution decreases with the increase in the TD temperature and the presence of an induced nucleation at 8-10 nm observed for 50-80 nm. The nucleation has also been reported in other TD designs (Cerully et al., 2014) .

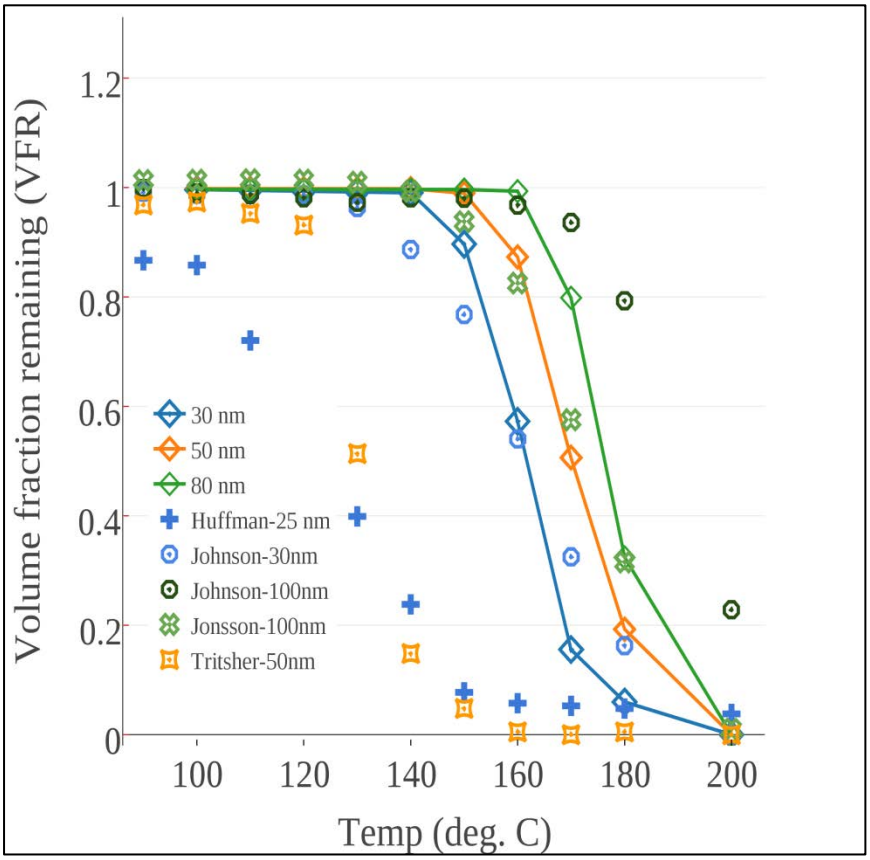

Figure 4.9 Volatility profile of ammonium sulfate at 30, 50 and 80 nm generated from the current TD. Also shown are the AS response from other TD designs. The line plot indicates the VFR profile from the current TD whereas the scatter plots are the VFR profile of AS from other design. The VFR in the y-axis is calculated using equation 4.2 and x-axis indicate the temperature maintained in the TD.

It is likely due to sharp change in temperature as the particle exits the TD and also contributed by high mass loading used in the laboratory experiments. Size distribution analysis also shows that the system does not induce any artificial bi-modal distribution at higher temperatures, which might compound the mixing state estimation.

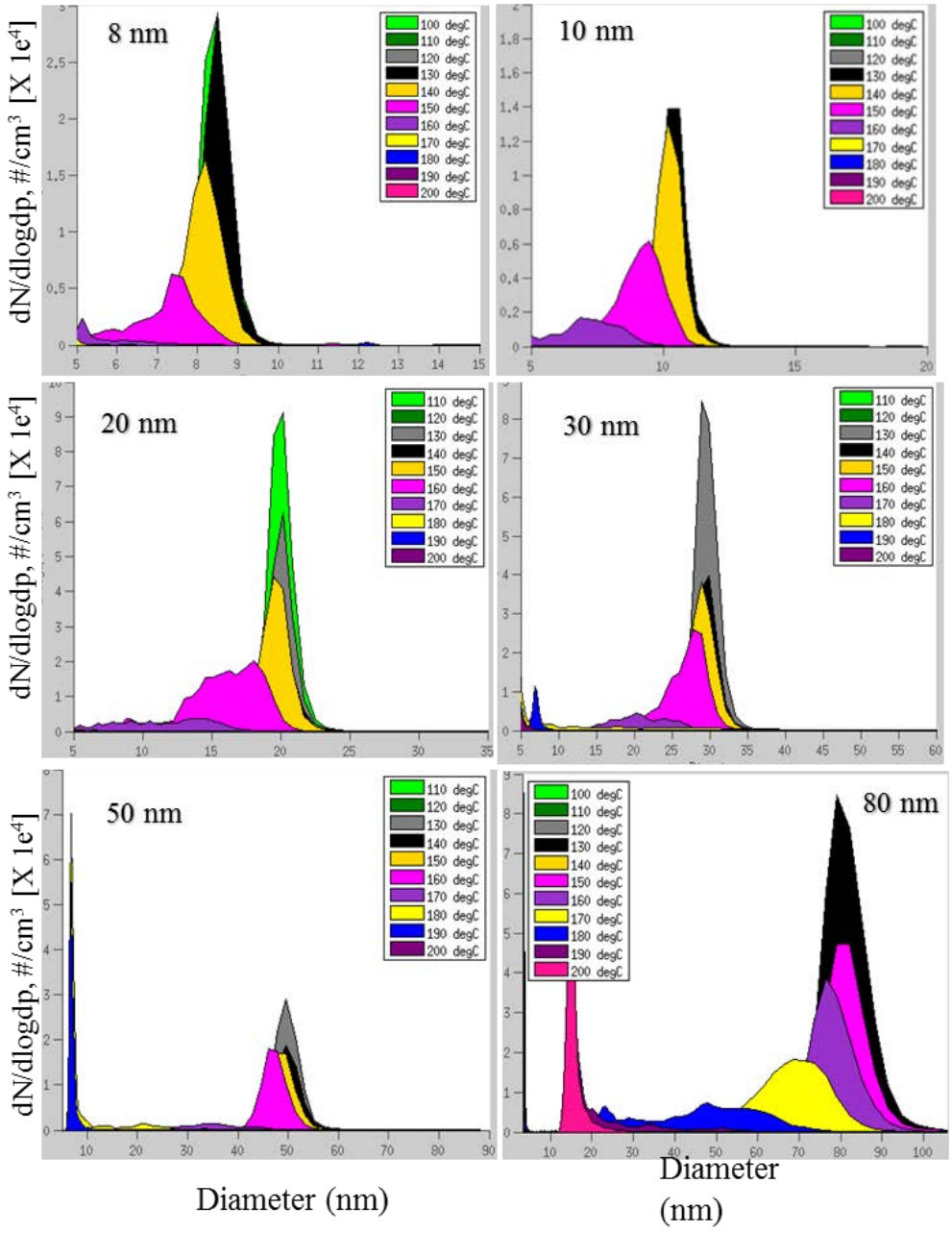

Figure 4.10 Response of particle size distribution to temperature increase. The test particle is ammonium sulfate and sizes from 8 to 80 nm were characterized from temperature from 100 to 200 ^{o}C. The y-axis of the each subpanel is the particle concentration and x-axis is the particle size.

4.4.2 Final TD Design

The schematic of the final TD design and the cooling mechanism is shown in **Figures 4.11 and 4.12.** The dimensions of the TD including various aspects of the V-DMA are listed in **Table 4.1**. In the TD, the wall temperature or the set point temperature is measured at two points along the length of TD; approximately 20-25 cm and 60-65 cm from the inlet of TD.

Each controller has a RS-485 to RS-232 converter to communicate with the LabVIEW software that allows them to be controlled, as indicated by the green color in **Figure 4.11**. As shown in **Figure 4.12**, the switching of the samples between the bypass and heated tubes and the operation of the cooling system are controlled by the valve controller box. The controller box contains five solid state relays which transmit the pulse voltage to the solenoid valves to close and open it. The valve controller box communicates with the LabVIEW software using a SCB-68 NI card which acts as input-output channel.

Typical operation of the V-TDMA temperature and sample run is shown in **Figure 4.13.** This operation is controlled by the V-TDMA program written in the LabVIEW software. Details on the V-TDMA program are provided in the **Appendix** (Section 9.2. VTDMA Program Structure and V-TDMA program set up for a typical experimental run).

Briefly, the V-TDMA program constitute of multiple sub-vi to control blower flow rate in the classifier, set voltage (applied) to the N-DMA, control temperature controller sub-vi, and a sub-vi to control the solenoid valves. The example temperature cycles during a typical V-TDMA experimental run is shown in **Figure 4.13**. In a typical

cycle include steady ramp up of temperature from T1 to T4 and with various D1-D3[48] at a programmable sampling frequency. A typical cycle of 4 temperatures, 3 diameters with 2 samples per diameter will requires approximately 60 minutes per cycle.

Also indicated in **Figure 4.13** is the sample timing, which indicates that bypass samples are taken while the heating tube is transitioning between set points. The timing of the transition can also be manually defined, and synced with the SMPS sampling interval.

Another important operational consideration of the V-TDMA is the initiation and closing of the cooling system. As evident in the **Figure 4.13**, the cooling system will be initiated after completing the sampling at the highest temperature sample (~T4). At this point the sample flow switches to the bypass tube while dry air is run through the heated (via valve 3 (air in) and valve 2 (air out)) tube at 25-30 psi until the heated tube temperature reaches the lowest heated temperature.

Once the bypass samples are complete the sample flow switches back to the heated tube, which is then at the lowest heated temperature. The cooling system is set to run until the heater temperature reaches to the T1 and is synched with SMPS sampling.

Overall the system is built and programmed so that the user can define the temperature, diameter and flow settings before running the experiments and can also look at the values when the experiments are running. For efficiently running the system, familiarity with LabVIEW may be required.

[48] Different temperature and diameter are user defined.

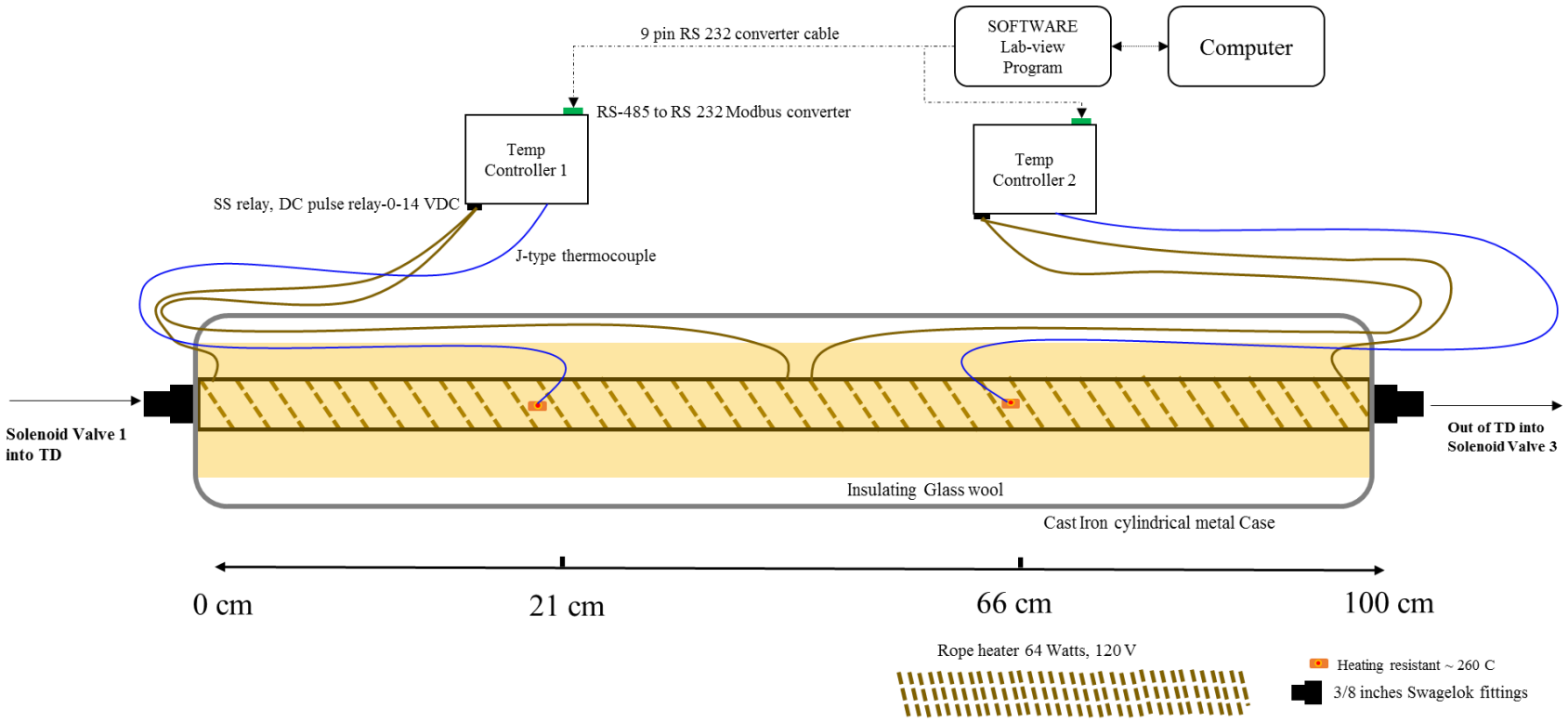

Figure 4.11 Detailed schematic of the TD components; hardware components of heating system, control mechanism, placement of thermocouple, and casing of the TD.

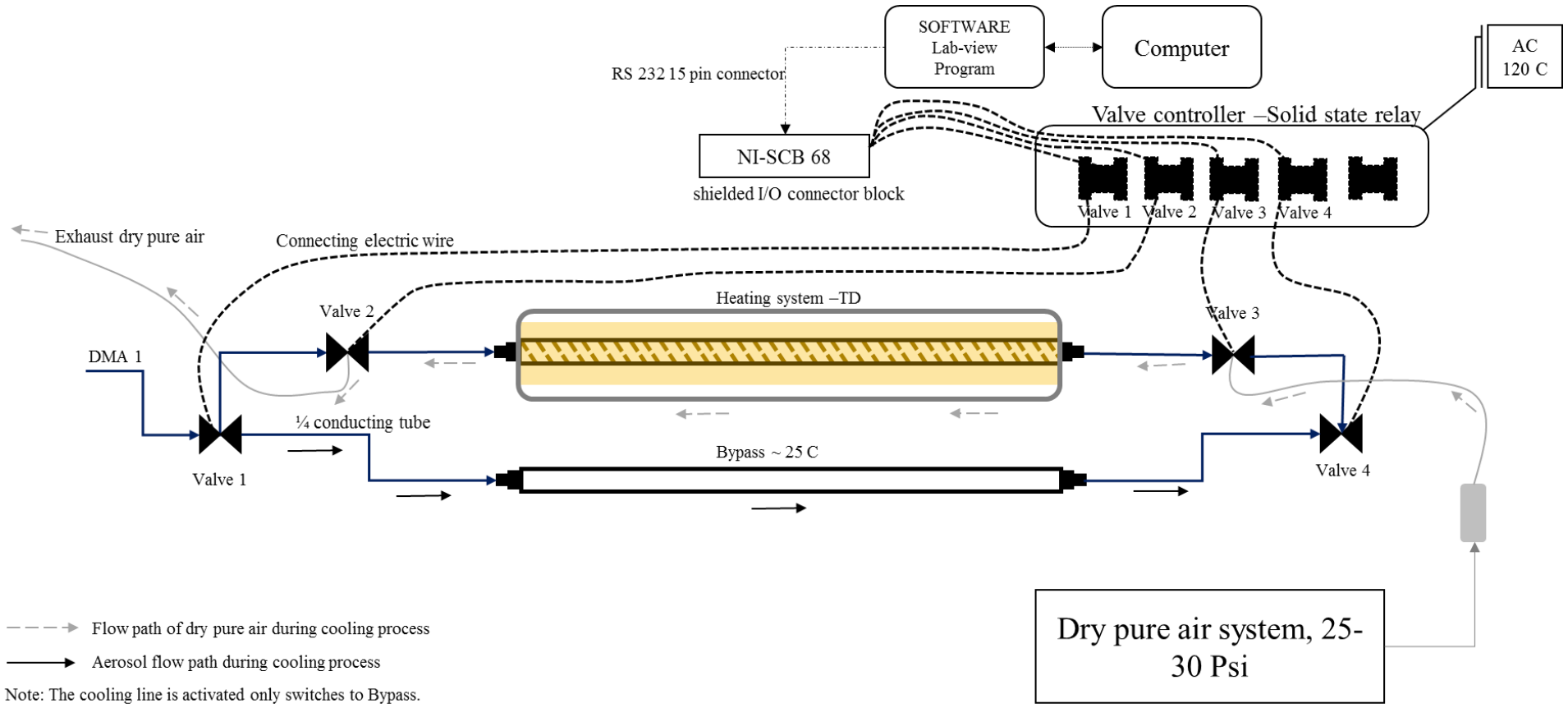

Figure 4.12 Detailed schematic of the cooling system in the TDMA system including the controlling mechanism for solenoid valves and flow of dry air pure through the TD.

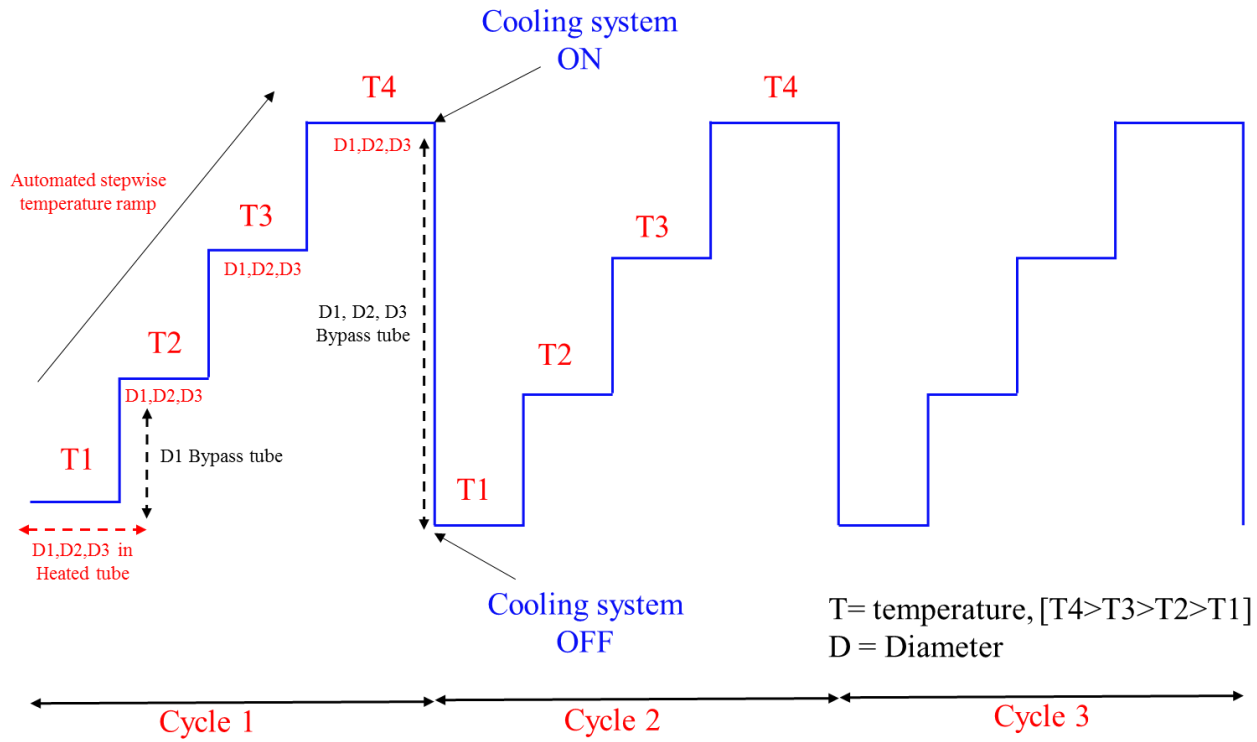

Figure 4.13 Detailed schematic of the operational of the current TDMA system; dotted arrow indicate the tube being sampled by SMPS in the TDMA; T1 to T4 are the set point temperature and D1, D2 and D3 are the diameter of interest the TDMA.

Table 4.1 Design details and operating condition for V-TDMA

Tube specific details	Details
Tube Diameter	9.5 mm OD, 7.7 mm ID
Tube Length	100 cm in length
Volumetric flow rate	0.3 to 1.5 lpm
Residence time	2 s at 1.00 lpm
Reynolds number	150-210 at 1 lpm
Denuder/adsorbing section	None
Temperature range	50 to 250 ^{o}C, J type thermocouple
Heating method	• 2 Rope heater coiled over the tube, and controlled by 2 temperature controllers • LabVIEW program for automatic temperature, diameter and valve switching • Programmable cool air flush for temperature control and continuous run
Particle measurement	• CPC 3785, Classifier 3080 and NDMA-3085, TSI Inc.
Valve system	• 4 Three way solenoid valves, Parker Automatic Inc.

4.5 Potential limitation and challenges

The system is built to operate for a long term unattended deployment in the field. It is crucial that the synchronization be achieved between the SMPS sampling time and the V-TDMA LabVIEW time stamp. The SMPS is controlled using the TSI's software[49] and is not directly linked with the V-TDMA LabVIEW program. The system operation has been improved to fix the error with time synchronization by setting or initiating both

[49] Aerosol Instrument Manager (AIM)

systems (SMPS and V-TDMA program at the same computer time) at the same computer time. If this is done the TD is capable of running for 15-25 h without manual assistance before the SMPS and V-TDMA samples fall significantly out of sync with each other. However if left running for prolonged periods of time the SMPS and LabVIEW time stamps can differ by more than 15 s. This is a major problem as this can cause particles from two separate V-TDMA runs to appear on the same SMPS samples.

Another operational challenge is the use of the V-TDMA at temperatures greater than 250 ^{o}C. The rope heated and thermocouples (to measure the set point) are rated to run at 260 ^{o}C continuously. Therefore for experiment requiring operation of TD at > 260 ^{o}C will require changes in the rope heater and adding conducting cement into the existing thermocouple sensing area.

The induced nucleation, associated with higher mass loading and larger sizes, were observed in the laboratory condition. Induced nucleation was not observed during field operation of the same V-TDMA setup. Nonetheless, the current system is not able to prevent the appearance of strong 8-10 nm for higher mass loading and larger sizes. The presence of an activated charcoal denuder section did not affect the presence of induced nucleation. The induced nucleation is caused by the sharp drop in temperature at the end of the TD, which likely causes the vapor to supersaturate and nucleate into particles. Because their volume and mass contribution is <2%, this effect can be neglected.

An additional in a system such as V-TDMA is the effect of heat on particle surface and likelihood of initiation of any heat sensitive chemical reaction. Although this issue has been raised in many other TD design such as the Donahue et al. (2012), Saleh et al. (2011), Huffman et al. (2008) and Brooks et al. (2001), quantitative investigation of

the heat related artifact in volatility response is still not reviewed comprehensively for many inorganics and organics aerosol composition. Experimental studies using organics aerosol such as alpha-pinene ozonolysis (Kuwata et al., 2011), ambient OA measurement studies (Dekenberger et al. (2007) have linked high temperature (>100 ^{o}C) with the presence of oligomers in the particles. For instance Kuwata et al. (2010) found that at 100 ^{o}C the secondary organics matter showed the presence of oligomers which was absent at 25 ^{o}C. Likewise, field measurements of OA at temperatures (>175 ^{o}C) showed increase in the oligomer mass by a factor of five compared to measurements below those temperatures. Oligomers have high molecular weights and thereby significantly influence CCN and the volatility response such as the presence of the residue.

4.6 Conclusion and future work

Volatility characterization provides information related to the thermodynamics and kinetics of evaporation, which are related to the composition of atmospheric particles. Particle volatility is often analyzed using TDMA systems. In this work, the development, fabrication and characterization of a Volatility Tandem Differential Mobility Analyzer have been described. The TD in the V-TDMA system discussed in this thesis consists of only one heated tube and heated by a pair of OMEGA rope heaters and temperature controllers. The residence time in the TD for a flow rate of 1 lpm is 2 s and the aerosol flow is laminar (Re~ 150-200). Estimated penetration efficiency is close to 85% for 10 nm and maintains a uniform temperature profile across the length of TD. Laboratory test showed that for UFP studies, the presence of a denuder does not change the volatility profile of the studied particles. Ammonium sulfate volatility profiles within

the TD discussed in this thesis agree most closely with those of TDs with less than ten second residence times.

Operationally the V-TDMA system can be user-defined with respect to temperature, diameter of interest and sampling frequency. This was achieved using a LabVIEW V-TDMA program that controls the SMPS, temperature controllers and valves within the V-TDMA.

Some minor design changes in the operation of the V-TDMA may include switching to gas temperature rather than wall temperature of TD. Measurement of direct gas temperature in the current set up was challenging due to the diameter of the TD tube. This requires a rod-type thermocouple probe and will have to be customized in its dimensions (such as its diameter). The current system was not able to prevent the appearance of strong 6-8 nm peaks at temperature >150 ^{o}C for particle such as 50 and 80 nm and also for high mass loading (~ >3-5 μg/m^{3}). The volume contributions due to these peaks were less than 2%, and were seen mainly in the laboratory conditions. However it is interesting to see if these were associated with large concentration load or the use non-conducting tubing in the aerosol flow path which could be sensitive to heat. Therefore changing the tubing to copper would be another minor change recommended in the current design.

Some exploratory changes in the V-TDMA system may include using a pair of CPC after heating the aerosol. Particle may activate (super saturation flow) differently in the CPC which also reflect their composition. Using water and butanol based CPC which similar D_{50}, bulk aerosol composition have been inferred (which mean aerosol with organic or inorganic) based on the amount of activation. Similar design could be merged

with the V-TDMA could better the current system for inferring chemistry of the aerosol. Likewise CPC, with modification in the saturation temperature, has been used to measure the cloud condensation nuclei of atmospheric aerosol. Method and modification to integrate water based CPC as CCN will also add new features and functionality to the V-TDMA system.

The major challenge in the V-TDMA design has been the question of equilibrium time and its effects on aerosol volatility. Observed evaporation of aerosol is likely to be strong function of residence time in the TD. Lacking equilibration in a TD may result in the measurement of aerosol evaporation rate than volatility. If the loss in the ultrafine particle range is not significant, ideally a V-TDMA should have multiple heating units running at multiple residence time from 1 to as high 50 seconds or higher. Running a V-TDMA at multiple residence time will assist in evaluating actual volatility of the aerosol. This will also require an evaporation model which will be used in an inverse sense. Measurement of volatility at multiple residence time will also offer estimation of heat of vaporization, saturation concentration, evaporation coefficient and others. Constraining these values is one of the major challenges in the V-TDMA data analysis which has implication on over or under estimation of aerosol volatility.

The idea of longer timescale in order to achieve equilibrium using isothermal dilution could be another direction. If applied on its own, studies have shown that isothermal dilution may lead to worse estimates of the volatility distribution compared to the TD. However application of TD with isothermal dilution has been shown to lead better estimates of parameters related to aerosol volatility.

Another challenge for the application of heat to study aerosol volatility is the likely of chemical reaction such as oligomerization in the organic aerosol. Although this has been highlighted in many studies as a potential artifact, but almost all the V-TDMA studies have not evaluated its significance. Field measurements studies using combinations of V-TDMA, CCNC or hygroscopicity will need to incorporate a method to verify the presence of such artifact. Aerodyne High-resolution Time-of-flight Aerosol Mass Spectrometer (HR-ToF-AMS) have been used in parallel configuration to detect the change in O, H and C ratio to verify the presence of temperature related oligomerization.

4.7 Acknowledgements

The author would like to acknowledge the wonderful support of Mr. Frank Turner from the Chemistry machine shop in helping the construction of various component of the V-TDMA system. Thanks to Mike Estenson at the Chemistry Department for assembling the various components of a temperature controller and other feedbacks to the author. Likewise, thanks to the Steve Struckman at the Engineering Machine shop for help with the construction of the adsorbing section of V-TDMA. I would like to thank Robert Bullard for his help in writing the V-TDMA program in LabVIEW. I would like to thank undergraduate researcher who assisted during this project, including Matt Johnson, Zachary Behrendt, Andrew Hesselink. Funding was provided by the National Science Foundation under Grant No. ATM-0748602.

4.8 References

Allan, J.D., Alfarra, M.R., Bower, K.N., Coe, H., Jayne, J.T., Worsnop, D.R., Aalto, P.P., Kulmala, M., Hyotylainen, T., Cavalli, F., Laaksonen, A., 2006. Size and composition measurements of background aerosol and new particle growth in a Finnish forest during QUEST 2 using an Aerodyne Aerosol Mass Spectrometer. Atmospheric Chemistry and Physics 6, 315-327.

Almeida, J., Schobesberger, S., Kuerten, A., Ortega, I.K., Kupiainen-Maatta, O., Praplan, A.P., Adamov, A., Amorim, A., Bianchi, F., Breitenlechner, M., David, A., Dommen, J., Donahue, N.M., Downard, A., Dunne, E., Duplissy, J., Ehrhart, S., Flagan, R.C., Franchin, A., Guida, R., Hakala, J., Hansel, A., Heinritzi, M., Henschel, H., Jokinen, T., Junninen, H., Kajos, M., Kangasluoma, J., Keskinen, H., Kupc, A., Kurten, T., Kvashin, A.N., Laaksonen, A., Lehtipalo, K., Leiminger, M., Leppa, J., Loukonen, V., Makhmutov, V., Mathot, S., McGrath, M.J., Nieminen, T., Olenius, T., Onnela, A., Petaja, T., Riccobono, F., Riipinen, I., Rissanen, M., Rondo, L., Ruuskanen, T., Santos, F.D., Sarnela, N., Schallhart, S., Schnitzhofer, R., Seinfeld, J.H., Simon, M., Sipila, M., Stozhkov, Y., Stratmann, F., Tome, A., Troestl, J., Tsagkogeorgas, G., Vaattovaara, P., Viisanen, Y., Virtanen, A., Vrtala, A., Wagner, P.E., Weingartner, E., Wex, H., Williamson, C., Wimmer, D., Ye, P., Yli-Juuti, T., Carslaw, K.S., Kulmala, M., Curtius, J., Baltensperger, U., Worsnop, D.R., Vehkamaki, H., Kirkby, J., 2013. Molecular understanding of sulphuric acid-amine particle nucleation in the atmosphere. Nature 502, 359-+.

An, W.J., Pathak, R.K., Lee, B.-H., Pandis, S.N., 2007. Aerosol volatility measurement using an improved thermodenuder: Application to secondary organic aerosol. Journal of Aerosol Science 38, 305-314.

Bullard, R.L., Stanier, C.O., Ogren, J.A., Sheridan, P.J., 2013. Determination of Seasonal, Diurnal, and Height Resolved Average Number Concentration in a Pollution Impacted Rural Continental Location, 19th International Conference on Nucleation and Atmospheric Aerosols (ICNAA), Colorado State Univ, Ctr Arts, Fort Collins, CO, pp. 583-586.

Burtscher, H., Baltensperger, U., Bukowiecki, N., Cohn, P., Huglin, C., Mohr, M., Matter, U., Nyeki, S., Schmatloch, V., Streit, N., Weingartner, E., 2001. Separation of volatile and non-volatile aerosol fractions by thermodesorption: instrumental development and applications. Journal of Aerosol Science 32, 427-442.

Cappa, C., 2010. A model of aerosol evaporation kinetics in a thermodenuder. Atmospheric Measurement Techniques 3, 579-592.

Cappa, C.D., Onasch, T.B., Massoli, P., Worsnop, D.R., Bates, T.S., Cross, E.S., Davidovits, P., Hakala, J., Hayden, K.L., Jobson, B.T., 2012. Radiative absorption enhancements due to the mixing state of atmospheric black carbon. Science 337, 1078-1081.

Cerully, K.M., Hite, J.R., Jr., McLaughlin, M., Nenes, A., 2014. Toward the Determination of Joint Volatility-Hygroscopicity Distributions: Development and Response Characterization for Single-Component Aerosol. Aerosol Science and Technology 48, 296-312.

Donahue, N.M., Robinson, A.L., Stanier, C.O., Pandis, S.N., 2006. Coupled partitioning, dilution, and chemical aging of semivolatile organics. Environmental Science & Technology 40, 2635-2643.

Ehn, M., Petaejae, T., Aufmhoff, H., Aalto, P., Haemeri, K., Arnold, F., Laaksonen, A., Kulmala, M., 2007a. Hygroscopic properties of ultrafine aerosol particles in the boreal forest: diurnal variation, solubility and the influence of sulfuric acid. Atmospheric Chemistry and Physics 7, 211-222.

Ehn, M., Petaejae, T., Birmili, W., Junninen, H., Aalto, P., Kulmala, M., 2007c. Non-volatile residuals of newly formed atmospheric particles in the boreal forest. Atmospheric Chemistry and Physics 7, 677-684.

Engler, C., Rose, D., Wehner, B., Wiedensohler, A., Brueggemann, E., Gnauk, T., Spindler, G., Tuch, T., Birmili, W., 2007. Size distributions of non-volatile particle residuals (D-p < 800 nm) at a rural site in Germany and relation to air mass origin. Atmospheric Chemistry and Physics 7, 5785-5802.

Frey, A., Rose, D., Wehner, B., Mueller, T., Cheng, Y., Wiedensohler, A., Virkkula, A., 2008a. Application of the Volatility-TDMA technique to determine the number size distribution and mass concentration of less volatile particles. Aerosol Science and Technology 42, 817-828.

Häkkinen, S., Äijälä, M., Lehtipalo, K., Junninen, H., Backman, J., Virkkula, A., Nieminen, T., Vestenius, M., Hakola, H., Ehn, M., 2012. Long-term volatility measurements of submicron atmospheric aerosol in Hyytiälä, Finland. Atmospheric Chemistry and Physics 12, 10771-10786.

Huffman, J.A., Ziemann, P.J., Jayne, J.T., Worsnop, D.R., Jimenez, J.L., 2008. Development and Characterization of a Fast-Stepping/Scanning Thermodenuder for Chemically-Resolved Aerosol Volatility Measurements. Aerosol Science and Technology 42, 395-407.

Johnson, G., Ristovski, Z., Morawska, L., 2004a. Application of the VH-TDMA technique to coastal ambient aerosols. Geophysical Research Letters 31.

Johnson, G.R., Ristovski, Z., Morawska, L., 2004d. Method for measuring the hygroscopic behaviour of lower volatility fractions in an internally mixed aerosol. Journal of Aerosol Science 35, 443-455.

Jonsson, A.M., Hallquist, M., Saathoff, H., 2007. Volatility of secondary organic aerosols from the ozone initiated oxidation of alpha-pinene and limonene. Journal of Aerosol Science 38, 843-852.

Joutsensaari, J., Vaattovaara, P., Vesterinen, M., Hämeri, K., Laaksonen, A., 2001. A novel tandem differential mobility analyzer with organic vapor treatment of aerosol particles. Atmospheric Chemistry and Physics 1, 51-60.

Kulmala, M., Mordas, G., Petäjä, T., Grönholm, T., Aalto, P.P., Vehkamäki, H., Hienola, A.I., Herrmann, E., Sipilä, M., Riipinen, I., 2007. The condensation particle counter battery (CPCB): A new tool to investigate the activation properties of nanoparticles. Journal of aerosol science 38, 289-304.

Lee, B.H., Kostenidou, E., Hildebrandt, L., Riipinen, I., Engelhart, G.J., Mohr, C., DeCarlo, P.F., Mihalopoulos, N., Prevot, A.S.H., Baltensperger, U., Pandis, S.N., 2010. Measurement of the ambient organic aerosol volatility distribution: application during the Finokalia Aerosol Measurement Experiment (FAME-2008). Atmospheric Chemistry and Physics 10, 12149-12160.

Meyer, N.K., Ristovski, Z., 2007. Ternary nucleation as a mechanism for the production of diesel nanoparticles: Experimental analysis of the volatile and hygroscopic properties of diesel exhaust using the volatilization and humidification tandem differential mobility analyzer. Environmental science & technology 41, 7309-7314.

Orsini, D.A., Wiedensohler, A., Stratmann, F., Covert, D.S., 1999. A new volatility tandem differential mobility analyzer to measure the volatile sulfuric acid aerosol fraction. Journal of Atmospheric and Oceanic Technology 16, 760-772.

Park, D., Kim, S., Choi, N.K., Hwang, J., 2008. Development and performance test of a thermo-denuder for separation of volatile matter from submicron aerosol particles. Journal of Aerosol Science 39, 1099-1108.

Philippin, S., Wiedensohler, A., Stratmann, F., 2004. Measurements of non-volatile fractions of pollution aerosols with an eight-tube volatility tandem differential mobility analyzer (VTDMA-8). Journal of Aerosol Science 35, 185-203.

Pryor, S.C., Spaulding, a.M., Barthelmie, R.J., 2010. New particle formation in the Midwestern USA: Event characteristics, meteorological context and vertical profiles. Atmospheric Environment 44, 4413-4425.

Riipinen, I., Pierce, J.R., Donahue, N.M., Pandis, S.N., 2010. Equilibration time scales of organic aerosol inside thermodenuders: Evaporation kinetics versus thermodynamics. Atmospheric Environment 44, 597-607.

Ristovski, Z., Fletcher, C., D'Anna, B., Johnson, G.R., Bostrom, J., 2006. Characterization of iodine particles with volatilization-humidification tandem differential

mobility analyser (VH-TDMA), Raman and Sem techniques. Atmospheric Chemistry and Physics Discussions 6, 1481-1508.

Ristovski, Z., Suni, T., Kulmala, M., Boy, M., Meyer, N.K., Duplissy, J., Turnipseed, A., Morawska, L., Baltensperger, U., 2010a. The role of sulphates and organic vapours in growth of newly formed particles in a eucalypt forest. Atmospheric Chemistry and Physics 10, 2919-2926.

Sakurai, H., Fink, M.A., McMurry, P.H., Mauldin, L., Moore, K.F., Smith, J.N., Eisele, F.L., 2005. Hygroscopicity and volatility of 4–10 nm particles during summertime atmospheric nucleation events in urban Atlanta. Journal of Geophysical Research: Atmospheres (1984–2012) 110.

Saleh, R., Shihadeh, A., Khlystov, A., 2011. On transport phenomena and equilibration time scales in thermodenuders. Atmospheric Measurement Techniques 4, 571-581.
Seinfeld, J.H., Pandis, S.N., 2012. Atmospheric chemistry and physics: from air pollution to climate change. John Wiley & Sons.

Shiraiwa, M., Seinfeld, J.H., 2012. Equilibration timescale of atmospheric secondary organic aerosol partitioning. Geophysical Research Letters 39.

Smith, J., Moore, K., McMurry, P., Eisele, F., 2004. Atmospheric measurements of sub-20 nm diameter particle chemical composition by thermal desorption chemical ionization mass spectrometry. Aerosol Science and Technology 38, 100-110.

Smith, J.N., Moore, K.F., Eisele, F.L., Voisin, D., Ghimire, A.K., Sakurai, H., McMurry, P.H., 2005. Chemical composition of atmospheric nanoparticles during nucleation events in Atlanta. Journal of Geophysical Research-Atmospheres 110.

Stolzenburg, M.R., McMurry, P.H., Sakurai, H., Smith, J.N., Mauldin, R.L., Eisele, F.L., Clement, C.F., 2005. Growth rates of freshly nucleated atmospheric particles in Atlanta. Journal of Geophysical Research-Atmospheres 110.

Swietlicki, E., HANSSON, H.C., Hämeri, K., Svenningsson, B., Massling, A., McFiggans, G., McMurry, P., Petäjä, T., Tunved, P., Gysel, M., 2008. Hygroscopic properties of submicrometer atmospheric aerosol particles measured with H-TDMA instruments in various environments—A review. Tellus B 60, 432-469.

Tiitta, P., Miettinen, P., Vaattovaara, P., Joutsensaari, J., Petaja, T., Virtanen, A., Raatikainen, T., Aalto, P., Portin, H., Romakkaniemi, S., Kokkola, H., Lehtinen, K.E.J., Kulmala, M., Laaksonen, A., 2010. Roadside aerosol study using hygroscopic, organic and volatility TDMAs: Characterization and mixing state. Atmospheric Environment 44, 976-986.

Tritscher, T., Dommen, J., DeCarlo, P., Gysel, M., Barmet, P., Praplan, A., Weingartner, E., Prévôt, A., Riipinen, I., Donahue, N., 2011. Volatility and hygroscopicity of aging

secondary organic aerosol in a smog chamber. Atmospheric Chemistry and Physics 11, 11477-11496.

Villani, P., Picard, D., Marchand, N., Laj, P., 2007a. Design and validation of a 6-volatility tandem differential mobility analyzer (VTDMA). Aerosol Science and Technology 41, 898-906.

Wang, J., Cubison, M.J., Aiken, a.C., Jimenez, J.L., Collins, D.R., 2010. The importance of aerosol mixing state and size-resolved composition on CCN concentration and the variation of the importance with atmospheric aging of aerosols. Atmospheric Chemistry and Physics 10, 7267-7283.

Wehner, B., Berghof, M., Cheng, Y., Achtert, P., Birmili, W., Nowak, A., Wiedensohler, A., Garland, R., Pöschl, U., Hu, M., 2009. Mixing state of nonvolatile aerosol particle fractions and comparison with light absorption in the polluted Beijing region. Journal of Geophysical Research: Atmospheres (1984–2012) 114.

Wehner, B., Petäjä, T., Boy, M., Engler, C., Birmili, W., Tuch, T., Wiedensohler, A., Kulmala, M., 2005. The contribution of sulfuric acid and non-volatile compounds on the growth of freshly formed atmospheric aerosols. Geophysical research letters 32.

Wehner, B., Philippin, S., Wiedensohler, A., 2002. Design and calibration of a thermodenuder with an improved heating unit to measure the size-dependent volatile fraction of aerosol particles. Journal of Aerosol Science 33, 1087-1093.

Weiden, S.-L., Drewnick, F., Borrmann, S., 2009. Particle Loss Calculator–a new software tool for the assessment of the performance of aerosol inlet systems. Atmospheric Measurement Techniques 2, 479-494.

Wu, Z., Poulain, L., Wehner, B., Wiedensohler, A., Herrmann, H., 2009. Characterization of the volatile fraction of laboratory-generated aerosol particles by thermodenuder-aerosol mass spectrometer coupling experiments. Journal of Aerosol Science 40, 603-612.

Zhang, Q., Stanier, C.O., Canagaratna, M.R., Jayne, J.T., Worsnop, D.R., Pandis, S.N., Jimenez, J.L., 2004. Insights into the chemistry of new particle formation and growth events in Pittsburgh based on aerosol mass spectrometry. Environmental science & technology 38, 4797-4809.

Zordan, C.A., Pennington, M.R., Johnston, M.V., 2010. Elemental composition of nanoparticles with the nano aerosol mass spectrometer†. Analytical chemistry 82, 8034-8038.

CHAPTER 5: VOLATILITY MEASUREMENT OF PRIMARY AND SECONDARY ULTRAFINE AEROSOL IN THE RURAL CONTINENTAL MIDWEST[50]

5.1 Abstract

Volatility measurement of UFP particles (10-100 nm) provides important information about particle growth pathways and thermodynamic properties, and can assist in constraining chemical composition. Midwest US has a diverse land use pattern and multiple of sources for UFPs. However the pathways of particle formation, and growth and the contribution of key gaseous precursors are still not examined or measured. Furthermore, the volatility of UFPs using V-TDMA has not been reported for many sites in the Midwestern U.S. Consequently, the relative contributions of organic and inorganic constituents to particle growth in the UFP size ranges, and also the presence or absence of low-volatile particle cores in 10-100 nm particles, has not been determined.

This study presents size resolved volatility analysis of UFPs from a yearlong field campaign in Bondville, IL. Analysis of volatility profile was performed using K-means cluster analysis. At least three types of profile in 15, 30, 50 and 80 nm is observed and qualitatively their volatility profile resembles illustrate; significant evaporation resistant residue at 200 ^{o}C and relative volatile profile before 200 ^{o}C , a mixture of ammonium

[50] This work is under preparation to be submitted to *Atmospheric Environment*. A. Singh, and C. Stanier designed the study and A. Singh performed all the field sampling, measurement analysis and manuscript preparation. Robert Bullard co-led the field sampling for the Stanier group.

sulfate and possible organics, and profiles resembling the profiles of ammonium sulfate. The presence of a volatility profile at various sizes is further explored during particle formation and growth period.

Evaporation resistant residue is consistently observed at 200 ^{o}C in all sizes from 15 to 80 nm. The amount of residue was positively correlated with particle size; volume fraction of residue increases from 10-15% in 15 nm to 30-40% in 80 nm. External mixture was examined using size distribution of the residue and was observed in 20-30% samples, especially at 30, 50 and 80 nm. The timing and characterization of the external mixture with respect to different mode were also analyzed.

The occurrence of the residue was evaluated by analyzing its association with trace gases, atmospheric condition, meteorology and different atmospheric condition. Strong associations were observed with ozone (O_3), sulfur dioxide (SO_2) and solar radiation.

5.2 Introduction

Ultrafine atmospheric particles (UFPs) have important effects on human health and climate. On a number basis, the concentration of particles is dominated in most locations by UFPs, particles with diameters below 100 nm. These particles determine the abundance of cloud condensation nuclei (CCN) and therefore are important to aerosol indirect climate forcing (Kuang et al., 2009; Spracklen et al., 2008). UFPs and the processes that govern the size and concentrations of UFPs are also important to determining the entire aerosol size distribution, including the larger particles that are primarily responsible for direct climate forcing due to scattering and absorption (Spracklen et al., 2006).

The two main pathways or sources through which UFP enters the atmosphere are nucleation and primary or direct emission. The contribution of nucleation to UFP concentration dominate in the remote continental areas by more than factor of two (Spracklen et al., 2006), and can be a dominant fraction in urban environment such as Pittsburg, US with more than 90% number fraction from UFP (Posner and Pandis, 2015). Of the small fraction (~10%) contributed by primary source to total UFP concentration, gasoline and industrial sources constitute the majority (~60%) among primary sources.

In the Midwest region of the United States, secondary production of UFPs through new particle formation has been shown to be significant. Pryor (2010) reported that 46% of sampling days exhibited new particle formation at a regionally polluted forested site. The frequency of particle formation is either comparable or higher than other locations such as Hyytiala, Finland (Dal Maso et al., 2005) and Pittsburg, US (Stanier et al., 2004). Regional modeling shows that the total particle concentration in the Midwest are sensitive to trace gas such as sulfur dioxide (SO_2), nitrogen oxides (NO_x), ammonia (NH_3) (Crippa et al., 2013).

The compounds responsible for the particle growth after nucleation vary with region. In less polluted regions, particle growth is dominated by compounds other than sulfuric acid (Kulmala et al., 2004), while in locations with significant urban or primary emissions of SO_2, a larger portion of growth is attributable to sulfuric acid (Bzdek et al., 2012; Stolzenburg et al., 2005; Wang et al., 2011; Yue et al., 2010). Normally ultrafine particles from particle formation are dominated by sulfate, ammonium, and organic carbon, and nitrate (Bzdek et al., 2012, Park et al., 2009). The presence of other compounds such as amine, silicon, elemental carbon, organo-sulfates, organo-nitrates,

carboxylic and hydroxyl carboxylic organic acid, aldehydes, and alcohols have also been reported in the freshly nucleated particle (Smith et al., 2008; Bzdek et al., 2014; Fanizza et al., 2010; Zhang et al., 2012).

Parameterization of New Particle Formation (NPF) in the Midwest indicates that concentrations of sulfuric acid (H_2SO_4) along with UV are important variable for nucleation rate (Crippa et al., 2012). Direct measurements of aerosol composition in freshly formed particles and growth thereafter have not been conducted in the Midwest and thus detailed parameterization of particle growth has not been performed. Few studies have shown the likely associations of biogenic organics to the particle growth in the Midwest. In a forested site (MMSF) in Indiana, weakening of the growth rate was found associated with the drought severity which provides causal evidence of semi-volatile partition of biogenic VOC (Pryor et al., 2014). Pryor et al. (2010) further found during the NIFty campaign that a condensing vapor concentration of approximately $5.2x10^7$ molecules/cm^3 is required for growth from 6-30 nm after a spring particle formation event. The estimated H_2SO_4 concentration was $1.2x10^7$ molecules/cm^3, 24% of the total required for condensation growth. For the same day mass closure experiment using nano-MOUDI and FMPS accounted the total particle mass below ≤30 nm from was accounted by $NH4^+$ and $SO4^{2-}$. This indicates that ammonia is playing an important role in neutralizing the sulfuric acid in the nuclei mode (<30 nm) and limited for larger sizes because of the limited availability of sulfuric acid (Zhang et al., 2009). The mass discrepancy increases for particles > 30 nm (chemically not quantified) is likely due to organic (Pryor et al., 2011; Yu et al., 2014). This was also supported by observations from Ozark forest in Missouri, where stronger positive correlation was observed between

the growth of the nucleated particles with biogenic VOC, O_3 than SO_2 indicating O_3 led oxidation of the biogenic VOC (Yu et al., 2014). Similarly measurements from CABINEX campaign in a forest area in Michigan found clear air mass from North is associated with particle formation, and lowering of the hygroscopicity than anthropogenic air mass from south and east with higher hygroscicpity, and increased presence of ammonium and sulfate (VanReken et al., 2015).

In contrast AMS measurement of $N_{<100}$ particles during a NPF event in Egbert, ON (which in contrast to the earlier studies has more anthropogenic influence) found decreasing organic to sulfate ratio as the nucleation aged, which was an indication of increasing sulfate condensation as the NPF particle grew (Shantz et al., 2012).

Based on the studies conducted so far, ammonia is a likely to dominate the composition for particle below 30 nm, via neutralization reaction in forested and urban location. Other precursors may dominate the growth of particle > 30 nm, which could be site specific. The concentration of the biogenic VOC (0.1-0.2 ppb) reported by these studies are at least one order of magnitude lower than SO_2 (1-1.5 ppb). It is likely that the concentration of these trace gases are not a strong indicator of nucleation rate and growth, rather specific oxidation products and meteorology such as UV may be significant.

This paper is a part of yearlong study to provide a complete perspective on particle formation and growth in a rural and agricultural Midwestern site. In this paper, volatility characterizations of UFPs were conducted to enable in direct inference about particle chemistry, and formation of evaporation resistant residue in the UFP in the Midwest. This study addresses few specific objectives which include identification of the volatility signature of particles in the UFP size range, quantification of physical

differences of UFPs between NPF and non-NPF events and relation of evaporation resistant residue with particle size, seasonality and mixing state.

The V-TDMA described in Chapter five was deployed during several multi-day periods during the yearlong campaign to study the volatility of the UFP in the Midwest United States. Tandem differential mobility measurements (TDMA) are well-established tool to study aerosol volatility (Clarke, 1991; Pinnick et al., 1987; Rader and McMurry, 1986). Design and calibration of the current V-TDMA is discussed in chapter five. Tandem differential mobility measurements (TDMA) are well-established tool to study aerosol volatility (Clarke, 1991; Pinnick et al., 1987; Rader and McMurry, 1986). Detailed design and calibration of the V-TDMA used in this work is provided as supplement. V-TDMA is often used with a thermodenuder to infer the chemical composition from volatility measurements of particles. Sub-15 nm particles were heated to 100 ^{o}C to identify the presence of ammonium sulfate from sulfuric acid (Sakurai et al., 2003). Heating to temperature > 150 ^{o}C will evaporate any sulfate salts and can be useful to indicate the presence of non-sulfate component such as nonvolatile organics (Smith et al., 2010; Sakurai et al., 2005). Likewise, heating to 280-300 ^{o}C has been used to determine the nonvolatile core, presumably polymerized organic. The nonvolatile core may account for 20-40% of volume in 3-25 nm particles (Wehner et al., 2005; Hakkinen et al., 2012). The nonvolatile core was found to influence growth of the freshly formed particles (Ehn et al., 2010), with the ratio of particle growth rate positive correlated to the amount of nonvolatile core. Varied sources, atmospheric conditions and chemical pathways have been reported as the possible underlying cause for these nonvolatile core including secondary organics (Ehn and Pet, 2007; Kokkola et al., 2014), other organics

such as PAH, BC and organic nitrate (Hakkinen et al., 2012) and traffic sources, polluted urban environments (Birmili et al., 2010; Wehner et al., 2009).

5.3 Methodology

The V-TDMA system used at Bondville, IL was designed to study the volatility of UFPs with rapid automated stepping for temperatures and particle size achieved using LabVIEW. The schematic of the V-TDMA system is shown in **Figure 4.1**. The TD, in this V-TDMA, is a stainless steel tube (length = 1 m, inner diameter = 0.305 inch (or 7.7 mm). The residence time of the particles in the heating column varies based on the CPC used (0.3 to 1.5 lpm). The field campaign was conducted with CPC 3785 which has an aerosol flow of 1 lpm resulting in a center line residence time of 2 s. A typical operation of V-TDMA with 4 temperature points and 3 diameters (see **Fig. 4.13**) takes approximately 60 minutes to complete.

The heating arrangement in the TD (**Fig. 4.11**) is similar in construction to Huffman (2008), Johnson (2004) and Tritscher (2011) with heating ropes controlled by a commercial temperature controller. To achieve controlled and uniform heating along the length, a pair of rope heaters (OMEGA HTC, 64 W, 1 m in length each) was wrapped around the walls of the pipe. Each rope heater was controlled by a commercial temperature controller (OMEGA CN 7523). Two fast (<2 s) response J-type thermocouples with heat resistant tape (SA1XL-J series rated to 260 ^{0}C, OMEGA) were placed on the surface of the TD to provide an input wall temperature for the controllers. The error in this J-type thermocouple is ±1.1 to 2.2 ^{o}C and both are calibrated to NIST standards. The TD was insulated with glass wool insulation (3 inches thick) and enclosed in a cylindrical cast iron casing.

The activated carbon denuder in a typical TD is used to remove gas phase species and minimize re-condensation onto partially evaporated particles. Theoretical examination of the evaporation with the presence of adsorption in TD show no difference in volatility of aerosol, especially for UFP sizes and atmospheric relevant particle concentration (Fuentes and McFiggans, 2012; Riipinen et al., 2010; Saleh et al., 2011). Our own laboratory evaluation showed that the absence of adsorbing system did not limit the removal rate of volatilized particulate material compared to the case when absorption section was used. This was in conformation with other experimental design (Ehn et al., 2007; Saleh et al., 2011; Tritscher et al., 2011). Thus the final TD design in our V-TDMA system did not include an adsorbent system. The lack of an absorbent section is further justified by the low concentrations encountered in ambient studies in the upper Midwest, which are significantly below the high loadings (>100 $\mu g/m^3$) needed to require an adsorbent (Cappa, 2010; Saleh et al., 2011).

5.3.1 Field deployment

The V-TDMA system was deployed on specific days of a 10 month field study at the Bondville Environment and Atmospheric Research Site **(**BEARS, 40.0523 N 88.3726 W). In the 10 month study period, five short campaigns between August 2013 and May 2014 were conducted, with each deployment consisting of 2-4 sampling days with 8-24 hours of sampling per day. The temperature used in the TD ranges between 80 and 250 °C and sizes between 6 and 80 nm. The dates and associated information on sizes, temperatures, and atmospheric conditions are in **Table 5.1**.

The 10 month campaign measurement of the full aerosol size distribution from 3 nm to 2.5 microns supplemented the extensive routine measurements at this site

(AERONET,[51] IMPROVE, [52] NOAA-GMD ESRL,[53] CASTNET, IL-EPA, [54] AIRMoN-Dry[55] and NADP[56]). In addition to extensive collocated instrumentation, a ten year (or longer) instrument record from many of these monitoring systems exists. The site was chosen because of its long measurement history and its representativeness of a perturbed rural continental site with intensive agriculture. Finally, the site is complementary to other UFPs studies in the site which have taken place in urban-industrial and deciduous forest locations.

Details on the various instruments deployed during this campaign and ongoing measurements by EPA, NADP, NASA, NOAA, NCore and other agencies are provided in Bullard et al. (2015). A short description is provided here.

Four sets of particle instrumentations were deployed: SMPS (3025 CPC/3080 Classifier, 2.5-60 nm), SMPS (3786 CPC/3080 Classifier, 10-500 nm), SMPS 3091 (10-500 nm), Aerosol Particle Sizer (TSI 3321, 0.542-20μm). In addition to an hourly EPA National Core (NCore)[57] SO_2 measurement, additional SO_2 measurement via Teledyne 100-E at 1 min average time resolution was also deployed. Other continuous traces gas measurements included in this study are CO, NO, NO_Y, [58] and O_3 were provided by the co- located EPA Ncore site. Incident solar radiation and weather variables were also provided from the NCore (Bullard et. al., 2015).

[51] http://aeronet.gsfc.nasa.gov/
[52] http://www.epa.gov/ttnamti1/visdata.html
[53] http://www.esrl.noaa.gov/gmd/
[54] http://www.epa.illinois.gov/
[55] http://www.atdd.noaa.gov/?q=node/46
[56] http://nadp.sws.uiuc.edu/
[57] http://www.epa.gov/ttnmain1/amtic/ncore/index.html
[58] NOy consists of all oxides of nitrogen. The oxidation state of the N atom is +2 or greater, i.e, the sum of all reactive nitrogen oxides including NOx (NO + NO2) and NO_z, http://www.epa.gov/ttn/amtic/files/ambient/pm25/spec/noysum2.pdf

Table 5.1 Summary of V-TDMA sampling periods

Sampling period	**Date Range**	**Diameters** (nm)	**Temperature** (^{o}C)	**Comments**
TDMA 1	8/25 – 8/29/2013	20, 30, 50, 80	80, 100, 150, 200, 250	Regional aerosol, cloudy condition, possible influence of regional biomass fire
TDMA 2	9/5-9/9/2013	10, 15, 20, 30, 50 80	80, 100, 150, 170, 200, 250	Particle burst event (PBE), high temperature, humidity and ozone period
TDMA 3	03/16/-03/17/ 2014	20, 30, 50, 80	100, 130, 150, 200	Regional aerosol
TDMA 4	04/21-04/ 24/2014	6,8,10, 15, 20, 30, 50 ,80	100, 130, 150, 200	Particle burst event and localized plumes
TDMA 5	05/22-05/26/2014	6, 8,10, 15, 20, 30, 50, 80	100, 130, 150, 200	Particle burst event and localized plumes; sensitivity to residence time

Samples were categorized into four categories based on trace gas concentrations and the particle number size distribution. The four categories are regional background (RB), local emission (LE), particle burst event with smooth growth (PBE-S) and particle burst with short discontinued growth (PBE-D). A detailed description of the atmospheric conditions is provided in the **Appendix** (Section 9.3. Classification of atmospheric conditions)**.** Regional background (RB) condition was defined as periods of NO_y > 1 ppb and particle concentrations was dominated mainly by accumulation mode particles (>100 nm). Localized emission (LE) was associated significant enhancement in NO concentration and variable concentration of SO_2 and observed during the early morning period (5-8 am). Local emissions also showed enhanced concentration with particle mode

in 15-30 nm. Two particle burst were observed: particle burst event with smooth growth over the day (PBE-S) and particle burst event with short discontinued growth (PBE-D) (See **Appendix** Section 9.3 figurative description of particle formation). Beside differences in the nature of growth, PBE-D events captured during TDMA operation were associated with stronger SO_2 enhancement (1-10 ppb) and rapid particle growth from 10 to 50 nm for few hours (1-3 h).

5.4 Data analysis

5.4.1 Volume fraction remaining (VFR)

Volume fraction remaining (VFR) is a non-dimensional measure of how much of an aerosol has evaporated. The VFR is the ratio of total heated aerosol volume (V_{heated}) to the total volume of bypass or unheated aerosol (V_{bypass}) (Hakkinen et al., 2012; Hong et al., 2014).

5.4.2 Cluster analysis of the volatility data

Cluster analysis of multi-variable data, such as the particle size distribution, has been used as a source apportionment method (Beddows et al., 2009; Brines et al., 2014; Kanawade et al., 2012; Sabaliauskas et al., 2013; Salimi et al., 2014). As in other techniques such as positive matrix factorization where factors are not constrained but are rather determined from data, a 2^{nd} step is inference of the sources that may contribute to clusters based on the meteorology, back trajectory, time of day, wind direction and associated trace gases. In this study, clustering technique was applied to identify and discriminate unique volatility profile observed within each particle size.

Clustering was performed using R statistical software. R offers "clValid" package which was used to test various clustering algorithm suitable for the volatility profile data and also determine the optimum number of clusters (Brock et al., 2008). Detail discussion on the clustering technique is in the **Appendix** (9.3 Cluster techniques for volatility data). "clValid" uses two broad groups of indices, internal and stability indices, to determine appropriate clustering algorithm and minimum number of clusters. The performance of various clustering algorithm was evaluated and is tabulated in the **Appendix** (Section 9.3. Cluster Analysis). In summary, no single clustering algorithm produced optimum values across the tested indices. K-means and hierarchical performed relatively better, at least with higher Dunn and Silhouette indices. Clustering method employing K-means algorithm consistently performs better with Dunn and Silhouette indices (Beddows et al., 2009; Salimi et al., 2014. In this work, K-means was thus chosen among the two best performing algorithm. In K-means, a pre-defined number of centroid for the dataset is set and iterates until it reduces the error function (Everitt et al., 2005). The iterative process stops when the error function[59] does not change significantly or the membership of the clusters no longer changes.

5.4.2.1 Volatility data processing for cluster analysis

This study focused on four diameters for the study period: 15, 30, and 50, and 80 nm. Samples were from August and September (in 2013), April and May (in 2014). The volatility data at each size were measured at multiple temperature ranging from 80 to 250 ^{o}C, but for consistency the clustering was applied for VFR data with three temperature points (100, 150 and 200 ^{o}C). This resulted in a total of 68 VFR distributions (VFR at

[59] The error function is a squared of the differences between the centroid and each observation and thus tries to reduce the variances within each cluster.

these three temperature points) for 15 nm, 170 for 30 nm, 165 for 50 nm and 120 for 80 nm for the total study period.

5.5 Results

5.5.1 Transmission loss in the TD

Two characteristics particle loss features in the current TD design is presented in **Figure 4.5 and 4.6.** Detailed description of these figures is also provided in Section 4.4 of this thesis. In summary, more than 85% transmission efficiency is estimated for 10 nm particles for a residence time of 2 s in the TD. This other loss characterization is the relative transmission loss shown in **Figure 4.6.** The error bar, in the figure, is the uncertainty calculated using the **Equation 4.3**. The transmission ratio indicates that the ratio is close to 1 for particles >10 nm, within 5% of each other. At 10 nm, the difference is close to 15% implying that the heated tube count is marginally higher than bypass tube. This results in a 2-5% difference in the total volume of all exiting particles between the heated and bypass tubes. Therefore these differences are not taken into account during the VFR calculation.

5.5.2 Comparison of VFR profile of AS between different TDs

The volatility profiles of ammonium sulfate aerosols are commonly used to compare different V-TDMA designs (An et al., 2007; Frey et al., 2008). In Section 4.4.1.2 of the thesis, detailed description of the volatility signature of AS and comparison with other design is shown using **Figure 5.8.** The complete volatilization of 30 and 50 nm occurs at 170-180 ^{o}C. The complete volatilization for diameter 15 and 20 nm is close to 160-170 ^{o}C. In summary, the volatility profile of ammonium sulfate is similar to the

signature from Jonsson et al. (2007) and Johnson et. al. (2004). Also comparison of volatility profile from TD design with residence time >10 s indicate a significant difference with the current TD.

5.5.3 Overview of the size-resolved UFPs volatility

Figure 5.1 shows the volatility profile of a range of particle sizes using all data from the field campaign, with the size- and temperature-dependent VFR shown as a box-and whisker plot. A distinction can be drawn in the behavior of 6-10 nm particles vs. those at 20 nm and larger. The small particles showed no evaporation[60] at 100 ºC, while larger particles lose 15% by volume at this low temperature (i.e. VFR of 0.85). These small particles, resistant to evaporation at 100ºC, showed significant evaporation at the next temperature interval investigated (130 ºC). At 150 ºC, 6-8 nm particles volatilized completely and 10 nm particles have a median VFR of 0.6 at 130 ºC.

The temperature range where 50% evaporation (by volume) occurs increases with particle size. For 6-10 nm particles, this transition occurs between 130 and 150 ºC. For 15 nm and above, this transition occurs between 150 and 200 ºC.

The residue, defined in this work as the VFR at 200 ºC, increases with particle size. Except for some outliers at 10 nm that reach up to 0.15, the residue of 6-10 nm particles is below 0.05. At 15 nm, the median residue is 0, but the range extends up to 0.2. At 20 nm, the median residue is 0.15, and the residue increases with particle size up to its greatest median value, which is 0.3 for 80 nm particles.

The VFR of pure AS, measured in laboratory experiments with the same system, is also shown in **Figure 5.1** as a function of particle size and temperature. The VFR of

[60]If the VFR do not change by no greater by 5 %, the VFR is classified as no evaporation.

AS shows resistance to evaporation until 150 ºC and then rapid volatilization in the 150-170 ºC range, followed by complete evaporation by 180 ºC. Compared to AS the VFR profile of all particle sizes in Bondville has a more gradual evaporation behavior, with all particle sizes having some evaporation (0.10-0.30) at 130 ºC where AS does not evaporate. Gradual evaporation is a signature of a multi-component aerosol mixture (Riipinen et al., 2010; Ristovski et al., 2010).

5.5.4 Cluster analysis of the volatility profile

The K-means clustering was applied to a total of 68 (15 nm), 170 (30 nm), 165 (50 nm) and 120 (80 nm) volatility profiles from the study. Each volatility profile is approximately 60 minutes in length and the data represent a total of 12 days of measurement. The cluster analysis results three volatility or VFR profile for 15 nm, and four clusters for 30, 50 and 80 nm (**Fig. 5.2)**. The resultant VFR cluster estimated/identified in each size are described in the **Table 5.2** and plotted in **Figure 5.2.** Within a particle size the observed VFR cluster/profile showed differences in VFR values especially at 100, and 150 ^{o}C. Values of VFR at these temperatures including 200 ^{o}C are provided in **Table 5.2**. Qualitatively, VFR cluster within each size show three different qualitative behaviors; significant evaporation at 100 to 150 ^{o}C, less than 15% evaporation at 100 ^{o}C but significant evaporation (> 15%) at 150 ^{o}C and small evaporation (<15%) till 150 ^{o}C and significant evaporation between 150-200 ^{o}C. It is likely that the variation observed in VFR clusters within a size may be associated with some known aerosol chemistry. This was also insinuated using **Figure 5.1.**

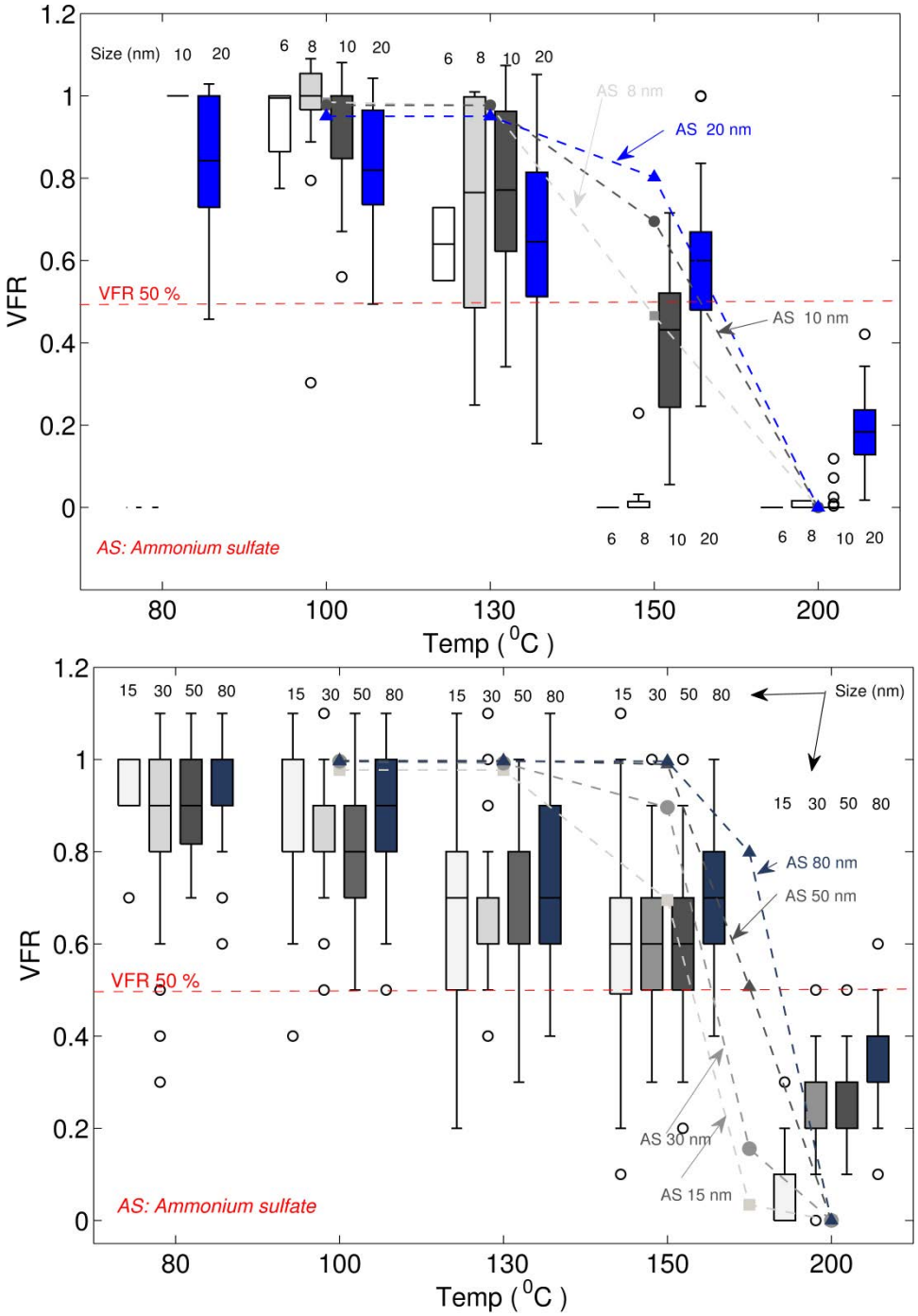

Figure 5.1 Average volatility profile of 6-80 nm particles during the BND-UIOWA campaign. The x-axis is the heater temperature in Celsius and the y-axis is the volume fraction remaining (VFR) calculated for different particle size. Top Panel contains shows the box plot of field observed VFR for 6,8,10, and 20 nm (discriminated with colors) and the line plots are pure AS VFR(indicated by arrow). Bottom panel contains the box plot of field observed VFR 15, 30, 50 and 80 nm and the line plots are the pure AS VFR.

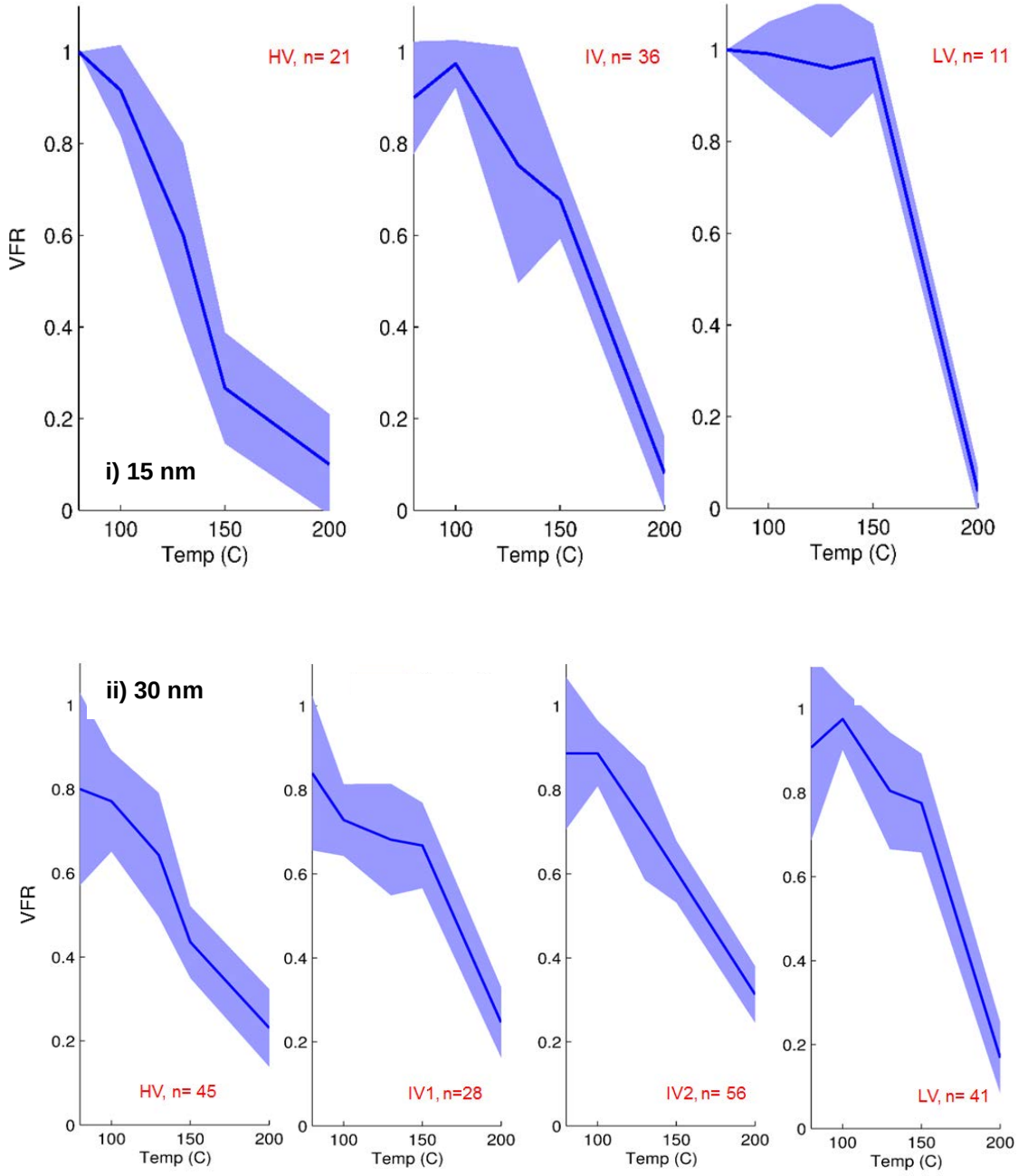

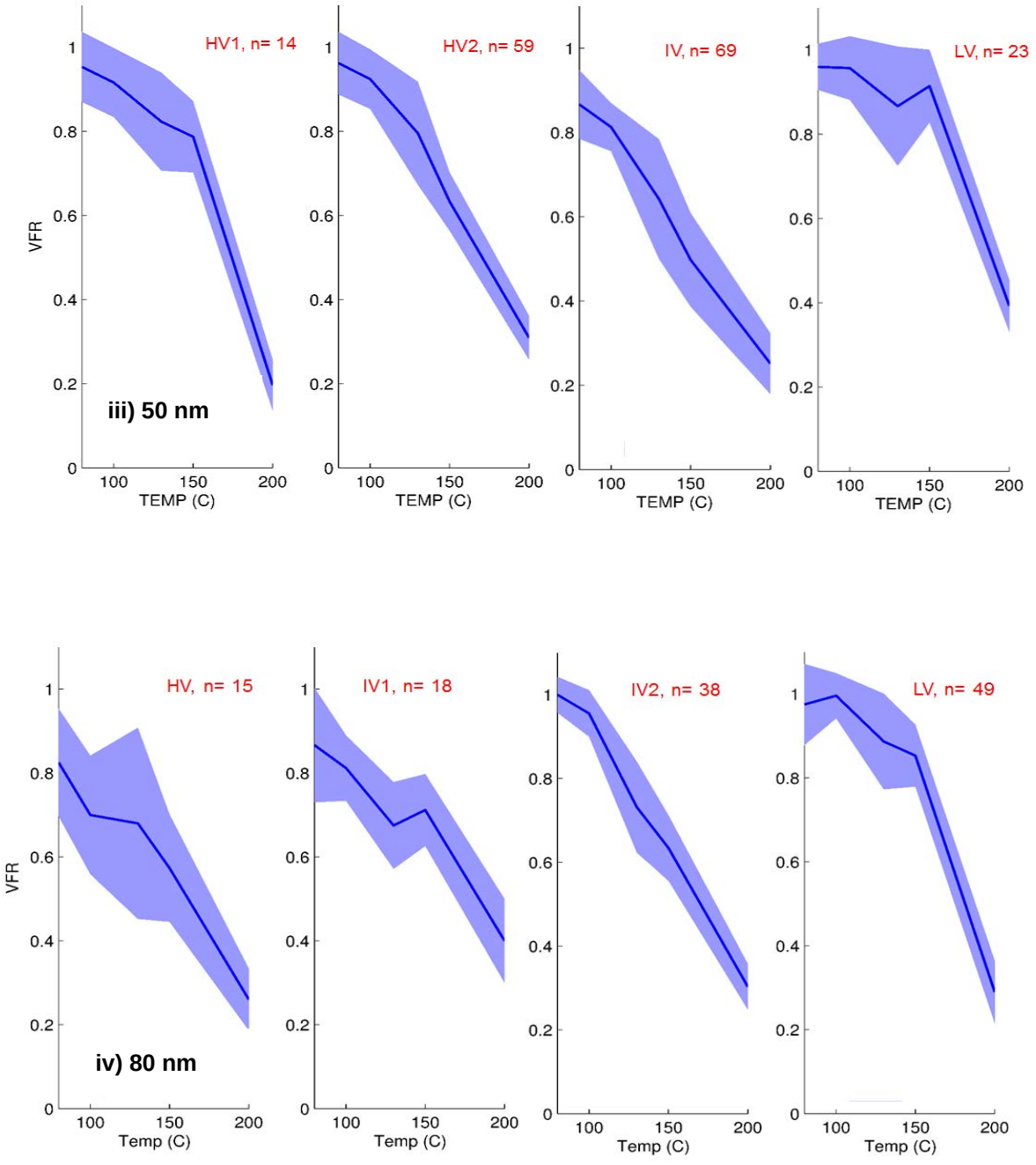

Figure 5.2 Results of K-means clustering unique volatility cluster in 15 nm (panel i), 30 nm (panel ii), 50 nm (panel iii) and 80 nm (panel iv) during the BND-UIOWA campaign (values for each cluster is also provided in Table 5.2). Each subplot in each panel shows heater temperature (x-axis) and mean VFR (y-axis). The subplots are also classified into high (HV), intermediate (IV) and least volatile (LV) profile according to average volatility. The *n* in the each subplot is the sample number.

Differences between volatility clusters are visualized in **Figure 5.3** which is a plot of VFR at 100 ^{o}C (x-axis) and 150 ^{o}C (y-axis) for each cluster. The distribution of volatility cluster in **Figure 5.3** broadly indicated three volatility class based on the *average volatility*: high volatile, (HV, 0.6 or less), intermediate volatile, (IV,0.6-0.8) and least volatile group, (LV, >0.8). The average volatility is mean of VFR at 100 ^{o}C and 150 ^{o}C. Significant evaporation (>40%) was observed at 200 ^{o}C in all sizes, and therefore is not included in the average volatility calculation. These classifications are not mutually exclusive and we observe certain overlap, especially between the HV and IV groups at 15 and 30nm.

Similar temperature dependent classification has been employed in the past (Kim et al., 2011; Paulsen et al., 2006; Tiitta et al., 2010; Wu et al., 2009).

Table 5.2 Characteristics of the VFR clusters

Dia. (nm)	**Assigned Cluster Name**	**N** (%)	**T100, T 150, T200** (VFR)	**SO_2** (ppb)	**NO_y** (ppb)	**O_3** (ppb)	**Solar Radiation** (W/m^2)	**Amb. Temp** (^{o}C)
15	High volatile	21 (31)	0.80,0.39,0.09	2.2	3.1	53.0	660.7	22.7
	Intermediate volatile	36 (53)	0.92,0.65,0.08	2.7	3.6	51.4	757.7	26.8
	Least volatile	11(16)	0.99,0.98,0.04	2.4	3.4	47.5	-	-
30	High volatile	45 (26)	0.75,0.43, 0.23	1.8	4.6	34.1	153.2	
	Intermediate volatile 1	28 (16)	0.73,0.67,0.25	2.0	3.9	43.2	388.9	20.2
	Moderately volatile 2	56 (33)	0.89,0.60,0.35	2.3	3.2	41.9	328.9	21.3
	Least volatile	41 (24)	0.95,0.76,0.16	2.1	3.3	47.5	311.7	22.8
50	High volatile1	14 (8)	0.80,0.40, 0.20	1.8	4.2	37.0	197.7	18.4
	High volatile2	59 (36)	0.66,0.52,0.27	1.5	4.7	31.9	119	15.3
	Intermediate volatile	69 (42)	0.83,0.63,0.23	1.5	3.9	39.0	211.5	19.7
	Least volatile	23 (14)	0.95,0.90, 0.39	2.2	3.6	41.2	276.6	22.3
80	High volatile	15 (13)	0.65,0.54,0.24	1.6	4.4	29.7	96.9	19.5
	Intermediate volatile 1	18 (15)	0.82,0.73,0.43	1.9	4.4	35.3	182.4	19.4
	Intermediate	38 (32)	0.93,0.62,0.29	1.7	4.1	37.2	173.4	17.1

volatile 2							
Least volatile	49 (41)	0.98,0.84,0.28	2.4	3.6	43.3	344.7	22.7

Across all particle sizes, the high volatile group (HV) is characterized by significant evaporation >20% at 100 ^{o}C to 40% at 150 ^{o}C. The intermediate volatility group (IV) is characterized by 10-15% evaporation at 100 ^{o}C and 30-40% evaporation at 150 ^{o}C. The least volatile group (LV) is characterized by 10% or less evaporation at 100 ^{o}C and < 30% at 150 ^{o}C. The frequency distribution of these three volatile profiles is similar, dominate by IV (40-50% of the total sample, see **Table 5.2**) and HV (30-40%).

Although VFR is insufficient to establish chemical composition definitively, LV profile, in **Figure 5.3,** across various sizes (except 15 nm) may be characteristically similar to the pure AS. For comparison the field TD-AMS profile of sulfate by Huffman (2009) also showed minor evaporation until 150 ^{o}C, and transition to vapor phase > 150 ^{o}C, with a minor or low residue (< 10%) at 200 ^{o}C. IV and LV profiles in 15 nm both show similar proximity to the pure AS. For each size, the IV profile is also associated with higher ambient SO_2 concentration and solar radiation, compared to other profile (see **Table 5.2**).

The nature of evaporation observed with HV profile (significant evaporation at 150 ^{o}C and significant residue at 200 ^{o}C) and is association with period of higher NO_x indicate particle from fresh or local emission. IV group, mostly in 30-80 nm depict gradual nature of evaporation from 100-200 ^{o}C and is likely a result of inorganic and organic mixture (Riipinen et al., 2010) or a complex mixture of semi-volatile organics over a wide range of volatilities (Donahue et al., 2006; Huffman et al., 2009).

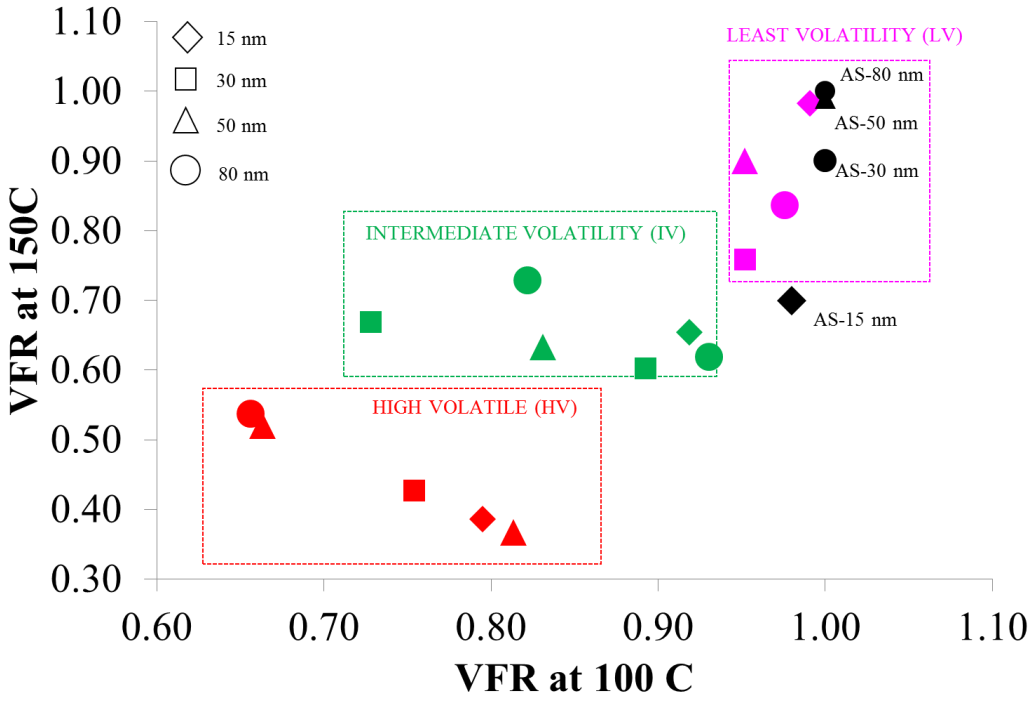

Figure 5.3 Cluster visualized by their VFR at 100 and 150 ^{o}C (x-axis VFR 100 ^{o}C and y-axis VFR at 150 ^{o}C) observed in each size during the BND-UIOWA campaign. The distribution of pure AS is also shown for each of the size categories (indicated by a black color). The three volatility class identified in Figure 5.2 is distinguished by different colors; HV (red), IV (green) and LV (magenta).

5.5.5 PBE events and volatility profile of nuclei mode particles

The change in particle composition during particle burst events was explored using the 15 and 30 nm clusters. Five particle formations (PBE events) were examined during TDMA operation. Three of the five days (5 Sept. 5th 2013, 22 and 23rd April 2014) were classified as PBE-S events with smooth and continuous growth and relatively lower SO_2 concentration (<1 ppb). The remaining two days (6 Sept. 2013 and 25th May 2014) were PBE-D events. In **Figure 5.4,** the left two panels are the frequency distribution of different VFR profiles during all the five PBE events. The right two panels graph the frequency distribution for each day separately. As evident in **Figure 5.4**, PBE-D are typically associated SO_2 concentrations in excess of 3 ppb, while PBE-S events

have concentrations below 1 ppb. Increase in the concentration of SO_2 correlates with the enhancement of LV profile, especially for 15 nm. In contrast, PBE-S events in both sizes have significant presence IV profile.

Within PBE-D there are slight differences in the presence of volatility profile. The Sept. 5 event, IV is the major profile in 15 nm compared to April events dominated by HV. This is also consistent with the observation in 30 nm particles.

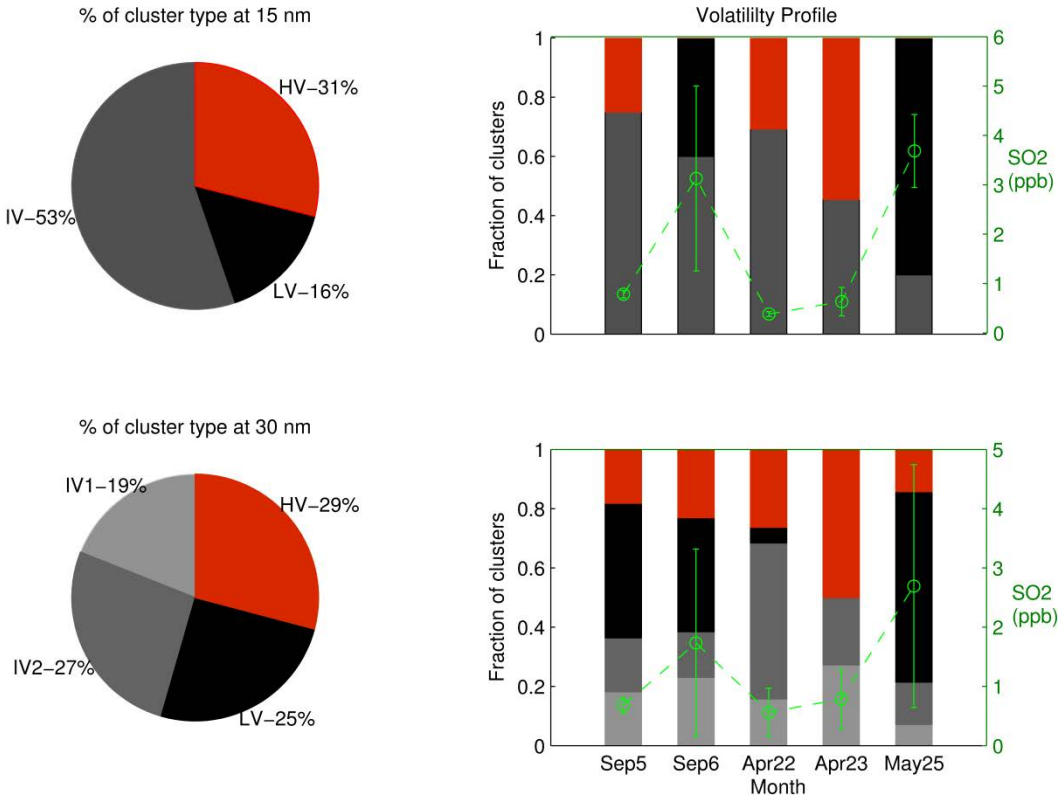

Figure 5.4 Frequency distribution of different cluster types (HV, IV and LV) in 15 and 30 nm during 5 PBE events during the TDMA operation during BND-UIOWA campaign. The left two panels (pie chart) show the aggregate frequency distribution of clusters during the PBE events for 15 and 30 nm. The right two panels (stacked bar charts) show the each day frequency distribution volatility profiles in these two particle sizes. The different volatility profiles are also indicated by distinct color on both left and right panel. SO_2 concentration (in ppb) is indicated by the *green line plot*, and is overlaid on the bar chart and the concentration is indicated by the right-hand side axis of the bar chart. The error bars in the SO_2 indicate the standard deviation.

5.5.6 Evaporation resistant residue at 200 ^{o}C

Multitude of source, atmospheric condition and chemical has been reported in the literature for the presence of residue in the particles. These include traffic and combustion (Philippin et al., 2004; Wehner et al., 2004), polluted and moderately polluted condition (Birmili et al., 2010; Wehner et al., 2009a), particle formation events (Wehner et al., 2005c), secondary organics (Ehn and Pet, 2007; Kokkola et al., 2014), other organics such as PAH, BC and organic nitrate (Hakkinen et al., 2012).

Residue in each particle size is presented in **Figure 5.5** (also shown are VFR values at 100 ^{o}C and 150 ^{o}C). This increasing trend in residue fraction with particle size has been observed in other volatile studies (Wehner et al., 2009a; Wehner et al., 2004). The average residue fraction for the aggregate sample is above 20% for 30-80 nm, compared to <10-15% in 15 nm. Also presented in the **Figure 5.5** (right panel), the average mode diameter at 200 ^{o}C for 10 to 80 nm to illustrate the particle size of the residue. Steady rise in the mode diameter is observed, but as also evident in the volume fraction, the mode values sharply rise at or after 20 nm.

Examining the presence of residue with respect to different volatility clusters (**Figure 5.2**) indicate that residue is present in all the cluster type (**Table 5.2**). The HV group in all sizes shows proportionate residue fraction to intermediate and least volatile cluster. The presence of residue in the most volatile cluster could be associated with fresh emission from local sources or freshly formed organics, which are reported to have heat resistant core (Wehner et al., 2004).

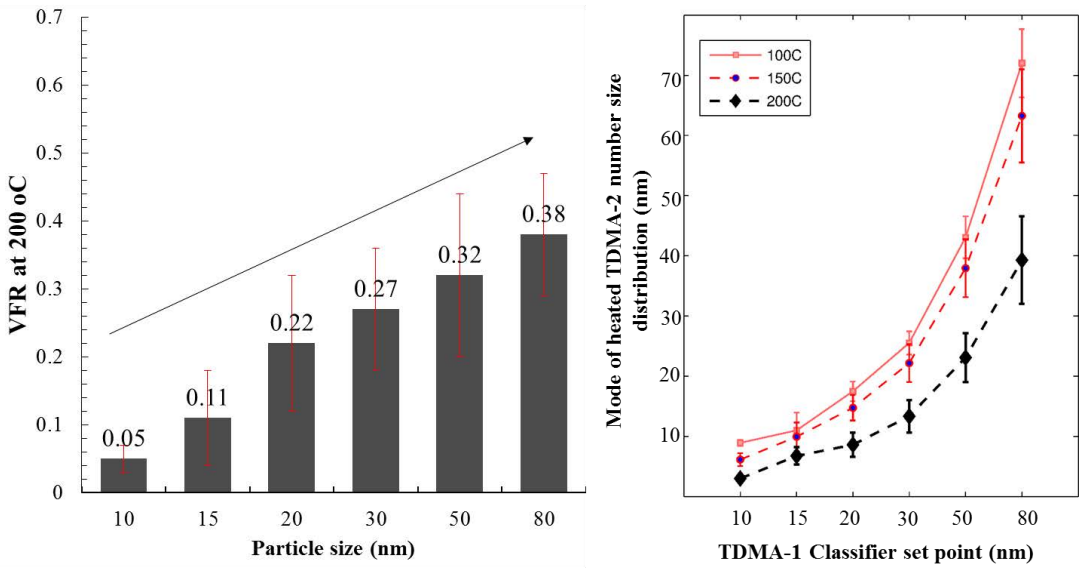

Figure 5.5 Fraction of VFR at three temperatures (100°C, 150 °C and 200 °C) at 6 sizes from 10 nm to 80 nm (left panel) and average mode diameter of the size distribution at three temperatures (right panel).

5.5.6.1 Size distribution of the residue

The size distributions of the residue at 15, 30, 50 and 80 nm at four different sampling months are shown in **Figure 5.6**. The mode of size distribution varies with different sampling period, shifting to the higher sizes in April and May compared to August and September. This shift is prominent for 30-80 nm, but not at 15 nm. Hakkinen et al., (2012) also reports higher residue mode in spring time than summer, also observed by although in a different atmospheric regime (Boreal forest) than the current study.

Likewise mean VFR in April for 30 and 50 nm are ~ 0.35 compared to mean VFR is in the range of 0.2-0.25 in other sampling months where the (See **Appendix** Section 9.3 Presence of residue across four sizes in four different months). Mean VFR of 15 nm, in September, April and May, contributed by PBE-S or D events and local emission showed significant variation in the residue. Residue of 15 nm in April clearly shows higher residue (~15%) compared to September (PBE events) and May which showed no residue to ~ 10% residue.

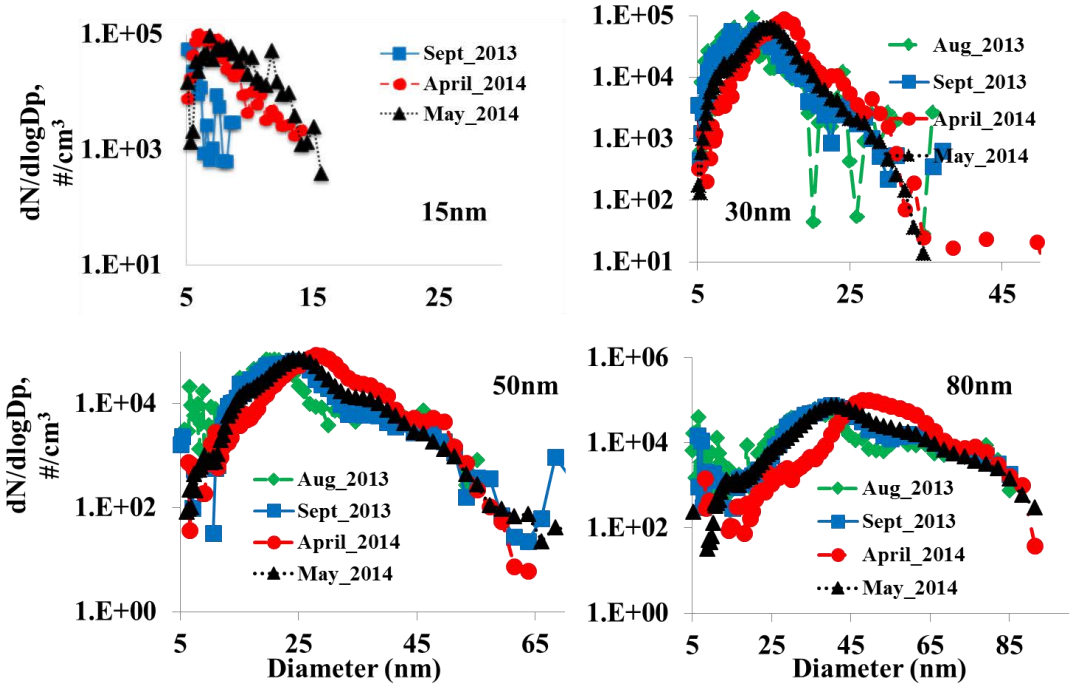

Figure 5.7 The resultant particle size distribution of the residue (or after heating to 200°C) for four different particle size (15, 30, 50 and 80 nm) observed during the four sampling periods in BND-UIOWA. The figure is a semi-log axis (y-axis is in log scale) and shows the number concentration and x-axis shows the particle diameter in nm.

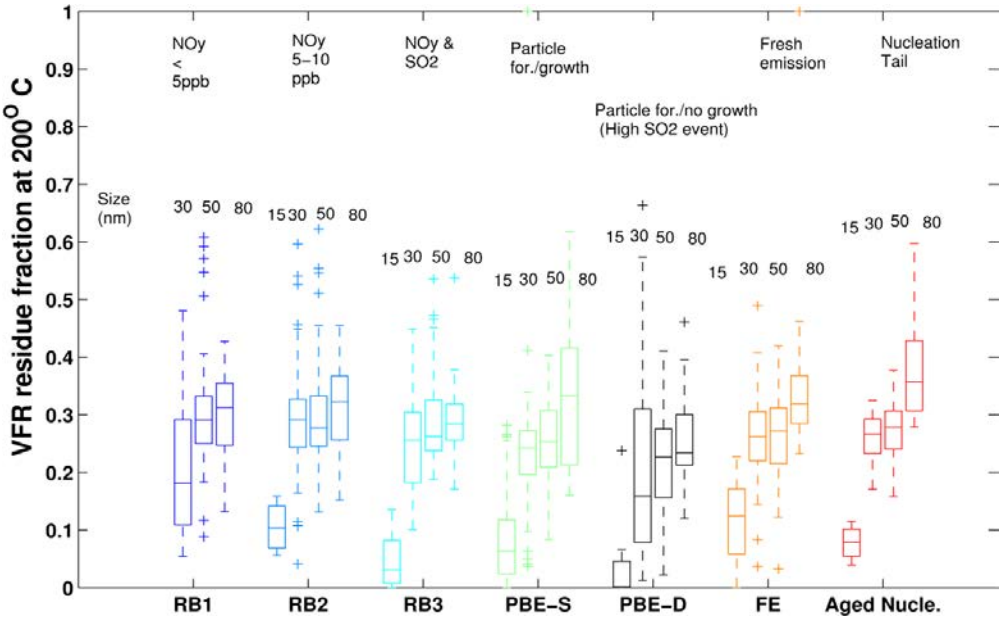

Figure 5.6 Association of different atmospheric condition (background, PBE-S, PBE-D, aged nucleation and fresh emission) and residue in four particle sizes during the BND-UIOWA campaign in Bondville, IL. Atmospheric conditions (distinguished by a unique color) are arranged along the x-axis and mean VFR for various particles are in y-axis.

To explicitly relate specific atmospheric condition in each sampling month to residue variability, volatility data was categorized based on the atmospheric conditions. Four specific atmospheric conditions were observed during the complete study period.

The majority of sampling time was background (RB, 50% of total sample), followed by particle burst with growth (PBE-S, 18% of total sample), particle burst with no growth (PBE-D, 15%) and local emission (LE, 7%).

In general, concentration of sulfur indicates sensitivity with residue fraction. High sulfur time period was associated low residue across all sizes. Residue in particle below 15 and 30 nm were more sensitivity to sulfur than 50 and 80 nm (**Fig. 5.7**). The NO_y levels varies during the sampling period from < 3 ppb levels to ≥ 10 ppb, but the presence of residue did not show any trends to changes in a levels. The background condition were divided into three categories (RB1, RB2 and RB3) based on the varying levels of NO_y and SO_2 (as indicated in Fig. 5.7), however no clear difference is observed within them.

Presence of residue in 15 nm was observed during particle formation with growth (PBE-S) atmospheric condition (VFR ~ 15%) and also observed during period of local emission impact (early morning and evening). To closely analyze how residue changes during the particle burst and growth, the five PBE events were further selected for residue analysis (**Figure 5.9**). Residue in 15 nm during particle formation events were observed only during PBE-S and disappeared during PBE-D period. Within the PBE-S, the median residue in 15 nm is 25% for Sept. 5th event compared to 10% in April 22 and 23rd. Similar to 15 nm, residue in 30 and 50 nm particles is higher in PBE-S than PBE-D. The differences in residue in PBE-S and PBE-D may indicate that changes in SO_2 levels are associated with the variation of residue. It is likely that during low SO_2 condition, organic

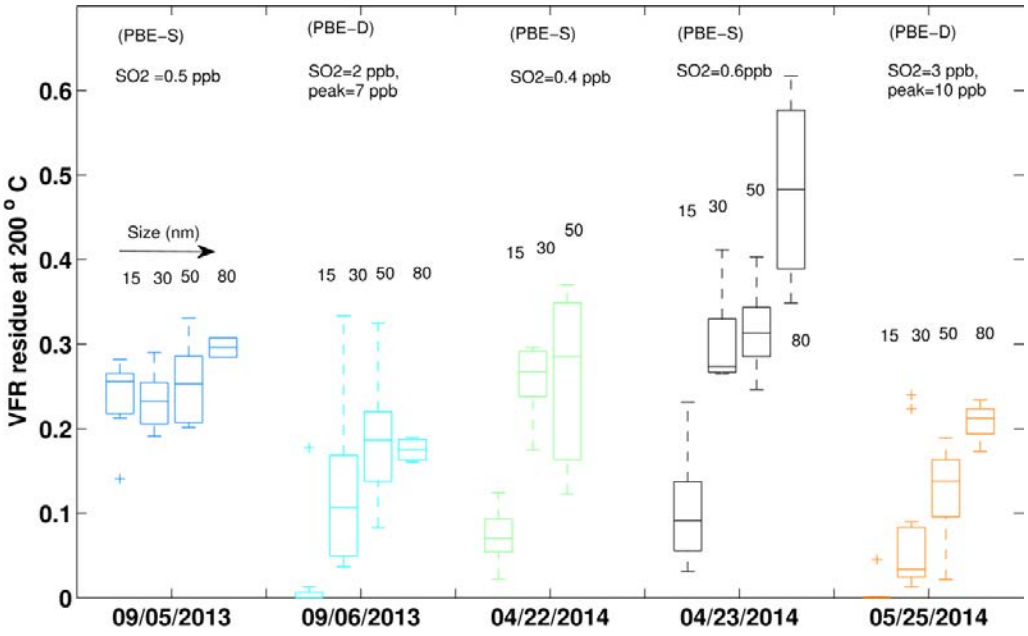

Figure 5.8 Variation of Residue during PBE-S and PBE-D events across different particle size during the BND-UIOWA campaign in Bondville, IL. Five PBE events are shown here (distinguished by color). The y-axis is the mean VFR for different sizes.

condensation is favored (Ehn et al., 2007), which may lead to higher residue, compared to strong SO_2 events where sulfuric acid condensation on particle may be significant (Sakurai et al., 2005b; Stolzenburg et al., 2005).

To statistically relate the presence or absence of residue with various trace gases, a Pearson linear correlation (95% confidence interval, Cl), between various trace gases and residue at 15, 30 50 and 80 nm, was performed. Correlation coefficients are shown in **Figure 5.9**. Histograms of the variables appear along the matrix diagonal in the figure. The correlation coefficients highlighted in red indicate which pair of the variables have correlations significant different from zero. All the trace gases, shown in the figure, are in ppb, temperature is in ^{o}C, solar radiation (SR) is in W/m^2. The correlation coefficient provides some confirmation of the relation of SO_2 level to the residue presence. However

other trace gas such as O_3 and solar radiation (SR) also show significant negative relationship with the residue.

The correlation between residue of different particle size (15, 30, 50 and 80 nm) and SO_2 showed negative correlation and the correlation is statistically significant at 95% confidence interval. Increase in SO_2 concentration favors less residues which may indicate that particles are composed mainly of ammonium sulfate. Pure ammonium sulfate are completely volatilized at 200 ^oC, and may be leading to low residue during strong SO_2 event and thus shows overall negative correlation. Among the four particle size, the correlation is much stronger (R = -0.29 and -0.45, 0.95 Cl) at 15 and 30 nm compared to 50 and 80 nm (R = -0.12, -0.19).

Strong influence of SO_2 at nuclei size is evident other field studies (Häkkinen et al., 2012; Sakurai et al., 2005a; Wehner et al., 2009c) and as the particles grows the influences of SO_2 weakens. Pryor et al. (2013) indicated, through mass closure experiment, the likelihood of organic condensation for particle size greater than 30 nm. This study, via residue analysis, indicates residue presence is weakly related to SO_2 at 50 and 80 nm, but has significant relation with particle 15 and 30 nm.

Likewise, residue at all the particle size showed negative correlation with ozone (O_3) and SR. However the strength of relation does not show any size dependence as observed with SO_2. SR can indirectly influence the presence of residue. Organic vapor condensation is usually a photochemical reaction and thus reducing photochemistry is likely to reduce the oxidization product for partitioning into particle (Wehner et al., 2005a). Studies shows indicate that low volatility compounds are associated with oxidation of secondary organic aerosol from ozone oxidation, larger “oligomers” and

very low volatility organo-sulfates (Ehn et al., 2014; Fry et al., 2013). Although it is not clear what fraction of these secondary organic aerosol (SOA) are low volatile, but the estimated range from 0.33 to 0.5 (Donahue et al., 2014). Association of temperature is relatively weak, but significant in 30-80 nm.

i) 15 nm

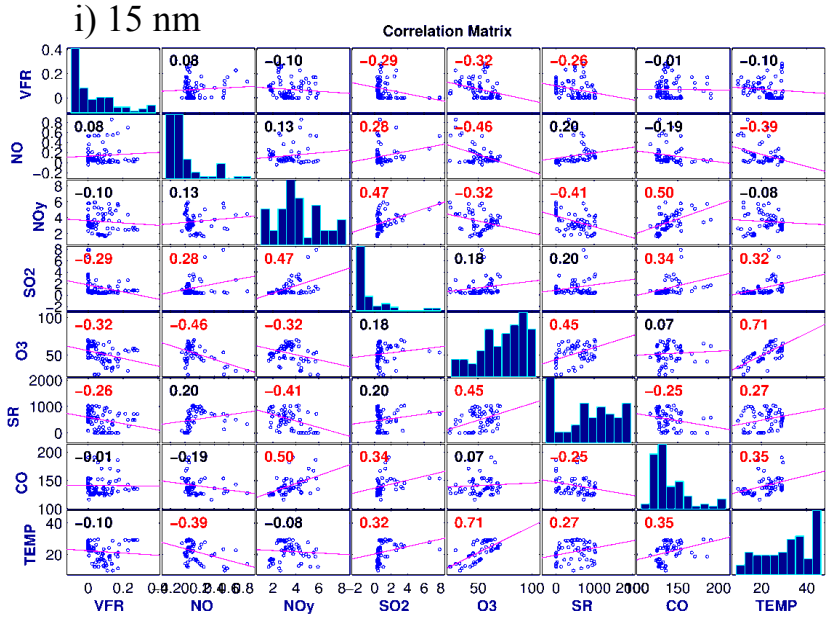

ii) 30 nm

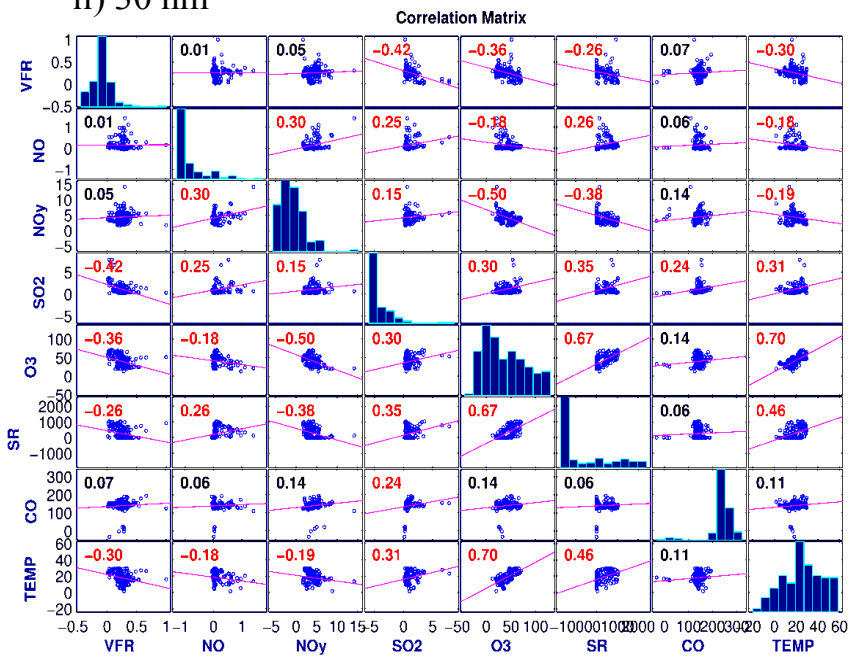

ii) 50 nm

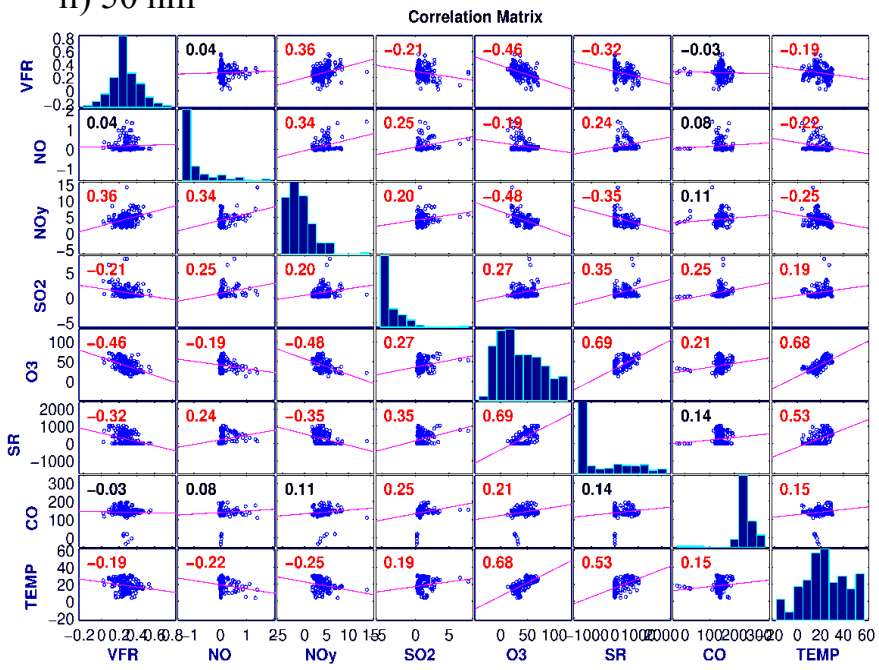

iv) 80 nm

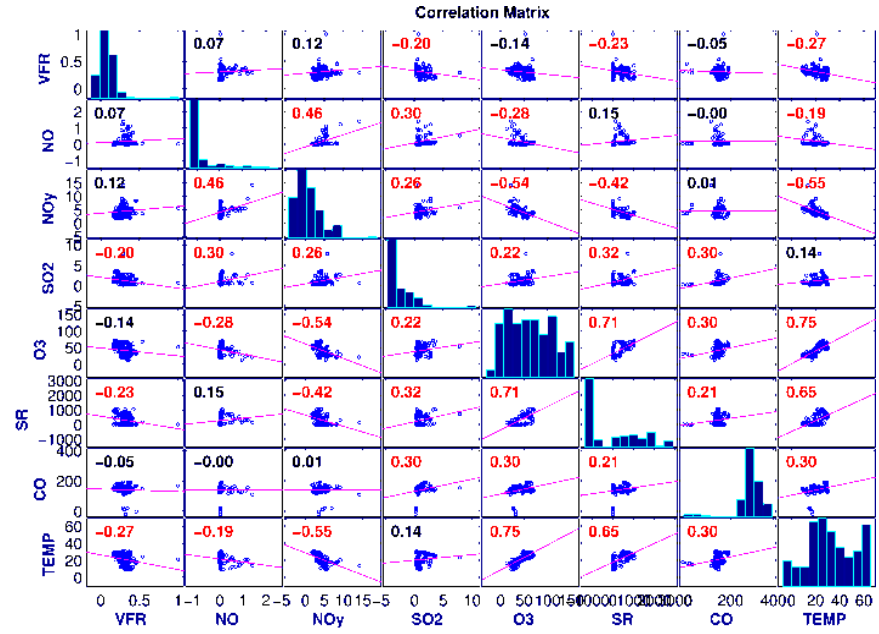

Figure 5.9 Paired correlation between residue, trace gas and meteorology. Four panels (i, ii, iii and iv) indicate four particle size studied during the BND-UIOWA campaign in Bondville, IL. Histogram of the variables appears along the matrix diagonal; scatter plots of variables pair appear off diagonal. The slopes of the least square reference lines in the scatter plots are equal to the displayed correlation coefficients. All the trace gases are in ppb, temperature is in ^{o}C, solar ration (SR) is in W/m^2. The correlation coefficients highlighted in red indicate which pair of the variables have correlations significant different from zero.

5.5.7 External or internal mixture

Evidence of multiple modes in the size distribution of the residue indicates the presence of external mixture in the V-TDMA analysis. Analysis of size distribution reveals that presence of external mixture predominantly at 50 and 80 nm and observed during night time and early morning (5-9 am). External mixture observed in the morning is likely due to the impact of local emission. The increase in the non-volatile core during night time is also reported by Hakkinen et. al., (2012).

At higher sizes, (20 to 80 nm) external mixtures account for 20-30% of the total sample number. Less than 5% (5 /123, see **Appendix**) of heated samples in 15 nm indicated evidence of external mixture 20-30% compared to >15 nm. Size distribution also revealed that the mode of the external mixture consistently observed at 9-15 nm, 22-26 nm, 23-26 nm, 35-40 nm and 60-65 nm.

The frequency of external mixture (of the total sample during that season) is relatively higher in April compared to other sampling period which co-incident is consecutive particle formation events (PBE-S).

5.5.8 Broader picture of aerosol chemistry in the Midwest

5.5.8.1 General overview

The sources of ultrafine particles in the Midwest are likely to be dominated by secondary sources in Bondville IL which represent a vast area with agriculture land use. During the TDMA operation period, the other two sources were fresh emission likely from the nearby city centers and industrial emission and late afternoon burst observed during high ozone and temperature period. The exact contributions from these three sources need to be quantified.

The TDMA operation was conducted for four different months: August, September, April and May. August and September 2013 had meteorologically above average temperature compared to earlier years. The AQI during these two months was also moderate and were frequently impacted by smoke from forest fire events in North West and South West US. Early weeks of September 2013 (or when TDMA II was deployed) showed relatively high ozone concentration which also was the highest temperature and humidity days of the month. April 2014 was one of the cleanest month (in terms of AQI, forest fire impact, O_3 concentration etc.) during the whole Bondville campaign especially the third week of April. Strong low pressure system dominates the region during this period, accompanied by a warm front moving from North West to South East with precipitation.

Particle formation events observed during April and May were associated with a cleaner environment (low particulate mass and low pressure system) for the initiation of nucleation. During the third week of April, enhancement in the aerosol sulfate concentration is reported by IMPROVE measurements (see Appendix 9.3 IMPROVE time series for April and May 2014) and Navy Aerosol Analysis and Prediction System (NAAPS) which also results in moderate AQI in the region. By the time the third TDMA was deployed on the 21st of April, 2014, a high pressure system leaves Bondville moving from north to south east. Particle formation events were observed on the 22nd of April and as the high pressure system dissipates completely, stronger nucleation was observed on 23rd and 24th of April.

May 2014 is also another clean month during the field campaign. TDMA was deployed on the fourth week of May 2014 from starting May 22nd to 26th 2014. NAAPS

model showed unusual dust impact at the Midwest region during this period which is coming from South west. At the start of TDMA deployment on May 22nd, moderate air quality exists due to dust and sulfate enhancement (as indicated by NAAPS and IMPROVE). Consequently no particle formation was recorded during this period, except on May 25th when a strong particle burst was observed with elevated mean sulfate concentration.

5.5.8.2 Associating particle volatility with regional changes

Comparing the volatility of aerosol across various sampling months, 15, 30 and 50 nm particle show all the volatility clusters. However a distinct difference was observed between August, September to April and May. As described in the previous section, meteorological conditions were different in August and September compared to April and May. August and September are characterized by particles with strong IV and LV clusters compared to April and May when IV dominate among the three clusters.

The month of April has the relatively lowest mean SO_2 concentration, and with consecutive nucleation days. This coincides with the dominance of IV cluster dominates in 15, 30 and 50 nm. The weak SO_2 events in April also coincide with the arrival of northerly air mass. Prior studies (Pryor et al., 2014; Shantz et al., 2012; Yue et al., 2014) in the Midwest have indicated that the northerly air mass to be rich in biogenic VOC such as mono-terpenes, toluene, isoprene. Rich biogenic VOC in the northerly air mass may assist in the growth of the freshly nucleated particles in the Midwest (VanReken et al., 2015). However the nature of reaction mechanism (condensation, semi-volatile partition or heterogeneous reaction) causing the growth is still not known. We also observed that during low sulfur condition, significant (10-15 %) fraction of the nuclei mode particle,

especially 15 nm, has a evaporation resistant residue. Dominance of IV clusters and the presence of low or non-volatile core from our measurement indicate that nucleation and growth of particle may be associated with organics along with sulfate. The higher presence (or frequency) of IV clusters in larger size such as 50 nm compared to 15 nm also indicate that organic constitute a larger fraction with increasing size.

Air mass from South East or West impacting the Bondville site was usually rich in SO_2 concentration as evident during May campaign and September. Among other parameters, the enhancement of SO_2 was associated with the LV clusters in the particle size with no residue. LV clusters have a similar volatility profile to a pure ammonium sulfate. This evidence suggests that air mass from south which is likely due to anthropogenic source is related to a LV cluster.

5.6 Conclusions and future work

This chapter has summarized size-resolved volatility analysis of UFPs from a yearlong field campaign in Bondville, IL. Analysis of volatility profile was performed using K-means cluster analysis. At least three types of profile in 15, 30, 50 and 80 nm is observed. Among the three profiles, high volatile profile showed significant evaporation resistance residue at 200 ^{o}C and relative volatile profile before 200 ^{o}C. Intermediate volatile profile is likely to be a mixture of ammonium sulfate and possible organics, and least volatile profile resembles to that of pure ammonium sulfate. The presence of a volatility profile at various sizes was further explored during particle formation and growth period.

Residue is consistently observed at 200 ^{o}C in all sizes from 15 to 80 nm. The amount of residue was positively correlated with particle size; volume fraction of residue

increases from 10-15% in 15 nm to 30-40% in 80 nm. External mixture was examined using size distribution of the residue and was observed in 20-30% samples, especially at 30, 50 and 80 nm. The timing and characterization of the external mixture with respect to different mode were also analyzed.

The occurrence of the residue was evaluated by analyzing its association with trace gases, atmospheric condition, meteorology and different atmospheric condition. Strong associations were observed with ozone (O_3), sulfur dioxide (SO_2) and solar radiation.

The future work should involve adding an evaporation model to generate a volatility basis set for the identified clusters. At this point the quantitative differences in the identified volatility cluster are based on temperature. A stronger chemical basis can be approximated by quantifying their volatility basis set using an evaporation model. Relevant to building a robust evaporation model and constrain it to field data, estimation of key thermodynamic parameters is essential. The application of parameters is reliant on the assumption that equilibrium is achieved in the V-TDMA system. The V-TDMA future field work should focus on adding measurement of volatility at multiple residence time to constraint the equilibrium sensitive parameters in the evaporation model.

It was felt that inter-comparison of TDMA results with the existing TDMA design are complicated and subject to uncertainty with temperature profile, heating mechanism, adsorber and other artifact. Huffman et al. (2010) provides a wonderful library of volatility profile from many different TDMA conducted in laboratory and field environment. Use of such profile for comparing with our identified clusters was thus not performed. Therefore V-TDMA field operation will require a building up of a volatility

profile library of many different aerosol types which can be compared with the field data for many different analyses including inferring composition of the aerosol.

Evidence of residue is detected in the study at all sizes. However it is unclear whether these residue are the resultant product of heating or the aerosol do have an actual non-volatile core which is resistant even at high temperature. The likely solution to this issue can only be solved using a mass spectrophotometry (Kuwata et al., 2012).

Laboratory experimentation using various mixture of aerosol types to quantify this effect which will aid many V-TDMA results reporting these clusters. Aerosol dominated by organics is reported to undergo oligomerization in the laboratory and field environment where as the no evidence exist for common inorganic aerosol types with or without a fraction of organics. These are interesting experiment that needs to be quantified to trust V-TDMA operation above 100 ^{o}C.

5.7 Acknowledgements

I would like to thank Mike Snider for his continual effort in maintaining and operating the BEARS site including our temporary station. I would like to acknowledge Christopher Lehmann to collaborate in this field campaign and allow access to the facilities at the Illinois State Water Survey. From Stanier research group, I would like to thanks Robert Bullard for leading this campaign and helping me in many different ways. Also Matt Johnson, undergraduate in the Stanier research group, who has been instrumental in interpreting TDMA data, manuscript write up and feedback.

Funding was provided by the National Science Foundation under Grant No. ATM-0748602.

5.8 Author's contributions

This work is under preparation to be submitted to *Atmospheric Environment*. A. Singh, and C. Stanier designed the study and A. Singh performed all the field sampling, measurement analysis and manuscript preparation. Robert Bullard co-led the field sampling for the Stanier group.

5.9 References

An, W.J., Pathak, R.K., Lee, B.-H., Pandis, S.N., 2007. Aerosol volatility measurement using an improved thermodenuder: Application to secondary organic aerosol. Journal of Aerosol Science 38, 305-314.

Beddows, D.C.S., Dall'Osto, M., Harrison, R.M., 2009. Cluster Analysis of Rural, Urban, and Curbside Atmospheric Particle Size Data. Environmental Science & Technology 43, 4694-4700.

Beddows, D.C.S., Dall'Osto, M., Harrison, R.M., Kulmala, M., Asmi, A., Wiedensohler, A., Laj, P., Fjaeraa, A.M., Sellegri, K., Birmili, W., Bukowiecki, N., Weingartner, E., Baltensperger, U., Zdimal, V., Zikova, N., Putaud, J.P., Marinoni, A., Tunved, P., Hansson, H.C., Fiebig, M., Kivekas, N., Swietlicki, E., Lihavainen, H., Asmi, E., Ulevicius, V., Aalto, P.P., Mihalopoulos, N., Kalivitis, N., Kalapov, I., Kiss, G., de Leeuw, G., Henzing, B., O'Dowd, C., Jennings, S.G., Flentje, H., Meinhardt, F., Ries, L., van der Gon, H.A.C.D., Visschedijk, A.J.H., 2014. Variations in tropospheric submicron particle size distributions across the European continent 2008-2009. Atmospheric Chemistry and Physics 14, 4327-4348.

Birmili, W., Heinke, K., Pitz, M., Matschullat, J., Wiedensohler, A., Cyrys, J., Wichmann, H.E., Peters, A., 2010. Particle number size distributions in urban air before and after volatilisation. Atmospheric Chemistry and Physics 10, 4643-4660.

Brines, M., Dall'Osto, M., Beddows, D.C.S., Harrison, R.M., Querol, X., 2014. Simplifying aerosol size distributions modes simultaneously detected at four monitoring sites during SAPUSS. Atmospheric Chemistry and Physics 14, 2973-2986.

Brock, G., Datta, S., Pihur, V., Datta, S., 2008. clValid: An R package for cluster validation. Journal of Statistical Software 25, 1-22.

Burtscher, H., Baltensperger, U., Bukowiecki, N., Cohn, P., Huglin, C., Mohr, M., Matter, U., Nyeki, S., Schmatloch, V., Streit, N., Weingartner, E., 2001. Separation of

volatile and non-volatile aerosol fractions by thermodesorption: instrumental development and applications. Journal of Aerosol Science 32, 427-442.

Clarke, A.D., 1991. A thermo optic technique for insitu analysis of size-resolved aerosol physicochemistry. Atmospheric Environment Part a-General Topics 25, 635-644.

Crippa, P., Spracklen, D., Pryor, S.C., 2013. Satellite-derived estimates of ultrafine particle concentrations over eastern North America. Journal of Geophysical Research-Atmospheres 118, 9968-9981.

Dal Maso, M., Kulmala, M., Riipinen, I., Wagner, R., Hussein, T., Aalto, P.P., Lehtinen, K.E.J., 2005. Formation and growth of fresh atmospheric aerosols: eight years of aerosol size distribution data from SMEAR II, Hyytiala, Finland. Boreal Environment Research 10, 323-336.

Donahue, N.M., Robinson, A.L., Stanier, C.O., Pandis, S.N., 2006. Coupled partitioning, dilution, and chemical aging of semivolatile organics. Environmental Science & Technology 40, 2635-2643.

Donahue, N.M., Robinson, A.L., Trump, E.R., Riipinen, I., Kroll, J.H., 2014. Volatility and Aging of Atmospheric Organic Aerosol, in: McNeill, V.F., Ariya, P.A. (Eds.), Atmospheric and Aerosol Chemistry, pp. 97-143.

Ehn, M., Petaejae, T., Birmili, W., Junninen, H., Aalto, P., Kulmala, M., 2007. Non-volatile residuals of newly formed atmospheric particles in the boreal forest. Atmospheric Chemistry and Physics 7, 677-684.

Ehn, M., Thornton, J.A., Kleist, E., Sipila, M., Junninen, H., Pullinen, I., Springer, M., Rubach, F., Tillmann, R., Lee, B., Lopez-Hilfiker, F., Andres, S., Acir, I.H., Rissanen, M., Jokinen, T., Schobesberger, S., Kangasluoma, J., Kontkanen, J., Nieminen, T., Kurten, T., Nielsen, L.B., Jorgensen, S., Kjaergaard, H.G., Canagaratna, M., Dal Maso, M., Berndt, T., Petaja, T., Wahner, A., Kerminen, V.M., Kulmala, M., Worsnop, D.R., Wildt, J., Mentel, T.F., 2014. A large source of low-volatility secondary organic aerosol. Nature 506, 476-+.

Fierz, M., Vernooij, M.G.C., Burtscher, H., 2007. An improved low-flow thermodenuder. Journal of Aerosol Science 38, 1163-1168.

Frey, A., Rose, D., Wehner, B., Mueller, T., Cheng, Y., Wiedensohler, A., Virkkula, A., 2008. Application of the Volatility-TDMA technique to determine the number size distribution and mass concentration of less volatile particles. Aerosol Science and Technology 42, 817-828.

Fry, J.L., Draper, D.C., Zarzana, K.J., Campuzano-Jost, P., Day, D.A., Jimenez, J.L., Brown, S.S., Cohen, R.C., Kaser, L., Hansel, A., Cappellin, L., Karl, T., Roux, A.H., Turnipseed, A., Cantrell, C., Lefer, B.L., Grossberg, N., 2013. Observations of gas- and

aerosol-phase organic nitrates at BEACHON-RoMBAS 2011. Atmospheric Chemistry and Physics 13, 8585-8605.

Fuentes, E., McFiggans, G., 2012. A modeling approach to evaluate the uncertainty in estimating the evaporation behaviour and volatility of organic aerosols. Atmospheric Measurement Techniques 5, 735-757.

Häkkinen, S., Äijälä, M., Lehtipalo, K., Junninen, H., Backman, J., Virkkula, A., Nieminen, T., Vestenius, M., Hakola, H., Ehn, M., 2012. Long-term volatility measurements of submicron atmospheric aerosol in Hyytiälä, Finland. Atmospheric Chemistry and Physics 12, 10771-10786.

Hong, J., Hakkinen, S.A.K., Paramonov, M., Aijala, M., Hakala, J., Nieminen, T., Mikkila, J., Prisle, N.L., Kulmala, M., Riipinen, I., Bilde, M., Kerminen, V.M., Petaja, T., 2014. Hygroscopicity, CCN and volatility properties of submicron atmospheric aerosol in a boreal forest environment during the summer of 2010. Atmospheric Chemistry and Physics 14, 4733-4748.

Huffman, J.A., Docherty, K.S., Aiken, A.C., Cubison, M.J., Ulbrich, I.M., DeCarlo, P.F., Sueper, D., Jayne, J.T., Worsnop, D.R., Ziemann, P.J., Jimenez, J.L., 2009. Chemically-resolved aerosol volatility measurements from two megacity field studies. Atmospheric Chemistry and Physics 9, 7161-7182.

Huffman, J.A., Ziemann, P.J., Jayne, J.T., Worsnop, D.R., Jimenez, J.L., 2008. Development and Characterization of a Fast-Stepping/Scanning Thermodenuder for Chemically-Resolved Aerosol Volatility Measurements. Aerosol Science and Technology 42, 395-407.

Johnson, G., Ristovski, Z., Morawska, L., 2004. Application of the VH-TDMA technique to coastal ambient aerosols. Geophysical Research Letters 31.

Jonsson, A.M., Hallquist, M., Saathoff, H., 2007. Volatility of secondary organic aerosols from the ozone initiated oxidation of alpha-pinene and limonene. Journal of Aerosol Science 38, 843-852.

Kalberer, M., Paulsen, D., Sax, M., Steinbacher, M., Dommen, J., Prevot, A.S.H., Fisseha, R., Weingartner, E., Frankevich, V., Zenobi, R., Baltensperger, U., 2004. Identification of polymers as major components of atmospheric organic aerosols. Science 303, 1659-1662.

Kanawade, V.P., Benson, D.R., Lee, S.-H., 2012. Statistical analysis of 4-year observations of aerosol sizes in a semi-rural continental environment. Atmospheric Environment 59, 30-38.

Karnezi, E., Riipinen, I., Pandis, S.N., 2014. Measuring the atmospheric organic aerosol volatility distribution: a theoretical analysis. Atmospheric Measurement Techniques 7, 2953-2965.

Karydis, V.A., Capps, S.L., Moore, R.H., Russell, A.G., Henze, D.K., Nenes, A., 2012. Using a global aerosol model adjoint to unravel the footprint of spatially-distributed emissions on cloud droplet number and cloud albedo. Geophysical Research Letters 39.

Kim, J.S., Kim, Y.J., Park, K., 2011. Measurements of hygroscopicity and volatility of atmospheric ultrafine particles in the rural Pearl River Delta area of China. Atmospheric Environment 45, 4661-4670.

Kokkola, H., Yli-Pirila, P., Vesterinen, M., Korhonen, H., Keskinen, H., Romakkaniemi, S., Hao, L., Kortelainen, A., Joutsensaari, J., Worsnop, D.R., Virtanen, A., Lehtinen, K.E.J., 2014. The role of low volatile organics on secondary organic aerosol formation. Atmospheric Chemistry and Physics 14, 1689-1700.

Kuang, C., McMurry, P.H., McCormick, A.V., 2009. Determination of cloud condensation nuclei production from measured new particle formation events. Geophysical Research Letters 36.

Kuhn, T., Biswas, S., Fine, P.M., Geller, M., Sioutas, C., 2005. Physical and chemical characteristics and volatility of PM in the proximity of a light-duty vehicle freeway. Aerosol Science and Technology 39, 347-357.

Kulmala, M., Vehkamäki, H., Petäjä, T., Dal Maso, M., Lauri, a., Kerminen, V.M., Birmili, W., McMurry, P.H., 2004. Formation and growth rates of ultrafine atmospheric particles: a review of observations. Journal of Aerosol Science 35, 143-176.

Leng, C., Zhang, Q., Tao, J., Zhang, H., Zhang, D., Xu, C., Li, X., Kong, L., Cheng, T., Zhang, R., Yang, X., Chen, J., Qiao, L., Lou, S., Wang, H., Chen, C., 2014. Impacts of new particle formation on aerosol cloud condensation nuclei (CCN) activity in Shanghai: case study. Atmospheric Chemistry and Physics 14, 11353-11365.

Matsui, H., Koike, M., Takegawa, N., Kondo, Y., Takami, A., Takamura, T., Yoon, S., Kim, S.W., Lim, H.C., Fast, J.D., 2013. Spatial and temporal variations of new particle formation in East Asia using an NPF-explicit WRF-chem model: North-south contrast in new particle formation frequency. Journal of Geophysical Research-Atmospheres 118.

Orsini, D.A., Wiedensohler, A., Stratmann, F., Covert, D.S., 1999. A new volatility tandem differential mobility analyzer to measure the volatile sulfuric acid aerosol fraction. Journal of Atmospheric and Oceanic Technology 16, 760-772.

Park, D., Kim, S., Choi, N.K., Hwang, J., 2008. Development and performance test of a thermo-denuder for separation of volatile matter from submicron aerosol particles. Journal of Aerosol Science 39, 1099-1108.

Paulsen, D., Weingartner, E., Alfarra, M.R., Baltensperger, U., 2006. Volatility measurements of photochemically and nebulizer-generated organic aerosol particles. Journal of Aerosol Science 37, 1025-1051.

Philippin, S., Wiedensohler, A., Stratmann, F., 2004. Measurements of non-volatile fractions of pollution aerosols with an eight-tube volatility tandem differential mobility analyzer (VTDMA-8). Journal of Aerosol Science 35, 185-203.

Pierce, J.R., Adams, P.J., 2009. Uncertainty in global CCN concentrations from uncertain aerosol nucleation and primary emission rates. Atmospheric Chemistry and Physics 9, 1339-1356.

Pinnick, R.G., Jennings, S.G., Fernandez, G., 1987. Volatility of aerosols in the arid southwestern united-states. Journal of the Atmospheric Sciences 44, 562-576.

Pryor, S.C., Barthelmie, R.J., Sorensen, L.L., McGrath, J.G., Hopke, P., Petaja, T., 2011. Spatial and vertical extent of nucleation events in the Midwestern USA: insights from the Nucleation In ForesTs (NIFTy) experiment. Atmospheric Chemistry and Physics 11, 1641-1657.

Pryor, S.C., Spaulding, a.M., Barthelmie, R.J., 2010. New particle formation in the Midwestern USA: Event characteristics, meteorological context and vertical profiles. Atmospheric Environment 44, 4413-4425.

Rader, D.J., McMurry, P.H., 1986. Application of the tandem differential mobility analyzer to studies of droplet growth or evaporation. Journal of Aerosol Science 17, 771-787.

Riipinen, I., Pierce, J.R., Donahue, N.M., Pandis, S.N., 2010. Equilibration time scales of organic aerosol inside thermodenuders: Evaporation kinetics versus thermodynamics. Atmospheric Environment 44, 597-607.

Riipinen, I., Pierce, J.R., Yli-Juuti, T., Nieminen, T., Hakkinen, S., Ehn, M., Junninen, H., Lehtipalo, K., Petaja, T., Slowik, J., Chang, R., Shantz, N.C., Abbatt, J., Leaitch, W.R., Kerminen, V.M., Worsnop, D.R., Pandis, S.N., Donahue, N.M., Kulmala, M., 2011. Organic condensation: a vital link connecting aerosol formation to cloud condensation nuclei (CCN) concentrations. Atmospheric Chemistry and Physics 11, 3865-3878.

Ristovski, Z.D., Suni, T., Kulmala, M., Boy, M., Meyer, N.K., Duplissy, J., Turnipseed, A., Morawska, L., Baltensperger, U., 2010. The role of sulphates and organic vapours in growth of newly formed particles in a eucalypt forest. Atmospheric Chemistry and Physics 10, 2919-2926.

Sabaliauskas, K., Jeong, C.-H., Yao, X., Jun, Y.-S., Evans, G., 2013. Cluster analysis of roadside ultrafine particle size distributions. Atmospheric Environment 70, 64-74.

Sakurai, H., Fink, M.A., McMurry, P.H., Mauldin, L., Moore, K.F., Smith, J.N., Eisele, F.L., 2005a. Hygroscopicity and volatility of 4-10 nm particles during summertime atmospheric nucleation events in urban Atlanta. Journal of Geophysical Research-Atmospheres 110.

Sakurai, H., Park, K., McMurry, P.H., Zarling, D.D., Kittelson, D.B., Ziemann, P.J., 2003. Size-dependent mixing characteristics of volatile and nonvolatile components in diesel exhaust aerosols. Environmental Science & Technology 37, 5487-5495.

Saleh, R., Shihadeh, A., Khlystov, A., 2011. On transport phenomena and equilibration time scales in thermodenuders. Atmospheric Measurement Techniques 4, 571-581.

Salimi, F., Ristovski, Z., Mazaheri, M., Laiman, R., Crilley, L.R., He, C., Clifford, S., Morawska, L., 2014. Assessment and application of clustering techniques to atmospheric particle number size distribution for the purpose of source apportionment. Atmospheric Chemistry and Physics 14, 11883-11892.

Shantz, N.C., Pierce, J.R., Chang, R.Y.W., Vlasenko, A., Riipinen, I., Sjostedt, S., Slowik, J.G., Wiebe, A., Liggio, J., Abbatt, J.P.D., Leaitch, W.R., 2012. Cloud condensation nuclei droplet growth kinetics of ultrafine particles during anthropogenic nucleation events. Atmospheric Environment 47, 389-398.

Smith, J.N., Barsanti, K.C., Friedli, H.R., Ehn, M., Kulmala, M., Collins, D.R., Scheckman, J.H., Williams, B.J., McMurry, P.H., 2010. Observations of aminium salts in atmospheric nanoparticles and possible climatic implications. Proceedings of the National Academy of Sciences of the United States of America 107, 6634-6639.

Spracklen, D.V., Carslaw, K.S., Kulmala, M., Kerminen, V.-M., Sihto, S.-L., Riipinen, I., Merikanto, J., Mann, G.W., Chipperfield, M.P., Wiedensohler, A., Birmili, W., Lihavainen, H., 2008. Contribution of particle formation to global cloud condensation nuclei concentrations. Geophysical Research Letters 35.

Spracklen, D.V., Carslaw, K.S., Kulmala, M., Kerminen, V.M., Mann, G.W., Sihto, S.L., 2006. The contribution of boundary layer nucleation events to total particle concentrations on regional and global scales. Atmospheric Chemistry and Physics 6, 5631-5648.

Stanier, C.O., Khlystov, A.Y., Pandis, S.N., 2004. Nucleation events during the Pittsburgh air quality study: Description and relation to key meteorological, gas phase, and aerosol parameters. Aerosol Science and Technology 38, 253-264.

Stolzenburg, M.R., McMurry, P.H., Sakurai, H., Smith, J.N., Mauldin, R.L., Eisele, F.L., Clement, C.F., 2005. Growth rates of freshly nucleated atmospheric particles in Atlanta. Journal of Geophysical Research-Atmospheres 110.

Tiitta, P., Miettinen, P., Vaattovaara, P., Joutsensaari, J., Petaja, T., Virtanen, A., Raatikainen, T., Aalto, P., Portin, H., Romakkaniemi, S., Kokkola, H., Lehtinen, K.E.J., Kulmala, M., Laaksonen, A., 2010. Roadside aerosol study using hygroscopic, organic and volatility TDMAs: Characterization and mixing state. Atmospheric Environment 44, 976-986.

Tritscher, T., Dommen, J., DeCarlo, P.F., Gysel, M., Barmet, P.B., Praplan, A.P., Weingartner, E., Prevot, A.S.H., Riipinen, I., Donahue, N.M., Baltensperger, U., 2011. Volatility and hygroscopicity of aging secondary organic aerosol in a smog chamber. Atmospheric Chemistry and Physics 11, 11477-11496.

Tsimpidi, A.P., Karydis, V.A., Pandis, S.N., 2007. Response of inorganic fine particulate matter to emission changes of sulfur dioxide and ammonia: The eastern United States as a case study. Journal of the Air & Waste Management Association 57, 1489-1498.

Villani, P., Picard, D., Marchand, N., Laj, P., 2007. Design and validation of a 6-volatility tandem differential mobility analyzer (VTDMA). Aerosol Science and Technology 41, 898-906.

Villani, P., Picard, D., Michaud, V., Laj, P., Wiedensohler, A., 2008. Design and validation of a volatility hygroscopic tandem differential mobility analyzer (VH-TDMA) to characterize the relationships between the thermal and hygroscopic properties of atmospheric aerosol particles. Aerosol Science and Technology 42, 729-741.

Wang, L., Khalizov, A.F., Zheng, J., Xu, W., Ma, Y., Lal, V., Zhang, R., 2010. Atmospheric nanoparticles formed from heterogeneous reactions of organics. Nature Geoscience 3, 238-242.

Wang, Z.B., Hu, M., Yue, D.L., Zheng, J., Zhang, R.Y., Wiedensohler, A., Wu, Z.J., Nieminen, T., Boy, M., 2011. Evaluation on the role of sulfuric acid in the mechanisms of new particle formation for Beijing case. Atmospheric Chemistry and Physics 11, 12663-12671.

Wegner, T., Hussein, T., Haemeri, K., Vesala, T., Kulmala, M., Weber, S., 2012. Properties of aerosol signature size distributions in the urban environment as derived by cluster analysis. Atmospheric Environment 61, 350-360.

Wehner, B., Berghof, M., Cheng, Y., Achtert, P., Birmili, W., Nowak, A., Wiedensohler, A., Garland, R., Pöschl, U., Hu, M., 2009a. Mixing state of nonvolatile aerosol particle fractions and comparison with light absorption in the polluted Beijing region. Journal of Geophysical Research: Atmospheres (1984–2012) 114.

Wehner, B., Petäjä, T., Boy, M., Engler, C., Birmili, W., Tuch, T., Wiedensohler, A., Kulmala, M., 2005c. The contribution of sulfuric acid and non-volatile compounds on the growth of freshly formed atmospheric aerosols. Geophysical research letters 32.

Wehner, B., Philippin, S., Wiedensohler, A., Scheer, V., Vogt, R., 2004. Variability of non-volatile fractions of atmospheric aerosol particles with traffic influence. Atmospheric Environment 38, 6081-6090.

Westervelt, D.M., Pierce, J.R., Riipinen, I., Trivitayanurak, W., Hamed, A., Kulmala, M., Laaksonen, A., Decesari, S., Adams, P.J., 2013. Formation and growth of nucleated particles into cloud condensation nuclei: model-measurement comparison. Atmospheric Chemistry and Physics 13, 7645-7663.

Wu, Z., Poulain, L., Wehner, B., Wiedensohler, A., Herrmann, H., 2009. Characterization of the volatile fraction of laboratory-generated aerosol particles by thermodenuder-aerosol mass spectrometer coupling experiments. Journal of Aerosol Science 40, 603-612.

Yu, F., Luo, G., 2009. Simulation of particle size distribution with a global aerosol model: contribution of nucleation to aerosol and CCN number concentrations. Atmospheric Chemistry and Physics 9, 7691-7710.

Yue, D.L., Hu, M., Zhang, R.Y., Wang, Z.B., Zheng, J., Wu, Z.J., Wiedensohler, A., He, L.Y., Huang, X.F., Zhu, T., 2010. The roles of sulfuric acid in new particle formation and growth in the mega-city of Beijing. Atmospheric Chemistry and Physics 10, 4953-4960.

Yue, D.L., Hu, M., Zhang, R.Y., Wu, Z.J., Su, H., Wang, Z.B., Peng, J.F., He, L.Y., Huang, X.F., Gong, Y.G., Wiedensohler, A., 2011. Potential contribution of new particle formation to cloud condensation nuclei in Beijing. Atmospheric Environment 45, 6070-6077.

Zhang, Q., Worsnop, D.R., Canagaratna, M.R., Jimenez, J.L., 2005. Hydrocarbon-like and oxygenated organic aerosols in Pittsburgh: insights into sources and processes of organic aerosols. Atmospheric Chemistry and Physics 5, 3289-3311.

CHAPTER 6 UNCONTROLLED COMBUSTION OF SHREDDED TIRES IN A LANDFILL: POPULATION EXPOSURE, PUBLIC HEALTH RESPONSE, AND AN AIR QUALITY INDEX FOR URBAN FIRES[61]

6.1 Abstract

The Iowa City Landfill in eastern Iowa, United States, experienced a fire lasting 18 days in 2012, in which a drainage layer of over 1 million shredded tires burned, generating smoke that impacted the surrounding metropolitan area of 130,000 people. This emergency required air monitoring, risk assessment, dispersion modeling, and public notification. This paper quantifies the impact of the fire on local air quality and proposes a monitoring approach and an Air Quality Index (AQI) for use in future tire fires and other urban fires. Individual fire pollutants are ranked for acute and cancer relative risks using hazard ratios, with the highest acute hazard ratios attributed to SO_2, particulate matter, and aldehydes. Using a dispersion model in conjunction with the new AQI, we estimate that smoke concentrations reached unhealthy outdoor levels for sensitive groups out to distances of 3.1 km and 18 km at 24-h and 1-h average times, respectively. Modeled and measured concentrations of $PM_{2.5}$ from smoke and other

[61] This work is published as two peer review papers, Singh et al., (2015) and Downard et al., (2015). A. Singh, B. Stone, R. Bullard, C. Stanier and S. N. Spak designed the study. For Singh et al., (2015), A. Singh performed all the field sampling, measurement analysis and draft write up. S. N. Spak provided all the AERMOD dispersion maps. E. Stone and J. Downard provided all the provided all the integrated measurement, and feedback on analysis. Robert Bullard co-led the field sampling for the Stanier group. All authors contributed to the final form of the manuscript. For Downard et al., (2015), A. Singh conducted field experiments related to smoke characterization and assisted in analysis and draft write up.

compounds such as VOCs and benzo[a]pyrene are presented at a range of distances and averaging times, and the corresponding cancer risks are discussed. Through reflection on the air quality response to the event, consideration of cancer and acute risks, and comparison to other tire fires, we recommend that all landfills with shredded tire liners plan for hazmat fire emergencies. A companion paper presents emission factors and detailed smoke characterization.

6.2 Introduction

Shredded tire chips are commonly used as landfill drainage lining material. They are permeable to leachate and protect the landfill liner (Cecich et al., 1996; FEMA/USFA, 2002; Fiksel et al., 2011; IWMB, 2002; Warith and Rao, 2006). This practice also offers a way to dispose of scrap tires (FEMA/USFA, 2002). However, shredded and whole tires pose a significant fire risk; they are difficult to extinguish once ignited and emit criteria pollutants and air toxics when combusted (Lemieux et al., 2004; Lemieux and Ryan, 1993; USFA, 1998; Wang et al., 2007).

The Iowa City landfill's shredded tire drainage layer was accidentally ignited and burned openly for 18 days beginning May 26, 2012 (**Figure 6.1**). The exposed shredded tire drainage layer was 1-m thick and covered 30,000 m^2 and the fire consumed an estimated 1.3 million tires (20,540 metric tons, assuming 15.8 kg $tire^{-1}$; RMA 2013). The Iowa City landfill was close enough to population centers of Johnson County, Iowa (population 152,586, U.S. 2010 Census) to impact people through smoke exposure, including densely populated neighborhoods.

Figure 6.1 Photograph of the Iowa City landfill fire, with smoke primarily from the burning shredded tire drainage layer (Photo courtesy- Thomas Peters)

Over a dozen major tire fires have occurred in the United States and Canada since 1983 (see CalEPA, 2002; DEQ, 1989, USFA, 1998; EPA 1997; Ritter, 2013). The Iowa City landfill fire was approximately five times smaller than the largest U.S. tire fire, the 1983 Rhinehart fire (Ritter, 2013). These types of fires often exceed one month in duration and pose threats to the health and safety of both firefighters and the public. In some cases, fires have prompted voluntary evacuations, school closings, and increased respiratory complaints. On occasion, tire fires have been documented through published air concentration measurements from environmental agencies (CalEPA, 2002; EPA, 1997; OMOE, 1990; Sidhu et al., 2006; USFA, 1998). Sampling results for polycyclic aromatic hydrocarbons (PAH) and metal residues on vegetation are also reported

(CalEPA, 2002; Steer et al., 1995), as well as cancer risk assessment conducted using B[a]P concentrations (Sidhu, et al., 2006). While the Iowa City fire shares many similarities to the listed tire fires, it is, to our knowledge, the first major U.S. tire fire occurring in a landfill liner system instead of at a tire stockpile location.

From public health and air quality perspectives, the response to a large scale tire fire includes many decisions – what compounds to monitor; where to locate air monitors; whether to use mobile or fixed samplers; whether to use integrating or continuous techniques; interpretation of multi-pollutant mixture results across varied averaging times; action levels for warnings, evacuations, and closures; wording of public notices; recommended actions for reducing exposure; and best practices for using dispersion modeling.

The combustion of tires emits hazardous gases and particles to the atmosphere. These emissions reflect the chemical composition of tires, which are 50% natural or synthetic rubber by weight, 25% black carbon, 10% metal (mostly in the steel belt), 1% sulfur, 1% zinc oxide, and trace quantities of other materials (Seidelt et al., 2006). Laboratory studies of tire combustion report significant emissions of CO_2 (*2890 g* kg^{-1}), CO (*71 g* kg^{-1}), NOx (*6.0 g* kg^{-1}), and SO_2 (28 g kg^{-1}) (Stockwell et al., 2014), total suspended particles (*TSP,65-105 g* kg^{-1}), gaseous and particle-phase PAH (*3.4-5.3 g* kg^{-1}), and volatile organic compounds (*VOC, 12-50 g* kg^{-1}*, e.g. benzene, toluene, xylene*) (Lemieux and Ryan, 1993). Many pollutants emitted from tire burning are toxic, carcinogenic, and/or mutagenic; together, they present significant health hazards.

Existing reports from past fires have major shortcomings as a guide to the public health response (JCPHD, 2012, Downard et al., 2015). Shortcomings include a lack of

prioritization on what to measure and where to measure it, and a focus on reporting concentrations with limited interpretation of the public health impact. Past ambient studies rarely incorporate correction for dilution levels – limiting ability to generalize from measurements. Finally, variety in analyte selection and monitoring protocol is a challenge, with the monitoring focus varying among PAH, volatile organic compounds (VOCs), fine particulate matter ($PM_{2.5}$), and CO (CalEPA, 2002).

During the Iowa City incident, the public health response was led by the Johnson County Department of Public Health (JCDPH) supported by State Hygienic Lab (SHL), the Iowa Department of Natural Resources (IDNR), EPA Region 7, and the University of Iowa. The combined measurement of various pollutants (see Downard et al., 2015) and modeling work by these organizations enabled retrospective characterization of ambient concentrations.

This paper attempts to improve on the air quality response through a hierarchy of monitoring priorities for large scale tire fires, a tire fire irritant Air Quality Index (AQI) for interpretation of the measured values, and a ranking of tire fire components by acute and cancer hazard ratios. We also examine public health response guidelines and estimate emissions of some compounds not yet sampled in tire burning by using emissions profiles from open burning of oil (Booher, 1997; Lemieux, 2004). The field-based approach used in this study provides a real-world perspective on the open burning of tires, which has previously only been examined in small-scale, laboratory experiments (Lemieux and Ryan, 1993; Stockwell et al., 2014). Ambient measurements of particle number (*PN*), mass, and size distribution, EC, PAH, SO_2, and CO are used to derive emission factors (*EF*) of key pollutants per kilogram of combusted tire. Furthermore, the EF determined

in this study are used to assess the health risks posed by the tire fire smoke and to formulate recommendations on air monitoring needs in response to large-scale tire fires. This work focuses on ambient air pollutants, and does not deal with the many other aspects of the emergency response.

6.3 Methodology

6.3.1 Monitoring sites and instrumentation

Ambient air, often impacted with smoke, was examined at a variety of sites as mapped in **Figure 6.2**. Number of locations were employed in monitoring the fire, and augmented by mobile, grab, and handheld monitoring (shown in **Fig. 6.2.** and **Table 6.1**). This range of monitoring locations supported assessment of atmospheric concentrations within the smoke plume at a range of distances from the fire; at long-term monitoring sites in the area (see **Fig. 6.2.** Hoover Elementary); and at representative sites near population centers (see **Fig. 6.2.**, IA-AMS, BDR).

Other overlapping reasons include: chemical characterization, physical characterization, calculation of numerical emission factors, determination of hazard ratios and air quality index**.** Terrain in the area is not a major concern for concentration gradients or air pollution meteorology; the local terrain is gently rolling with less than 50 m elevation differences and the sharpest topography near the Iowa River, ~7.5 km east of the fire.

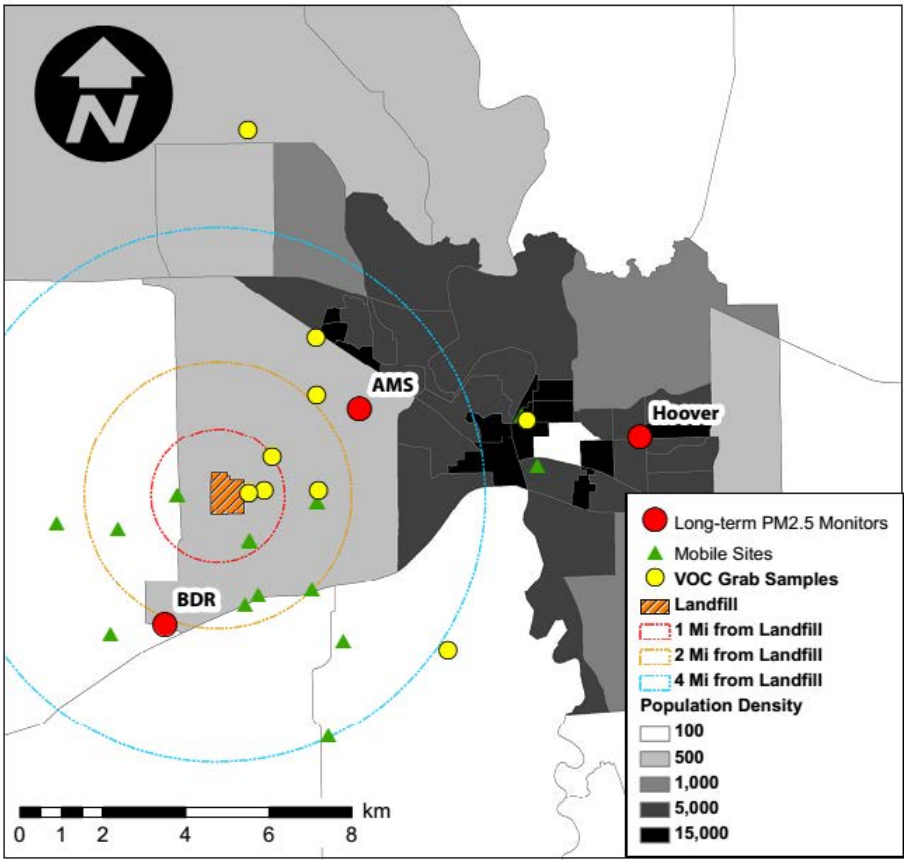

Figure 6.2 Map of the study area shaded by Census 2010 block group population density (persons/km2). Symbols mark locations of air quality samples from mobile sampling (green triangles), VOC grab samples (yellow circles), and long-term PM2.5 monitors (red circles). Concentric circles mark radii of 1.6 km (1 mi, red), 3.2 km (2 mi, yellow), and 6.4 km (4 mi, blue) from the fire location.

Measurements at the Iowa City landfill were taken near the edge of tire fire and around the periphery of landfill. Measurement near the fire edge were short term (10 minute sample integration or less), and included VOCs, $PM_{2.5}$, and CO. For an immediate survey of the fire, handheld $PM_{2.5}$ (TSI Dustrak 8520) and CO (TSI Q-Trak 7575) monitors were deployed at the edge of fire and downwind areas.

The IA-AMS site is situated among recreational fields, low use parking areas, and woodlands 4.2 km northeast of the landfill. This site has two stationary $PM_{2.5}$ inlets (3000 ABC, medium vol. URG corp.) used by the University of Iowa for collection of Quartz

and Teflon filters (47 mm) for $PM_{2.5}$ chemical speciation. Another Thermo-2025 medium volume PM_{10} sampler for 24 h integrated sampling was installed by the State Hygienic Laboratory (SHL) as a response to the fire and ran from May 31st - June 10th 2012. Details on the collection, mass and chemical analysis of filter samples are described by Downard et al. (2015).

Monitoring at the IA-AMS was further supplemented by the Stanier research trailer from June 1-4. The trailer was equipped with: a Scanning Mobility Particle Sizer (TSI Classifier 3080, CPC 3025 with DMA 3081) for particles 14.6-661 nm at 135 s intervals; an Aerosol Particle Sizer (TSI APS Model 3321) for particles 0.54-20 μm at 10 s intervals; a condensation particle counter (TSI CPC 3786); a Vaisala 343 GMP flow-through CO2 monitor; an NDIR CO monitor (Thermo Scientific Model 48i-TLE); a SO_2 UV fluorescence monitor (Teledyne 100E); and a roof-mounted weather station (DAVIS Vantage Pro2 Console). CO data was available only from May 29-31, 2012 (See **Table 6.1**).

The Hoover Elementary monitoring site (EPA site 191032001) is a routine EPA state and local air monitoring station (SLAM) and the designated Iowa $PM_{2.5}$ monitoring site for the metropolitan area. This site is located 10.5 km east of the Iowa City landfill in a residential area. This station monitors 24 h average and hourly $PM_{2.5}$ using a low volume FRM sequential air sampler (R&P Model 2025 w/VSCC gravimetric) and a beta attenuation sampler (Met One BAM-1020 w/SCC beta attenuation), respectively.

The primary objective for monitoring at Hoover station is to assess population exposure in the neighborhood area with a spatial scale from 0.5 to 4.0 kilometers range (IDNR, 2013).

Stanier research trailer was also deployed to a private farm on Black Diamond Road (3.2 km southwest of the landfill) on May 31 and June 1, 2012 to intercept the landfill plume. Land use around the Black Diamond Road (BDR) sampling site is primarily row-crop farming with scattered areas of grasses and deciduous trees. The site was 300 m north of the nearest principal road (Highway 1) and 5 km from the nearest limited access highway. Minor roads in the area are unpaved (gravel) and are an important source of localized PM.

On June 1, real-time instrumentation was deployed on a customized High Mobility Multipurpose Wheeled Vehicle (HMMWV or Humvee), which permitted mobile sampling at distances of 1.3, 3.2, and 4.8 km at different dilution ratio for its characterization from the landfill. Samples were collected only while the Humvee was stopped and operating on batteries to avoid sampling of the vehicle's exhaust. Instrumentation used during the transect included the SMPS, APS, and CPC from the trailer described in **Table 6.1.**

Additional information on detailed site locations, instruments deployed, and laboratory methodologies are also provided in **Appendix** (Section 9.4. Characterization method overview, organized by sampling method (offline or real-time) and compound class).

Table 6.1 Measurement Location and Measurement Methods

Site	Latitude, Longitude	Distance to landfill site (km)	Observations	Dates
University of Iowa Air Monitoring Site (IA-AMS)	41.6647, -91.5845	4.2	Particle Size Distribution, PN, CO_2, SO_2, CO (6/1-6/4); $PM_{2.5}$ filters for speciation (05/27-06/10); PM_{10} mass (05/31-06/10)	see dates at left
Hoover Elementary Site[a]	41.6572, -91.5035	10.5	Continuous 1 h $PM_{2.5}$, 24 h $PM_{2.5}$ (gravimetric)	ongoing routine monitoring site
Black Diamond Road (BDR)	41.6188, -91.6422	3.2	Particle Size Distribution, PN, CO_2, SO_2, CO	05/30/2012-06/01/2012
Plume Transect				
1. Site A	41.6366,-91.6173	1.3		06/01/2012
2. Site B	41.6248, -91.6150	3.2	Particle size distribution, PN, BC	06/01/2012
3. Site C	41.6143, -91.5907	4.8		06/01/2012
Landfill	41.6469, -91.6194	0.3	VOC (TO-15, TO-12 Air Toxic)	06/01/2012
Community Samples				
Weber School	41.6472, -91.5969	2.4	VOC (TO-15 & 12)	5/28/2012
University of Iowa, Pentacrest	41.6614, -91.5361	7.6	"	06/02/2012
Camp Cardinal Rd.	41.6678, -91.5969	3.4	"	05/27/2012
Dane Road, SW	41.6117, -91.5605	6.7	"	06/01/2012
Slothower St.	41.6548, -91.6100	1.6	"	06/01/2012
First Ave. and 22nd Ave. Coralville	41.6803, -91.5967	4.5	"	05/27/2012
Forever Green Rd. and Route 965, N. Liberty	41.7257, -91.6151	8.3	"	05/27/2012

[a] EPA SLAMS Network in Iowa City for residential population exposure at Hoover Elementary School

Ambient VOC concentrations were determined by EPA methods TO-12 and TO-15 (EPA, 1999). Ten grab samples, representing background and plume-impacted air, were collected in pre-cleaned 6-L Summa canisters (Entech Silonite^{TM}). Analysis was by gas chromatography (GC) mass spectrometry (Agilent Technologies 7890A, 5975C; 60 m DB-1 column). These were analyzed using EPA method TO-15 (EPA, 1999) using an Entech 7016 canister auto sampler, Entech Model 4600A dynamic dilutor, Entech Model 7100A pre-concentrator, Agilent 7890A GC and an Agilent 5975C MS.

6.3.2 Calculation of emission factors of the plume

Equation 6.1 has been is used in many emission studies to calculate the EF for particle mass, number and black carbon (Baalbaki et al., 2013; Ban-Weiss et al., 2009; Kalafut-Pettibone et al., 2011; Paul M Lemieux et al., 2004; Ning et al., 2008; Yli-Tuomi et al., 2005. EF for PM2.5, SO_2 (g kg^{-1} fuel burned), and PN (#/cm^3) were calculated using Equation 1 (Lemieux et al., 2004):

$$EF_i = \frac{[\mathrm{i}]_{plume} - [\mathrm{i}]_{background}}{[\mathrm{C}]_{plume} - [\mathrm{C}]_{background}} \times f_c \qquad (6.1)$$

where i is the pollutant, C represents carbon from CO and CO_2, and fc is the mass fraction of carbon in the fuel, which is 0.85 for shredded tires (Quek and Balasubramanian, 2013). Concentrations of gases measured in real-time were averaged over 10 minutes. The conversion of CO_2 mixing ratio to mass concentration assumed 25^{o}C and atmospheric pressure (i.e. 1 ppm CO_2 is equivalent to 0.498 mgC m^{-3}).

Plume-impacted samples were identified by visual inspection of time series data, field notes (where odor of the plume was noted), and wind direction. Background concentrations for $PM_{2.5}$, CO, CO_2, PN, and SO_2 were calculated by averaging 30 minutes before and after each plume intercept, or from shorter time periods when plume

intercepts occurred in quick succession. Enhancement of CO above background and the average CO: CO_2 ratio was determined by P1-P4 in **Figure 6.3.** **Equation 6.1** assumes tire carbon is emitted as CO_2 and CO, ignoring VOC and PM, and does not account for up to 25% of tire carbon forming pyrolytic oil (Unapumnuk et al., 2006).

In cases where CO_2 data was not available at the required location or time interval, **Equation 6.2** (Lemieux et al., 2004) was used to calculate EF for species j relative to a species (k) for which EF_k had been determined:

$$EF_j = \frac{[j]_{plume} - [j]_{background}}{[k]_{plume} - [k]_{background}} EF_k \qquad (6.2)$$

Size-resolved EFPN were determined relative to $PM_{2.5}$, while EFPAH were calculated relative to EC following the assumption that EC comprised 45% of $PM_{2.5}$ (Slowik et al., 2004).

6.3.3 Hazard ratios for tire fire smoke

Hazard ratios compare the ambient concentrations of pollutants to reference concentrations for a similar averaging period (EPA, 1989). The hazard ratio concept can be used to target specific pollutants in an exposure situation (Austin, 2008; EPA, 1989; McKenzie et al., 2012; Silverman et al., 2007). The hazard ratio (HR_i) for species *i* is

$$HR_i = \frac{C_i}{C_{ref}} \qquad (6.3)$$

where c_i is the ambient concentration and c_{ref} is the reference concentration. For the acute hazard ratio (HRA) we adopt 1-h Acute Exposure Guideline Levels (*AEGL-1*) (NRC, 2001) for c_{ref}. AEGL-1 is defined as "the airborne concentration of a substance above which it is predicted that the general population, including susceptible individuals, could experience notable discomfort, irritation, or certain asymptomatic non-sensory

effects. However, the effects are not disabling and are transient and reversible upon cessation of exposure." AEGL values were selected because they were developed specifically for emergency exposures and are thoroughly documented. For species with no 1-h AEGL, a Short Term Exposure Limit (*STEL*) from the American Conference of Industrial Hygienists (ACGIH, 2014), with the NIOSH STEL, OSHA STEL, and five times the TLV-TWA for the compound as alternate c_{ref} depending on availability (OSHA, 2006, NIOSH, 1996). For the cancer risk hazard (HRC), the inverse of the inhalation unit risk factor (*IUR*) from IRIS (EPA, 2011) or CalEPA (CalEPA, 2003) was used for c_{ref}.

Because individual tire fire studies lack comprehensive species coverage, ratios were calculated from multiple studies (EPA, 1997; CalEPA, 2002; Downard et al., 2015), ranked within study, and then merged into a unified ranking. Because no tire fire study included some compounds such as formaldehyde, a laboratory study of pooled crude oil burning was also included (Lemieux et al., 2004).

6.3.4 Development of Air Quality Index (AQI) for tire fires

Air quality indices (AQI) are useful for communication of the level of hazard (Chen et al., 2013; Dimitriou et al., 2013; EPA, 2006; Gurjar et al., 2008; OEHHA, 2012). However, traditional AQI formulas have drawbacks when applied to an emergency fire situation – 1-h, 8-h and 24-h averaging time AQI are needed but are not available for all pollutants, and it is not clear how to account for the multi-pollutant nature of the smoke. Factors such as tire particulate toxicity and the high mutagenicity of tire fire smoke relative to wood smoke (Lemieux and Ryan, 1993; Lindbom et al., 2006) suggest that conventional indices may be insufficient for tire fire smoke. We propose an

AQI formula for total air quality index (a_{tot}) from summation of the impacts from multiple pollutants:

$$a_{tot} = \left[a_{PM}^p + o_1^p + o_2^p + \cdots + o_m^p + u_1^p + u_2^p + \cdots + u_n^p\right]^{1/p} \qquad (6.4)$$

Equation 4 includes the concentrations of $PM_{2.5}$ (a_{PM}), m co-pollutants (o_m), and n unmeasured compounds (u_n). Summation is appropriate when pollutants share a common health effect and mode of action (Murena, 2004; Plaia and Ruggieri, 2011). In the case of the tire fire smoke, most of the pollutants are respiratory irritants, and we propose summation over the irritant compounds. The exponent (p) controls the nature of the summation process; as p increases, the summation becomes dominated by the highest air quality index in the summation. A fixed p value of 2.5 has been proposed (Kyrkilis et al., 2007), which heavily weights the maximum AQI. In this study, results from p exponents of both 1 and 2.5 are explored, and the main results and discussion are reported using a p exponent of 1.

The AQI values for all compounds were calculated using linear interpolation between AQI breakpoints (EPA, 2009). Breakpoints for $PM_{2.5}$ were from OEHHA (2012), which are based on the EPA NAAQS but extend to 8-h and 1-h averaging periods. The NAAQS-based SO_2 AQI breakpoints are adopted uniformly for 24-h, 8-h, and 1-h averaging times.

For all other species, NAAQS based thresholds are not available, and AEGL were used if available. A full complement of AEGL mixing ratios consists of 15 values, corresponding to 5 averaging times and 3 thresholds: AEGL-1 (defined in section 2.2), AEGL-2 (irreversible or other serious adverse health effects), and AEGL-3 (life-threatening). For some compounds, AEGL concentrations are not available, and the AQI

breakpoints rely on STEL instead, as described in section 2.2. Due to the high concentrations involved in the tire fire, and the high STEL and AEGL of some compounds, linear extrapolation of AQI values in excess of 500 was performed.

SO_2 has NAAQS-based AQI breakpoints as well as AEGL values and a STEL. Therefore, it is used to translate from concentrations relative to AEGL or STEL (available for many compounds) to concentrations relative to an AQI (available for SO_2). Specifically, the AQI of pollutant i is calculated by

$$a_i = a_{SO2}(f_{AEGL}^{-1}(\overline{AEGL}_{SO2}, f_{AEGL}(\overline{AEGL_i}, c_i))) \quad (6.5)$$

where f_{AEGL} is a piecewise linear function with two inputs: (a) the 3 AEGL values of species i (denoted by the vector $\overline{AEGL_i}$), and (b) c_i. f_{AEGL} is 0 at c_i of 0, and 1, 2 and 3, respectively at concentrations of AEGL-1, AEGL-2, and AEGL-3. f_{AEGL}^{-1} is the inverse function that returns the concentration that will give a specific value of f_{AEGL}. For SO_2, the AEGL-1, 2, and 3 mixing ratios are 200, 750, and 30,000 ppb, respectively. The 1-h NAAQS (also the value for an AQI of 100) is 75 ppb, and the STEL is 250 ppb. Therefore, for SO_2, the AEGL-1, 2, and 3 values occur at AQI values of 224, 700, and 28,000, respectively, and the SO_2 STEL occurs at an AQI value of 256.

$PM_{2.5}$ was used as a tracer of the tire fire smoke. That is, we considered tire fire smoke by its $PM_{2.5}$ concentration (denoted PM_t), and then calculate the concentrations of all co-pollutants (e.g. SO_2, formaldehyde, VOCs) using the ratio of the co-pollutant emission factor to that of PM_t. The various AQI values are combined according to equation 6.2. An example 1-h AQI calculation is shown in Supplementary materials.

6.3.5 Dispersion modeling

Two dispersion models, Hazard Prediction and Assessment Capability model (HPAC) version 5.0 MB (Sykes and Gabruk, 1997) and AERMOD (EPA-454/R-03-004, September 2004 release 0726) (EPA, 2004) were run independently, with results first available beginning on May 30, the fourth full day of the fire. Both models were provided to the incident command group to help plan activities, and to understand potential impacts on populated areas (Holmes and Morawska, 2006; Kakosimos et al., 2011; Morra et al., 2009).

The Iowa National Guard's 71st Civil Support Team requested dispersion modeling from the Defense Threat Reduction Agency (DTRA). DTRA modeled the landfill fire as combustion of oil using HPAC.

AERMOD was used with regional forecast meteorology (60 hour forecast) from the Weather Research and Forecasting model (WRF) 3.3.1 (Skamarock et al., 2008). The WRF configuration included 24 vertical layers from the surface to 5 km, 4 km horizontal resolution, ACM2 planetary boundary layer scheme (Pleim, 2007), and initial conditions and observational constraint from the North American Mesoscale Model. WRF profiles were processed for AERMOD using MCIP2AERMOD (Davis et al., 2008).

WRF/AERMOD simulated dispersion to a 100 m receptor grid from an area source covering the burning landfill cells. All receptors were placed 2 m above terrain height. In forecasting, the smoke $PM_{2.5}$ emission rate was set at 0.4 g/s (10 $\mu g/m^2$-s) to match early field observations of the plume (site BDR on May 30, 20:00). For retrospective modeling to reconstruct concentrations, the emission rate for smoke was adjusted to minimize the average of the absolute fraction errors of observed plumes.

Specifically, the peak model concentration at the distance of the monitoring location was compared to the observed peak at 10 min averaging time (where available) or hourly average concentration. Cases with the modeled plume more than 40° away from the measurement location were excluded.

6.4. Results and Discussion

The fire was first reported during the evening of May 26, 2012. The impact of the landfill fire plume on individual stationary sites was episodic and depended strongly on wind direction, dilution, and emission rates that vary due to firefighting activities, temperature, and atmospheric conditions (Akagi et al., 2012; CalEPA, 2002; JCPHD, 2012; Kwon and Castaldi, 2009). The tire fire was declared under control and smoke emission was almost eliminated as of June 12, 2012. The plume was well dispersed during a majority of the fire-affected period due to meteorology. During these periods, its influence was localized. Conversely, two stable periods with low boundary layer heights and significant smoke accumulation over more widespread areas were identified (June 1-3 and June 7-8). Chronology of weather, PM concentrations, sampler activities, and model highlights are found in **Appendix** (Section 9.4: Chronology of the tire fire and response**).** Concentrations of $PM_{2.5}$, SO_2, and PAH were used to develop emission factors and are also discussed in Downard et al. (2015).

6.4.1 Meteorology and smoke impact

Initial winds were from the southeast, carrying the plume to the northwest and away from populated areas. Populated areas to the north of the landfill were first impacted on May 27, and then areas to the southeast of the landfill on May 28. VOCs

were sampled by canisters starting on the May 27. Monitoring systems especially deployed for the landfill fire began operation on May 29 (handheld PM and CO, size distribution and gas monitors) and 30 (PM_{10} sampler at IA-AMS). Two independent dispersion model forecasts began on May 30, the 4th full day of the fire. The condition least conducive to dispersion and the highest impact on Iowa City occurred during June 1-3, during a downtown outdoor arts festival. June 2 was the day of the highest EC filter loading at IA-AMS (Downard et al., 2015). During the early morning of June 3, calm conditions and fog formed, and high concentrations were recorded at the sites to the east of the landfill (**Fig. 6.3** hourly values of 48 and 71 $\mu g/m^3$ at IA-AMS and Hoover, respectively). Atmospheric stabilities on June 2 and 3 ranged from neutral to slightly stable (Pascal-Gifford stability E and D) as determined by NOAA READY (NOAA, 2013). Boundary layer heights were limited to 200 m during periods of the highest plume impact.

Dispersion improved throughout the day on June 3, reaching unstable conditions and a boundary layer height in excess of 2 km during the afternoon of June 3. A tire, burn and cover operation began on June 4 to manage the fire. In general, the plume was dispersed very effectively during June 4-7, and then had moderate impacts north of the landfill during June 7-10. The fire was declared fully under control and the emergency operation - stopped on June 12. Additional detail on weather, PM concentrations, sampler activities, and forecasting activities predictions are found in **Appendix** (Section 9.4 Chronology of the tire fire and response).

Appendix (Section 9.4. Enhancement of pollutants in the smoke at different measurement sites during Iowa City Tire fire) summarizes background and increment

above background (Δ) results at several different sites around the landfill. Examples of smoke impacts at fixed monitoring locations are shown in Figure 3, which depicts a six-day record of 10-min averages of particle mass concentration ($PM_{2.5}$) and SO_2. The black line in **Figure 6.3** shows 10-min $PM_{2.5}$ at BDR (prior to June 1) and at IA-AMS (after June 1) while the blue line graphs hourly $PM_{2.5}$ at Hoover. Four periods identified as smoke plumes at BDR are marked on the figure as P1-P4. Six periods identified as smoke plumes at IA-AMS are marked P5 to P10, and three smoke plumes identified at the Hoover site are labeled H1-H3. SO_2 data prior to 14:00 on June 30 are from a mobile sampling location on Country Club Dr. in Iowa City which sampled background air while the plume was slightly to the west of the site. Smoke plumes were identified based on the simultaneous increase above background of multiple pollutants ($PM_{2.5}$, CO, particle number, and SO_2). The duration of plumes at BDR and IA-AMS ranged from a few minutes to impacts lasting several hours. At the Hoover site (7.3 km from the landfill), plumes H1 to H3 measured 19.6 to 71.0 $\mu g/m^3$ relative to background concentrations of 5-11 $\mu g/m^3$.

After 17:00 on June 3, a number of SO_2 plumes can be seen in Figure 3(d), often in excess of 15 ppb. These were not associated with the landfill fire because the wind direction during this period was from the east and southeast and the correlation of $PM_{2.5}$ and SO_2 characteristic of the tire fire smoke was not observed in these SO_2 peaks after 17:00 June 3. The University of Iowa power plant, located south east of IA-AMS, is a likely source of these SO_2 peaks.

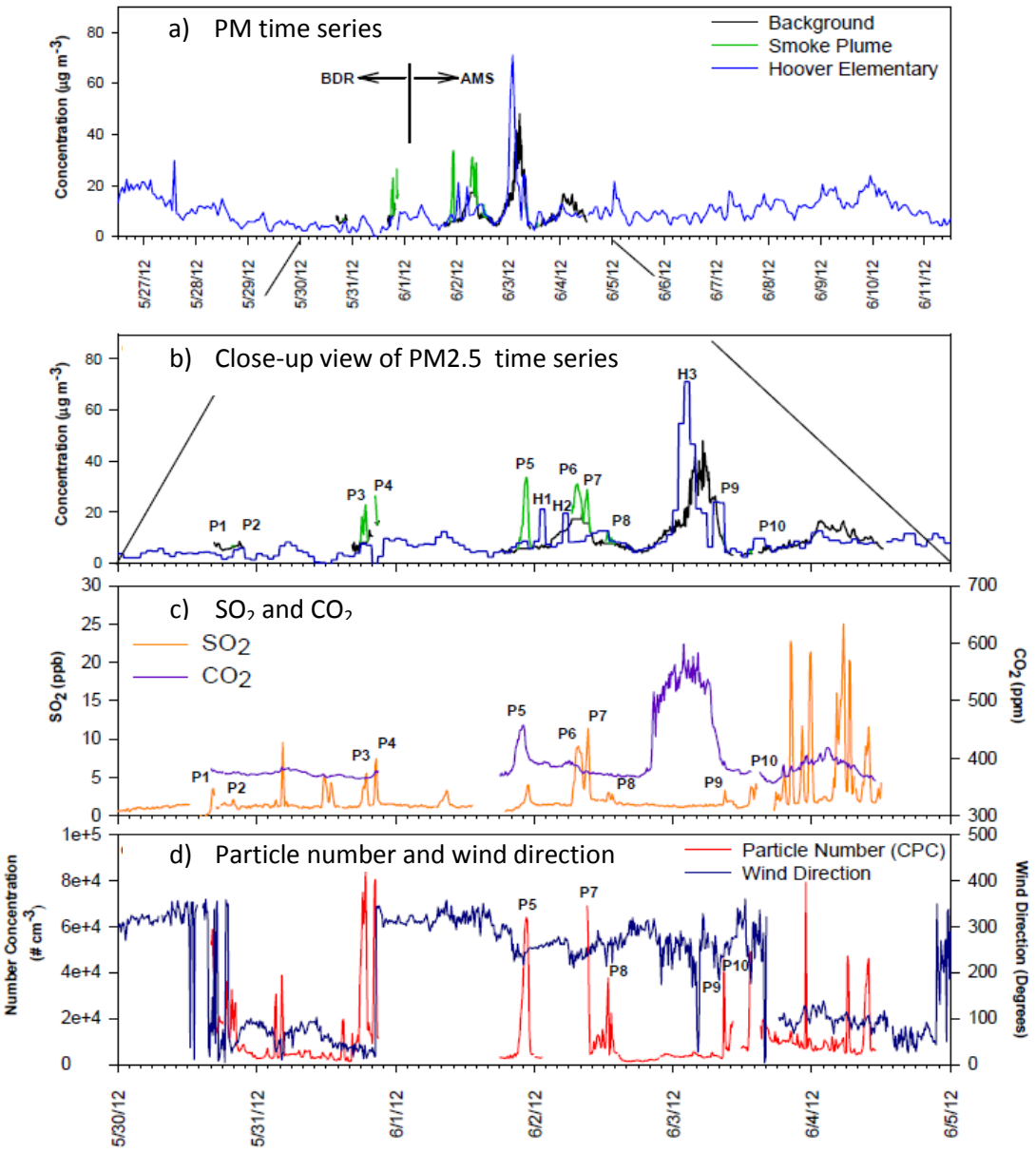

Figure 6.2 Time series of continuous measurement at BDR and IA-AMS site during the landfill fire in Iowa City. Panel (a) show continuous hourly measurement of PM2.5 at BDR, IA-AMS and Hoover Elementary (blue line). Panel (b) is the close up of panel (a) from May 29 to June 4 2014 and the P1-P10 are the identified fire plumes intercepted at the measurement site. Panel (c) Continuous measurement of SO2 and CO2 for the study period. Panel (d) total particle number (>2.5 nm) and Wind direction for the study period.

6.4.2 Volatile organic compounds (VOC)

A total of 54 VOCs were quantified from May 27 to June 2 in both background and impacted locations. Tire fires are known to be a major source of VOCs (Lemieux and Ryan, 1993). **Table 6.2** reports a selected list of VOC concentrations in a representative plume-impacted sample taken on May 28 at 300 m from the fire with additional data in **Appendix** (Section 9.4. All TO-15 and selected TO-12 VOC measured during the tire fire). Significant increments in concentration over background were observed for many aromatic VOCs such as benzene, toluene, ethyl toluene, dimethyl benzene, xylene and styrene, as well as aliphatics (e.g., propane, butane). Fewer carbonyls were measured, but acrolein showed enhancement. Several hydrocarbon concentrations were below detection limit.

Benzene concentrations ranged from 0.05-0.07 ppbv in background samples and increased to 8.3 ppbv and remained elevated in some samples (e.g., 0.63 ppbv 8.0 km downwind). Toluene was present at 8.7 ppbv in the plume and 0.50 ppbv downwind. Synthetic rubber components butadiene and styrene are typically below detection limits in Iowa City but were 0.5-1 ppbv at 300 m from the fire. The benzene concentrations were well below a number of relevant reference concentrations, such as the OSHA STEL (1000 ppb), the ACGIH TLV-TWA (100 ppb), and the AEGL-1 (52,000 ppb, 1-h) but close to the lower ATSDR minimum risk level of 9 ppb (ATSDR 2013).

6.4.3 Tire smoke profile

The tire smoke profile was based on the average of P1-P10 plume identified in Figure 2. The enhancement in each plume event is presented in Table 6.3. The average

emission factor values for $PM_{2.5}$ mass, particle number, SO_2 are presented in the **Table 6.3**.

Average emission factors for total particle number was $3.5e^{16}$ kg^{-1} tire. In the absence of any prior reference of emission factor for particle number for tire fire, comparison of emission factor are made with vehicular emission, biomass and agriculture burning. The EF for particle number is similar in range to light and heavy duty vehicles under cruise and acceleration conditions (Kittelson et al.2006). The lower cut off in Kittelson et al. (2006) is 3 nm, similar to the current study. Reported values of biomass burning (due to various burn condition and fuel type) have wide range, but found around in the range of 3.1 to $5.9e^{16}$ #/cm^3 (Janhaell et al. 2010, Akagi et al 2011). Substantial variation is observed in the size resolved particle emission factors which could be due to the nature of burn, dilution, and atmospheric condition. But the size resolved emission factor also shows significant emission of nuclei mode (<30nm) particles compared to higher sizes (**Fig. 6.4**). Fresh emission of organics and Sulphur is likely to lead particle formation which could be associated with the dominance of nuclei mode particles.

The average EF of $PM_{2.5}$ estimated in this study 5.35 g kg^{-1} of tire. This differs by an order of magnitude lower than the EF of TSP reported by Lemieux and Ryan (1993) at 65 -105 g kg^{-1}. The average EF of SO_2 from the open-burning of tires was 7.1 g kg^{-1}. This value is a factor of 4-5 lower than EF of SO_2 reported by Levendis et al. (1996) at 35 g kg^{-1} and Stockwell et al. (2014) at 28 g kg^{-1}, and an order of magnitude greater than the than $EFSO_2$ of 0.1-0.8 g kg^{-1} reported by Shakya et al. (2008), all of which correspond to laboratory studies.

Table 6.2 Increment over background for EPA TO-12 and TO-15 VOCs in the tire smoke plume at various measurement sites.

Species	Method detection limit (ppbv)	Method of detection	Tire plume[a] ppbv	Background air[b] ppbv	Δ VOC[c] ppbv	Enhancement over background[e]	Enhancement relative to benzene ($\Delta VOC_i / \Delta VOC_{benzene}$)
Aromatic							
Benzene	0.17	GCMS volatiles, EPA TO-15	8.27	0.05	8.22	164	1
Toluene	0.16		8.64	0.05	8.59	172	1.0
Ethylbenzene	0.18		0.66	<0.18	0.48[d]	3	1.6E-02
m,p Xylene	0.26		2.03	<0.26	1.77[d]	7	4.0E-02
o-Xylene	0.11		0.62	<0.11	0.51[d]	5	2.7E-02
Styrene	0.1		0.59	<0.1	0.49[d]	5	2.9E-02
1,2,4-Trimethylbenzene	0.14		0.27	<0.14	0.13[d]	1	5.4E-03
1,3,5-Trimethylbenzene	0.16		0.14	<0.16	0.0	0	
Isopropyl benzene	0.07	To-12 Speciated non-Methane Organics	0.6	<0.07	0.53[d]	8	4.4E-02
m-ethyltoluene	0.08		1.53	0.12	1.41	12	6.8E-02
p-ethyltoluene	0.1		0.76	0.05	0.71	14	8.3E-02
m-dimethyle benzene	0.05		0.08	<0.05	0.03[d]	1	3.5E-03
p-dimethyl benzene	0.04		0.49	<0.04	0.45[d]	11	6.5E-02
Halocarbon compounds							
Carbon tetrachloride	0.33	GCMS volatiles, EPA TO-15	0.09	0.1	0	0	
Dichlorodifluoromethane	0.23		0.53	0.51	0.02	0	2.3E-04
Trichloroflurormethane	0.17		0.25	0.22	0.03	0	7.9E-04
1,1,2 Trichloro,1,2,2-trifluroethane	0.18		0.08	0.08	0	0	0.0E+00
Aliphatic compounds							
Acetylene	0.73	GCMS volatiles, EPA TO-15	0.72	0.12	0.6	5	2.9E-02
Propylene	0.16		5.54	<0.16	5.38[d]	34	2.0E-01
1,3 butadiene	0.24		0.91	<0.24	0.67[d]	3	1.6E-02

Ethane	0.03	To-12 Speciated non-Methane Organics	41.7	2.5	39.2[d]	16	9.1E-02
propane	0.1		20.4	0.59	19.81	34	2.0E-01
Butane	0.1		6.07	0.29	5.78	20	1.2E-01
Isopentane	0.08		3.67	0.3	3.37	11	6.5E-02
Hexane	0.18		1.1	0.08	1.02	13	7.4E-02
Nonane	0.05		0.37	0.21	0.16	1	4.4E-03
1-decene	0.08		2.58	0.15	2.43	16	9.4E-02
Decane	0.08		1.13	<0.08	1.05[d]	13	7.6E-02
Dodecane	0.08		0.13	<.08	0.05[d]	1	3.6E-03
Carbonyl compounds							
Acrolein	0.08	GCMS volatiles, EPA TO-15	1.5	<0.08	1.42[d]	18	1.0E-01
Terpenoid compounds		To-12 Speciated non-Methane Organics					
α-Pinene	0.06		0.08	0.1	0.02		
Isoprene	0.08		2.49	0.14	2.35	17	9.8E-02

[a]Tire plume sample is based on the VOC canister measurement 300 meters away from fire; [b]Background sample is based on the Iowa Pentacrest (06/01/2012, 15:20); [c] ΔVOC is tire plume minus background sample; [d] Minimum detection limit values were used for the calculate of delta;

[e] Enhancement is the ratio of ΔVOC over background concentration. For background concentration below MDL, MDL values were substituted for the background.

Table 6.3 Fuel based emission factor from P1-P10 tire plume

		Ambient Concentrations			EF (g kg^{-1} or # kg^{-1})		
	Formula	Bck	Plume-impacted	Units	Mean	Stdev.	Median
Carbon dioxide[a]	CO_2	378.9	383.1	(ppm)	-	-	-
Sulfur dioxide[a]	SO_2	1.69	3.75	(ppb)	7.1	8.3	2.91
$PM_{2.5}$[a]	-	9.81	15.1	(mg m^{-3})	5.35	5.39	3.05
Particle number	-	9800	39400	(cm^{-3})	3.49E+16	3.41E+16	2.05E+16

a) Determined from samples collected 30 May to 3 June, 2012 (n = 10);

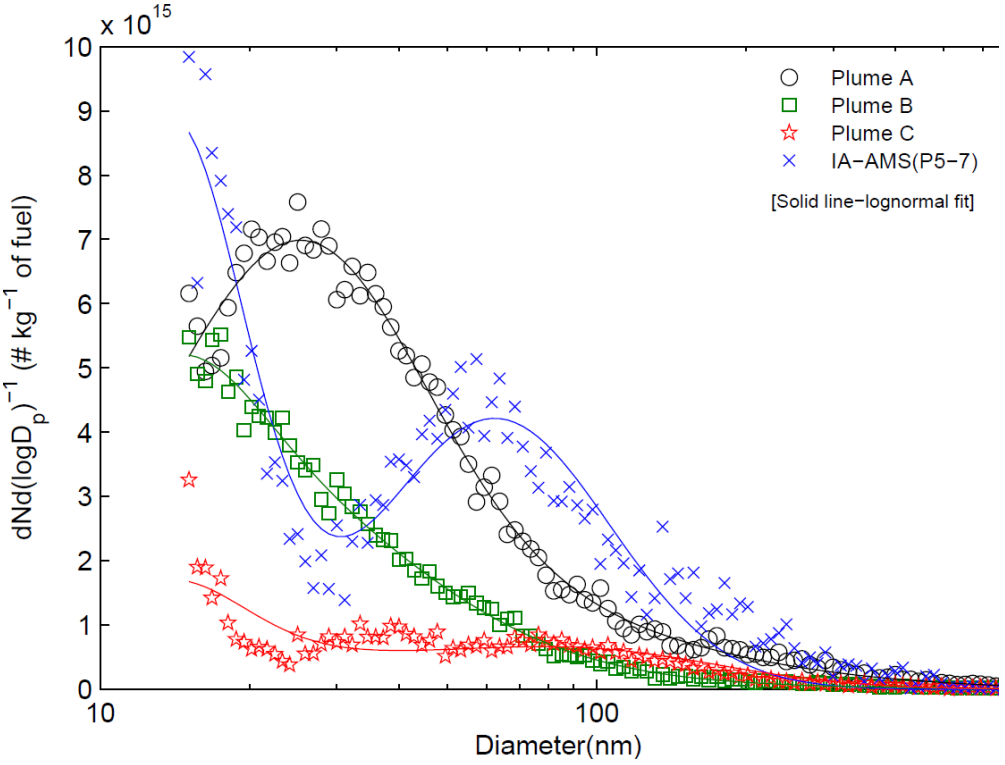

Figure 6.3 Size resolved emission factor calculated (10 nm-500 nm) from Plume transect and IA-AMS measurement. Plume A, B and C are from Plume transect study located at 1.3m 3.2 and 4.8 km downwind of fire. Plume P5, 6, and 7 were used from IA-AMS.

6.4.4 Identification of key pollutants from hazard ratio analysis

Calculated cancer and acute hazard ratios (HRA and HRC) are summarized in Tables 4 and 5, respectively, with details on ambient concentration measurements and reference concentration values, from multiple studies in Supplementary materials. Acute hazard ratios can be found in the parenthesis in **Table 6.4**. Note that hazard ratios from different ambient concentration measurements (e.g., the Westley vs. the Iowa City VOCs) cannot be directly compared to each other or to the hazard ratios based on emission factors. Only the relative orderings can be compared. SO_2, $PM_{2.5}$, black carbon (BC), and air toxic VOCs had the highest rankings when assessed using concentrations or emission factors from Iowa City. In other studies with tire smoke, BC, biphenyl, benzene, benzaldehyde, PM, and CO was highly ranked hazards. SO_2, which receives the highest ranking by AEGL-based hazard ranking, has limited published emission factors. For example, it is not listed as an emission factor in Lemieux and Ryan (1993); however, Lemieux and Ryan did publish an SO_2 and CO time series for a tire fire test that corroborates the high placement of SO_2 in our hazard ratio ranking. The test had an SO_2/CO mixing ratio of ~0.2-0.33 which corresponds to HRA_{SO2}/HRA_{CO} of 400-660.

Aldehydes have not been extensively measured in tire fire emissions, but are known components of smoke from burning oil. Aldehydes include strong irritants with low reference concentrations, and formaldehyde, benzaldehyde, and acrolein have high rankings according to their HRA. Accordingly, we expect these compounds to play a role in the health impacts of the smoke, and recommend further study of their emissions.

Hazard ratio rankings within an order of magnitude of each other were grouped to generate a merged ranked list of the most hazardous compounds found in the right hand column of Table 4. Compounds common to multiple studies (benzene, 1,3-butadiene,

PM and CO) provided benchmarks for relative rankings. The unified acute hazard ratio for tire fires includes SO_2 > PM > BC> Acrolein, Formaldehyde > CO > Benzene, Benzaldehyde, Biphenyl, 4-Vinyl-1-Cyclohexene, and Phenol as the higher ranked compounds. Monitoring and risk assessment should prioritize compounds with high hazard ratios.

Table 6.5 lists the cancer hazard ratio results. These were calculated using two alternate methods. One method was to consider B[a]P, which has been used in past cancer risk screenings of tire fires, as well as gases for which there are URF values. The resulting ordering is B[a]P > benzene > 1,3-butadiene > naphthalene > formaldehyde > acetaldehyde > ethylbenzene. B[a]P has the highest HRC in all tire fire datasets examined, using a URF of 1.1×10^{-3} $(\mu g/m^3)^{-1}$. The alternate method is to also include tire fire $PM_{2.5}$ as a potential carcinogen, applying the diesel particulate matter URF [3.04×10^{-4} $(\mu g/m^3)^{-1}$, CalEPA, 2003]. In that case, the cancer risk is dominated by $PM_{2.5}$, as the $PM_{2.5}$ risk factor exceeds that of B[a]P by more than 2 orders of magnitude. Future research and cancer screenings should consider this more conservative approach of treating the PM in tire fire smoke as a carcinogen.

Table 6.4 Ranked order of acute hazard ratios from multiple studies and unified ranked order list of hazard ratios. Numbers in parentheses are the hazard ratios (see text).

Study					
This study, emission factors	EPA, emission factors	Pooled oil burn	This study, VOC Canisters	Westley, CA	Unified Ranking by Hazard Ratio*
SO_2 (13,500)	PM_{10} (2980)	Acrolein (160), Formaldehyde (126)	Acrolein (49)	PM_{10} (11)	SO_2
$PM_{2.5}$ (357)	CO (262)	CO (65)	Benzene (0.16)	BC (0.46) CO (0.5)	PM
BC (138)	Biphenyl (52), Vinyl-cyclohenene (49), Benzaldehyde (38)	Benzaldehyde (2.5), Benzene (1.5)	Toluene (0.04)	Benzene (0.06)	BC
	Naphthalene (13), Benzene (15), Phenol (12)	Napthalene (0.6), Isovaler-aldehyde (0.3)	Ethylbenzene (0.02) Styrene (0.03), Xylene (0.02)	1,3-Butadiene (<0.01)	Acrolein, Formaldehyde
	Styrene (7.6), Indene (4.8), Ethylbenzene (4.4), Xylenes (3.6), Toluene (3.3)	Acetone (0.04), Xylene (0.04), TMB (0.05), Toluene (0.06)	TMB (0.002), 1,3-Butadiene (0.001)		*CO*
	TMB (1.2), Cumene (1.6), Limonene (1.2)	MEK (0.01), Nonane (0.003)			Benzene, Benzaldehyde, Biphenyl, Vinyl-cyclohexene, Phenol
	1,3-Butadiene (0.1)				Naphthalene, Isovaleraldehyde
					Styrene, Indene, Ethylbenzene,Toluene, Acetone, Xylene, TMB, Cumene, Limonene
					1,3-Butadiene, MEK, Nonane

← Lower Hazard Ratio Higher →

*In the unified list (rightmost column), regular typeface indicates respiratory irritation or reduced lung function as part of the acute effect; italic typeface indicates that respiratory irritation or reduced lung function is NOT part of the acute effect. This is the case only for carbon monoxide.

Table 6.5 Cancer hazard ratios derived from concentrations or emission factors from this work and from other ambient and laboratory combustion studies.

.	Species of Interest	Unit Risk Factor (URF)	EPA Classification	Laboratory open tire fire burn			Westley Tire Fire			This study (VOC canister)			This study (emission factors)			Pooled Oil Burning		
		[$(\mu g/m^3)^{-1}$]		EF (mg kg^{-1})	HRC	Rank	Conc. ($\mu g\ m^{-3}$)	HRC	Rank	Conc. ($\mu g\ m^{-3}$)	HRC	Rank	EF (mg kg^{-1})	HRC	Rank	EF (mg kg^{-1})	HRC	Rank
	PM2.5	$3.0x10^{-4}$											5350	1.6	1			
71-43-2	Benzene	$2.9x10^{-5}$	A	2205	0.064	2	9.2	$2.7x10^{-4}$	1	26.4	$7.7x10^{-4}$	1				251	$7.3x10^{-3}$	1
91-20-3	Naphthalene [(a)]	$3.4x10^{-5}$	C	1195	0.041	3												
106-99-0	1,3-Butadiene	$1.7x10^{-4}$	B2	160	0.027	3	1.1	$1.9x10^{-4}$	2	1.5	$2.6x10^{-4}$	2						
100-41-4	Ethylbenzene	$2.5x10^{-6}$	D	632	0.0016	4				2.9	$7.2x10^{-6}$	3				10	$2.5x10^{-5}$	4
50-00-0	Formaldehyde	$6.0x10^{-6}$	B1													139	$8.3x10^{-4}$	2
75-07-0	Acetaldehyde	$2.7x10^{-6}$	B2													44	$1.2x10^{-4}$	3
50-32-8	Benzo(a)pyrene	$1.1x10^{-3}$	A	113.9	0.13	1	0.15	$1.7x10^{-4}$	2				3.56	$3.9x10^{-3}$	2	7	$7.7x10^{-3}$	1

(a) Volatile and semi-volatile phase

6.4.5 Tire fire irritant smoke AQI

The 24-h AQI of tire fire smoke measured as $PM_{2.5}$ (PM_t) is shown in **Figure 6.5**. It is calculated for two values of p (1 and 2.5, respectively) in the absence of background PM. 26 $\mu g/m^3$ of tire fire smoke equates to an AQI of 100 using p=1, which can be contrasted to the ambient $PM_{2.5}$ concentration of 35.4 $\mu g/m^3$ required for the same AQI. When tire fire smoke $PM_{2.5}$ is 26 $\mu g/m^3$, it is expected to contain 13 ppb of SO_2 and 3.4 ppb of benzene. The contribution to the AQI at that concentration was 80% from $PM_{2.5}$, 19% from SO_2, and 1% from other gases. The p=2.5 curve crosses the AQI 100 threshold at a PM_t concentration of 34.8 $\mu g/m^3$. Tabulated results from a tire fire irritant smoke calculation for a 1-h AQI at a PM_t value of 100 $\mu g/m^3$ can be found in **Table 6.6**, and a lookup table of AQI values as a function of tire fire smoke and ambient $PM_{2.5}$ is in **Table 6.7**. It is anticipated that an incident command team could use a lookup table such as **Table 6.7**, or an equivalent tool, during a fire response to interpret monitoring and/or dispersion modeling data.

Carbon monoxide and B[a]P were included in **Table 6.3** but not in the AQI calculation because their health impacts do not include respiratory irritation. Carbon monoxide has serious health effects and should be considered during tire fires; however, using the emission ratios of this work, and the concentrations needed to reach levels equivalent to an AQI of 100, a tire fire smoke AQI for CO will be less than 10% of the value calculated from PM_t alone, and less than 17% of that calculated from SO_2 alone. H_2S is a respiratory irritant with a low AEGL-1 possibly in tire fire smoke (WDHFS, 2006). Its emission factor is largely unknown, and it is not included in reported AQI values from Iowa City, but including it using an emission factor derived from reported

H_2S/CO ratios would increase the AQI values by about 5%. A detailed example of a tire fire smoke AQI calculation can be found in Supplementary Material.

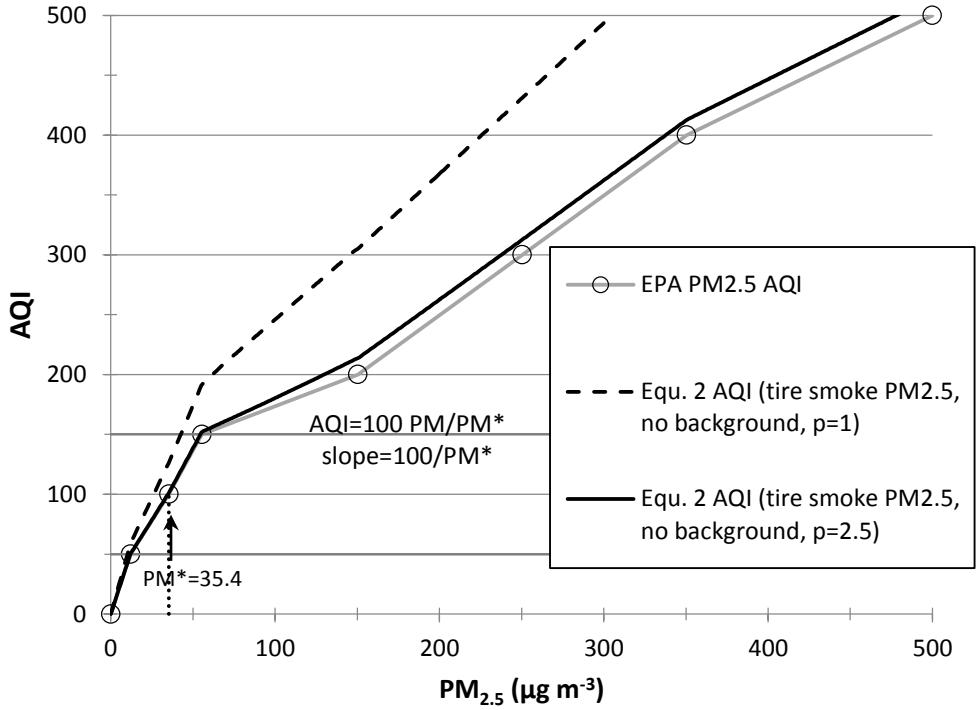

Figure 6.4 Relationship between $PM_{2.5}$ concentrations (x-axis) and Air Quality Index (AQI) (y-axis). Two $PM_{2.5}$ vs. AQI relationships from equation 6.2 are compared to the current US EPA $PM_{2.5}$ Air Quality Index.

Some factors may cause the AQIs presented in this work to be lower limits than those that could (and perhaps should) be calculated. These include the fact that (1) we treat tire fire smoke $PM_{2.5}$ the same as ambient $PM_{2.5}$ without any multiplier to account for its properties; (2) we neglect the impacts of the coarse fraction of tire fire smoke; (3) the AEGL-1 concentrations for many of the VOCs in this work are higher than other threshold concentrations that could also be justified. Counterbalancing these are the use of p=1 in AQI in the figures and tables of this work (besides **Figure 6.3** which includes both), and the use of the NAAQS 24-h $PM_{2.5}$ value of 35.4 µg m^{-3} as a key threshold for

the AQI when other higher thresholds could also be justified, such as the occupational limit of respirable dust, which ranges from 3-5 mg/m^3. We feel that summing over irritating components of the tire fire smoke (i.e., using p=1) is justified because it is a conservative, protective assumption, and furthermore, it counterbalances some of the factors listed above that serve reduce the AQI.

Table 6.6 Variables necessary for calculation of the multicomponent air quality index (AQI)

Species	EF_i/EF_t	Concentration* for an individual pollutant AQI of 100			Method**	Fraction of total AQI at 100 µg/m^3, p=1, 1 h
		1 h	8 h	24 h		
$PM_{2.5}$	1.0	88	50	35	NAAQS	0.71
SO_2	1.33	0.075	0.075	0.075	NAAQS	0.282
Acrolein	0.0021	0.0112	0.0112	0.0112	AEGL	0.0035
Formaldehyde	0.026	0.34	0.34	0.34	AEGL	0.00273
Benzene	0.41	19.5	3.4	3.4	AEGL	0.00167
Vinylcyclohexene	0.021	0.186	0.186	0.186	est. STEL	0.00107
Benzaldehyde	0.124	1.50	1.50	1.50	STEL	0.00083
Biphenyl	0.062	0.96	0.44	0.44	AEGL	0.00097
Phenol	0.133	5.6	2.36	2.36	AEGL	0.00064
Naphthalene	0.223	5.6	5.6	5.6	STEL	0.00033
Styrene	0.121	7.5	7.5	7.5	AEGL	0.00016
Indene	0.063	5.6	5.6	5.6	STEL	0.00010
Ethyl benzene	0.118	12.4	12.4	12.4	AEGL	9.58E-05
1,2,4-Trimethylbenzene	0.154	52	16.9	16.9	AEGL	8.11E-05
Xylene, mixed	0.38	49	49	49	AEGL	7.74E-05
Toluene	0.47	75	75	75	AEGL	7.26E-05
Limonene	0.61	187	187	187	est. STEL	2.53E-05
Cumene	0.074	18.7	18.7	18.7	AEGL	3.52E-05
Acetaldehyde	0.0060	16.9	16.9	16.9	AEGL	8.57E-06
Isovaleraldehyde	0.00093	2.47	2.47	2.47	est. STEL	4.67E-06
1,3-Butadiene	0.0299	251	251	251	AEGL	2.34E-06
Acetone	0.0037	75	75	75	AEGL	9.14E-07
Methyl ethyl ketone	0.0013	75	75	75	AEGL	2.58E-07
Nonane	0.0024	375	375	375	est. STEL	5.38E-08
Hydrogen sulfide	0.22†	0.19	0.12	0.12	AEGL	0.05

*Units are µg/m^3 for $PM_{2.5}$, and ppm for all other entries
**est. STEL indicates the AQI breakpoints were based on the SO_2 breakpoints scaled to the ratio of the SO_2 STEL to an estimated species STEL (5 times TLV-TWA)
†H_2S was not included in the reported AQI in this work because the high uncertainty on its presence in the smoke. The 0.22 emission ratio is based on a single H_2S/CO reading detected downwind of a tire fire. See text for discussion.

Table 6.7 AQI values (p=1) as a function of tire fire $PM_{2.5}$ smoke concentration and background $PM_{2.5}$ concentration. Colors correspond to ranges as follows: green 0-50 (good); yellow 51-100 (moderate); orange 101-150 (unhealthy for sensitive groups); red 151-200 (unhealthy); purple 201-300 (very unhealthy); maroon >300 (hazardous). An expanded table with smoke indicators other than $PM_{2.5}$ (e.g. CO, CO_2) can be found in the Appendix.

1hr Avg. Tire Fire PM2.5 (µg/m^3)	1hr Avg. Background PM2.5 (µg/m^3)					
	0	10	20	30	40	50
0	0	13	26	39	52	62
1	2	15	28	42	54	64
2	4	17	30	44	55	65
3	6	19	33	46	57	67
4	8	21	35	48	59	69
5	10	23	37	50	61	71
10	21	34	47	59	69	79
20	41	54[b]	67	77	87	97
30	62	74[a]	84	94	104	114
50	99	109	119	129	139	149
100	184	194	204	214	222	225
200	281	284	286	288	291	293
300	330	333	335	337	340	342

8hr Avg. Tire Fire PM2.5 (µg/m^3)	8hr Avg. Background PM2.5 (µg/m^3)					
	0	10	20	30	40	50
0	0	23	45	64	82	100
1	3	26	48	67	85	102
2	6	29	52	69	87	105
3	9	32	54	72	90	107
4	12	35	57	74	92	110
5	15	38	59	77	95	112
10	30	53	72	90	108	125
20	61	79	97	115	132	150
30	87	105[c]	123	140	157	173
50	138	155	172	188	192	196
100	231	235	239	244	248	252
200	318	328	338	348	358	368
300	444	449	454	459	465	470

24hr Avg. Tire Fire PM2.5 (µg/m^3)	24hr Avg. Background PM2.5 (µg/m^3)					
	0	10	20	30	40	50
0	0	42	67	88	112	137
1	5	47	70	91	115	140
2	10	52[e]	73	94	118	143
3	15	54	76	97	121	146
4	20	57	79	100	125	150
5	25	60	82	103	128	153
10	49	75[d]	96	119	144	160
20	82	104	127	152	167	173
30	111	134	159	175	180	186
50	174	190	195	201	206	211
100	246	251	257	262	267	272
200	368	378	388	398	408	418
300	494	504	514	524	534	544

[a]Cell corresponding to the most exposed 1h period at the Hoover site (measurements)

[b]Cell corresponding to the most exposed 1h period at IA-AMS (measurements)

[c]Cell corresponding to the most exposed 8h period at the Hoover site (measurements)

[d]Cell corresponding to the most exposed 24h period at the Hoover site (measurements)

[e]Cell corresponding to the most exposed 24h period at IA-AMS (dispersion model)

6.4.6 Application of AERMOD as an emergency response tool for landfill fire dispersion

The emission rate from the fire is a necessary parameter for quantitative dispersion modeling, and this was unknown during the initial days of the fire. Three particulate mass measurements at BDR (see **Figure 6.1**, May 30, Downard et al. 2015) were used to calculate a preliminary emission rate of 0.4 g/s to match observed plume impact. For retrospective assessment of ambient concentrations, this emission rate was scaled to minimize model error as described in the methods section, resulting in a minimum average absolute fractional error of 0.87 for a scaling factor of 3.6 (r^2 of model-observation pairs 0.61; model mean 26 µg/m^3; observation mean 19 µg/m^3; n=20).

Figure 6.6 maps AERMOD predicted tire fire smoke concentrations from May 26 - June 8, 2012 for the 1-h maximum (**Fig. 6.6a**) and 24 h maximum (**Fig. 6.6b**) $PM_{2.5}$. The 1-h maximum has an additional 2.6 multiplier to reflect potential temporal variability in emission rate, based on the ratio of the maximum to the average $PM_{2.5}$ emission factor in Downard et al. (2015). The highest concentration in the 1-h map is 3900 $\mu g/m^3$ located at the landfill. AERMOD 1-h maximum concentration of tire fire $PM_{2.5}$ smoke for the study period at distances of 1, 2, 3, 5 and 10 km were 243, 131, 80, 55 and 26 $\mu g/m^3$, respectively. Likewise 8-h (not shown) and 24-h maximum concentrations at the same distances were 107, 42, 27, 15 (8-h) and 60, 25, 16, 9 and 4 (24-h) $\mu g/m^3$, respectively.

AQI values in **Figure 6.6** were calculated for the p=1 case. Exposure risks within a radius of approximately 1.5 km from the fire were clearly in the unhealthy zone during at least 1 hour of the fire and smoke levels as far as 18 km downwind were also likely to exceed AQI values of 100 for at least 1 hour of the event. Risks based on 24-h max $PM_{2.5}$ concentration also suggest areas as far as 3.1 km from the fire reached an unhealthy AQI for sensitive subpopulations. The recommended action for such zones, according to the OEHHA air quality index, is to consider closing sensitive areas such as schools, and cancelling outdoor events. Air quality in areas further than 3 km downwind from the fire was moderate when considering 24 h and longer averaging time periods.

Based on the modelled $PM_{2.5}$ average for the duration of the tire fire, an increased cancer risk is calculated for B[a]P, the compound used in past tire fire cancer risk estimates, as well as $PM_{2.5}$.

The B[a]P to $PM_{2.5}$ ratio in the smoke is $7x10^{-4}$ (Downard et al., 2015). At the most impacted location (1 km) from the fire, the modeled mean concentrations during the fire period were 5.5 µg/m^3 and 3.8 ng/m^3 of tire fire $PM_{2.5}$ and B[a]P, respectively.

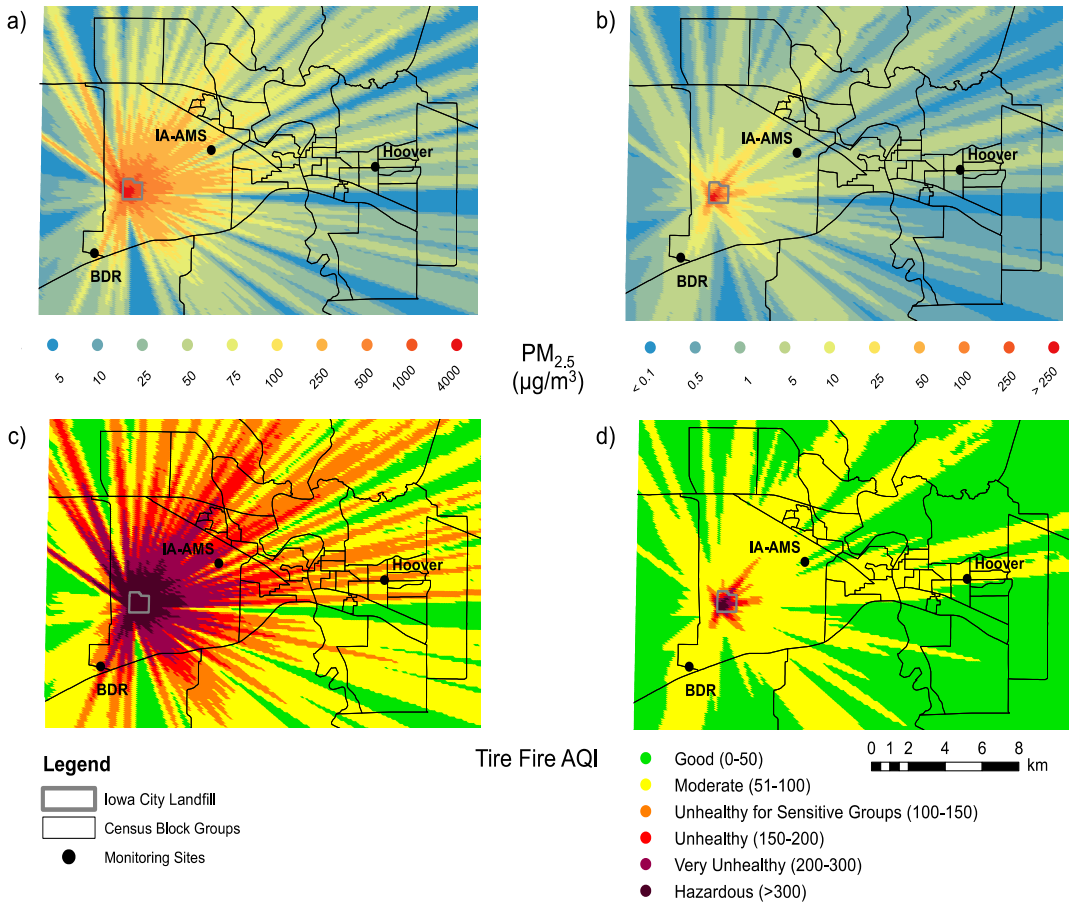

Figure 6.5 WRF-AERMOD dispersion model results for the period May 30 – June 12, 2012. (a) 1-h maximum concentration of tire fire smoke (µg/m^3 $PM_{2.5}$); (b) 24-h maximum concentration of tire fire smoke (µg/m^3 $PM_{2.5}$); (c) 1-h maximum AQI (p=1); and (d) 24-h maximum AQI (p=1)

The corresponding potential cancer risks are 1.2x10-6 and 3.0x10-9, respectively. To compare, the cancer risk for B[a]P of 7.0x10-9 during the Blair Township tire fire was similar (Sidhu et al., 2006). The B[a]P assessments of Sidhu and in Iowa City were both below the common acceptable risk threshold of 1x10-6, while the value for PM2.5, using

the diesel PM URF exceeded it. The applicability of the diesel particulate matter URF to PMt has not been established, but is used here due to the lack of other information about the cancer risks of the PM components of tire fire smoke.

6.4.7 Lessons learned for emergency response and monitoring

Review of notable tire fires in the US and Canada indicates a wide variety of air quality responses during emergency situations. We offer some recommendations for emergency air quality response in **Table 6.8**. The recommendations are in part based on a local multi-agency retrospective review (JCDPH, 2012) of the public health response to the Iowa City fire.

With respect to what compounds to target for monitoring and monitor placement, any of the high hazard ratio compounds (e.g., SO_2, $PM_{2.5}$, CO, black carbon PM, formaldehyde, acrolein) are sufficient. Concentrations of unsampled pollutants can be estimated using emission ratios. For example, the AQI in this work uses emission factor ratios based on PM. An example of an expanded AQI reference table with pollutants other than $PM_{2.5}$ as the smoke tracer can be found in Supplemental Materials.

A distance of 1-3 km radius from the fire provides the most actionable data for the public health response. At this distance, the plume will have undergone initial dispersion and plume processing and will allow for measurement of the plume and background air. Additional monitoring within 1 km of the source can be added if warranted by public health concerns with respiratory protection for monitoring personnel. Monitoring can be added at specific locations that may be of interest to determine or verify population exposure.

Stationary monitoring at 24-h time resolution is listed in Table 6 as lower priority, and this designation requires explanation. 24-h time resolution samples are useful for verifying impacts on populated areas, but they are not spatially representative (for example see **Figure 6.4**) and do not permit estimation of source strength and dispersion model calibration unless the duration of plume impact periods is well known. VOC speciation is similarly listed in **Table 6.6**. Because of the modest impact that VOCs had in the hazard ratio and AQI analysis, we list them as lower priority. However, the VOC sampling can be an important part of the monitoring response. VOCs do serve as a tracer for the smoke, and measurements can confirm uncertain source profile estimates.

Table 6.8 Recommended steps and detailed actions to respond to a large-scale urban fire.

Step	Detailed Actions
Prepare	• Practice multi-agency response • Map important sites and monitor placement • Establish how monitors will be obtained and operated
Monitor	• HIGHER PRIORITY: Monitor 1-hr $PM_{2.5}$, SO_2, CO, black carbon, or PM_{10} 1-3 km from source in populated areas. *These data can be used to assess population exposure, evaluate smoke intensity, calculate AQI values, and calibrate emissions for model.* • LOWER PRIORITY: Monitor above < 1 km from source (see text); Collect samples for VOC analysis (see text); 24-hr monitoring (see text); particulate matter chemical speciation
Model	• Forecast plume intensity, position, and AQI using AERMOD or equivalent • Adjust emission rates using monitoring data
Interpret	• Calculate AQI • Issue public health statements

Ideally, both rapid sampling (instantaneous to 10 min integration) and integrated sampling at 1, 8 or 24 h averaging time should take place at fixed locations for assessing population exposure potential. We recommend that (i) at least one compound be measured by both short term methods (<10 min) and integrated sampling (1 to 24-h) at the same location during plume impaction event(s); and (ii) that short term samplers, such

as grab measurements, be co-located and operated simultaneously for some samples. This sampling strategy has numerous desirable characteristics. It directly measures both background and plume concentrations (by the instantaneous and real-time instruments); it allows estimation of concentration impacts at longer averaging times (using integrated samplers); it allows inter-comparison of instruments (thus permitting calculation of concentration ratios and/or emission factors); it spatially constrains the plume (via a network of fixed site real-time instruments); and it is well-suited for calibration or evaluation of dispersion models.

We recommend that concentrations from dispersion modeling and monitors be converted to an AQI scale that the incident command team has been trained on; concentration predictions without interpretation may not be actionable for local responders. In the absence of other data, we recommend a $PM_{2.5}$ emission rate of 5.3 g per kg of combusted tire (Downard et al., 2015) if the mass burn rate can be estimated, and 36 μg $PM_{2.5}$ $m^{-2}s^{-1}$ if not but the extent of the fire is known.

As reiterated in the FEMA tire fire manual and other documents (IWMB, 2002; OSFM, 2004; USFA, 1998), a pre-planning incident plan is critical for responding intelligently to any hazmat fire. Landfills utilizing shredded tires should preplan for a hazmat fire in the liner system. One potentially transferrable preplanning structure is North Carolina's multiagency Air Toxic Analytical Support Team, or ATAST (NCDAQ, 2014).

As highlighted in Table 6, pre-planning should include a scheduled exercise where multiagency response is simulated. Such exercises are critical for developing competence with the necessary sampling protocols, and at identifying problems in the

emergency response, such as gaps in training, communication, incident command structure, or equipment. A scheduled exercise would deal with one item noted in the Iowa after action review: confusion on communication protocols for contacting state and federal resources, and uncertainty on the extent and nature of the federal response once contact was made. In the Iowa City event, the federal response was advisory (from EPA and DTRA), but in other tire fires EPA deployed equipment and personnel. The exercise should include predetermination of public health messages, distribution outlets, and public health protection measures (closures, cancellations, evacuations, etc.) relative to anticipated AQI level or other concentration-based action levels. Finally, it is important to identify agencies or service providers with equipment and expertise to implement or guide an air monitoring response, and to establish how resources will be procured (e.g., establish contracts or memoranda of understanding).

Several research needs were identified based on the Iowa incident and follow up analysis. Additional work is warranted on multiple pollutant risk assessment. Calibrated, low-cost, portable, and battery-powered monitors with wireless data reporting features are needed to streamline emergency monitoring network deployment. In terms of smoke composition, research needs include refinement of emission factors and their sensitivity to combustion conditions, with specific emphasis on H_2S, aldehydes, organic vs. elemental carbon, metals speciation, and organics speciation of total and size-resolved PM. Characterization of the mass distribution, deposition lifetime, and morphology of smoke particles is also needed. Finally, within the public policy and waste management community, reassessment of the costs, risks, and benefits of shredded tire landfill drainage systems is warranted given the potential fire and public health risk. Furthermore,

the relationship between open burning of an exposed liner and underground elevated temperature incidents (Jafari et al, 2015; Martin et al., 2013) should be investigated.

6.5 Conclusions

We have assessed the outdoor concentrations of pollutants generated from the 18 day 2012 Iowa City tire fire at a variety of averaging times. We estimated maximum concentrations (1-h) of tire fire $PM_{2.5}$ smoke at distances of 1, 5 and 10 km of 243, 55 and 26 $\mu g/m^3$, respectively. Likewise 24-h maximum concentrations at the same distances were 60, 9 and 4 $\mu g/m^3$, respectively. Use of hazard ratios to screen many components in the tire fire smoke, and adoption of a novel multi-pollutant AQI system for irritant smoke will improve decision support capabilities and streamline monitoring strategies. For example, the use of the AQI establishes that smoke concentrations reached unhealthy outdoor levels out to distances of 1.6 km and 11 km at 24-h and 1-h averaging times, respectively. The fire constituted a serious public health concern, and we report recommendations for responding to future comparable incidents – preplanning, monitoring, dispersion modeling, and future research needs. We stress that the emission rate, speciation, and meteorology of each tire fire are unique, and while we believe our findings are generalizable, the extent of variability, especially in emissions speciation, is not well quantified.

6.6 Acknowledgements

The authors would like to acknowledge Andy Gross of the Defense Threat Reduction Agency for discussion on dispersion modeling. We also thank Walker Williams for assistance with sample collection on Black Diamond Road and the Operator Performance Laboratory at the University of Iowa for help with the plume transect study.

Funding was provided by the University of Iowa Environmental Health Sciences Research Center through the National Institutes of Health (NIH, 428 P30 ES05605) and NASA grant NNX11AI52G.

6.7 Author's contributions

This work is published in Singh et al., (2015). A. Singh, C. Stanier and S. N. Spak designed the study and A. Singh performed all the field sampling, measurement analysis and draft write up. S. N. Spak provided all the AERMOD dispersion maps. E. Stone and J. Downard provided all the provided all the integrated measurement, feedback on analysis and draft write. Robert Bullard co-led the field sampling for the Stanier group. All authors contributed to the final form of the manuscript

6.8 References

Akagi, S.K., Craven, J.S., Taylor, J.W., McMeeking, G.R., Yokelson, R.J., Burling, I.R., Urbanski, S.P., Wold, C.E., Seinfeld, J.H., Coe, H., Alvarado, M.J., Weise, D.R., 2012. Evolution of trace gases and particles emitted by a chaparral fire in California. Atmospheric Chemistry and Physics 12, 1397-1421.

Austin, C., 2008. Wildland firefighter health risks and respiratory protection, Montreal, Canada, pp. 1-52.
CalEPA, 2002. Tire fire report office of environmental health hazard assessment. California Environmental Protection Agency, California, pp. 1-20.

CalEPA, 2003. Toxicity Criteria Database. California Environmental Protection Agency California Environmental Protection Agency, California.

Cecich, V., Gonzales, L., Hoisaeter, A., Williams, J., Reddy, K., 1996. Use of shredded tires as lightweight backfill material for retaining structures. Waste Management & Research 14, 433-451.

Chen, R., Wang, X., Meng, X., Hua, J., Zhou, Z., Chen, B., Kan, H., 2013. Communicating air pollution-related health risks to the public: An application of the Air Quality Health Index in Shanghai, China. Environment International 51, 168-173.

Davis, N., Arunachalam, S., Brode, R., 2008. MCIP2AERMOD: a prototype tool for preparing meteorological inputs for AERMOD. , 7 th Annual Models-3 CMAS Users Conference CMAS, Chappel Hill, North Carolina, p. 21.

Dimitriou, K., Paschalidou, A.K., Kassomenos, P.A., 2013. Assessing air quality with regards to its effect on human health in the European Union through air quality indices. Ecological Indicators 27, 108-115.

EPA, 1989. Risk Assessment Guidance for Superfund Volume I Human Health Evaluation Manual (Part A). Environmental Protection Agency, Washington D.C.

EPA, 1997. Air emissions from scrap tire combustion. Environment Protection Agency, Washington, D.C.

EPA, 1999. Copendium Methods TO-15: Determination of Volatile Organic Compounds (VOCs) in Air Collected In Specially-Prepared Canisters and Analyzed by Gas Chromatography/Mass Spectrometry (GC/MS)

EPA, 2004. Aermod : Description of model formulation. Environmental Protection Agency, North Carolina.

EPA, 2006. Guidelines for the Reporting of Daily Air Quality – the Air Quality Index (AQI). U.S. EnvironmentalProtection Agency, Research Triangle Park, North Carolina.

EPA, 2009. Technical Assistance Document for the Reporting of Daily Air Quality – the Air Quality Index (AQI). Environment Protection Agency, Research Triangle Park.

EPA, 2011. Integrated Risk Information System (IRIS). EPA, Washington DC.

FEMA/USFA, 2002. Landfill fires: Their magnitude, characteristics and mitigation. Federal Emergency Management Agency, Arlington , Virginia, pp. 1-26.
Fiksel, J., Bakshi, B.R., Baral, A., Guerra, E., DeQuervain, B., 2011. Comparative life cycle assessment of beneficial applications for scrap tires. Clean Technologies and Environmental Policy 13, 19-35.

Gurjar, B.R., Butler, T.M., Lawrence, M.G., Lelieveld, J., 2008. Evaluation of emissions and air quality in megacities. Atmospheric Environment 42, 1593-1606.

Holmes, N.S., Morawska, L., 2006. A review of dispersion modelling and its application to the dispersion of particles: An overview of different dispersion models available. Atmospheric Environment 40, 5902-5928.

IWMB, 2002. Tire Pile Fires : Prevention , Response , Remediation. Integrated Waste Management Board, Santa Ana, California.

JCPHD, 2012. After Action Review – Air Quality Monitoring Activities during Iowa City Landfill fire, in: Department of Public Health, J.C. (Ed.). Johnson County, Iowa City.

Kakosimos, K.E., Assael, M.J., Katsarou, A.S., 2011. Application and evaluation of AERMOD on the assessment of particulate matter pollution caused by industrial activities in the Greater Thessaloniki area. Environmental Technology 32, 593-608.

Kwon, E., Castaldi, M.J., 2009. Fundamental understanding of the thermal degradation mechanisms of waste tires and their air pollutant generation in a N2 atmosphere. Environmental science & technology 43, 5996-6002.

Kyrkilis, G., Chaloulakou, A., Kassomenos, P.A., 2007. Development of an aggregate Air Quality Index for an urban Mediterranean agglomeration: Relation to potential health effects. Environment International 33, 670-676.

Lemieux, P.M., Lutes, C.C., Santoianni, D.A., 2004. Emissions of organic air toxics from open burning: a comprehensive review. Progress in Energy and Combustion Science 30, 1-32.

Lemieux, P.M., Ryan, J.V., 1993. Characterization of Air-Pollutants Emitted from a Simulated Scrap Tire Fire. Journal of the Air & Waste Management Association 43, 1106-1115.

Lindbom, J., Gustafsson, M., Blomqvist, G., Dahl, A., Gudmundsson, A., Swietlicki, E., Ljungman, A.G., 2006. Exposure to wear particles generated from studded tires and pavement induces inflammatory cytokine release from human macrophages. Chemical Research in Toxicology 19, 521-530.

McKenzie, L.M., Witter, R.Z., Newman, L.S., Adgate, J.L., 2012. Human health risk assessment of air emissions from development of unconventional natural gas resources. Science of the Total Environment 424, 79-87.
Morra, P., Lisi, R., Spadoni, G., Maschio, G., 2009. The assessment of human health impact caused by industrial and civil activities in the Pace Valley of Messina. Science of the Total Environment 407, 3712-3720.

Murena, F., 2004. Measuring air quality over large urban areas: development and application of an air pollution index at the urban area of Naples. Atmospheric Environment 38, 6195-6202.

NCDAQ, 2014. Emergency Response Protocol. North Carolina Division of Air Quality, Raleigh, NC.

NOAA, 2013. READY Current & Forecast Meteorology. Air Resource Laboratry, NOAA, College Park, Maryland.

NRC, 2001. Acute Exposure Guideline Levels for Selected Airborne Chemicals: Volume 1. National Research Council, Washington D.C.

OEHHA, 2012. Wildfire Smoke : A guide for public health officials. Air Resource Board, OEHHA, California, pp. 23-24.

OMOE, 1990. Haggersville Tire Fire (1990) Survey: Technical Memorandum. Atmospheric Research And Special Programmes Section, Air Resource Branch, Ontario.

OSFM, 2004. Rings of Fire Revisited: Fire Prevention and Supprresion of outdoor Tire Storage. Office of the State Fire Marshal, California.

Plaia, A., Ruggieri, M., 2011. Air quality indices: a review. Reviews in Environmental Science and Bio-Technology 10, 165-179.

Pleim, J.E., 2007. A combined local and nonlocal closure model for the atmospheric boundary layer. Part I: Model description and testing. Journal of Applied Meteorology and Climatology 46, 1383-1395.

Ritter, K.S., 2013. Tire Inferno, C & EN NEWS, pp. 10-15.

Sidhu, K.S., Keeslarm, F.L., Warner, P.O., 2006. Potential health risks related to tire fire smoke. Toxicology international 13, 1-17.

Silverman, K.C., Tell, J.G., Sargent, E.V., 2007. Comparison of the industrial source complex and AERMOD dispersion models: Case study for human health risk assessment. Journal of the Air & Waste Management Association 57, 1439-1446.

Skamarock, W.C., Klemp, J.B., Dudhia, J., Gill, D.O., Barker, D.M., Duda, M., Huang, X.-Y., Wang, W., Powers, J.G., 2008. NCAR Technical Note: Description of the Advanced Research WRF Version 3. Mesoscale and Microscale Meteorology Division, National Center for Atmospheric Research, Boulder, Colorado.
Steer, P.J., Tashiro, C.H.M., McIllveen, W.D., Clement, R.E., 1995. PCDD AND PCDF IN AIR, SOIL, VEGETATION AND OILY RUNOFF FROM A TIRE FIRE. Water Air and Soil Pollution 82, 659-674.

USFA, 1998. Special Report : Scrap and Shredded Tire Fires, Technical Report Series. United States Fire Administration, Maryland.

Wang, Z., Li, K., Lambert, P., Yang, C., 2007. Identification, characterization and quantitation of pyrogenic polycylic aromatic hydrocarbons and other organic compounds in tire fire products. Journal of chromatography. A 1139, 14-26.

Warith, M.A., Rao, S.M., 2006. Predicting the compressibility behaviour of tire shred samples for landfill applications. Waste Management 26, 268-276.

WDHFS, 2006. Health Consultation : WATERTOWN TIRE FIRETOWN OF SHIELDS, DODGE COUNTY, WISCONSIN, Atlanta, Georgia.

CHAPTER 7: CONCLUSION AND FUTURE WORK

Improvement in the measurement techniques and tools for atmospheric particles, characterization of ultrafine physical properties, emission characterization of a primary source, and health risk assessment were some of the major themes in this thesis.

The goal of aim one was to address the challenges of obtaining real-time concentration of UFPs with sufficient temporal and spatial resolution. A TSI particle counter was modified to build mobile particle counter. The built mobile platform has an independent electric power system, a central controller with robust data acquisition, a GPS system, and a data visualization tool. Field measurements with the mobile CPC illustrated an example of particle concentration data with sufficient temporal and spatial resolution. The primary objective was thus achieved. In the context of providing complete information about particle source, diurnal variation and trace gas measurement, the next phase of the mobile particle counter should be multiplatform, and utilize recent technology development in low cost sensors. As described in Chapter three, the newly developed low cost electrochemical gas sensors such as NO_x, CO, O_3, SO_2, and VOCs as well as portable meteorology sensors, provides a wonderful opportunity in this direction. Additionally, possible integration of a mobile unit with a Quadcopter is another exciting novelty, which has the potential to collect vertical profiles of many pollutants. The data retrieval and graphical interface used in the current mobile CPC can be made more efficient by automating the data retrieval, processing, and visualization step. Replacing the GPS module with a *Wifi-GPS shield* will enable the capability to collect and transmit

the data into a server while sampling. This can also be useful when working with more than one mobile unit.

In aim two, a Volatility Tandem Differential Mobility Analyzer (V-TDMA) system was designed and built to characterize the volatility behavior of UFPs. This particle treatment successfully met all of the physical characterization requirements and showed agreement with volatility signal from other published designs. With experimental verification, the current design offered changes in the traditional design of a thermodenuder. The key design change includes removal of adsorbing system, and use of multiple heating rope and controllers. The design is fully operationally automatized by developing a LabVIEW based user-defined program. The system needs further improvement in time synchronization between different components, expanding the operating temperature higher than 260 ^{o}C, and measuring actual gas temperature rather than the wall temperature.

The major challenge in the V-TDMA design has been the question of equilibrium time and its effects on aerosol volatility. The current design could benefit from a system with multiple heating units running at multiple residence time from 1 to as high 50 seconds or higher. Volatility data at multiple residence time will assist in evaluating actual volatility of the aerosol and offer estimation of heat of vaporization, saturation concentration, evaporation coefficient and others.

Another design change may include experimentation by integrating isothermal dilution with the TD which has been shown to lead better estimates of parameters related to aerosol volatility.

The likelihood of heat-induced chemical reaction such as oligomerization in the organic aerosol could be significant (Kuwata et al. 2011). Field measurements studies using combinations of V-TDMA, CCNC or hygroscopicity will need to incorporate a method to verify the presence of such artifact. Aerodyne high-resolution time-of-flight Aerosol Mass Spectrometer (HR-ToF-AMS) have been used in parallel configuration to detect the change in O, H and C ratio to verify the presence of temperature related oligomerization.

In the third aim, physical characterization of the UFP in the Midwest was conducted with a goal to provide answers to source apportionment, chemical and physical characterization of UFPs, and relating the changes in properties with respect to time, meteorology, and land use pattern. This is the first known application of a V-TDMA system in the Midwest for the measurement of UFP volatility. Specifically, the study tried to answer three questions: relating the volatility signature of particles sized from 6 to 80 nm, identifying differences in the volatility profile with particle formation, and measuring the evaporation resistant residue in the UFP. New approaches to the analysis of multivariate data such as cluster analysis were applied and distinct volatility profiles for 15, 30, 50, and 80 nm were found. Although VFR analysis is insufficient to establish chemical composition definitely, simple graphical methods used in the work showed some volatility profiles resemble closely ammonium sulfate. Additional parameters such as hygroscopicity or CCNC would have added more specific information to the composition analysis. Residues were present in sizes as small as 15 nm and the extent of residue showed size dependence. And these low volatility cores show significant correlation to trace gases and meteorology, information about their chemical composition

and formation pathways are still not known. Particle formation periods during high SO_2 concentrations (1 > ppb) correlated well with increased presence of the least volatile cluster in particles, and low SO_2 concentrations were associated with the increased presence of a high volatile profile. It is consistent with the experimental data but conclusive that particle formation and growth during low SO_2 concentrations may have organic influence. The sampling frequency of external mixture in UFPs is provided in this work. Calculation of sampling frequency for external mixture indicate that larger sizes (>30 nm) have higher fraction of externally mixed sample compared to 15 nm. But the effect of the mixing state to particle growth could not be established.

The future work should involve adding an evaporation model to generate a volatility basis set for the identified clusters. At this point the quantitative differences in the identified volatility cluster are based on temperature. A stronger chemical basis can be approximated by quantifying their volatility basis set using an evaporation model. Relevant to building a robust evaporation model and constrain it to field data, estimation of key thermodynamic parameters is essential. The V-TDMA future field work should focus on adding measurement of volatility at multiple residence time to constraint the equilibrium sensitive parameters in the evaporation model.

Inter-comparison of TDMA results with the previously published TDMA designs is complicated and subject to uncertainty with residence time, temperature profile, heating mechanism, adsorber and other artifact. Huffman et al. (2009) provides a wonderful library of volatility profile from many different TDMA conducted in laboratory and field environment. Use of such profile for comparing with our identified clusters was thus not performed. Therefore V-TDMA field operation will require a

building up of a volatility profile library of many different aerosol types which can be compared with the field data for many different analyses including inferring composition of the aerosol.

Evidence of residue is detected in the study at all sizes. However it is unclear whether these residue are the resultant product of heating or the aerosol do have an actual non-volatile core which is resistant even at high temperature. The likely solution to this issue can only be solved using a mass spectrometry. Laboratory experimentation using various mixtures of aerosol types is required to quantify the effect of heat. This will aid many V-TDMA results reporting evaporation resistant residue. Aerosol dominated by organics is reported to undergo oligomerization in the laboratory and field environment (Kuwata et al., 2011) whereas the no evidence exists for common inorganic aerosol types with or without a fraction of organics. These are interesting experiment that needs to be quantified to trust V-TDMA operation above 100 ^{o}C.

The goal of aim four in this thesis was to build an urban air quality emergency system as a response to accidental fires near populated areas. Difficulty in determining air quality and public health risk during the accidental tire fire in Iowa City was the underlying rationale for the development of a proper air quality management and response system. This thesis made significant contribution in many aspects of the response system including risk assessment using target compounds, multi-pollutant air quality index, and dispersion modeling tied with mobile monitoring. Smoke characterization was another critical analysis presented in this thesis which provided improved emission factors for particle mass and aerosol-PAH, and new emission factors and enhancement ratio values for particles (0.001-2.5 μm) and trace gas. Overall this

thesis included a wide range of scientific and policy analysis specific to urban, landfill and tire fires.

This work can be further explored and expanded in many different ways. For smoke characterization, major missing information is the gas phase VOC emission factors and yield experiments to determine VOC (volatile, semi-volatile and least volatile compounds) partitioning into gas and aerosol phase. In terms of smoke composition, research needs include refinement of emission factors and their sensitivity to combustion conditions, with specific emphasis on H_2S, aldehydes, organic vs. elemental carbon, metals speciation, and organics speciation of total and size-resolved PM. Characterization of the mass distribution and morphology of smoke particles such as density and shape factor is also needed.

In terms of health risk assessment for a toxic smoke, the "additive of health risk" assumption formed the basis for the equation proposed in this study. It is not yet known if health risk posed by multiple toxic pollutants are additive. This is an active area of inquiry which is important for toxic sources such as biomass and tire fires. Accidental fire, in the future, will require a "ready to go" monitoring station. This could be facilitated by using calibrated, low-cost, portable, and battery-powered monitors with wireless data reporting features. This study identified basic online and offline techniques required during monitoring, however it is still suggestive and concrete model and method will need further discussion.

Communication of exposure and health risk, tied to AQI, was another area in which this thesis showed a useful integration of dispersion model, mobile measurements, and AQI. This can be further improved for application by non-academic actors such as

state officials by building an integrated system which will query the nature of the fire, provide instruction about the monitoring strategies, and analyze the air quality data to determine the impact. This could be initiated by developing a pre-planning incident plan especially areas that has shredded tires in their landfill. Existing examples such as the North Carolina's multiagency Air Toxic Analytical Support Team, or ATAST could be useful. In the case of fire accident with likely public health implication, a pre-planning event will help develop competence with the necessary sampling protocols, and at identifying many logistics gaps such training, communication, incident command structure, or equipment. The pre-planning should also include nature of public health messages, and public health protection measures (closures, cancellations, evacuations, etc.) based on the forecasted AQI level or other concentration-based action levels. Finally, within the public policy and waste management community, reassessment of the costs, risks, and benefits of shredded tire landfill drainage systems is warranted given the potential fire and public health risk. Furthermore, the relationship between open burning of an exposed liner and underground elevated temperature incidents (Jafari et al, 2015; Martin et al., 2013) should be investigated.

Overall the thesis adds new instrumentation to the research group to characterize ultrafine aerosol in laboratory and field environments. The application of such instrumentation and its benefits are amply highlighted with many different experiments performed in this thesis. This thesis also provides important insight into physical properties of atmospheric particles in a region of Midwest characterized by mixed dryland and cropland. The thesis showed that particles have distinct evaporation profiles which are indication of their composition. Physical characterization also quantify

evaporation resistant residue all particles size and these residue were correlated to SO_2, and related to the nature of particle formation events. A particle formation and growth event influenced by northern air mass, which is weak in SO_2 concentration, is likely to be influenced by organic. Important contributions were also made for in responding to a scenario in the context of urban air quality management. In that respect, this thesis can serve as a scientific and policy document toward determining risky pollutants in smoke, interpreting risk, and for developing a framework for air quality management during fires.

CHAPTER 8: GLOSSARY OF TERMS

Term	Descriptions
AC	Alternating Current
AERONET	AErosol RObotic NETwork
AIRMON	Atmospheric Integrated Research Monitoring Network
CASNET	The Clean Air Status and Trends Network
CCNC	Cloud Condensation Nuclei Counter
CO_2	Carbon dioxide
CPC	Condensation particle counter
EPA	Environmental Protection Agency
FE	Fresh Emission
GPS	Global Position System
HMMWV	Humvee
IA-AMS	Iowa, Atmospheric monitoring site
IMPROVE	Interagency Monitoring of Protected Visual Environments
LabVIEW	Laboratory Virtual Instrument Engineering Workbench
MOUDI	Precision cascade impactors
NADP	National Atmospheric Deposition Program
NAMS	Nano aerosol mass spectrometer
NCORE	National Core (NCore) multi-pollutant monitoring stations.
NPF	New particle formation
NOAA-GMD	National Oceanic and Atmospheric Administration Global Monitoring Division
NO_X	mono-nitrogen oxides NO and NO2 (nitric oxide and nitrogen dioxide)
NOy	Reactive nitrogen compounds
O_3	Ozone
PAH	Poly-aromatic hydrocarbon

PBE-	Particle burst event
PLC	Particle loss calculation
PSD	Particle size distribution
RB	Regional background
SHL	Stanley hydraulic lab
SLAMS	EPA umbrella network for air quality monitoring
SMPS	Scanning mobility particle spectrometer
SO_2	Sulfur dioxide
TD	Thermodenuder
TD-CIMs	Thermal Desorption Chemical Ionization Mass Spectrometry.
TSI	TSI | Precision Measurement Instruments
UFP	Ultrafine particles
VDC	Voltage differential current
VOC	Volatile organic compounds
V-TDMA	Volatility tandem differential mobility analyzer
WAAS	Wide Area Augmentation System (WAAS)

CHAPTER 9: APPENDIX

Appendix for Aim 1

Section 9.1.cr basic program

```
Public rmclongitude As String
Public rmce_w_indicator As String
Public rmcspeed As String
Public rmccourse As String
Public rmcutcdate As String
'Define the individual parameters of the string RAWDATA
Alias splitRawdata(1) = mode
Alias splitRawdata(2) = Flags
Alias splitRawdata(3) = CN                    ' CN: particle num
Alias splitRawdata (4) = ST                   ' ST: Sample Time
Alias splitRawdata(5) = LT                    ' LT: Live Time
Alias splitRawdata(6) = CNT                   ' Accumulated part
Alias splitRawdata(7) = PH                    ' Place holders
Alias splitRawdata(8) = RP                    ' RP : Raw photome
Alias splitRawdata(9) = FL                     ' S record for th
Alias splitRawdata(10) = AP
Alias splitRawdata(11)= STE
Alias splitRawdata(12) =GT
Alias splitRawdata(13) = OT

'Define Data Tables
DataTable(CO2,True,-1)
  DataInterval(0,10,Sec,10)
  Average(1,BattV,FP2,False)
  Average(1,co2_mv,FP2,False)
  Average(1,co2_ppm, FP2, False)
EndTable

DataTable(CPC, True, -1)  'you'll probably want to change this na
  DataInterval(0,1,Sec,10)
  Sample(1,co2_ppm,FP2)
  Sample (13,splitRawdata(1),Float)
  Sample (1,Rawdata,String)
EndTable

'Main Program
BeginProg
  SerialOpen(com1, 115200,0,0,140) ' communication parameter of t
  Outstring = "SM,4,10" + CHR(13)+ CHR(10)
  SerialOut(com1,Outstring,"",0,100)
  Scan(1,Sec,1,0)
    SerialInBlock(com1, Rawdata, 140)     ' 140 is the approximate
```

```
'CR800 Series
'Created by Ashish Singh 23rd 2012
'Declare Variables and Units

SequentialMode

'CPC
Public BattV
Public co2_mv
Public co2_volt
Public co2_ppm

Units BattV=Volts
Units co2_mv=mV

'CO2 Variables
Public PTemp_c,Temp_c, batt_volt  ' define general parameter of t
Public Rawdata As String * 140  ' define data type out of the sen
Public splitRawdata(13)  ' define individual value when the strin
Public NBytesReturned
Public Outstring As String *10

'GPS16X-HVS at Campbell Scientific Factory Defaults
Const GPSPort = Com2 'Com port where GPS is connected

'***Wiring***
'C7 GPS16X-HVS pulse per second (gray)
'C8 GPS16X-HVS RS-232 TxD (white)
'G GPS16X-HVS power control (yellow)
'12V GPS16X-HVS power (red)
'G GPS16X-HVS power and RS-232 signal reference (black)
'G Ground (blue)
'G Shield (shield)

Public GGAstring As String * 500
Public RMCstring As String * 500
'rmc variables
Public rmcid As String
Public rmcutc As String
Public rmcstatus As String
Public rmclatitude As String
Public rmcin_s_ind As String
```

```
    'SerialInRecord(com1,Rawdata, &h44,120,0,NBytesReturned,01) '
    SplitStr(splitRawdata(),Rawdata,",",13,4)
    SerialFlush(Com1)

    'Default Datalogger Battery Voltage measurement BattV
    Battery(BattV)
    'Generic Single-Ended Voltage measurements co2_mv
    VoltSe(co2_mv,1,mV5000,1,True,0,_60Hz,1,0)
    co2_volt = co2_mv/1000
    co2_ppm = co2_volt*400
    'Call Data Tables and Store Data
    CallTable(CPC)
    CallTable(CO2)
  NextScan
EndProg
```

Section 9.1. Simple diagram of the inlet

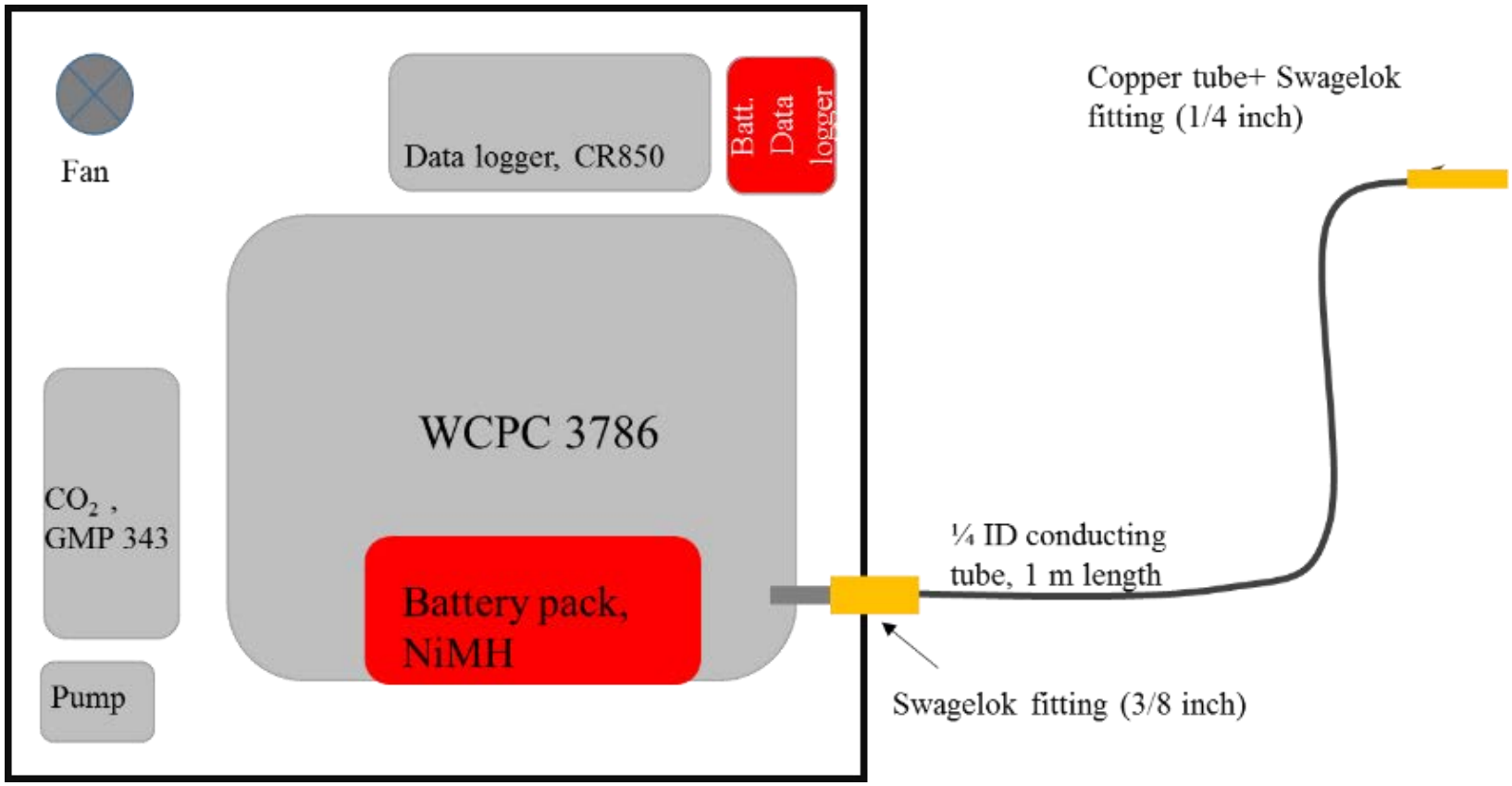

Section 9.1. Power supply design for the mobile CPC

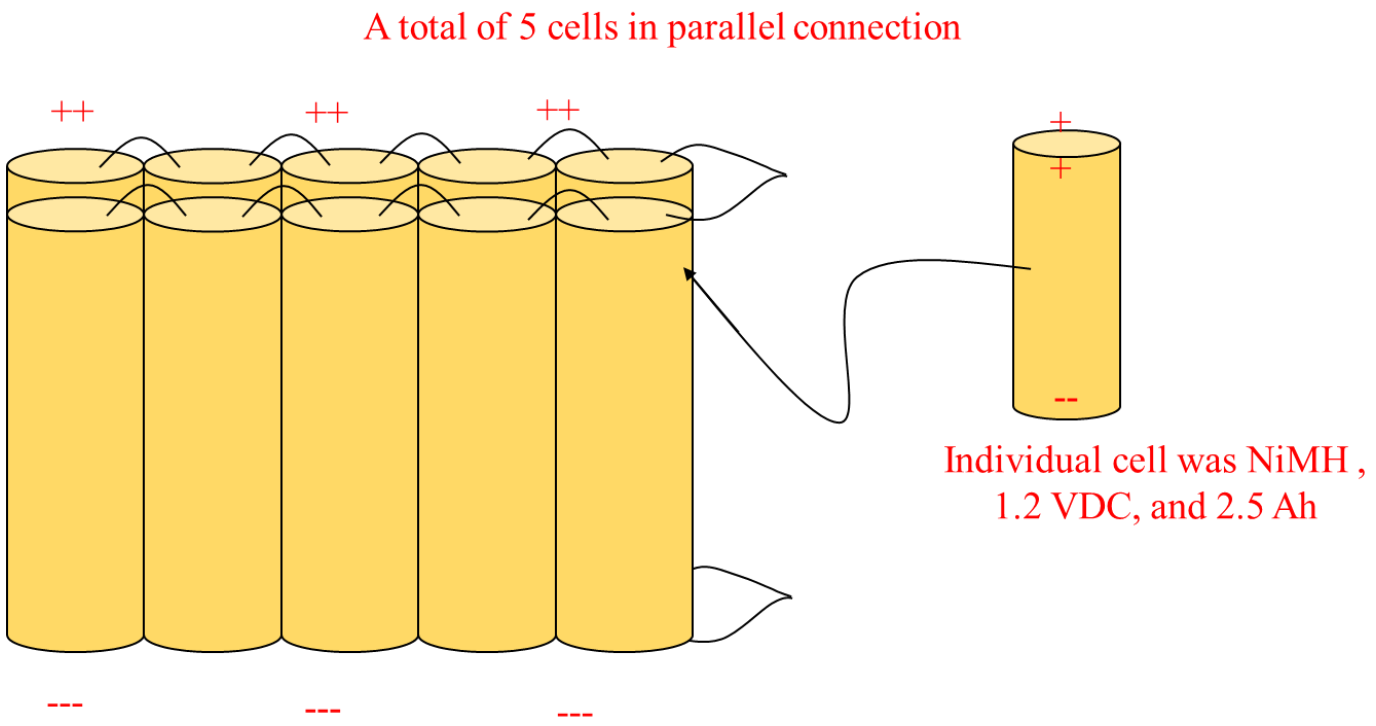

Section 9.1.other measurements results by mobile CPC

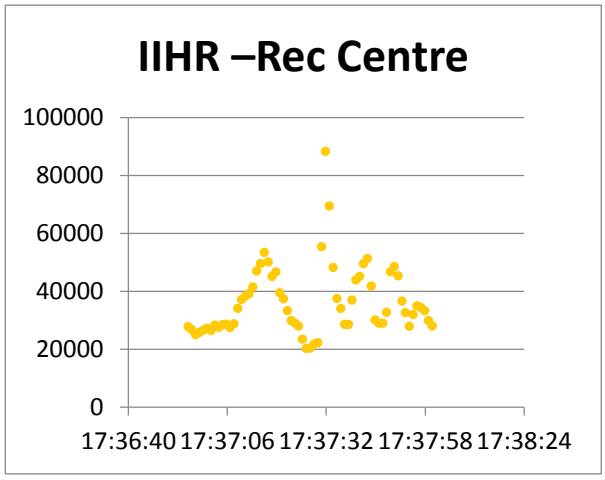

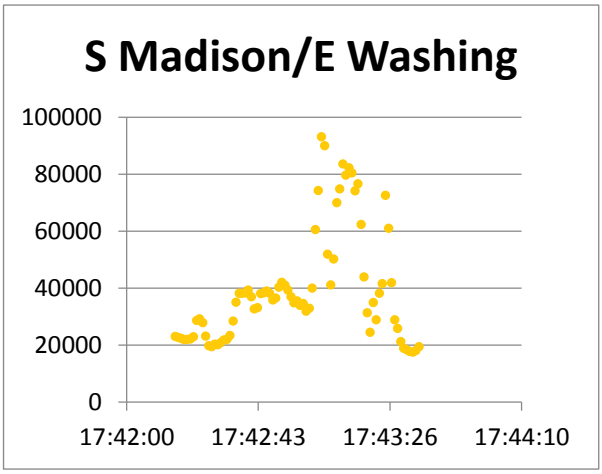

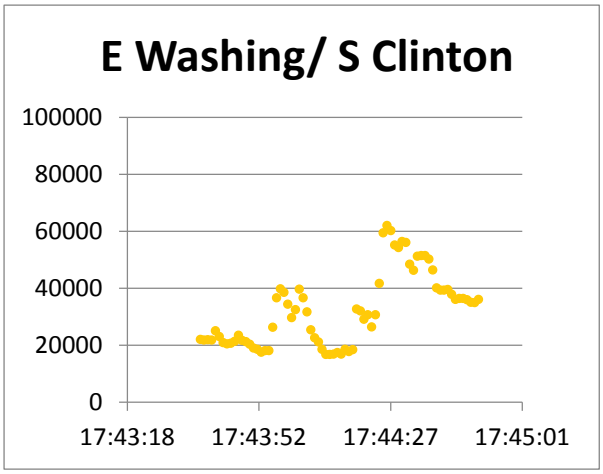

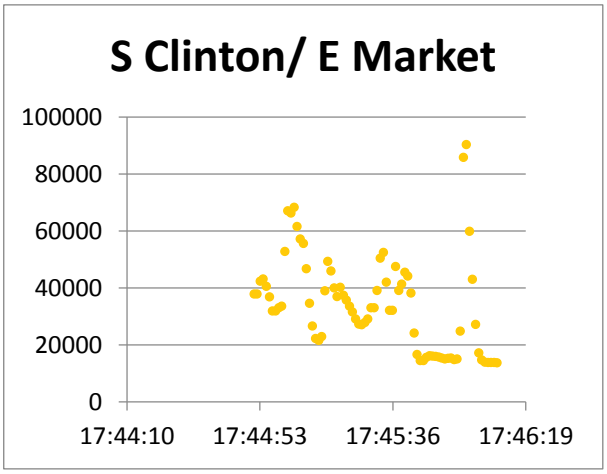

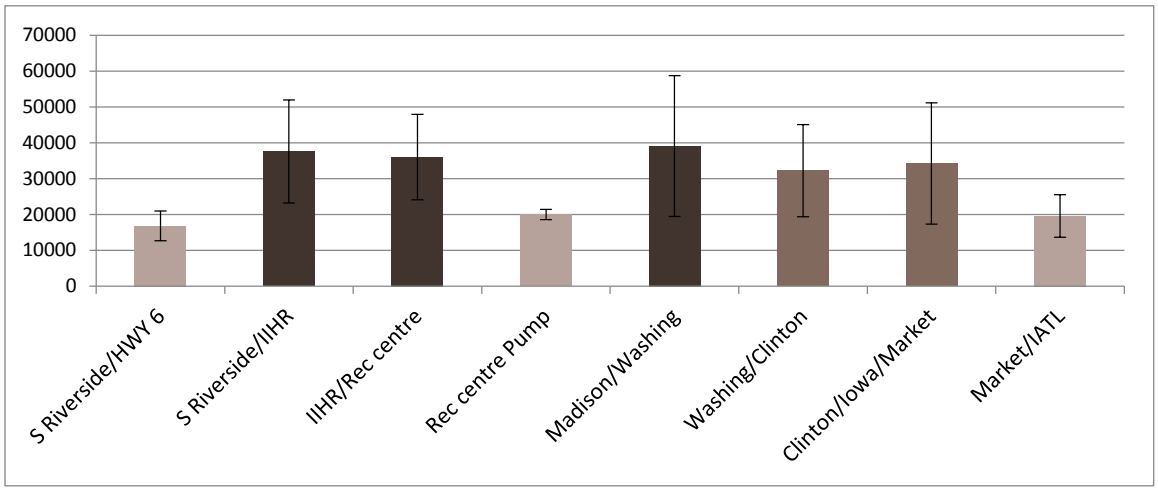

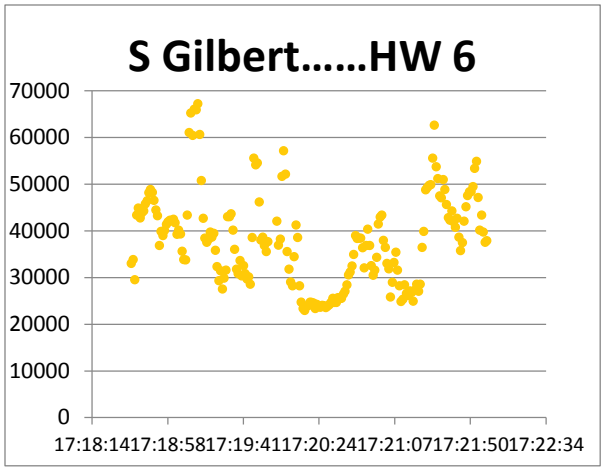

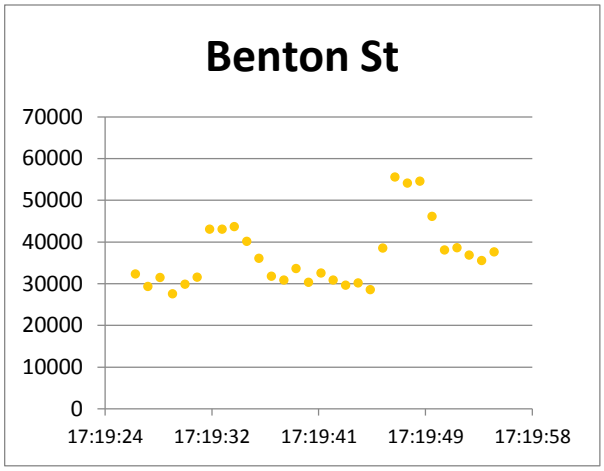

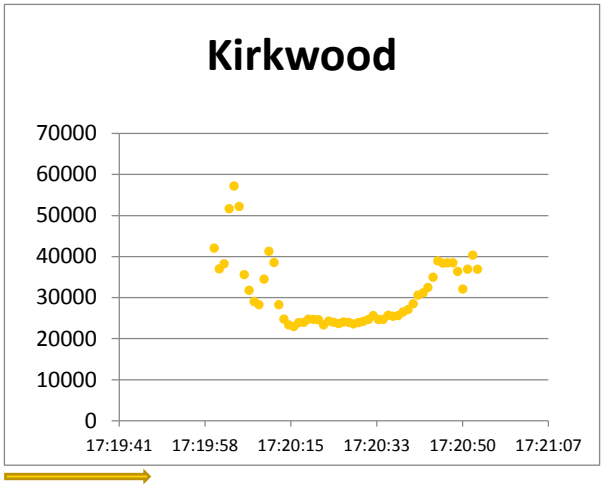

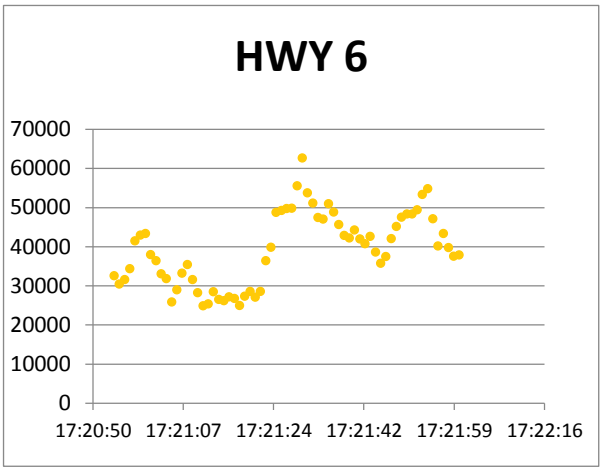

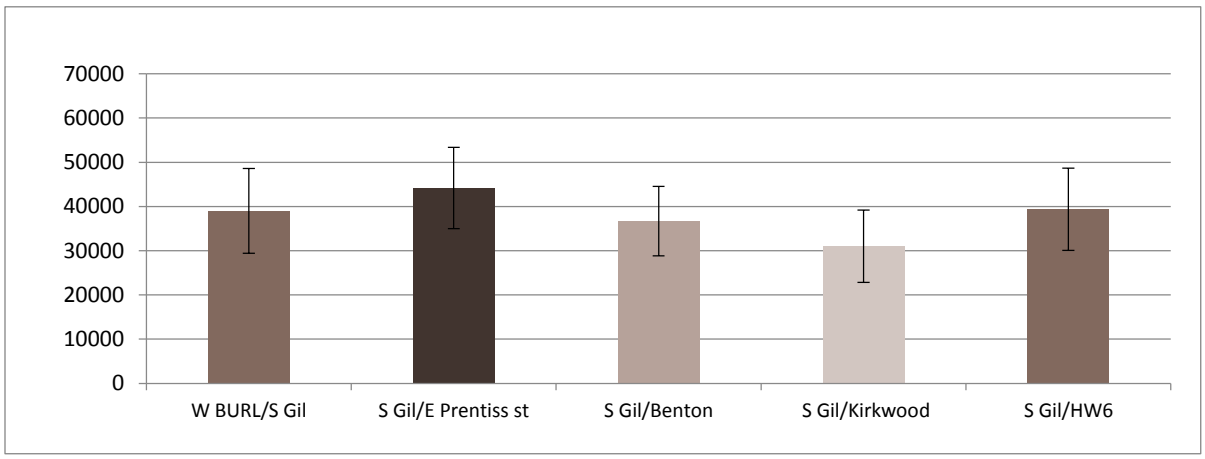

Appendix for Aim 2

Section 9.2. Typical design of the thermodenuder

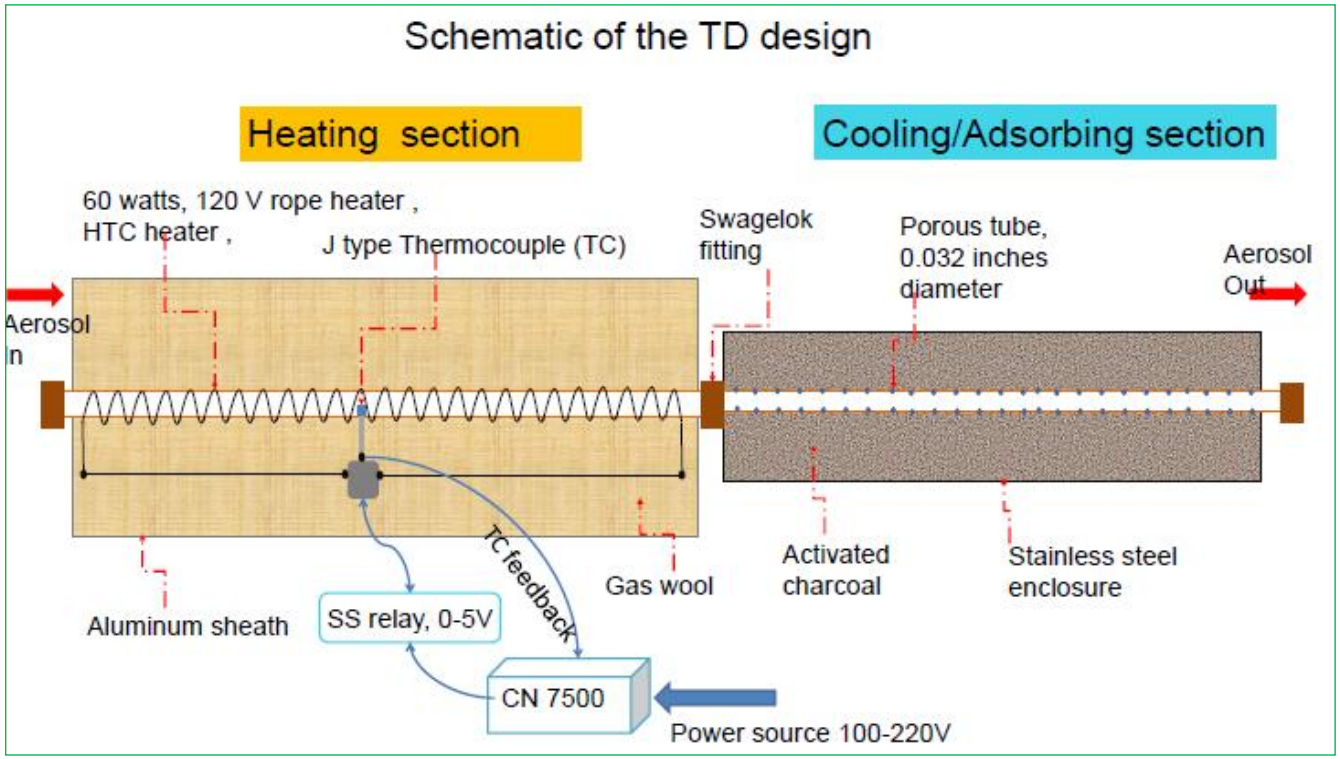

Section 9.2 Wall temperature profile measured at four points T1, T2 T3 and T4 along the wall of the TD during a typical temperature cycle in the V-TDMA operation

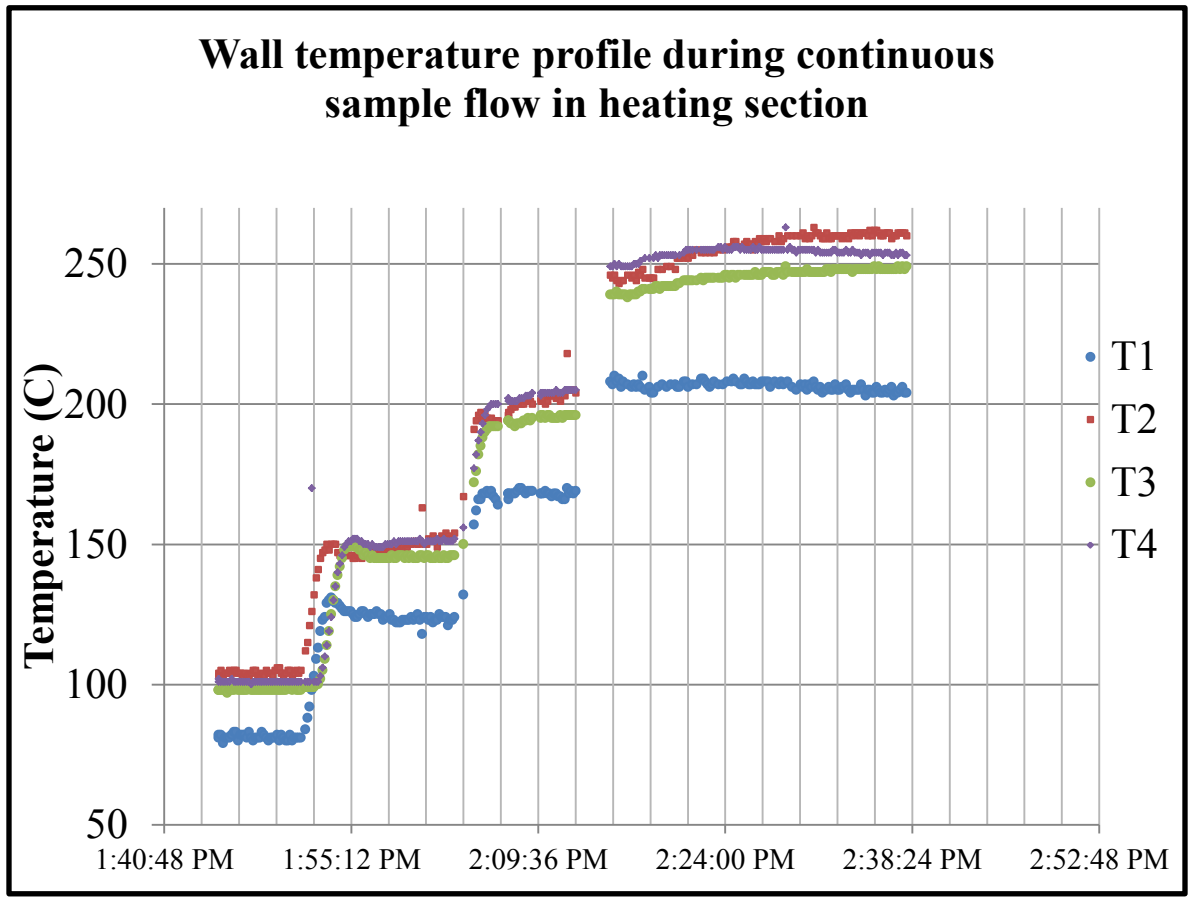

Section 9.2 Comparison of Denuder (AC) and No Denuder comparison with Adipic Acid (50nm)

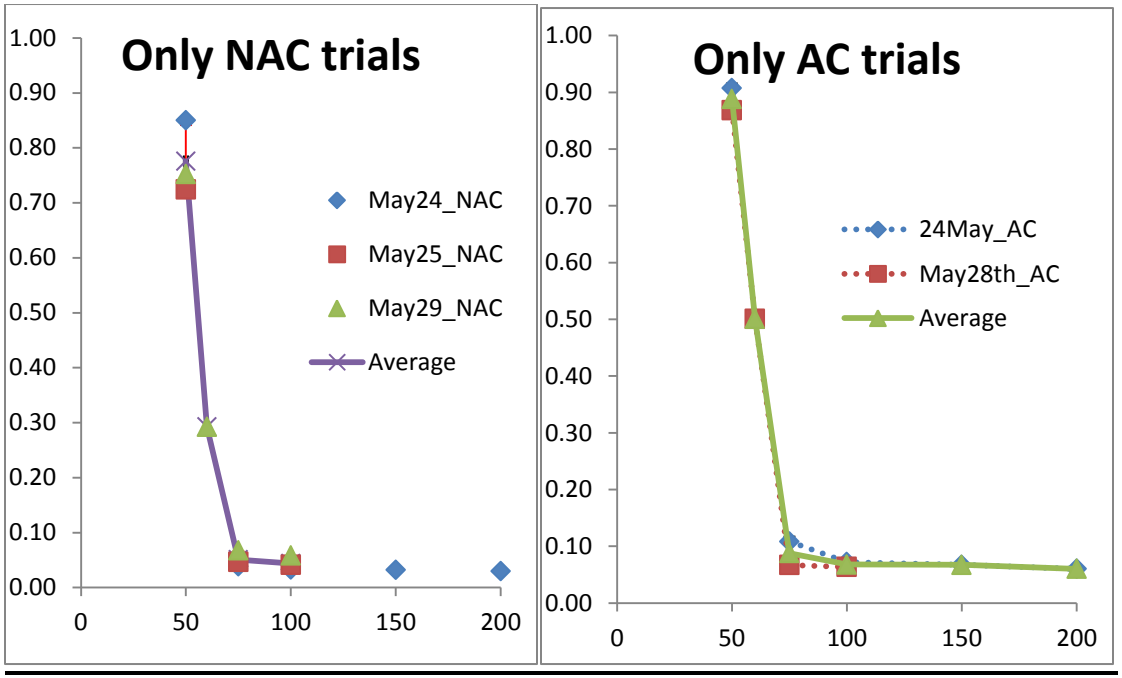

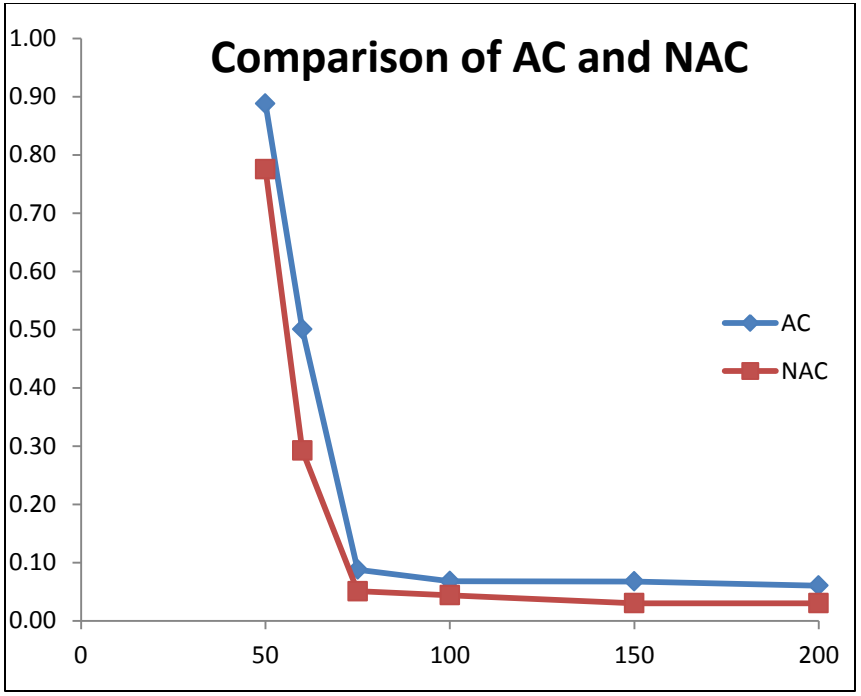

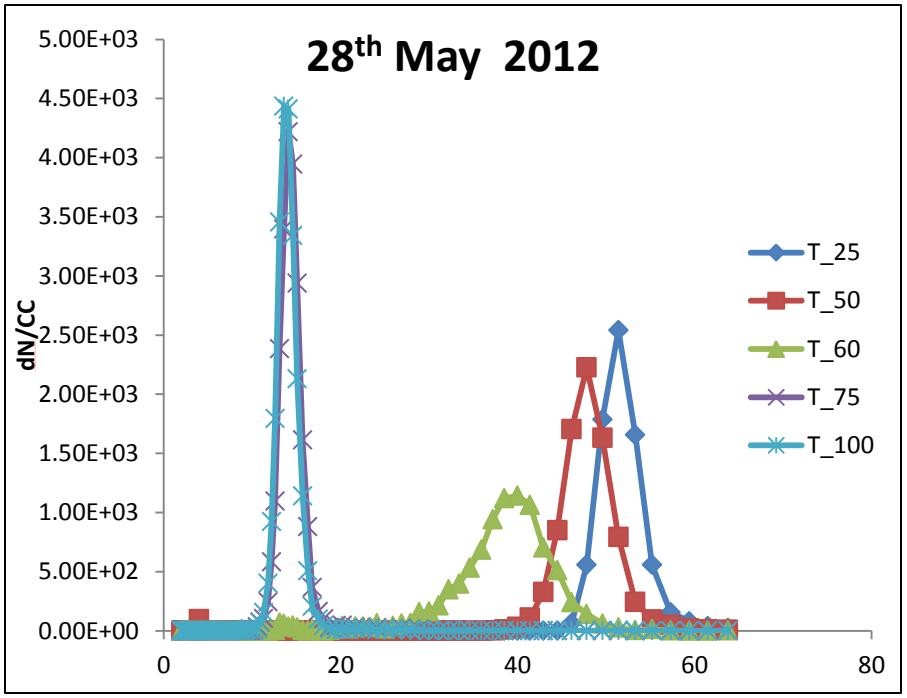

Section 9.2 V-TDMA Program structure

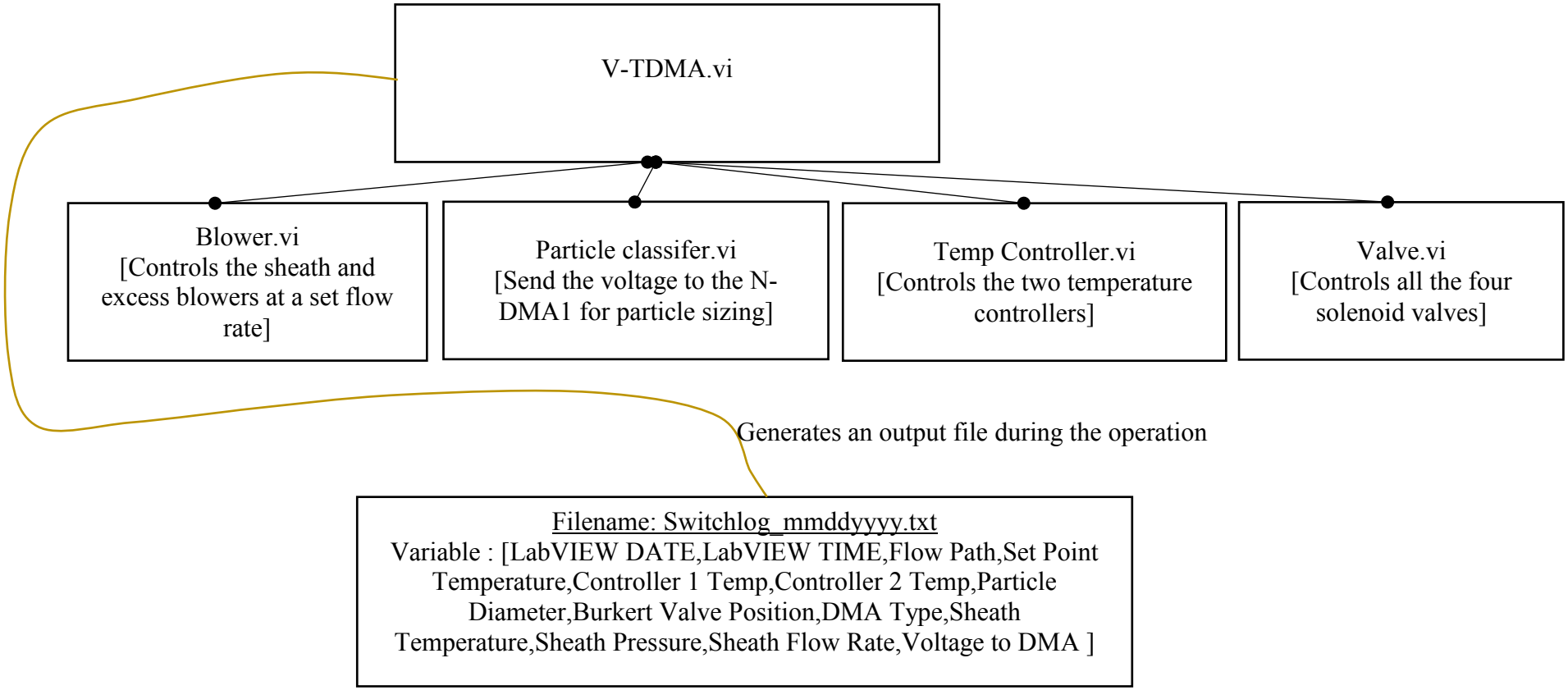

Section 9.2 V-TDMA program set up for a typical experimental run

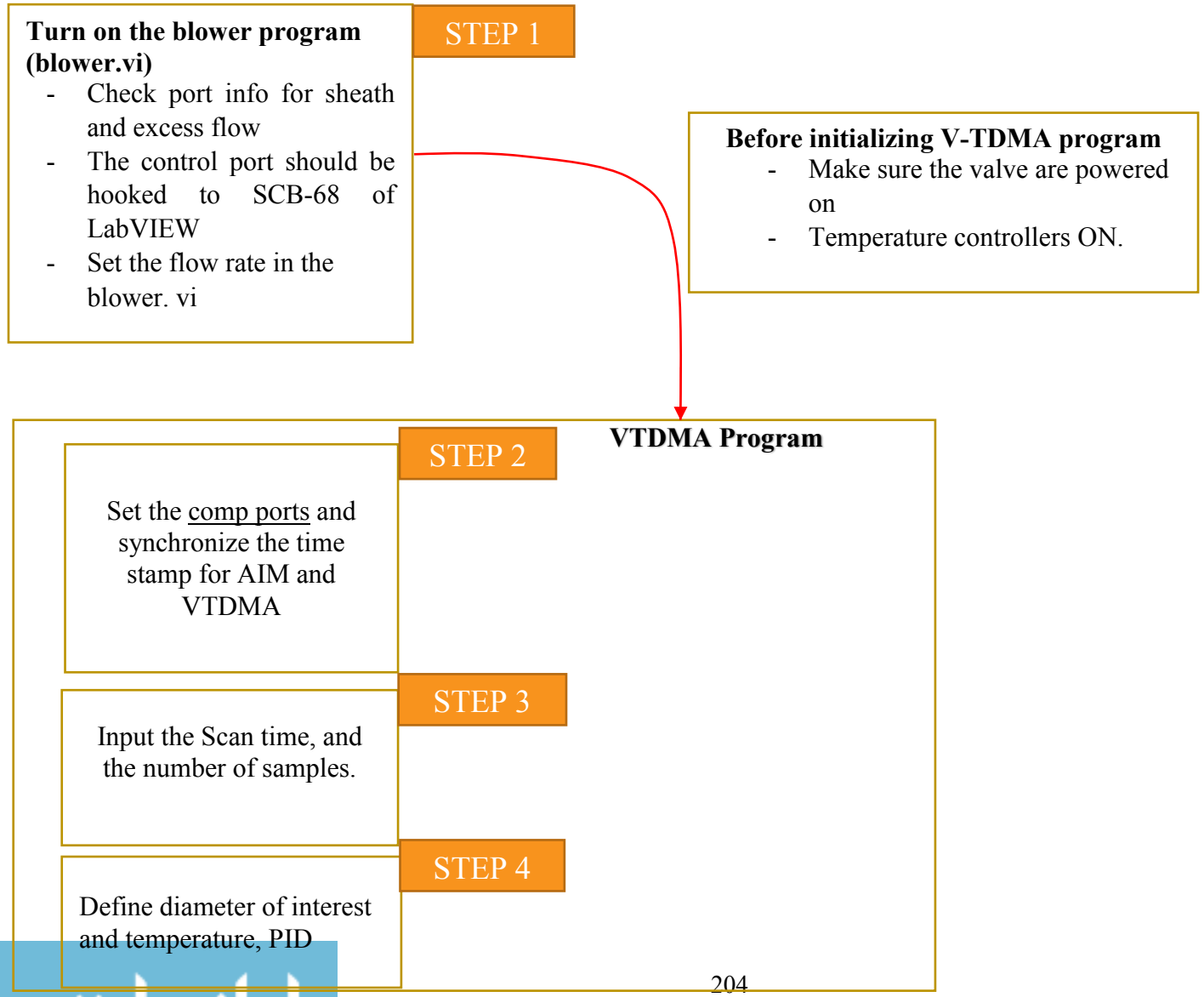

STEP 1

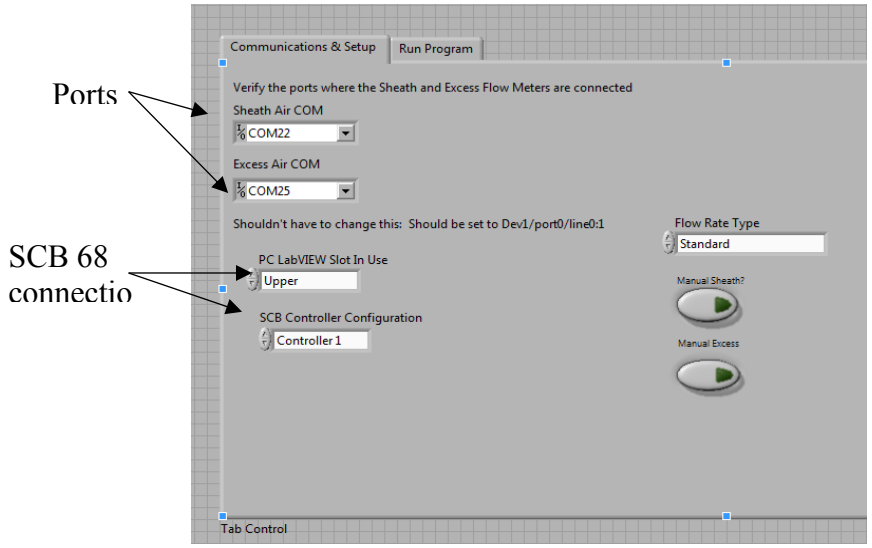

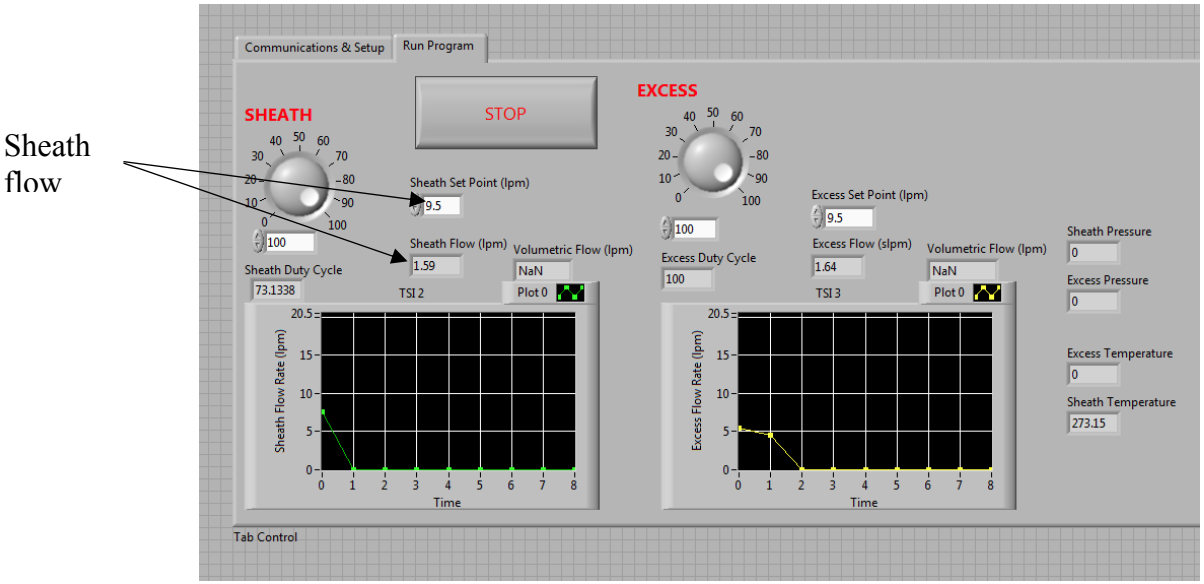

STEP 2

START UP TAB

Port number for two controllers

Define if you want to start with heated or bypass

For synchronizing with the AIM, define a scheduled time when you want to initiate the program

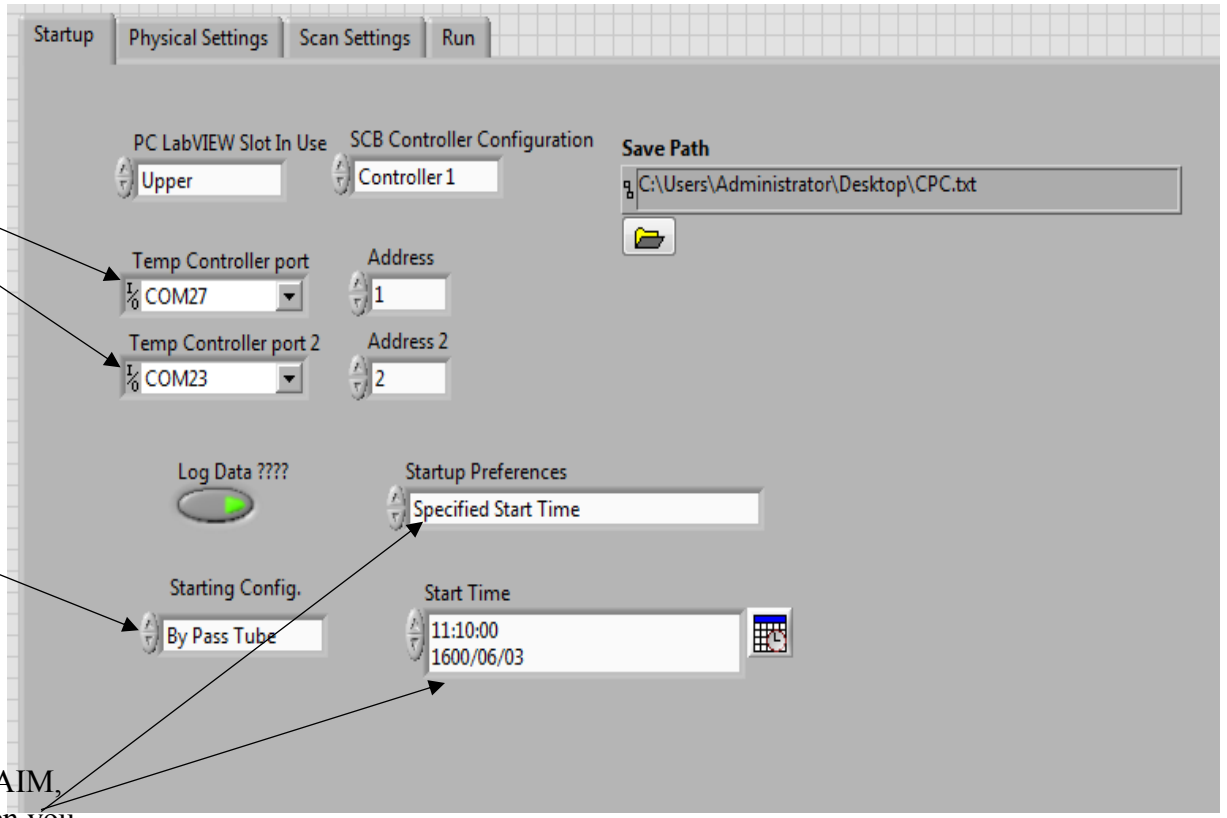

STEP 3

Physical Setting –Diameter, Temperature, Flush temperature and PID

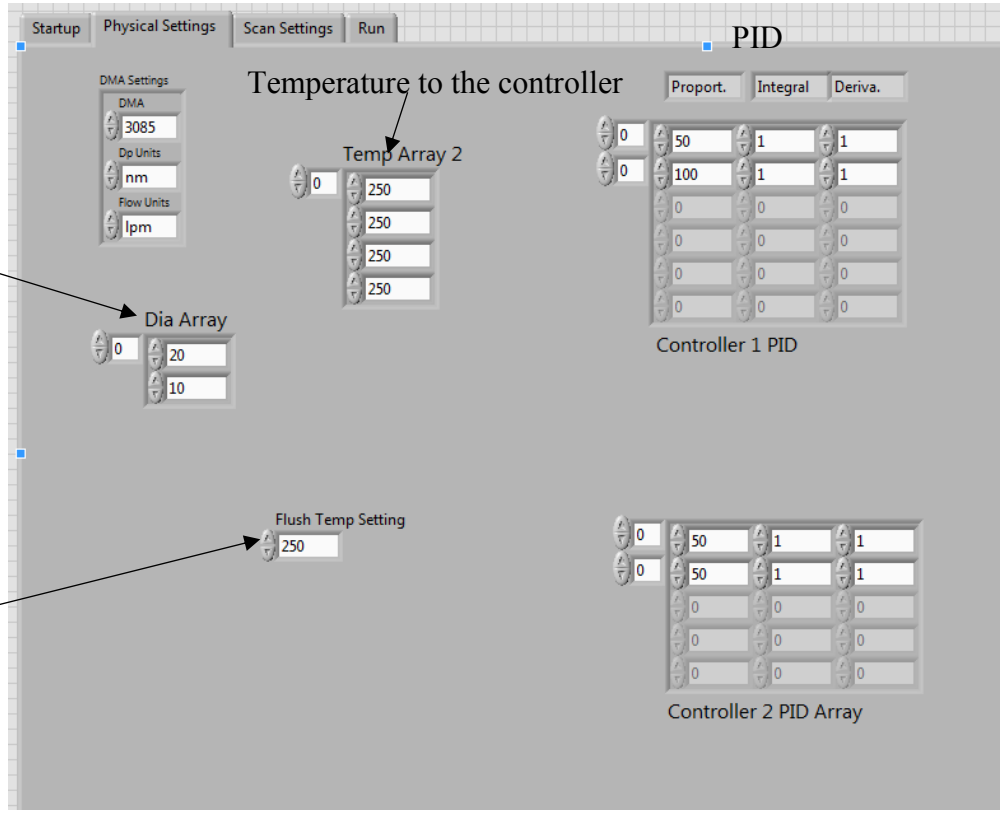

Flush temperature- needed for the cooling cycle – this is the temperature which determines where the cooling system has to reach

STEP 4

Determine the number of sample

This should match with upscan and down scan time used in the AIM for the SMPS

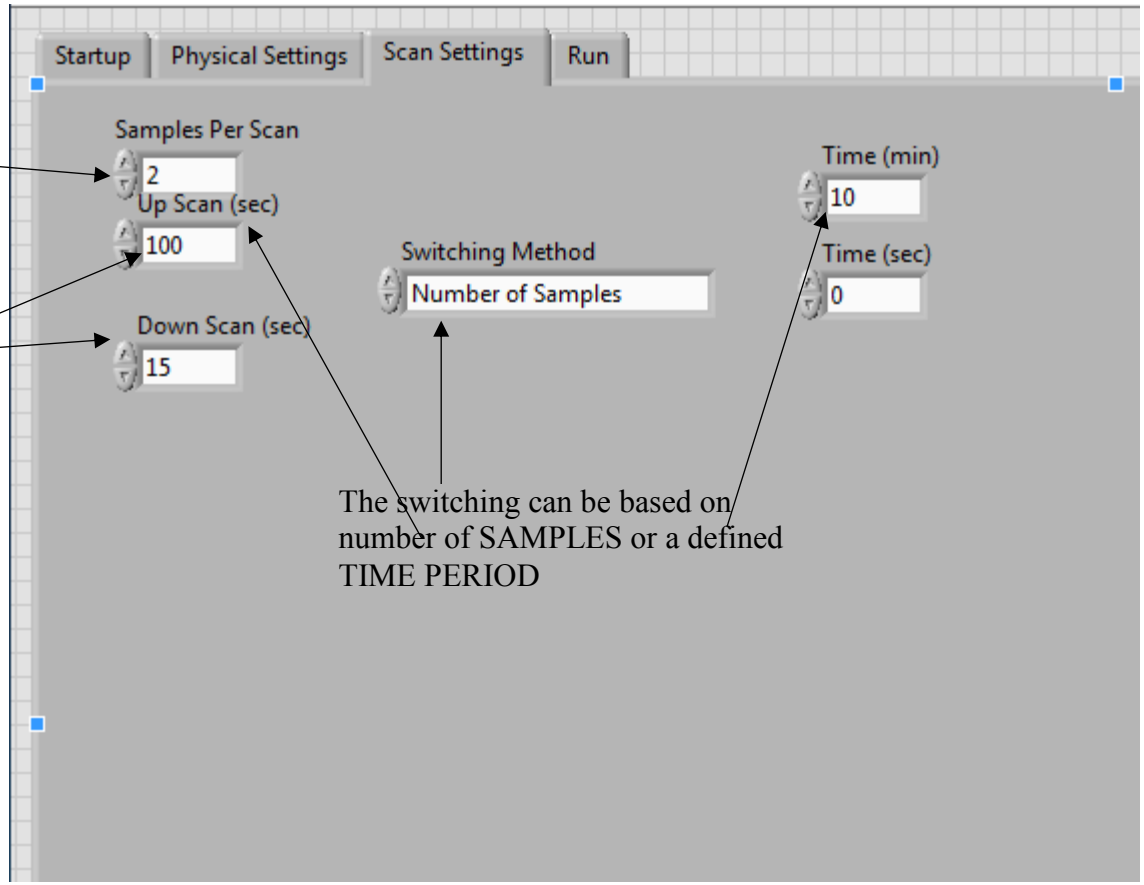

STEP 5

This is a read out of all the parameters including diameter, temperature, voltage, sheath flow, PID and timer

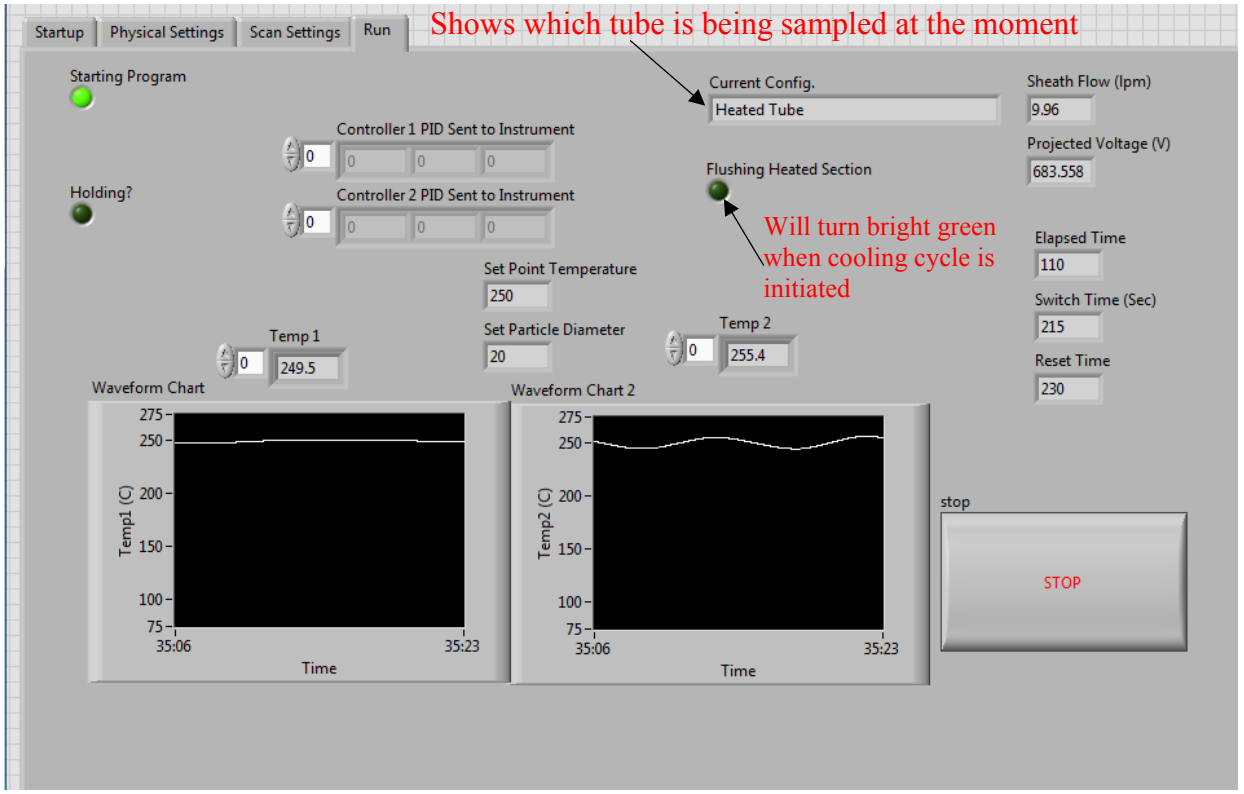

Safety concerns associated with using V-TDMA experiment

- Because the CPC pulls the air through the system (including the valves), it is essential to make sure the valves are open when you are starting the experiment or V-TDMA program. By default the bypass channel is open. But to make sure the CPC pump is not pressurized, unplug the CPC inlet from the V-TDMA operation and check the flow path by sucking into the conducting tube,
- Make sure you run a complete cycle to understand the set up diameter and temperature are cycling right, especially for high temperature run
- If you are sizing the particle, the V-TDMA program (in the run tab) will show following information
    - Current temperature on both controllers
    - Current PID on both controllers
    - Sheath and voltage sent to the DMA 1 (important if you are sizing the particle)
    - Timer (synchronized with the timer in AIM of SMPS). The timer follow the sample time loop of the AIM. So it restart after the end of a SCAN TIME.
    - Current sampled tube
    - All these values should be active and should not report NaN. If there is NaN or if the box is inactive, then it is likely that there is some problems

- Some commonly encountered problems
  - Blower ports not correctly set up
  - Blower stop running (report NaN in sheath and voltage box on the V-TDMA program)
  - The temperature box is inactive.
    - It is likely that the RS 232 cable may be lose
    - Or the temperature controller sub-vi has some bug
  - If you change the Rob's classifier (there are different version of classifier). The usual suspect in this case is the sheath flow 1 or 2 sub vi. Just need to play around to get this fixed.
  - Valve doesn't switch-
    - Check if it is powered on
    - Check the wiring in the valve
- DO NOT LEAVE the valve on after you complete the experiment. These valves will heat up.
- Make sure you have enough flush air during the cooling loop, otherwise it may not be cool down from high to your lowest temperature.

Section 9.2 Volatility response from organics and inorganics generated from the current design and measured by other group

1. **Response from our V-TDMA for a mixture aerosol containing ammonium sulfate, adipic acid and sodium chloride at the mass fraction (3:6:1). The figure summarizes three sets of experiments (VFR_1, VFR_2 and VFR_3) for a particle size of 20 nm.**

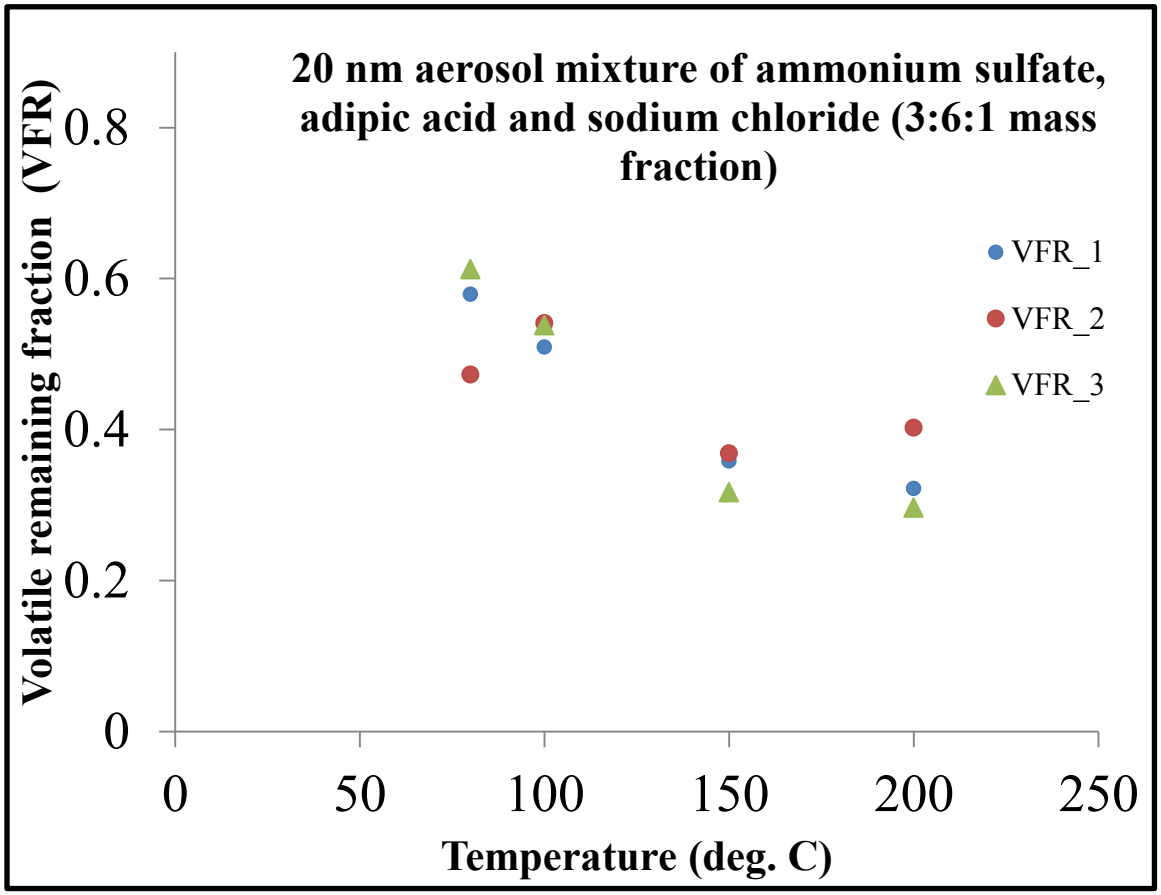

2. **Response from our V-TDMA for a mixture aerosol containing adipic acid and sodium chloride at the mass fraction (8:2) and pure adipic acid for 50 nm.**

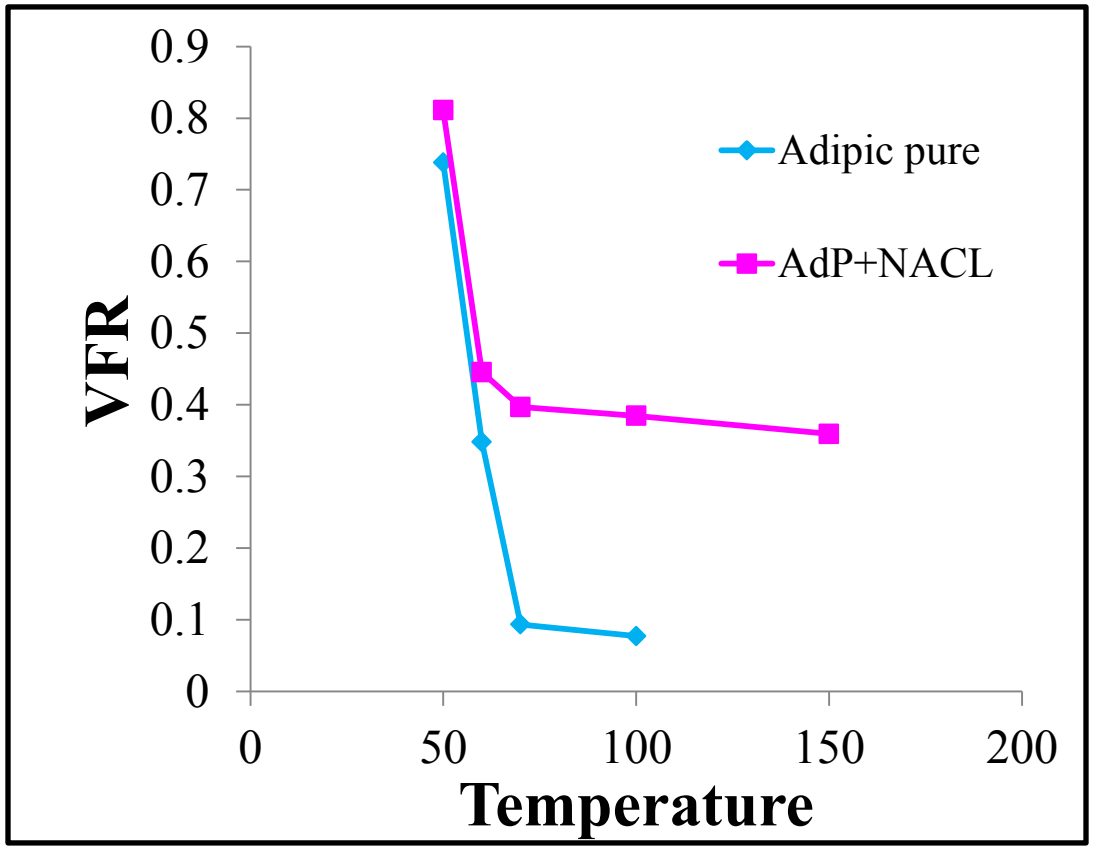

3. **Comparison of AS from our V-TDMA (30, 50 and 80 (blue line plot) with the response from Huffman V-TDMA (15.6 to 21.2 second of RT). From Huffman, VFR response of SO4, NH4, SOAR-OA,OAA and Milagro OA, OAA**

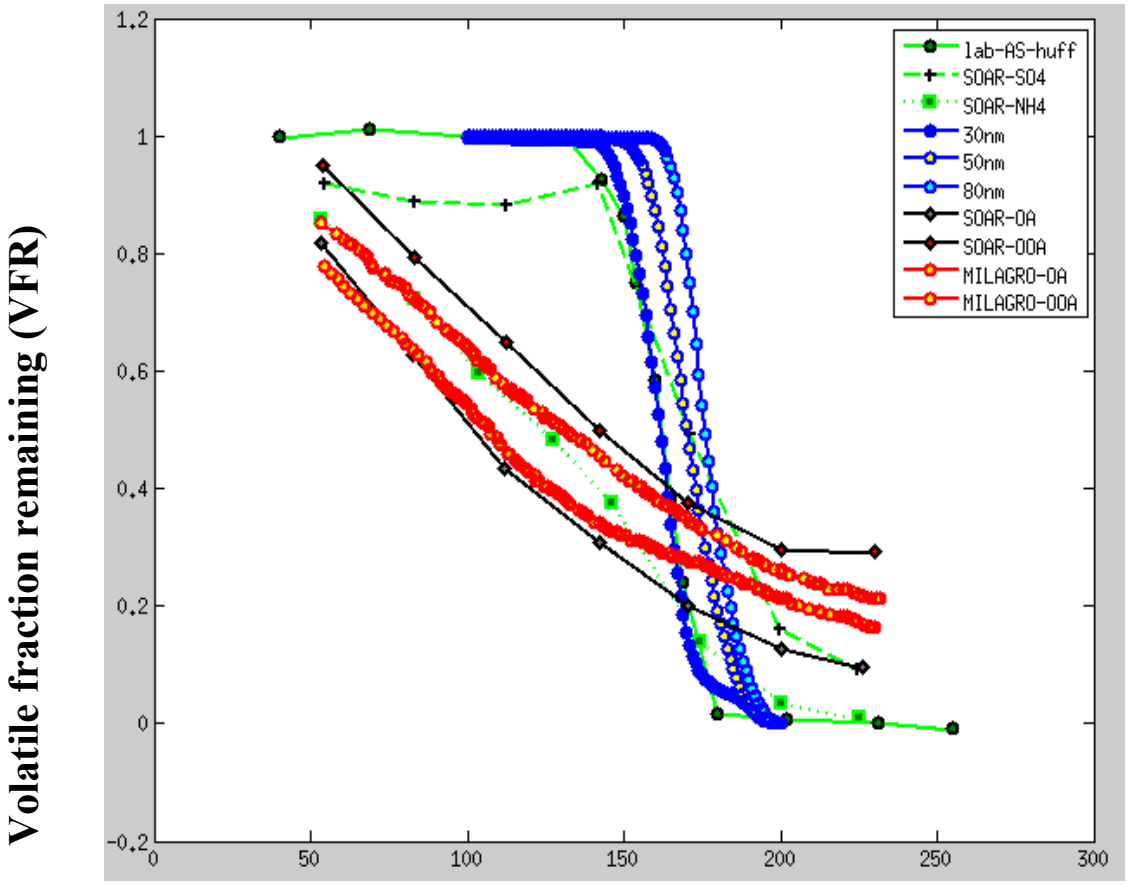

4. **VFR response of multiple species from illustration from the Johnson Group V-TDMA. Johnson Group AS profile was similar to our design. In this figure below, VFR profile for partially neutralized sulfuric acid (with ammonia) , Diesel aerosol, Alpha-pinene response and response during nucleation events are shown**

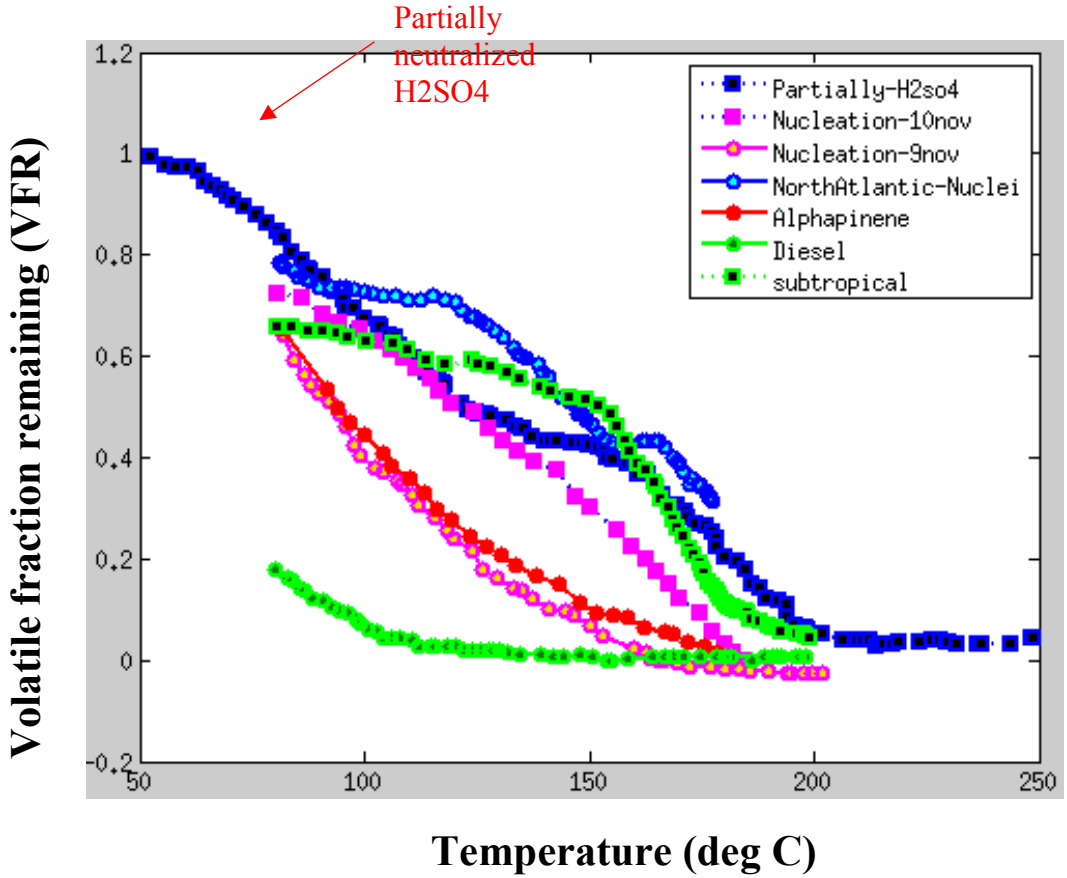

Appendix for Aim 3

Section 9.2. Cluster Analysis

Selection of the minimum number of clusters was based on the Dunn and silhouette index. However other validation indices such as connectivity, APN and AD were considered. The results from these indices often disagree regarding the number of clusters (Beddows et al., 2009; Sabaliauskas et al., 2013; Wegner et al., 2012).. For example the Dunn index was highest for 10 clusters in 15nm. This was inconsistent with other indices. The silhouette index became worse as the number of clusters increased which is used to rule out unreasonable high cluster number (Wegner et al., 2012). Details on the indices and clustering model are provided in the supplementary section.

Particle size: 15nm
Clustering Methods:
Hierarchical kmeans pam som model clara sota

Cluster sizes:
3 4 5 6 7 8 9 10

Cluster model	Internal consistency indicator	3	4	5	6	7	8	9	10
hierarchical	Connectivity	14.4	20.3	27.9	29.3	30.4	31.9	33.5	40.2
	Dunn	0.2	0.2	0.2	0.2	0.3	0.3	0.3	0.3
	Silhouette	0.4	0.4	0.4	0.4	0.4	0.3	0.3	0.4

kmeans	Connectivity	21.0	24.2	32.5	34.2	34.6	41.1	45.6	50.3
	Dunn	0.2	0.2	0.2	0.2	0.3	0.3	0.3	0.3
	Silhouette	0.4	0.4	0.4	0.4	0.4	0.4	0.4	0.4
pam	Connectivity	24.9	32.5	35.6	41.6	43.4	47.5	49.7	54.3
	Dunn	0.1	0.2	0.2	0.2	0.2	0.2	0.3	0.3
	Silhouette	0.4	0.4	0.3	0.3	0.3	0.3	0.4	0.4
som	Connectivity	21.1	33.3	39.0	43.4	49.8	50.4	57.7	62.0
	Dunn	0.1	0.1	0.2	0.2	0.2	0.3	0.2	0.3
	Silhouette	0.4	0.3	0.3	0.4	0.4	0.4	0.3	0.4
model	Connectivity	32.6	35.9	45.0	62.4	60.1	60.1	53.8	55.5
	Dunn	0.1	0.1	0.1	0.1	0.1	0.1	0.3	0.3
	Silhouette	0.2	0.2	0.3	0.0	0.3	0.3	0.4	0.4
clara	Connectivity	25.9	40.6	36.1	39.0	39.9	43.7	49.9	56.2
	Dunn	0.1	0.1	0.2	0.2	0.2	0.2	0.2	0.2
	Silhouette	0.4	0.3	0.3	0.3	0.3	0.4	0.3	0.3
sota	Connectivity	32.4	38.3	41.4	46.1	47.4	51.3	51.3	53.4
	Dunn	0.2	0.2	0.2	0.2	0.2	0.2	0.2	0.2
	Silhouette	0.3	0.3	0.3	0.3	0.3	0.3	0.1	0.2

Optimal Scores:

	Score	Method	Clusters
Connectivity	14.4111	hierarchical	3
Dunn	0.3333	kmeans	9
Silhouette	0.4144	hierarchical	3

Cluster Model	**Validation index**	**3**	**4**	**5**	**6**	**7**	**8**	**9**	**10**
hierarchical	APN	0.11	0.17	0.19	0.27	0.24	0.30	0.31	0.35
	AD	0.26	0.22	0.21	0.21	0.20	0.19	0.19	0.18

	ADM	0.09	0.07	0.08	0.09	0.09	0.09	0.09	0.11
	FOM	0.14	0.13	0.13	0.13	0.13	0.13	0.13	0.13
kmeans	APN	0.21	0.21	0.26	0.34	0.38	0.37	0.39	0.37
	AD	0.26	0.22	0.21	0.21	0.21	0.19	0.19	0.17
	ADM	0.10	0.08	0.10	0.11	0.12	0.11	0.11	0.11
	FOM	0.14	0.13	0.13	0.13	0.13	0.13	0.13	0.13
pam	APN	0.27	0.29	0.31	0.42	0.45	0.36	0.38	0.33
	AD	0.23	0.22	0.21	0.21	0.20	0.18	0.17	0.16
	ADM	0.09	0.08	0.10	0.12	0.12	0.11	0.11	0.10
	FOM	0.13	0.13	0.13	0.13	0.13	0.13	0.13	0.13
som	APN	0.33	0.42	0.35	0.44	0.38	0.34	0.33	0.34
	AD	0.26	0.23	0.21	0.21	0.19	0.18	0.17	0.17
	ADM	0.14	0.12	0.10	0.12	0.11	0.10	0.10	0.11
	FOM	0.13	0.13	0.13	0.13	0.13	0.13	0.13	0.13
model	APN	0.26	0.42	0.42	0.55	0.40	0.42	0.30	0.42
	AD	0.26	0.27	0.24	0.27	0.22	0.20	0.17	0.18
	ADM	0.10	0.13	0.13	0.16	0.12	0.12	0.10	0.12
	FOM	0.14	0.14	0.13	0.14	0.13	0.13	0.13	0.13
clara	APN	0.29	0.35	0.39	0.38	0.41	0.37	0.38	0.35
	AD	0.24	0.22	0.21	0.21	0.20	0.18	0.18	0.17
	ADM	0.09	0.10	0.12	0.11	0.12	0.11	0.11	0.11
	FOM	0.13	0.13	0.13	0.13	0.13	0.13	0.13	0.13
sota	APN	0.25	0.29	0.31	0.34	0.46	0.45	0.45	0.41
	AD	0.26	0.23	0.22	0.22	0.21	0.20	0.20	0.19
	ADM	0.10	0.10	0.11	0.12	0.13	0.12	0.12	0.11
	FOM	0.13	0.13	0.13	0.13	0.13	0.13	0.13	0.13

Optimal Scores:

	Score	Method	Clusters
APN	0.1136	hierarchical	3
AD	0.1648	pam	10
ADM	0.0729	hierarchical	4
FOM	0.1304	sota	7

Particle size: 30nm
Clustering Methods:
Hierarchical kmeans pam som model clara sota

Cluster sizes:
3 4 5 6 7 8 9 10

Cluster Model	Internal validation	3	4	5	6	7	8	9	10
hierarchical	Connectivity	5.8579	16.2738	19.3694	19.5694	28.4437	51.2	59.7885	67.6
	Dunn	0.3194	0.1601	0.1601	0.1601	0.1132	0.1361	0.1741	0.1741
	Silhouette	0.494	0.356	0.2588	0.2156	0.1666	0.2348	0.2383	0.2228
kmeans	Connectivity	30.9976	44.5333	60.8881	80.9393	83.8377	95.9873	100.638	109.794
	Dunn	0.1414	0.1543	0.1543	0.1429	0.1715	0.1857	0.2294	0.2294
	Silhouette	0.3503	0.2987	0.271	0.2568	0.2552	0.2859	0.2826	0.279
pam	Connectivity	52.0774	67.7111	87.5127	94.331	109.851	92.9397	96.9135	108.275
	Dunn	0.0874	0.1162	0.1162	0.1162	0.1162	0.1162	0.1179	0.1179
	Silhouette	0.2469	0.2463	0.2401	0.2427	0.2336	0.2444	0.2333	0.2347
som	Connectivity	43.8956	53.9532	57.3143	69.9972	91.5381	88.1869	93.5774	105.91
	Dunn	0.0962	0.1222	0.1222	0.1491	0.1491	0.1961	0.1961	0.1491
	Silhouette	0.3035	0.2824	0.2596	0.2712	0.2484	0.2849	0.2797	0.2818
model	Connectivity	71.3317	83.6012	63.304	75.1306	141.299	142.787	110.385	156.893

	Dunn	0.0874	0.0874	0.1491	0.1491	0.0933	0.0933	0.1374	0.0933
	Silhouette	0.2667	0.0287	0.2897	0.285	0.091	0.0986	0.1013	0.065
clara	Connectivity	42.8861	75.0929	71.3123	85.05	78.9698	100.189	83.8361	100.025
	Dunn	0.0962	0.1179	0.1302	0.1826	0.1491	0.1857	0.1857	0.1925
	Silhouette	0.2362	0.2119	0.2282	0.2124	0.2409	0.2464	0.2606	0.2462
sota	Connectivity	46.5476	59.5948	75.9262	87.819	92.6575	95.9821	96.0933	96.5433
	Dunn	0.0874	0.0874	0.0953	0.1302	0.1302	0.14	0.1508	0.1715
	Silhouette	0.2465	0.2379	0.2257	0.2193	0.2008	0.1383	0.1397	0.104

Optimal Scores:

	Score	Method	Clusters
Connectivity	5.8579	hierarchical	3
Dunn	0.3194	hierarchical	3
Silhouette	0.4940	hierarchical	3

Cluster Model	Internal validation	3	4	5	6	7	8	9	10
hierarchical	APN	0.0229	0.0849	0.237	0.3669	0.544	0.4036	0.4124	0.396
	AD	0.2823	0.2792	0.2761	0.2735	0.2701	0.2354	0.2277	0.2221
	ADM	0.0127	0.0355	0.0664	0.0959	0.1346	0.1059	0.1028	0.0995
	FOM	0.1333	0.1334	0.1318	0.1315	0.127	0.1265	0.1262	0.1264
kmeans	APN	0.3048	0.4257	0.3587	0.4127	0.4106	0.438	0.4513	0.3803
	AD	0.2566	0.2487	0.229	0.2206	0.2177	0.2119	0.209	0.2004
	ADM	0.1154	0.1361	0.1181	0.1223	0.1234	0.1227	0.1272	0.1098
	FOM	0.1306	0.1301	0.1283	0.129	0.127	0.1275	0.1276	0.1275
pam	APN	0.3036	0.4285	0.5134	0.4985	0.5093	0.4577	0.4816	0.4482
	AD	0.2387	0.2345	0.2297	0.2152	0.2074	0.197	0.1953	0.1894
	ADM	0.0931	0.1185	0.1248	0.1206	0.1133	0.1054	0.1136	0.1101
	FOM	0.1287	0.1288	0.1295	0.1284	0.1271	0.1274	0.1279	0.1274
som	APN	0.3353	0.4242	0.4906	0.4075	0.5059	0.3714	0.4667	0.4949
	AD	0.2439	0.2326	0.2243	0.2124	0.2087	0.1971	0.1946	0.1922
	ADM	0.1095	0.1212	0.1256	0.1114	0.121	0.1101	0.1135	0.1141
	FOM	0.129	0.1289	0.1295	0.127	0.1275	0.129	0.128	0.1289
model	APN	0.3321	0.3344	0.4025	0.5121	0.3605	0.3592	0.4719	0.372
	AD	0.2661	0.2577	0.2489	0.2529	0.2627	0.2569	0.2495	0.245
	ADM	0.1121	0.1043	0.1169	0.1325	0.1	0.0963	0.1142	0.1081
	FOM	0.1314	0.1298	0.1305	0.132	0.1316	0.1324	0.1309	0.1284
clara	APN	0.2815	0.4389	0.465	0.5015	0.4705	0.487	0.4971	0.4409
	AD	0.2373	0.2356	0.227	0.2186	0.208	0.2016	0.197	0.1883
	ADM	0.0835	0.1161	0.1146	0.1177	0.1097	0.1105	0.1092	0.1075
	FOM	0.1288	0.13	0.1291	0.1285	0.1274	0.1268	0.1266	0.1267
sota	APN	0.3104	0.4792	0.4556	0.4373	0.5009	0.5221	0.521	0.5235

	AD	0.2409	0.2353	0.2262	0.2193	0.2172	0.2144	0.212	0.2089
	ADM	0.0976	0.1138	0.1177	0.1166	0.123	0.1252	0.1246	0.123
	FOM	0.1273	0.1274	0.1268	0.127	0.1272	0.1275	0.1278	0.1276

Optimal Scores:

	Score	Method	Clusters
APN	0.0229	hierarchical	3
AD	0.1883	clara	10
ADM	0.0127	hierarchical	3
FOM	0.1262	hierarchical	9

Particle size: 20nm
Clustering Methods:
Hierarchical kmeans pam som model clara sota

Cluster sizes:
3 4 5 6 7 8 9 10

Cluster Model	**Internal Consistency**	**3**	**4**	**5**	**6**	**7**	**8**	**9**	**10**
hierarchical	Connectivity	11.6778	22.8964	24.2921	41.9286	49.3242	50.4671	54.0778	55.7528
	Dunn	0.1491	0.1814	0.1814	0.1988	0.2749	0.2749	0.2749	0.2749
	Silhouette	0.2398	0.2614	0.2483	0.2506	0.2874	0.2824	0.2834	0.2974
kmeans	Connectivity	28.4131	30.723	43.8655	45.4694	53.0552	56.9659	61.8226	65.3107
	Dunn	0.1865	0.1915	0.2279	0.1679	0.1734	0.1734	0.1817	0.3491
	Silhouette	0.3431	0.3078	0.3109	0.2981	0.2995	0.2835	0.3013	0.3359
pam	Connectivity	28.4131	36.5925	39.8869	44.0456	49.1448	53.6917	59.0996	61.9659
	Dunn	0.1865	0.1988	0.1988	0.1988	0.1988	0.2383	0.2468	0.1556
	Silhouette	0.3431	0.2998	0.2923	0.2863	0.2732	0.291	0.315	0.3255

som	Connectivity	28.2833	35.0996	44.4135	48.7881	57.0437	60.7738	63.3774	73.7425
	Dunn	0.1865	0.1988	0.2321	0.2345	0.1816	0.1776	0.2881	0.2068
	Silhouette	0.3399	0.2974	0.2891	0.278	0.2922	0.2857	0.2882	0.268
model	Connectivity	49.0508	53.35	76.0679	67.9746	87.0718	90.5377	59.4433	88.3143
	Dunn	0.0916	0.0916	0.0697	0.0897	0.151	0.1481	0.2468	0.1149
	Silhouette	0.1535	0.0916	0.0626	0.1517	0.1227	0.088	0.3344	0.1184
clara	Connectivity	28.4131	0.0916	43.7345	48.7726	50.5306	55.1694	56.7417	63.8393
	Dunn	0.1865	0.0916	0.1988	0.2383	0.1503	0.1503	0.2383	0.1503
	Silhouette	0.3431	0.0916	0.2825	0.28	0.2952	0.2894	0.2823	0.301
sota	Connectivity	26.371	0.0916	45.802	51.2552	57.1214	60.9183	68.7825	69.9254
	Dunn	0.1865	0.0916	0.1915	0.1915	0.1915	0.1915	0.2646	0.2646
	Silhouette	0.3341	0.0916	0.2405	0.2314	0.235	0.27	0.2703	0.275

Optimal Scores:

	Score	Method	Clusters
Connectivity	11.6778	hierarchical	3
Dunn	0.3491	kmeans	10
Silhouette	0.3431	kmeans	3

Cluster Model	**Internal Consistency**	**3**	**4**	**5**	**6**	**7**	**8**	**9**	**10**
hierarchical	APN	0.2223	0.4255	0.4225	0.4004	0.4297	0.441	0.4557	0.4665
	AD	0.2725	0.2537	0.2401	0.2193	0.2049	0.201	0.1924	0.1852
	ADM	0.0876	0.1405	0.1304	0.1254	0.119	0.119	0.1185	0.1184
	FOM	0.1307	0.1304	0.1307	0.1306	0.1312	0.1307	0.13	0.1295

kmeans	APN	0.3398	0.3544	0.3133	0.4667	0.4046	0.4795	0.4743	0.4328
	AD	0.246	0.2308	0.22	0.2161	0.2012	0.2027	0.1914	0.1766
	ADM	0.136	0.1252	0.1304	0.1301	0.1127	0.1266	0.1235	0.1133
	FOM	0.1283	0.1302	0.1303	0.1299	0.1313	0.1308	0.1294	0.1284
pam	APN	0.3558	0.3183	0.4366	0.4403	0.4511	0.4702	0.4467	0.4803
	AD	0.2454	0.2175	0.2107	0.205	0.1989	0.1926	0.1802	0.1768
	ADM	0.1235	0.0916	0.1076	0.1133	0.114	0.12	0.1094	0.1113
	FOM	0.1302	0.1292	0.1284	0.1289	0.1301	0.1297	0.1283	0.1293
som	APN	0.2866	0.4278	0.4309	0.4479	0.5084	0.4452	0.4727	0.4885
	AD	0.2342	0.2253	0.2167	0.2055	0.2003	0.1921	0.183	0.1814
	ADM	0.0918	0.1213	0.1224	0.1243	0.1244	0.1124	0.1149	0.1182
	FOM	0.1303	0.1296	0.1289	0.1303	0.1293	0.1294	0.1271	0.1287
model	APN	0.441	0.3208	0.5038	0.5603	0.3865	0.5475	0.5058	0.4852
	AD	0.2695	0.2422	0.2501	0.246	0.2188	0.2264	0.1914	0.2094
	ADM	0.1337	0.093	0.1383	0.1448	0.1067	0.1283	0.1232	0.131
	FOM	0.1313	0.129	0.1302	0.1299	0.1302	0.1289	0.1305	0.1308
clara	APN	0.3597	0.3239	0.4208	0.4685	0.4621	0.4894	0.4503	0.4452
	AD	0.2439	0.2181	0.2102	0.2092	0.2022	0.1956	0.1857	0.1792
	ADM	0.1242	0.0915	0.1031	0.1215	0.123	0.1245	0.1145	0.1158
	FOM	0.1287	0.1293	0.1281	0.1282	0.1291	0.131	0.1288	0.1275

Optimal Scores:

	Score	Method	Clusters
APN	0.2223	hierarchical	3
AD	0.1766	kmeans	10
ADM	0.0876	hierarchical	3
FOM	0.1271	som	9

Section 9.3.Cluster classification

15nm

Most likely	**3 clusters**	**100**	**130**	**150**	**200**	**Sample_size**	**Sam_frac**	**Avg.volatility**	
	Cluster1	0.92	0.71	0.65	0.08	36	**53**	0.79	IV
	Cluster2	0.99	0.96	0.98	0.04	11	**16**	0.99	LV
	Cluster3	0.80	0.60	0.39	0.09	21	**31**	0.59	MV
						68			

Other feasible classification	**4 clusters**					**Sample_size**	**Sam_frac**		
	Cluster1	0.99	0.80	0.90	0.03	11	16	0.95	
	Cluster2	0.93	0.60	0.27	0.09	7	10	0.60	
	Cluster3	0.97	0.75	0.68	0.08	31	46	0.83	
	Cluster4	0.70	0.59	0.47	0.08	19	28	0.59	
						68			

30nm

Most likely	**3 clusters**	**100**	**130**	**150**	**200**	**Sample_size**	**Sam_frac**	**Avg.volatility**	
	Cluster1	0.93	0.79	0.78	0.23	58	**34**	0.86	LV
	Cluster2	0.73	0.63	0.52	0.26	73	**43**	0.62	MV
	Cluster3	0.93	0.73	0.51	0.25	39	**23**	0.72	IV
						170			

Other feasible classification	**4 clusters**						Avg.volatility		
	Cluster1	0.73	0.68	0.67	0.25	28	16	0.70	IV
	Cluster2	0.89	0.73	0.60	0.33	56	33	0.75	IV
	Cluster3	0.95	0.77	0.76	0.16	41	24	0.85	LV
	Cluster4	0.75	0.62	0.43	0.23	45	26	0.59	MV

						170			

50nm

Most likely	**3 clusters**	**100**	**130**	**150**	**200**	**Sample_size**	**Sam_frac**	**Avg.volatility**	
	Cluster1	0.88	0.74	0.76	0.27	61	**37**	0.82	LV
	Cluster2	0.64	0.53	0.52	0.26	48	**29**	0.58	MV
	Cluster3	0.86	0.71	0.54	0.29	56	**34**	0.70	IV
						165			

Most likely	**4 clusters**					**Sample_size**	**Sam_frac**	Avg.volatility	
	Cluster1	0.813	0.567	0.367	0.207	14	8	0.59	MV1
	Cluster2	0.663	0.554	0.520	0.277	59	36	0.59	MV2
	Cluster3	0.952	0.823	0.900	0.396	23	14	0.93	LV
	Cluster4	0.83	0.70	0.63	0.23	69	42	0.73	IV
						165			

80nm

Most likely	**3 clusters**	**100**	**130**	**150**	**200**	**Sample_size**	**Sam_frac**	**Avg.volatility**	
	Cluster1	0.71	0.60	0.61	0.30	28	**23**	0.66	MV
	Cluster2	0.91	0.67	0.60	0.29	39	**33**	0.76	IV
	Cluster3	0.99	0.88	0.85	0.32	53	**44**	0.92	LV
						120			

Most likely	**4 clusters**					**Sample_size**	**Sam_frac**	Avg.volatility	
	Cluster1	0.656	0.567	0.538	0.244	15	13	0.60	MV

Cluster2	0.822	0.675	0.728	0.433	18	15	0.78	IV1
Cluster3	0.976	0.850	0.836	0.284	49	41	0.91	LV
Cluster4	0.93	0.70	0.62	0.29	38	32	0.77	IV2
					120			

Section 9.3. Classification of atmospheric conditions

Start_time	End_time	Atmospheric_Condition	Revised Atmospheric Condition
8/25/2013 18:00	8/26/2013 00:00	Background	Background1
8/26/2013 0:00	8/26/2013 15:00	Background	Background2
8/26/2013 14:00	8/26/2013 18:00	Burst, SO2 1 ppb	Burst
8/26/2013 18:00	8/27/2013 0:00	Background, Noy 3 ppb	Background1
8/27/2013 0:00	8/27/2013 5:00	Elevated NOY, 5-10 ppb	Background2
8/27/2013 5:00	8/27/2013 9:00	Fresh Emission	FE
8/27/2013 9:00	8/27/2013 18:00	Burst, Elevated SO2	Burst
8/27/2013 18:00	8/28/2013 3:00	Background, NOY ~ 5 ppb	Background2
8/28/2013 3:00	8/28/2013 9:00	Background, NOY <3 ppb	Background1
8/28/2013 9:00	8/28/2013 19:30	long duration Burst, Elevated SO2 1.5 ppb	Burst
8/28/2013 19:30	8/29/2013 0:00	Background, High NOY period, 5 ppb	Background2
8/29/2013 0:00	8/30/2013 0:00	Background, < 5 ppb NOY	Background1
9/5/2013 11:00	9/5/2013 20:00	Active Nucleation/growth 1, SO2 low, NOy 3 ppb	Nucleation
9/5/2013 20:00	9/6/2013 0:00	Changes in air mass (nucleation air mass disappears), NOY rises close to 4-5 ppb	Background2
9/6/2013 0:00	9/6/2013 6:00	Background, NOY continues to be at 4-5 , decreases by 6 am	Background1
9/6/2013 6:00	9/6/2013 18:00	Period of elevated SO2, NOY 3-4 ppb	Background3
9/6/2013 18:00	9/7/2013	Background, NOY reaches 10-15 ppb	Background2
9/7/2013 0:00	9/7/2013 6:00	Background, High NOy period, 5-10 ppb	Background2
9/7/2013 6:00	9/7/2013 9:00	Fresh Emission, NO, SO2 and NOY	FE
9/7/2013 9:00	9/7/2013 15:00	SO2 Spikes close to 3 ppb	Burst
9/7/2013 15:00	9/8/2013 0:00	Background, <3-4 ppb	Background1
9/8/2013 0:00	9/8/2013 9:00	High NOy period, 5-10 ppb	Background2
9/8/2013 9:00	9/8/2013 18:00	SO2 Spikes close to 2.5 ppb	Burst
9/8/2013 18:00	9/9/2013 0:00	High NOy period, 5-10 ppb	Background2
9/9/2013 0:00	9/9/2013 3:00	High NOy period, 5-10 ppb	Background2

9/9/2013 3:00	9/9/2013 15:00	SO2 Spikes close to 2.5 ppb, Burst in the noon time	Burst
9/9/2013 15:00	9/10/2013 0:00	Background, NOy period,3-4 ppb	Background1
3/16/2014 0:00	3/16/2014 12:00	Background, weak NOY 2 ppb	Background1
3/16/2014 12:00	3/17/2014 0:00	Nucleation and growth	Nucleation
3/17/2014 0:00	3/17/2014 6:00	Aged nucleation growth from yesterday	A_nucleation
3/17/2014 6:00	3/17/2014 18:00	NOY elevates to 5 ppb along with SO2 which increases to 2.5 ppbs	Background3
3/17/2014 18:00	3/18/2014 0:00	Background, Strong NOY to 10 ppbs	Background2
4/21/2014 0:00	4/21/2014 7:00	Background, Strong NOY to 10 ppbs, associated with t a strong particle band at 80 nm	Background2
4/21/2014 7:00	4/21/2014 18:00	SO2 spikes close to 4-5 ppbs, short term burst	Burst
4/21/2014 18:00	4/22/2014 0:00	Strong Noy period with > 5ppbs	Background2
4/22/2014 0:00	4/22/2014 5:00	NOY is dropping down, *2* ppb by 6 am (can be considered background), 1 PPB So2 IS PREVALENT DURING THIS PERIOD	Background3
4/22/2014 5:00	4/22/2014 8:30	Hint of Fresh Emission, NO and SO2	FE
4/22/2014 8:30	4/22/2014 18:00	SLIGHT RISE IN SO2 CONC. 9 am nucleation starts. Active nucleation and growth	Nucleation
4/22/2014 18:00	4/23/2014 0:00	Growth continue, but with elevated SO2 and NOY (5ppb) and change in wind direction	Aged_Nucleation
4/23/2014 0:00	4/23/2014 4:30	Background, NOY spike period	Background2
4/23/2014 4:30	4/23/2014 8:30	Hint of Fresh Emission, NO and SO2	FE
4/23/2014 8:30	4/23/2014 17:00	Nucleation period/growth, still see NO concentration	Nucleation
4/23/2014 17:00	4/24/2014 0:00	Growth continue, WITH So2 OF 1 PPB AND and NOY (5ppb) and change in wind direction	Aged_Nucleation
4/24/2014 0:00	4/24/2014 6:00	Noy CLOSE TO 5 PPB, PARTICLE MODE CONTINUES FROM YESTERDAY	Background2
4/24/2014 6:00	4/24/2014 9:00	SO2 spike, NO during the same time	FE
5/22/2014 0:00	5/22/2014 9:00	NOY 5-10 ppb	Background2
5/22/2014 9:00	5/22/2014 18:00	--	

5/22/2014 18:00	5/23/2014 0:00	Background, NOY 5 ppb	Background2
5/23/2014 0:00	5/23/2014 5:00	NOY continues to be around 5-10 , background conditions	Background2
5/23/2014 5:00	5/23/2014 8:30	Fresh Emission, CO,NO	FE
5/23/2014 8:30	5/23/2014 18:30	Weak nucleation, but changes in the wind direction during the day	Nucleation
5/23/2014 18:30	5/23/2014 20:30	Fresh Emission, CO	FE
5/23/2014 20:30	5/24/2014 0:00	Probably nearby combustion source, CO and SO2 elevated, change in the wind direction	FE
5/24/2014 0:00	5/24/2014 4:30	Elevated SO2 and NOy. SO2 `~2 ppb and NOy 5-7 ppb	Background3
5/24/2014 4:30	5/24/2014 6:00	NOY 5-7, SO2 <1	Background3
5/24/2014 6:00	5/24/2014 8:30	SO2 spikes again with NOY	Background3
5/24/2014 8:30	5/24/2014 18:00	SO2 and NOy remains consistent at 1.5 ppb and 4-5 ppbs	Background3
5/24/2014 18:00	5/24/2014 21:00	Noy RISES TO 5-7 ppb	Background2
5/24/2014 21:00	5/25/2014 0:00	SO2 rises to 2.5 ppb till midnight, so it CO, FRESH emission or FRESH COMBUSTION	FE
5/25/2014 0:00	5/25/2014 5:30	Strong NOY presence from 5 to 7 ppb	Background2
5/25/2014 5:30	5/25/2014 9:00	FRESH EMISSION, SO2 Rose to ~ 10 ppb, NOY close to 6 and NO 1.5 ppb	FE
5/25/2014 9:00	5/25/2014 19:30	Strong SO2 presence the whole day between 4-5 ppbs.	Burst
5/25/2014 19:30	5/25/2014 21:30	AS the evening kicks in , NOY rises to 6-7 ppbs with and visible Spike of SO2	Background3
5/25/2014 21:30	5/26/2014 0:00	SO2 weakens to <1 ppb, NOY still at 5-6 ppb	Background3
5/26/2014 0:00	5/26/2014 4:00	SO2 has been fluctuating, but remains. NOY 7-8 ppbs	Background3
5/26/2014 4:00	5/26/2014 8:30	Fresh Emission , NO 2 ppb, with minor SO2 and NOY spike	FE
5/26/2014 8:30	5/26/2014 11:00	SO2 maintain a conc of 2.5 ppb and by the end , it drops back to <1 ppb, NOY also drops to 2 ppb, a WEAK BURST is also seen	Background3
5/26/2014 11:00	5/26/2014 13:00	SO2 maintain a conc of 2.5 ppb and by the end , it drops back to <1 ppb, NOY also drops to 2 ppb,	Background3

5/26/2014 13:00	5/26/2014 18:00	Background	Background1

Section. 9.3. Classification of the residue

	least v	intermediate	high V
30 nm	35-22	22-15	005-015
in (% of Dp)	73	50	16-50
in (% of vol)	0.4	0.13	5E-03
% volume	0.6	0.3	0.1
50nm	58-35	35-22	05-022
in (% of Dp)	70	44	010-44
in (% of vol)	0.3	0.09	1E-03
% volume	0.7	0.3	0.08
80nm	88-70	70-50	035-05
in (% of Dp)	81	44	06-044
in (% of vol)	0.4	0.08	2E-04
% volume	0.6	0.3	0.08

Wehner distribution 2009			
Dp_cut	30 nm	50nm	80nm

82%	24.6	41	65.6
45%	13.5	22.5	36

Section9.3. Time series of the internal and external mixture during April 22 and 23 nucleation days

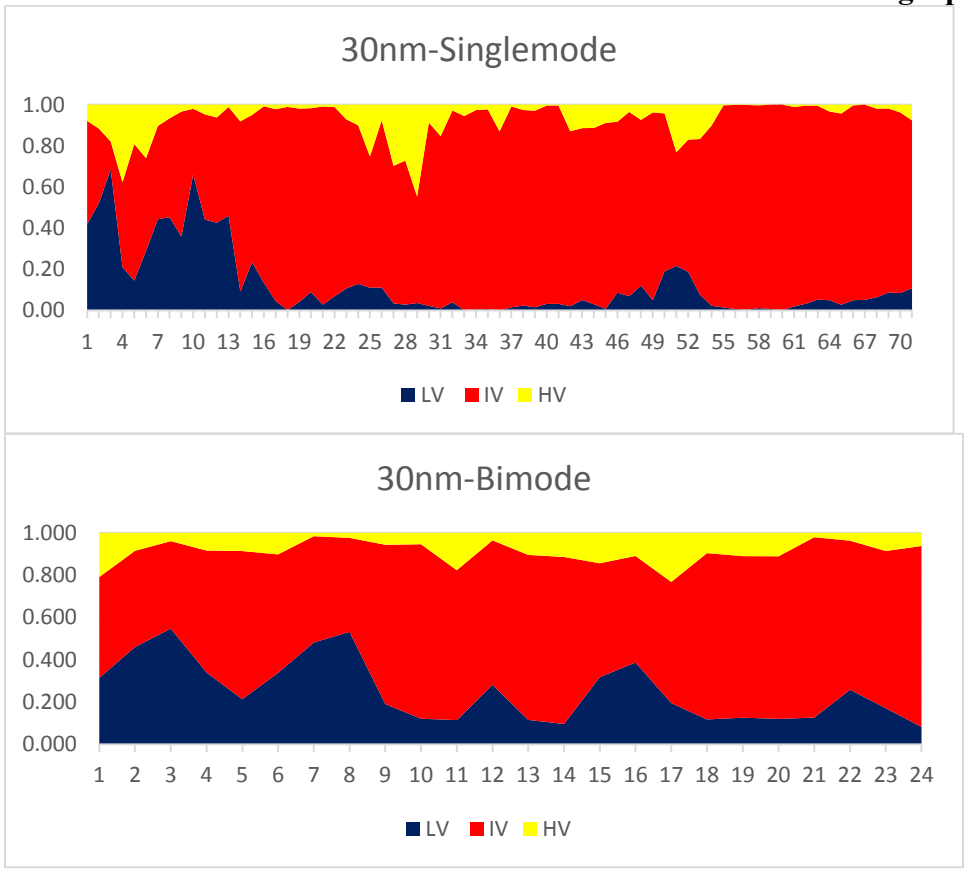

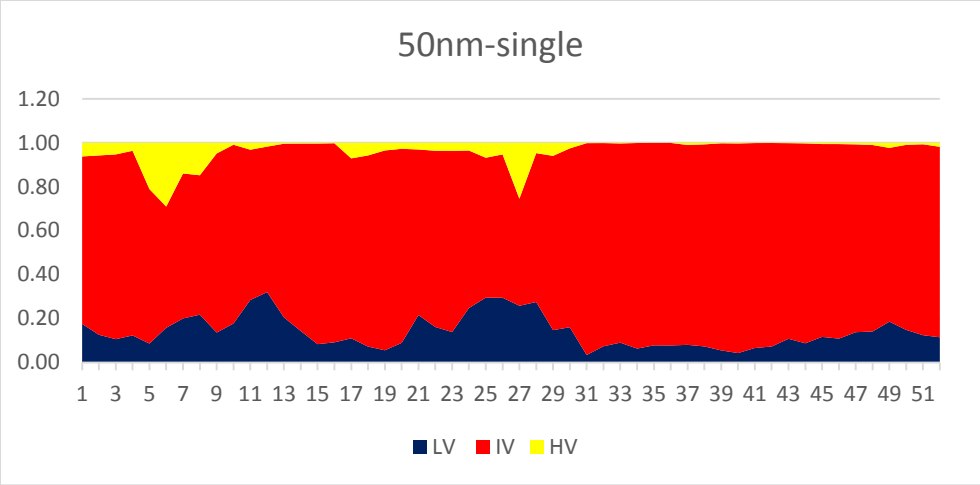

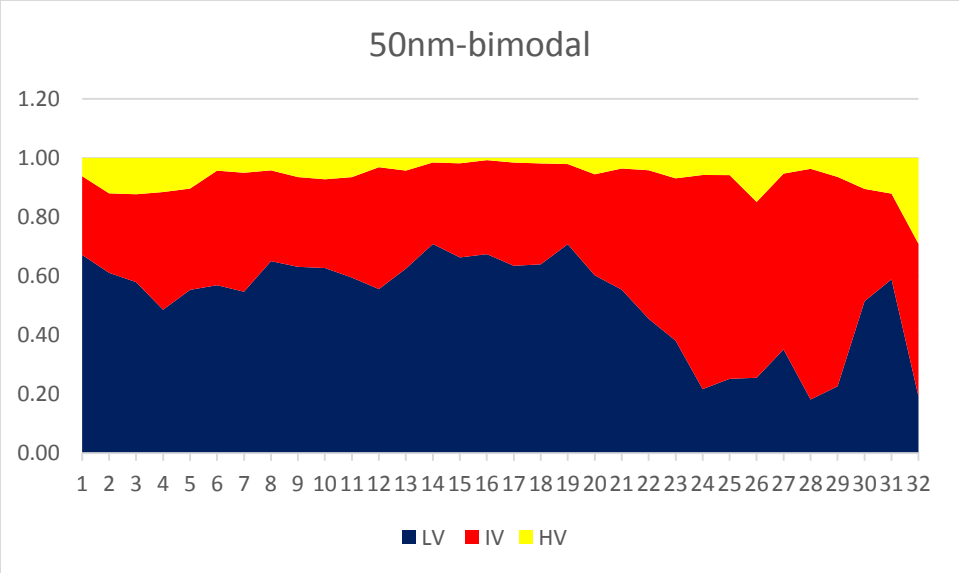

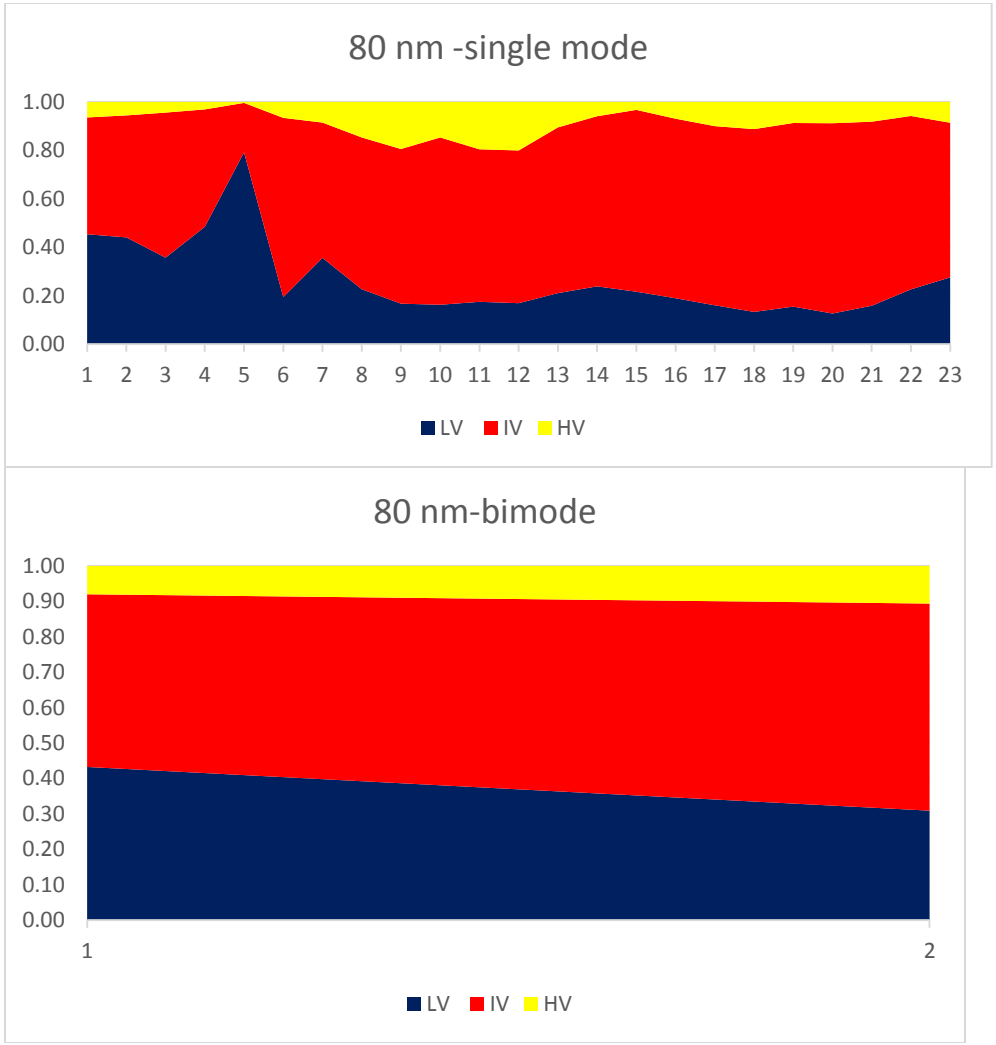

Section 9.3. Bimodal distribution observed in 30, and 50nm observed during the TDMA study period

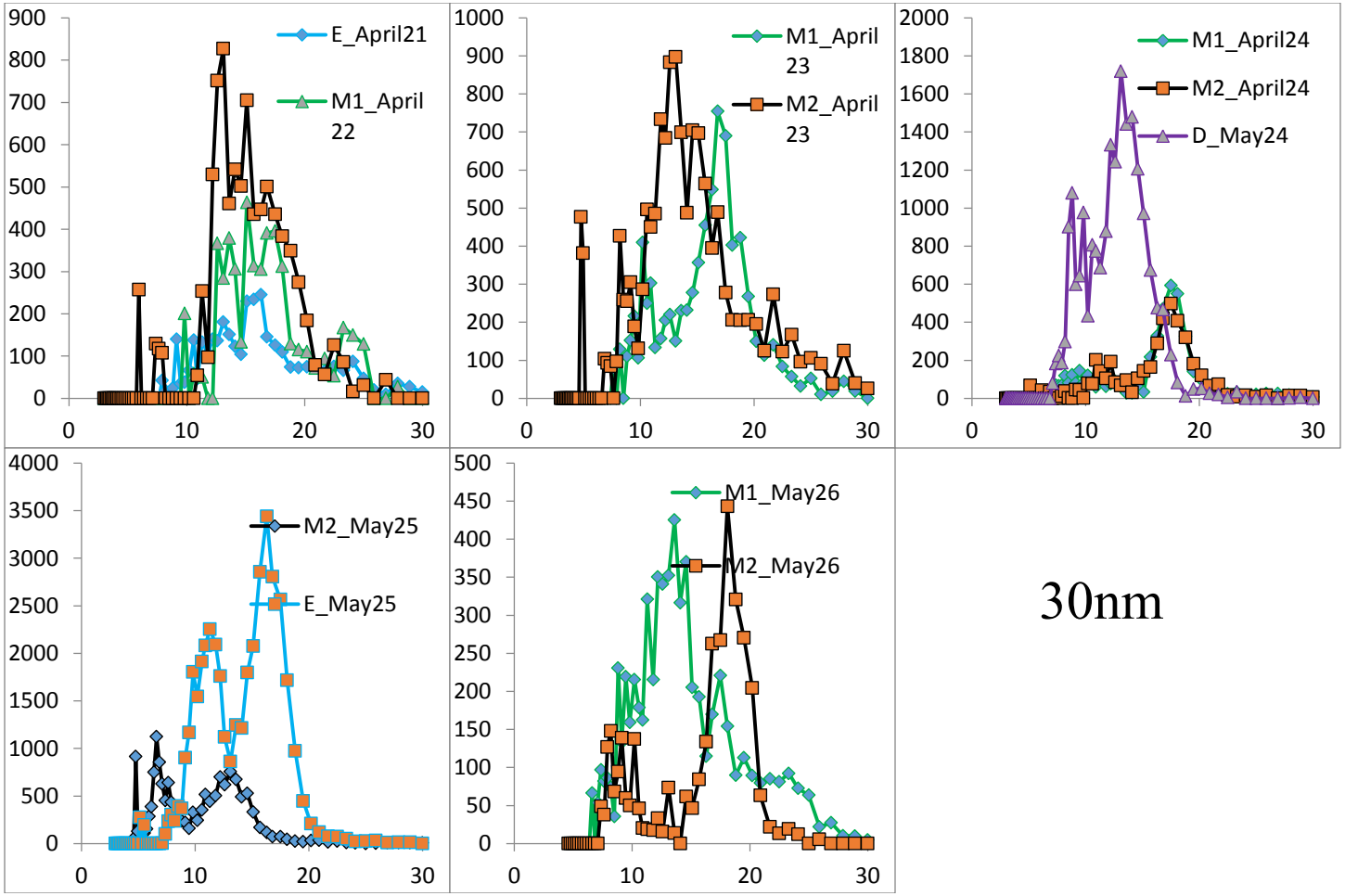

30nm

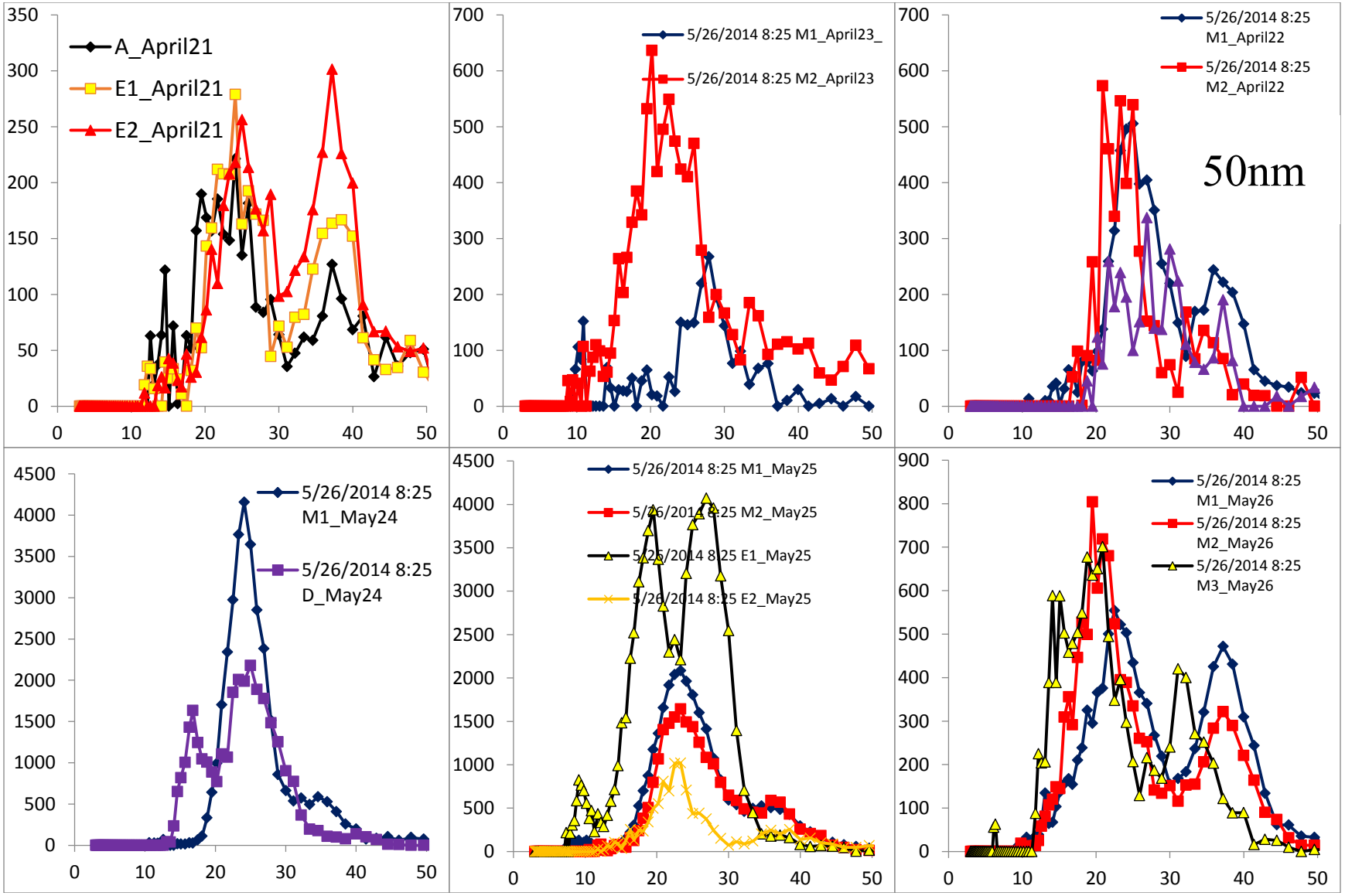

Secton 9.3 Description of internal and external mixing observed from the V-TDMA sampling in BND-UIOWA campaign

Aerosol mixing state definition:
Mixing state is a measure of distribution of chemical in the aerosol population. Mixing state is also referred to the distribution of chemical compounds within a particle. In this study the mixing state refers distribution of chemical in the aerosol population

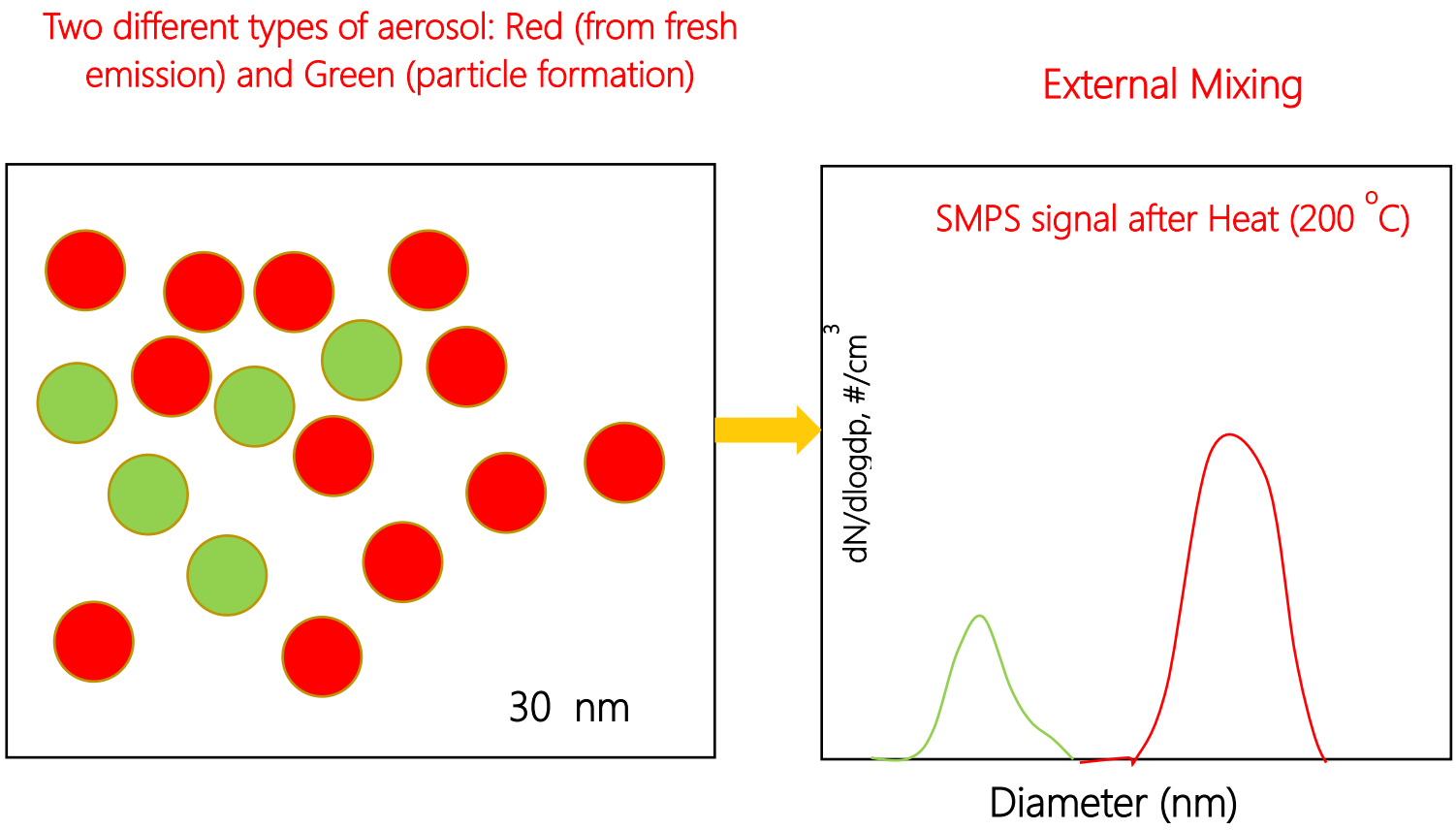

Two different types of aerosol: Red (from fresh emission) and Green (particle formation)

Internal Mixing

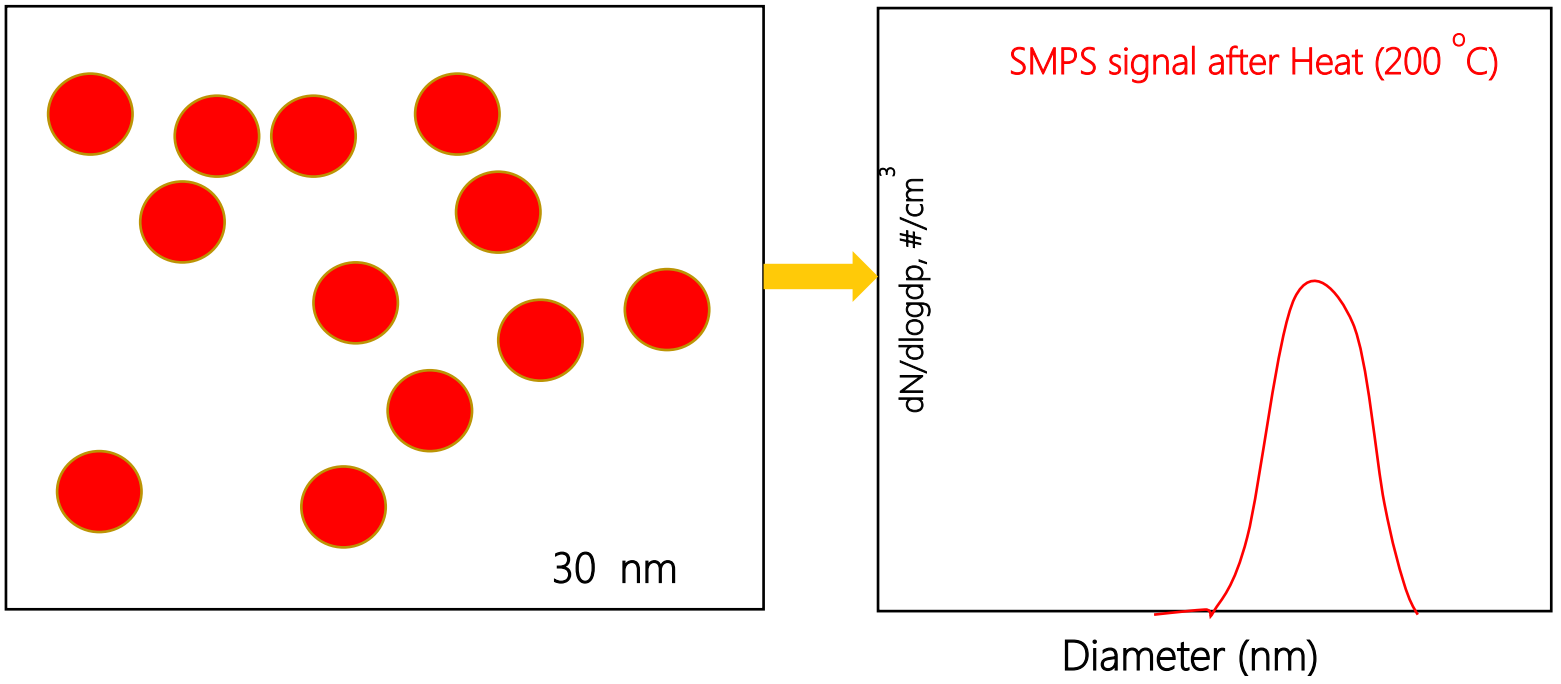

Example of external and internal mixing from field data in BND-UIOWA

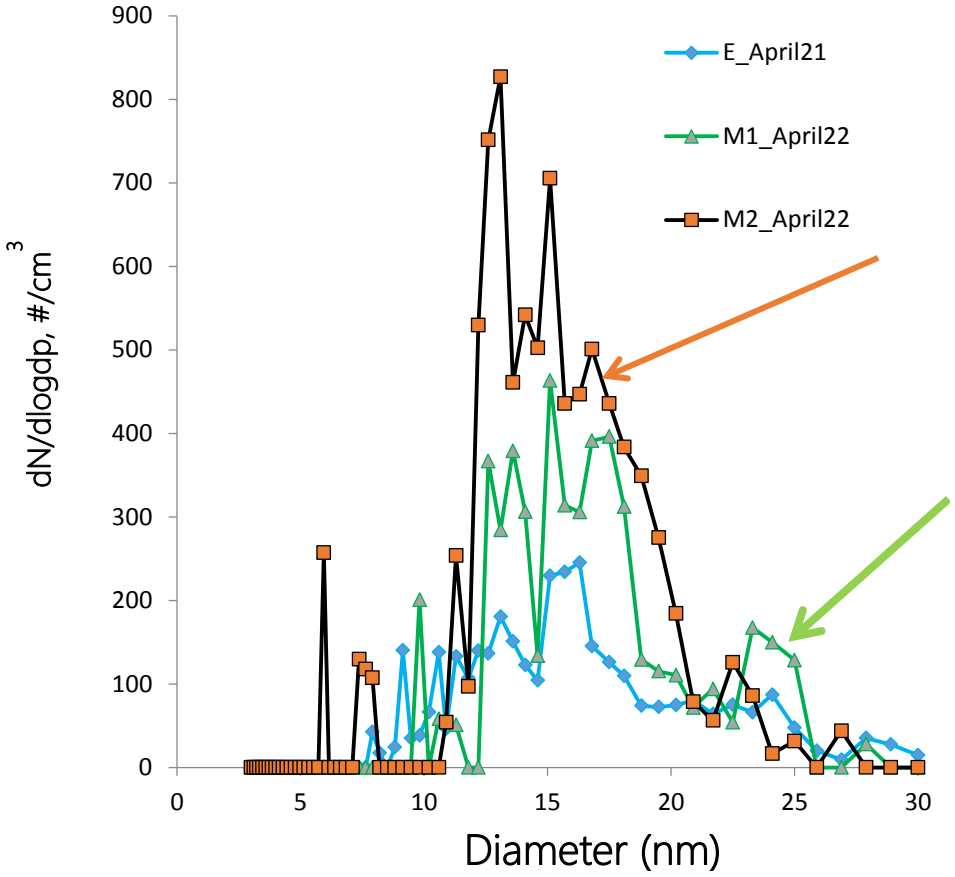

Internal mixing, single dominant mode (10-15 nm) of the size distribution

External mixing, two modes were observed with this size distribution. One at 15nm and other at 25 nm

Section 9.3. Change in the mode diameter for 30, 50 and 80

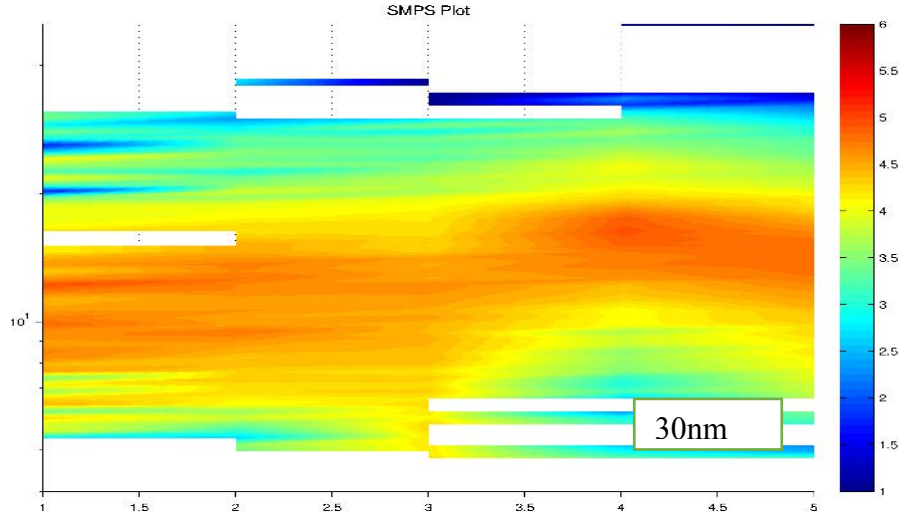

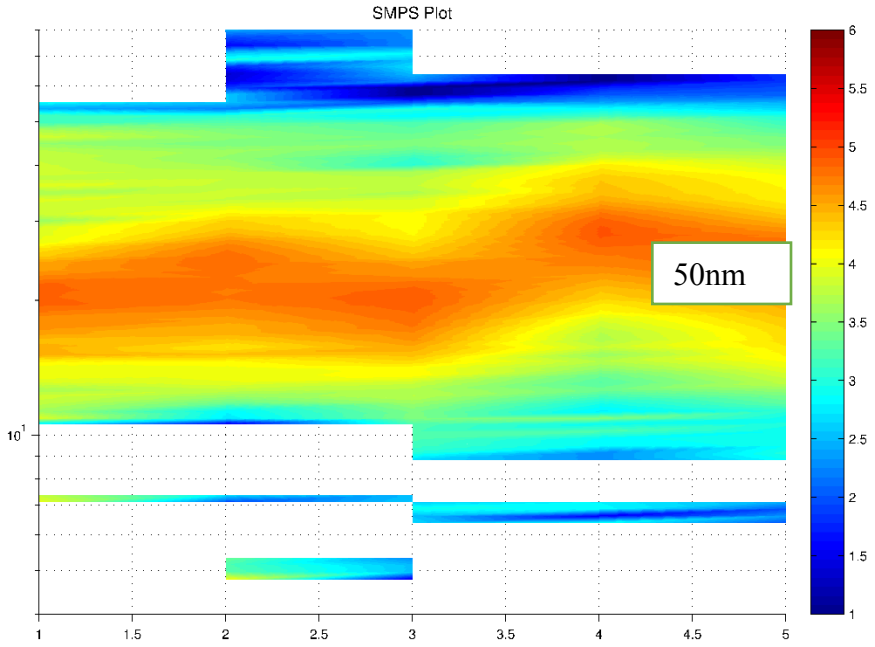

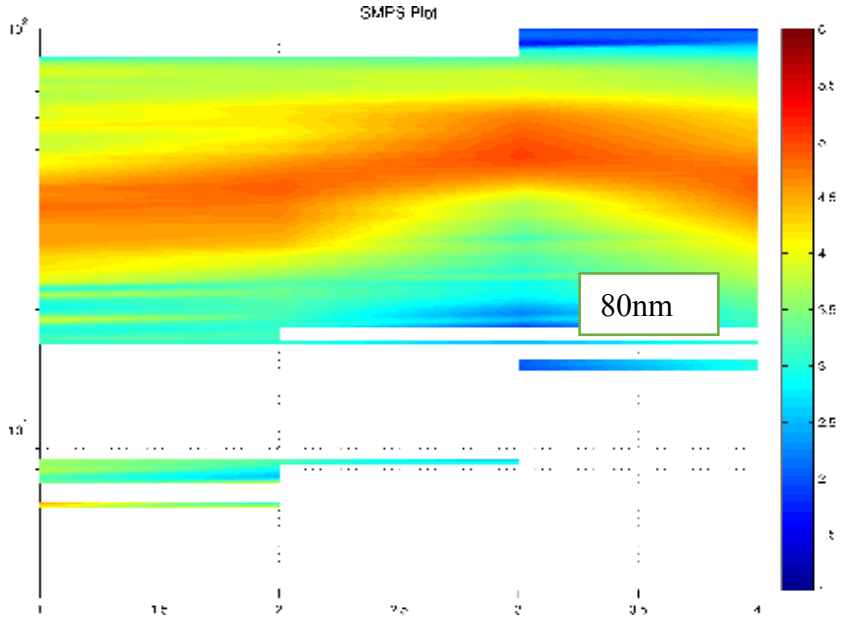

Section 9.3 IMPROVE measurement times series during April and May 2014

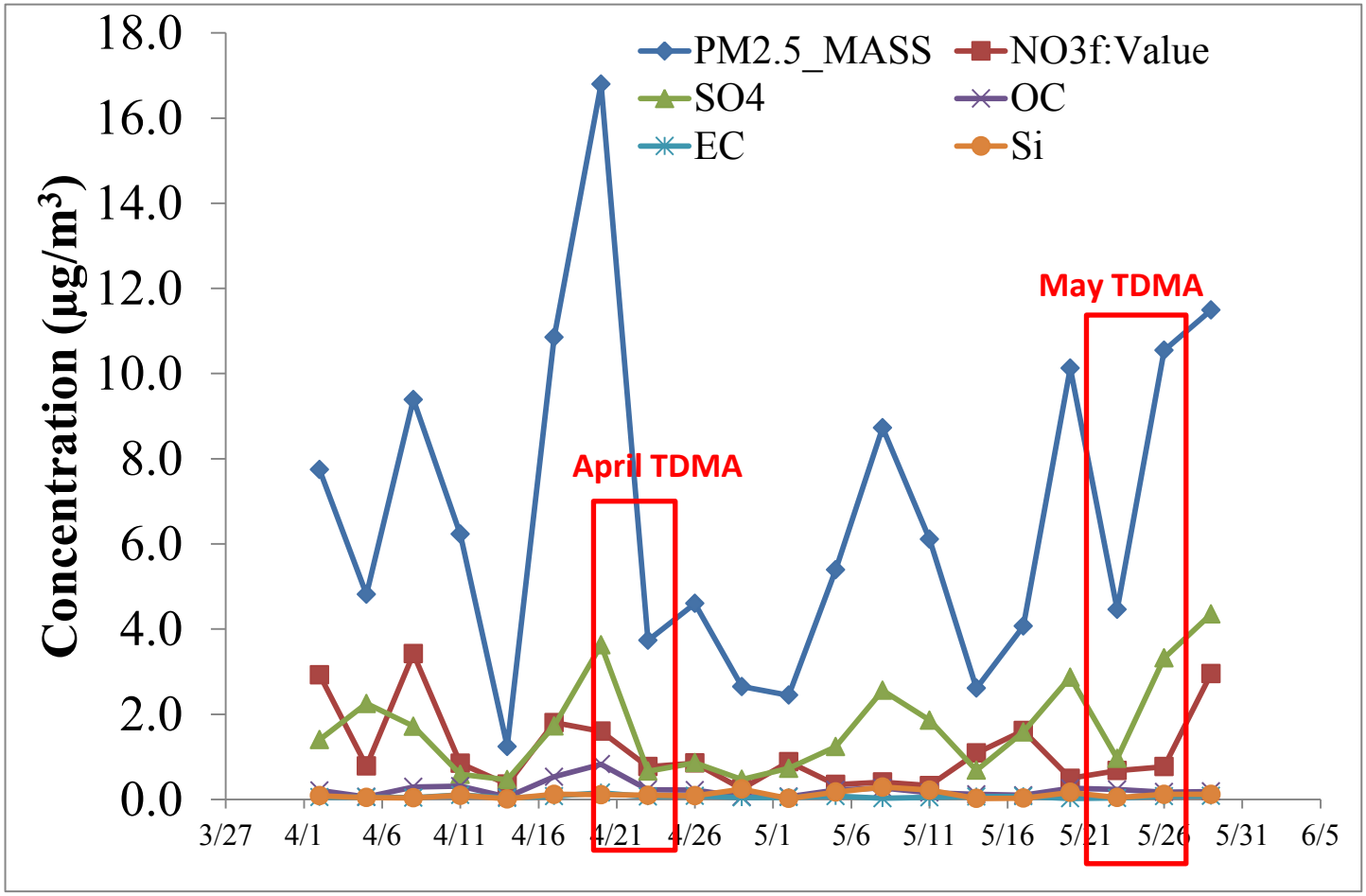

Appendix for Aim 4

Section 9.4

Supplementary Material for

Section 9.4: Chronology of the tire fire and response

The fire was first reported during the evening of May 26, 2012 under conditions of clear skies, low $PM_{2.5}$ levels, and warm temperatures. Initial winds were southeasterly, carrying the plume to the northwest and away from populated areas. Populated areas to the north of the landfill were first impacted on May 27, and then areas to the southeast of the landfill on May 28. The plume dispersed most efficiently from May 26 – 28, as indicated by retrospective dispersion modeling. Over the next few days, more stable atmospheric conditions led to higher concentrations of $PM_{2.5}$, measured up to 377 $\mu g\ m^{-3}$ at 8.4 km from the fire on May 30.

High concentrations impacted populated areas in the north, and northeast on June 2 and 3 during periods of low wind speeds, low boundary layer heights, and increased atmospheric stability. The fire-related pollutants $PM_{2.5}$, SO_2, particle number, EC, and PAH peaked in Iowa City from June 1-3 (Downard et al., 2015). Dispersion improved on June 3, as boundary layer heights increased to over 2 km.

A "stir, burn and cover" operation began on June 4 to manage the fire. In general, the plume was dispersed very effectively from June 4 until June 7, and then had moderate impacts north of the landfill during June 7-10. Retrospective dispersion model classifies June 7-8 as the period 2nd least conducive to dispersion, but the June 7 and 8 plumes were not captured by monitors. The

fire was declared under control and the emergency operation stopped on June 12. Additional detail on weather, PM concentrations, sampler activities, and associated AERMOD predictions are found in the following table.

Section 9.4. Chronology of Meteorology, Air Quality, and Air Quality Management

Table 4A 1. Chronology of Meteorology, Air Quality, and Air Quality Management Activities

Time period	Meteorology	Air Quality	Sampling, Forecasting, and Risk Management Activities
May 26 (Sat)	The fire was first reported during the evening (6:38 PM) of May 26, 2012. Conditions at the start of the fire were hot (high of 32°C), with clear skies and winds from the southeast. This carried the plume initially to sparsely populated areas to the northwest of the landfill.	Conditions at the start of the fire were clean ($PM_{2.5}$ of ~7 μg m^{-3}). Retrospective modeling shows the significant impact area (AQI>100, 1 h averaging time) extending a maximum distance of 1.3 km from the landfill.	Iowa City contacts Johnson County Public Health (JCPH) for public health concerns about smoke. JCPH contacts Linn County Public Health (LCPH) and the State Hygienic Laboratory (SHL).
May 27-28 (Sun-Mon)	Hot and clear or partly cloudy conditions continued on the 27th and 28th, but with shifting winds, first southerly winds which carried the plume into the populated Coralville area on May 27, and then westerly and northwesterly winds bringing the plume to a residential neighborhood and close to a school (Weber Elementary) on May 28.	The peak value of benzene sampled during the fire is taken: 8.3 ppb at 300 m away from the fire on the 28th. Retrospective dispersion modeling indicates excellent plume dispersion during this period. Maximum (modeled) peak 8 h smoke concentration in a densely populated area is in Coralville IA at ~0.6 μg/m^3 $PM_{2.5}$ smoke. Significant impact area (AQI>100, 8 h averaging time) is modeled to extend a maximum distance of 0.7 km from the landfill.	Public health advisory appears in the local newspaper.[1] JCPH in contact with the IDNR for technical assistance. TO-15 canister samples begin at 5:30 PM on May 27. May 27 is a 1-in-3 sampling day for the IA-AMS $PM_{2.5}$ speciation sampler. This sampler is changed to every day operation.
May 29-31 (Tue-Thu)	Conditions shifted to cooler (high of 27°C) on May 29 with strong northwesterly winds. Cool and windy conditions, with some rain, prevailed on the May 30 and 31, with wind directions from the north and east (and therefore carrying the plume away from the populated areas).	No impact of the fire on Iowa City, Coralville, or North Liberty is expected due to the wind direction; out of the plume, the 24 h PM_{10} filter (AMS site) reads 16 μg/m^3, while the Hoover $PM_{2.5}$ BAM averages 3.7 μg/m^3. Retrospective dispersion modeling has the plume to the south of the landfill for the entirety of this period, and the significant impact area (AQI>100, 8 h averaging time) modeled to extend up to 3.8 km to the southeast of the landfill. The Stanier group trailer achieves an interception of a well-diluted smoke plume	Handheld surveys of $PM_{2.5}$ and CO begin. JCPH sends an official request (on 5/31) for State and Federal assistance in air monitoring and assessment. The Stanier group trailer is first deployed on May 29 but is just to the east of the plume and records clean conditions. The first SHL PM_{10} sample at IA-AMS is taken on May 30 and the first WRF-AERMOD and HPAC dispersion model forecasts are produced.

Time period	Meteorology	Air Quality	Sampling, Forecasting, and Risk Management Activities
		at BDR on May 30 ($\Delta PM_{2.5}$ of 0.7 $\mu g/m^3$ on a 6.3 $\mu g/m^3$ background, 30 min average). A hand held Dust Trak reads an instantaneous reading of 377 $\mu g/m^3$ at a distance of 8.2 km from the fire.	
June 1-3 (Fri-Sun)	On June 1-3, under cool conditions (highs of 20-27 C) light westerly winds threaten downtown Iowa City with landfill smoke and bring the plume to the IA-AMS and Hoover sites. This Friday – Sunday period is of special concern because an outdoor music festival is scheduled with large crowds in downtown Iowa City. Low boundary layer heights and neutral / stable conditions during some portions of this period.	Instantaneous $PM_{2.5}$ by Dust Trak is 510 $\mu g/m^3$ on June 1 at 2.4 km from the fire. June 2 is the day of the highest EC filter loading (AMS). PAH (24 h) is ~140 times background levels (AMS). During early morning of June 3, calm conditions and fog form, and high concentrations are recorded at the sites to the east of the landfill (1 h values of 48 and 71 $\mu g/m^3$ at AMS and Hoover, respectively). Reports of strong odor and respiratory irritation on the east side of Iowa City are noted. The retrospectively modeled area of significant impact (AQI > 100, 8 h averaging) extends farthest on the 2nd, out to 5.8 km from the landfill into Coralville, and 4.4 km towards Iowa City, crossing Mormon Trek Blvd. into the west side neighborhood of University Heights (but not reaching downtown Iowa City under 8 h averaging). Maximum 8 h modeled concentrations of smoke in downtown Coralville and downtown Iowa City are 16 and 6 $\mu g/m^3$, respectively.	Iowa City mayor signs a Local Disaster Declaration document (June 1) facilitating access to state and federal resources. Also on June 1, EPA region 7 personnel on site in Iowa City and participate in coordination meetings (SHL, JCPH, DNR, EPA) reviewing sampling activities and assessment. WRF-AERMOD forecasts shared with the JCPH predict limited dispersion, with hourly smoke concentrations in excess of 50 $\mu g/m^3$ in populated areas up to 9 km from the landfill. A plume transect experiment samples plume size distribution and number concentration at 3 distances.
June 4-7 (Mon-Thu)	From June 4-7, light easterly winds and favorable conditions for vertical plume dispersion prevail, carrying the plume up and away from populated areas. Heavy equipment operation at the landfill site begins on June 3 as part of the "stir burn and cover" operation and this creates a darker and larger	The highest instantaneous concentration of the fire period is recorded on a DustTrak instrument, 2000 $\mu g/m^3$ at a distance of 1.0 km under very smoky conditions during the morning of June 4. Upwind of the plume, the average $PM_{2.5}$ in Iowa City (Hoover) during this time is 9.4 $\mu g/m^3$ and the	WRF-AERMOD forecasts predicting excellent vertical dispersion of the plume are shared with JCPH. Handheld and TO-15 canister sampling is suspended.

Time period	Meteorology	Air Quality	Sampling, Forecasting, and Risk Management Activities
	smoke plume.	highest 1 h concentration is 21 $\mu g/m^3$. The modeled area of significant impact (AQI > 100, 8 h averaging) extends to 1.5 km to the northwest of the landfill.	
June 7-12 (Thu-Tue)	The evening of June 7 to June 10 brings southerly winds carrying the plume north towards Coralville and North Liberty. Conditions transition to westerly and northwesterly winds and cooler temperatures on June 11 and 12. The fire is declared fully under control and the stir, burn and cover operation is stopped on June 12.	Elevated EC concentration (AMS) on June 7, and the highest IA-AMS PM_{10} sample (29 $\mu g/m^3$) is taken on June 8. No visible smoke from the landfill as of June 12. The modeled area of significant impact (AQI > 100, 8 h averaging) extends to 3.9 km to the north of the landfill, towards North Liberty. A peak 8 h average concentration of landfill smoke of 2.7 $\mu g/m^3$ is modeled for the North Liberty library, 11.4 km from the landfill.	

[1] (Source: Press Citizen) The Johnson County Health Department warns residents in the path of the smoke to avoid exposure to the smoke as much as possible. Persons who have respiratory, heart or other conditions which may be aggravated by smoke and the young and elderly should shelter in place with outside sources of air shut off. Most home air conditioning units recirculate air from the interior and should be sufficient. Businesses and other structures which draw in outside air should close outside air sources if the smoke plume is present. Avoid outdoor activities such as exercising if the smoke plume is present. Nursing homes, day cares and other businesses which care for the elderly, very young and persons with respiratory diseases should take special care to monitor the health of clients and to minimize exposure to the smoke plume.

By June 4, the public health advisory was unchanged in a press release by the City of Iowa City. However, the following two additional sentences were added: Concentration (increase and decrease) of particulate matter and other irritants in the smoke are greatly affected by weather conditions. Individuals are the best judges of their own health and should take appropriate protective measures based on their health status.

Section 9.4. Characterization method overview, organized by sampling method (offline or real-time) and compound class

Table 4A.2: Characterization method overview, organized by sampling method (offline or real-time) and compound class

Analyte	Method and Instrumentation	Research Group[4]	Site(s)	Smoke Characteriztaion[2]	Factor	Exposure Assessment[3]	Handheld	Hazard Ratio
TO-15, TO-12 VOCs	Collection in 6L canisters and GC/MS	SHL	Various	C		E, R		●
$PM_{2.5}$, PM_{10}	Beta Attenuation and Gravimetric filter (low volume)	SHL	Hoover ($PM_{2.5}$ & PM_{10}); IA-AMS (PM_{10})[5]			E, R		
$PM_{2.5}$ speciation (OC, EC, inorganic ions, metals and organic molecular markers)	Various, see text	Stone	IA-AMS	C	●	R		●
SO_2	UV fluorescence (Teledyne 100E)	Stanier	BDR, IA-AMS	C	●	R		●
CO_2	Infrared absorption (Vaisala 343 GMP)	Stanier	BDR, IA-AMS		●			
CO	NDIR absorption (Thermo 48i-TLE)	Stanier	BDR, IA-AMS	C	●			
CO	TSI 7575 Q-Track with electro-chemical CO sensor (IAQ-Probe Model 982)	JCPH	Various			E	●	
$PM_{2.5}$	Beta attenuation (BAM-1020)	SHL	Hoover			E, R		
$PM_{2.5}$	Light scattering photometer (TSI	JCPH	various			E	●	

	Dust Track-8532)[1]						
Particle size distribution	Scanning Mobility Particle Sizer and Aerosol Particle Sizer	Stanier	BDR, IA-AMS, plume transect	P	●	R	●
Particle number (PN)	Condensation particle counter (TSI CPC 3786)	Stanier	BDR, IA-AMS, plume transect	P	●	R	

[1]Sensitive in to particles from 0.1-10 µm; [2]C indicates chemical characterization; P indicates physical characterization; [3]E indicates used mainly for exposure assessment during the incident; R indicates mainly used for retrospective assessment; [4] State Hygienic Lab (SHL), Johnson County Public Health (JCPH); [5]PM10 at IA-AMS is gravimetric mid volume sampler installed just for the tire fire period.

Section 9.4. Enhancement of pollutants in the smoke at different measurement sites during Iowa City Tire fire

Analyte	Variable[a]	Units / Averaging Time	Landfill (17:24 sample on 5/28)[e]	Plume Transect A[b]	Plume Transect B[c]	Plume Transect C[d]	BDR	IA-AMS	Hoover[f]
CO_2	baseline	ppm 20 min – 2.3 h	--	--	--	--	365.6-376.7	370.2-406.0	--
	range of Δ		--	--	--	--	0.15-2.52	1.03-24.1	--
	mean of Δ (n)[b]		--	--	--	--	1.22 (4)	6.09 (6)	--
Particle Number (PN)	baseline	cm^{-3} 20 min – 2.3 h		3219	5949	4505	11,794-16,968	4400-8263	--
	range of Δ		--	--	--	--	5533-50520	6916-43,462	--
	mean of Δ (n)[b]		--	36,882	22,855	10,344	33,248 (4)	26,651 (5)	--
$PM_{2.5}$	baseline	$\mu g/m^3$ 20 min – 3 h	--	6.27	4.4	4.54	6.30-15.9	3.8-17.3	8.2-13.5
	range of Δ		--	--	--	--	0.67-7.5	1.09-11.8	11.5-44.0
	mean of Δ (n)[b]			49 (1)	9 (1)	6 (1)	5.07 (3)	5.37 (6)	22.2 (4)
SO_2	baseline	ppb 20 min – 2.3 h	--	--	--	--	0.78-1.89	1.33-2.94	--
	range of Δ		--	--	--	--	0.63-5.22	0.6-4.12	--
	mean of Δ (n)[b]		--	--	--	--	2.48 (3)	2.04 (6)	--
BaP	baseline	ng/m^3	--	--	--	--	--	0.02	--
	range of Δ		--	--	--	--	--	0.33-1.54	--
	mean of Δ (n)[c]		--	--	--	--	--	0.73 (3)	--
PAH	baseline	ng/m^3	--	--	--	--	--	0.24	--
	range of Δ		--	--	--	--	--	2.7-33	--

	mean of Δ (n)[c]		--	--	--	--	--	13.6 (3)	--
Benzene	baseline	ppb	0.07	--	--	--	--	--	--
	Δ		8.2	--	--	--	--	--	--
1,3 Butadiene	baseline	ppb	<0.24 [f]	--	--	--	--	--	--
	Δ		0.67	--	--	--	--	--	--

[a]Variables,

i. Except for VOC and PAH, the baseline refers to the concentration before and after the plume impaction.
ii. Δ is calculated as actual plume concentration minus baseline concentration.
iii. Of the 10 VOC measurement sites, sample collected on May 28th 2012 at 300 m from the fire (close to 41.646902, -91.619386) was used a plume concentration and sample collected on May 27 near Camp Cardinal Road and Melrose Avenue in Iowa City approximately 4 km from the landfill (44.65733, -91.59395) was used as "baseline". This sample was taken during non-plume impact period and had the lowest values of all the measured location and time.

[b](n)=10 plumes were identified from the continuous measurement at BDR and IA-AMS from 05/30 to 06/04 2012
[c](n) =3, the Δ values are based on three days during tire fire measured at IA-AMS ; 06/01, 06/02, and 06/03. For baseline of total PAH and BaP, 2011 summer average (n = 8) measured at the same site was used.
[d]Plume transect A is averaged over 0.92 h duration; the mean value is the average of individual 5 minute samples.
[e]Plume transect A is averaged over 1.17 h duration; the mean value is the average of individual 5 minute samples.
[f]Plume transect A is averaged over 0.58 h duration; the mean value is the average of individual 5 minute samples.
[g]Sample was below the minimum detection limit, which was 0.06 ppb for 1,3 butadiene and 0.16 ppb for ethylbenzene
[h]Hoover data is at 1 h time resolution, and the four plumes identified and averaged for this table have durations of 1, 1, 1, and 3 h

Table 4A.4: Summary data, including background, ambient enhancement (□), and emission factors (EF) for ten transects of the tire fire plume in Iowa City.

No.	Location[a]	Date in 2012	Start time[b]	End time[b]	Peak duration (h)	CO_2 background (ppm)	□CO_2 (ppm)	$PM_{2.5}$ background (□g m^{-3})	□$PM_{2.5}$ (□g m^{-3})	EF $PM_{2.5}$ (g kg^{-1})	SO_2 background (ppb)	□SO_2 (ppb)	EF SO2 (g kg^{-1})	PN background (# cm^{-3})	DPN (# cm^{-3})	EF PN (# kg^{-1})
1	BDR	30-May	16:20	16:50	0.67	376.74	2.52	NA[c]	NA[c]	NA[c]	0.78	2.13	4.1	16,968	30,863	2.3E+16
2	BDR	30-May	19:50	20:10	0.50	373.93	1.24	6.30	0.67	NA[c]	1.24	0.63	2.4	16,932	5,533	8.2E+15
3	BDR	31-May	18:00	19:10	1.33	365.56	0.15	8.19	7.06	NA[c]	1.38	1.96	NA[c]	13,434	46,077	NA[c]
4	BDR	31-May	20:20	20:50	0.33	376.45	0.99	15.93	7.47	14.0	1.89	5.22	25.6	11,794	50,520	9.4E+16
5	IA-AMS	1-Jun	21:20	23:30	2.33	406.00	24.10	5.86	11.77	0.9	1.35	0.80	0.2	4,400	28,382	NA[c]
6	IA-AMS	2-Jun	6:40	8:20	1.83	384.20	1.72	17.28	9.01	9.6	2.54	4.12	11.5	NA[c]	NA[c]	NA[c]
7	IA-AMS	2-Jun	8:40	9:40	1.17	374.54	1.42	15.76	6.50	8.4	2.94	3.92	13.3	4,757	43,462	5.6E+16
8	IA-AMS	2-Jun	12:20	14:00	1.67	370.21	1.03	7.76	1.71	3.0	1.80	0.60	2.8	8,263	6,916	NA[c]
9	IA-AMS	3-Jun	8:50	9:10	0.33	387.21	5.51	7.38	2.14	0.7	1.63	1.14	1.0	4,966	26,633	8.9E+15
10	IA-AMS	3-Jun	13:10	14:40	1.50	374.57	2.78	3.80	1.09	0.7	1.33	1.67	2.9	6,635	27,864	1.8E+16
	Mea					**378.94**	**4.15**	**9.81**	**5.27**	**5.35**	**1.69**	**2.22**	**7.1**			**3.5E**

n								**0**	**9,794**	**29,583**	**+16**
Standard Deviation	11.34	7.16	5.07	3.98	5.33	0.64	1.64	8.31	5,121	15,851	3.4E+16
Minimum	365.56	0.15	3.80	0.67	0.72	0.78	0.60	0.16	4,400	5,533	8.2E+15
Maximum	406.00	24.10	17.28	11.77	13.97	2.94	5.22	25.57	16,968	50,520	9.4E+16

a) BDR = Black Diamond Road; b) Local; c) NA = not available;

Section 9.4. All TO-15 and selected TO-12 VOC measured during the tire fire

Table 4A.5: All TO-15 and selected TO-12 VOC measured during the tire fire

	Species	Method detection limit	Method of detection	Coralville –End st/22nd Avenue	Iowa City- Camp Cardinal/Melrose	Iowa City near landfill	North Liberty, forevergreen road/965	Weber School, Iowa City	Iowa City Penta crest (not in plume)	Dane RD SW, Iowa city (in plume)	Iowa City, near fire	Slothower road, Iowa City (in plume)	Iowa City Penta crest (in plume)
		(ppbv)		05/27/2012/17:58	5/27/2012 18:11	5/27/2012 17:34	5/27/2012 17:40	5/28/2012 16:53	6/1/2012 15:20	6/1/2012 18:52	6/1/2012 15:32	6/1/2012 17:50	6/2/2012 7:00
	Aromatic												
1	Benzene	0.17		0.08	0.07	8.27	0.63	0.05	0.05	0.45	>10	0.08	0.18
2	Toluene	0.16		0.11	0.06	8.64	0.5	0.16	0.05	0.32	>10	0.11	0.15
3	Ethylbenzene	0.18		<0.18	<0.18	0.66	<0.18	<0.18	<0.18	<0.18	>10	<0.18	<0.18
4	m,p Xylene	0.26		<0.26	<0.26	2.03	<0.26	<0.26	<0.26	<0.26	>10	<0.26	<0.26
5	o-Xylene	0.11		<0.11	<0.11	0.62	<0.11	<0.11	<0.11	<0.11	10	<0.11	<0.11
6	Styrene	0.1		<0.1	<0.1	0.59	<0.1	<0.1	<0.1	<0.1	>10	<0.1	<0.1
7	1, 2 4-Trimethylbenzene	0.14		<0.14	<0.14	0.27	<0.14	<0.14	<0.14	<0.14	7.53	<0.14	<0.14
8	1, 3 5-Trimethylbenzene	0.16		<0.16	<0.16	0.14	<0.16	<0.16	<0.16	<0.16	3.52	<0.16	<0.16
9	Benzyl Chloride	0.31		<0.31	<0.31	<0.31	<0.31	<0.31	<0.31	<0.31	<0.31	<0.31	<0.31
10	Chlorobenzene	0.13		<0.13	<0.13	<0.13	<0.13	<0.13	<0.13	<0.13	0.21	<0.13	<0.13
11	1,3 Dichlorobenzene	0.09		<0.09	<0.09	<0.09	<0.09	<0.09	<0.09	<0.09	<0.09	<0.09	<0.09
12	1,4 Dichlorobenzene	0.1		<0.1	<0.1	<0.1	<0.1	<0.1	<0.1	<0.1	<0.1	<0.1	<0.1
13	1,2 Dichlorobenzene	0.2		<0.2	<0.2	<0.2	<0.2	<0.2	<0.2	<0.2	<0.2	<0.2	<0.2
14	1,2,4 Trichlorobenzene	0.23		<0.23	<0.23	<0.23	<0.23	<0.23			<0.23	<0.23	<0.23
	Halocarbon compounds												
15	Chloroform	0.11		<0.11	<0.11	<0.11	<0.11	<0.11	<0.11	<0.11	<0.11	<0.11	<0.11
	Tetrachloroethene	0.16		<0.19	<0.19	<0.19	<0.19	<0.19	<0.19	<0.19	<0.19	<0.19	<0.19
16	Carbon tetrachloride	0.33	GCMS volatiles, EPA TO-15	0.08	0.1	0.09	0.07	0.1	0.1	0.12	0.11	0.1	0.14
17	Dichlorodifluoromethane	0.23		0.51	0.51	0.53	0.5	0.56	0.51	0.61	0.56	0.48	0.65
18	Dichlorotetrafluoromethane	0.17		<0.17	<0.17	<0.17	<0.17	<0.17	<0.17	<0.17	<0.17	<0.17	<0.17
19	Chloromethane	0.3		0.62	0.64	0.59	0.54	0.67	0.71	0.66	0.67	0.59	0.74
20	Chloroethane	0.26		<0.26	<0.26	<0.26	<0.26	<0.26	<0.26	<0.26	<0.26	<0.26	<0.26
21	Trichloroflurormethane	0.17		0.23	0.24	0.25	0.22	0.24	0.22	0.26	0.24	0.19	0.3
22	1,1,2 Trichloro,1,2,2-trifluroethane	0.18		0.06	0.08	0.08	0.08	0.09	0.08	0.08	0.08	0.06	0.09
23	1,1 Dichoroethene	0.19		<0.19	<0.19	<0.19	<0.19	<0.19	<0.19	<0.19	<0.19	<0.19	<0.19
24	Trans 1,2 Dichloroethane	0.14		<0.14	<0.14	<0.14	<0.14	<0.14	<0.14	<0.14	<0.14	<0.14	<0.14
25	cis 1,2 Dichloroethane	0.22		<0.22	<0.22	<0.22	<0.22	<0.22	<0.22	<0.22	<0.22	<0.22	<0.22
26	Chloroprene	0.13		<0.13	<0.13	<0.13	<0.13	<0.13	<0.13	<0.13	<0.13	<0.13	<0.13
27	1,1,1 Trichloroethane	0.27		<0.27	<0.27	<0.27	<0.27	<0.27	<0.27	<0.27	<0.27	<0.27	<0.27
28	1,1 Dichoroethane	0.07		<0.07	<0.07	<0.07	<0.07	<0.07	<0.07	<0.07	<0.07	<0.07	<0.07
29	1,2 Dichoroethane	0.09		<0.09	<0.09	<0.09	<0.09	<0.09	<0.09	<0.09	<0.09	<0.09	<0.09
30	Trichloroethene	0.16		<0.16	<0.16	<0.16	<0.16	<0.16	<0.16	<0.16	<0.16	<0.16	<0.16
31	1,2 Dichloropropane	0.21		<0.21	<0.21	<0.21	<0.21	<0.21	<0.21	<0.21	<0.21	<0.21	<0.21
32	1,1,2 Trichloroethane	0.26		<0.26	<0.26	<0.26	<0.26	<0.26	<0.26	<0.26	<0.26	<0.26	<0.26
33	Bromodichloromethane	0.15		<0.15	<0.15	<0.15	<0.15	<0.15	<0.15	<0.15	<0.15	<0.15	<0.15
34	Dibromochloromethane	0.32		<0.32	<0.32	<0.32	<0.32	<0.32	<0.32	<0.32	<0.32	<0.32	<0.32
35	1,2 Dibromoethane	0.13		<0.13	<0.13	<0.13	<0.13	<0.13	<0.13	<0.13	<0.13	<0.13	<0.13

	Species	Method detection limit	Method of detection	Coralville –End st/22nd Avenue	Iowa City- Camp Cardinal/Melrose	Iowa City near landfill	North Liberty, forevergreen road/965	Weber School, Iowa City	Iowa City Penta crest (not in plume)	Dane RD SW, Iowa city (in plume)	Iowa City, near fire	Slothower road, Iowa City (in plume)	Iowa City Penta crest (in plume)
		(ppbv)		05/27/2012/17:58	5/27/2012 18:11	5/27/2012 17:34	5/27/2012 17:40	5/28/2012 16:53	6/1/2012 15:20	6/1/2012 18:52	6/1/2012 15:32	6/1/2012 17:50	6/2/2012 7:00
36	Bromoform	0.25		<0.25	<0.25	<0.25	<0.25	<0.25	<0.25	<0.25	<0.25	<0.25	<0.25
37	Bromomethane	0.19		<0.19	<0.19	<0.19	<0.19	<0.19	<0.19	<0.19	<0.19	<0.19	<0.19
38	1,1,2,2 Tetrachloroethane	0.2		<0.2	<0.2	<0.2	<0.2	<0.2	<0.2	<0.2	<0.2	<0.2	<0.2
39	Hexachlorobutadiene	0.24		<0.24	<0.24	<0.24	<0.24	<0.24			<0.24	<0.24	<0.24
	Aliphatic compounds												
40	Acetylene	0.73		0.13	0.17	0.72	0.39	0.18	0.12	0.15	7.73	0.35	0.28
41	Propylene	0.16		<0.16	<0.16	5.54	0.91	<0.16	<0.16	0.26	>10	<0.16	<0.16
42	1,3 butadiene	0.24		<0.24	<0.24	0.91	<0.24	<0.24	<0.24	<0.24	8.13	<0.24	<0.24
43	Vinyle Chloride	0.18		<0.18	<0.18	<0.18	<0.18	<0.18	<0.18	<0.18	<0.18	<0.18	<0.18
44	Methly-t-butyl ether (MBTE)	0.12		<0.12	<0.12	<0.12	<0.12	<0.12	<0.12	<0.12	<0.12	<0.12	<0.12
45	Ethly tert butly ether	0.19		<0.19	<0.19	<0.19	<0.19	<0.19	<0.19	<0.19	<0.19	<0.19	<0.19
46	tert amyl methyl ether	0.21		<0.21	<0.21	<0.21	<0.21	<0.21	<0.21	<0.21	<0.21	<0.21	<0.21
47	Ethly acrylate	0.1		<0.1	<0.1	<0.1	<0.1	<0.1	<0.1	<0.1	<0.1	<0.1	<0.1
48	Methyl methacrylate	0.14		<0.14	<0.14	<0.14	<0.14	<0.14	<0.14	<0.14	<0.14	<0.14	<0.14
49	Cis-1,3 Dichloropropene	0.16		<0.16	<0.16	<0.16	<0.16	<0.16	<0.16	<0.16	<0.16	<0.16	<0.16
50	Trans 1,3 Dicholoropropene	0.17		<0.17	<0.17	<0.17	<0.17	<0.17	<0.17	<0.17	<0.17	<0.17	<0.17
51	Octane	0.14		<0.14	<0.14	<0.14	<0.14	<0.14	<0.14	<0.14	<0.14	<0.14	<0.14
	Terpenoid compounds		To-12 Speciated non-Methane Organics										
52	α-Pinene	0.06		0.31	0.13	0.08	<0.06	<0.06	0.1	0.76	0.38	<0.06	<0.06
53	Isoprene	0.08		4.13	1.77	2.49	0.47	0.54	0.14	0.39	16.14	0.31	0.24
	Carbonyl compounds												
54	Acrolein	0.08	GCMS volatiles, EPA TO-15	0.17	0.17	1.5	0.24	0.14	<0.08	<0.08	1.7	<0.08	<0.08
55	Methly ethyl ketone	0.18		<0.18	<0.18	<0.18	<0.18	<0.18	<0.18	<0.18	<0.18	<0.18	<0.18
56	Methyl Isobutyl Ketone	0.16		<0.16	<0.16	<0.16	<0.16	<0.16	<0.16	<0.16	3.47	<0.16	<0.16
57	Ethane	0.03	To-12 Speciated non-Methane Organics	3.85	3.81	41.7	3.73	4.7	2.5	4.07	>20	2.5	3.07
58	propane	0.1		1.99	2.09	20.4	1.85	3.04	0.59	1.5	>20	0.59	1.68
59	Butane	0.1		1	1.06	6.07	0.74	1.4	0.29	1.08	>20	0.31	0.54
60	Isopentane	0.08		0.78	0.64	3.67	0.5	0.56	0.3	1.05	>20	0.37	0.75
61	Hexane	0.18		0.18	0.16	1.1	0.17	0.19	0.08	0.17	15.58	0.13	0.18
62	Nonane	0.05		0.11	0.07	0.37	<.05	0.17	0.21	0.16	5.39	<.05	0.06
63	Isopropyl benzene	0.07		<0.07	<0.07	0.6	<0.07	<0.07	<0.07	0.09	12.21	<.07	<.07
64	m-ethyltoluene	0.08		<0.08	<0.08	1.53	0.11	<0.08	0.12	0.22	>20	0.15	0.11
65	p-ethyltoluene	0.1		<0.1	<0.1	0.76	0.8	<0.1	0.05	0.15	>20	0.08	0.06
66	1-decene	0.08		0.11	0.09	2.58	0.09	0.09	0.15	0.17	>20	0.19	0.21
67	Decane	0.08		0.04	0.07	1.13	<0.08	<0.08	<0.08	0.11	18.3	0.09	<0.08
68	Dodecane	0.08		<0.08	<0.08	0.13	0.08	0.06	<.08	<0.08	3.4	0.03	<.08
69	m-dimethyle benzene	0.05		<0.05	<0.05	0.08	<0.05	<0.05	<0.05	0.19	1.75	<0.05	<0.05
70	p-dimethyl benzene	0.04		0.09	0.08	0.49	0.07	0.2	<0.04	<0.04	11.7	0.24	0.14

Section 4. Support on the acute hazard ratio calculation

Table 4A.6. Acute hazard ratios derived from concentrations or emission factors from this work and from other ambient and laboratory combustion studies.

CAS	Species	TLV-TWA[a] (mg/m3)	STEL or Ceiling[b] (mg/m3)	AEGL-1 (1 hr, mg/m3)	EPA Lab burn[d]			Westley,CA tire fire[e]			This study, VOC canister			This study emission factor			Pooled oil burn[f]		
					EF (mg/kg)	HR	Rank	Conc. (µg/m3)	HR x1000	Rank	Conc. (µg/m3)	HR x1000	Rank	EF (mg/kg)	HR	Rank	EF (mg/kg)	HR	Rank
none	$PM_{2.5}$	3	-	-	-	-		-	-		-	-		5350	357 **	2	-	-	
7446-09-5	SO_2	0.65	0.66[i]	0.52	-	-		-	-		-	-		7090	13528	1	-	-	
630-08-0	CO	29	458	-	1.2E+05	262 *	2	229	0.50 *	2	-	-		-	-		30000	65 *	3
none	PM_{10}	10	-	-	1.5E+05	2980 **	1	557	11.1 **	1	-	-		-	-		-	-	
none	BC	3.5	-	-	-	-		8	0.46 **	2	-	-		2410	138 **	3	-	-	
71-41-2	Benzene	1.6	16[ii]	166	2205	13.3	7	9.2	0.055	3	26.4	0.16	2	-	-		251	1.5	5
92-52-4	Biphenyl	1.26	-	-	330	52 **	3	-	-		-	-		-	-		-	-	
100-40-3	Vinylcyclohexene	0.44	-	-	108	49 **	4	-	-		-	-		-	-		-	-	
100-52-7	Benzaldehyde	8.8	17.4[i]	-	664	38 *	5	-	-		-	-		-	-		44	2.5 *	4
91-20-3	Naphthalene	52	79[i]	-	1195	15.2 *	6	-	-		-	-		-	-		44	0.6	6
108-95-2	Phenol	19.2	60[iii]	58	714	12.4	8	-	-		-	-		-	-		-	-	
106-99-0	1,3-Butadiene	4.4	11.1[ii]	1482	160	0.108	14	1.1	7E-4	4	1.5	0.001	6	-	-		-	-	
108-88-3	Toluene	75	565[iii]	754	2519	3.3	12	-	-		32	0.04	3	-	-		42	0.06	7
100-41-4	Ethyl benzene	87	543[iii]	143	632	4.4	11	-	-		2.9	0.02	4	-	-		10	0.07	7
95-13-6	Indene	23.7	71[iv]	-	339	4.8 *	10	-	-		-	-		-	-		-	-	
100-42-5	Styrene	85	170[i]	85	646	7.6	9	-	-		2.51	0.03	4	-	-		-	-	

CAS	Species	TLV-TWA[a] (mg/m3)	STEL or Ceiling[b] (mg/m3)	AEGL-1 (1 hr, mg/m3)	EPA Lab burn[d]			Westley,CA tire fire[e]			This study, VOC canister			This study emission factor			Pooled oil burn[f]		
					EF (mg/kg)	HR	Rank	Conc. (µg/m3)	HR x1000	Rank	Conc. (µg/m3)	HR x1000	Rank	EF (mg/kg)	HR	Rank	EF (mg/kg)	HR	Rank
95-63-6	1,2,4-Trimethylbenzene	123	-	688	826	1.2	13	-	-		1.3	0.002	5	-	-		32	0.05	7
138-86-3	Limonene	557	-	-	3239	1.16 **	13	-	-		-	-		-	-		-	-	
none	Xylene, mixed	434	651[i]	564	2013	3.6	12	-	-		9.9	0.017	5	-	-		25	0.04	7
98-82-8	Cumene	246	-	246	398	1.62	13	-	-		-	-		-	-		-	-	
107-02-8	Acrolein	0.23	0.23[i,C]	0.07	-	-		-	-		3.4	49	1	-	-		11	160	1
50-00-0	Formaldehyde	0.37	2.46[ii]	1.11	-	-		-	-		-	-		-	-		139	126	2
590-86-3	Isovaleraldehyde	4.7	-	-	-	-		-	-		-	-		-	-		5	0.3 **	6
75-07-0	Acetaldehyde	45	45[i,c]	81	-	-		-	-		-	-		-	-		32	0.4	6
67-64-1	Acetone	1188	1782[i]	475	-	-		-	-		-	-		-	-		20	0.04	7
111-84-2	Nonane	1050	-	-	-	-		-	-		-	-		-	-		13	0.003 **	9
338-23-4	Methyl ethyl ketone	590	885[i]	590	-	-		-	-		-	-		-	-		7	0.01	8
50-32-8	B[a]P	-	-	-	114	-		0.15	-		-	-		3.6	-		7	-	

Abbreviations: Emission factor (EF); Concentration (Conc.), and Hazard ratio (HR)

*STEL used in place of AEGL; **5 x TLV used in place of AEGL; **(a)** ACGIH: Documentation of the Threshold Limit Values (TLVs) and Biological Exposure Indices (BEIs). 2014. A summary of recent values can be found at https://www.osha.gov/dsg/annotated-pels/tablez-1.html; **(b)** STEL or Ceiling values (c) are based on (i) ACGIH, (ii) OSHA (iii) NIOSH (iv) Australian STEL; **(d)** Shredded tire combustion in EPA (1997). Values also reported in Lemieux et al. (2004); **(e)** Westley tire fire - 1 hr max concentration from Westley Livingston site at 4-5 miles downwind of the tire fire. **(f)** Crude oil emission factor are taken from Lemieux et al 2004 , table 8, page 20 [values are based from the original research work of Booher and Janke 1999]

Section 9.4. Support of the Multi-Pollutant AQI

An example calculation of the 1-h AQI resulting from 300 µg/m^3 of tire fire smoke.

The result can be seen from Table 5, and is 330. But additional details regarding the calculation are shown here.

- 300 µg/m^3 of $PM_{2.5}$ at 1-h averaging time alone, with no copollutants, carries an AQI of 188
- SO_2 is co-emitted, and will be at a concentration of 398 µg/m^3, or 152 ppb. This has a 1-h AQI of 135 as calculated at http://www.airnow.gov/index.cfm/index.cfm?action=resources.conc_aqi_calc
- The the SO_2 AQI contribution as 134.9.
- With p=1, these combine to 323
- These two compounds represent 97.9% of the total AQI.

The remaining 2.1% contribution are from a number of VOC compounds (listed in Table 6).
One of them is benzene, and its contribution is detailed here.
Benzene is coemitted with a mass ratio (relative to $PM_{2.5}$) of 0.41, so it is present in a concentration of 124 µg/m^3, or 38.7 ppb. This is associated with a benzene AQI contribution of 0.21. This is calculated as follows.

1. The first AQI breakpoint of SO_2 at the 1-h averaging time is AQI 50, concentration of 91.7 µg/m^3, or 35 ppb.
2. The AEGL-1 (1-h) for SO_2 is 200 ppb.
3. The AEGL-1 (1-h) for benzene is 52 ppm, or 52,000 ppb.
4. We convert from 38.7 ppb of benzene to a fraction of AEGL-1. The result is 7.44×10^{-4}
5. We construct an "equivalent" SO_2 concentration using 7.44×10^{-4} x $AEGL\text{-}1_{SO2}$, or 0.15 ppb SO_2
6. We determine the AQI for 0.15 ppb SO_2 (which is 0.15/35 x 50 = 0.21 AQI points).

We note that the OSHA STEL is a factor 10.4 lower than the AEGL-1, and using it as the basis for the calculation would increase the impact of benzene somewhat.
Some pollutants don't have an AEGL-1. For example, biphenyl. It has an AEGL-2 of 9.6 ppm. The estimate of the airborne concentration of biphenyl is 18.5 µg/m^3 (2.9 ppb), so the equivalent SO_2 concentration would be the AEGL-2 of SO_2 (750 ppb) x 2.9 / 9600 or 0.23 ppb of SO_2. This would have an AQI of 0.23 / 35 x 50 = 0.33 AQI units which matches the calculated value.

Section 9.4. AQI Categories

Table S6. AQI Categories (from Wildfire Smoke A Guide for Public Health Officials; Revised July 2008, With 2012 AQI Values)

Category	Notes
Good 0-50	If smoke exposure is forecast, implement communication plan.
Moderate 51-100	Issue public service announcements (PSAs) advising public about health effects and symptoms and ways to reduce exposure. Distribute information about exposure avoidance.
Unhealthy for Sensitive	If smoke event projected to be prolonged, evaluate and notify possible sites for cleaner air shelters. If

Subgroups 101-150	smoke event projected to be prolonged, prepare evacuation plans.
Unhealthy 151-200	Consider closing schools, possibly based on school environment and travel considerations. Consider canceling public events, based on public health and travel considerations.
Very unhealthy 201-300	Consider closing some or all schools (newer schools with a central air cleaning filter may be more protective than older leakier homes). Cancel outdoor events (e.g., concerts, sporting events).
Hazardous	Close schools. Cancel outdoor events (e.g., concerts, sporting events). Consider closing workplaces not essential to public health. If PM level is projected to remain high for a prolonged time, consider evacuation of sensitive subpopulations

Section 9.4. . Expanded version of Table 5 that includes additional tracers of the tire fire smoke

Table A4.7. Expanded version of Table 5 that includes additional tracers of the tire fire smoke (benzene, CO, and SO_2, 1,3 butadiene, acrolein, CO_2, and $PM_{2.5}$ B[a]P), using emission factor ratios. Additional columns can be added based on what measurements are available, using emission factor ratios, or Δconcentration ratios. These are prepared assuming p=1.

1-h Average Pollutant in Tire Smoke							1-h Average Background $PM_{2.5}$ (μg/m^3)					
Benzene (ppb)	Benzene (μg/m^3)	CO (ppb)	CO (μg/m^3)	SO_2 (ppb)	SO_2 (μg/m^3)	$PM_{2.5}$ (μg/m^3)	0	10	20	30	40	50
0	0	0	0	0	0	0	0	13	26	39	52	62
0.015	0.047	20	23	0.5	1.3	1	2	15	28	42	54	64
0.029	0.094	40	46	1.0	2.7	2	4	17	30	44	55	65
0.044	0.14	60	68	1.5	4	3	6	19	33	46	57	67
0.06	0.19	80	91	2.0	5	4	8	21	35	48	59	69
0.07	0.24	100	114	2.5	7	5	10	23	37	50	61	71
0.15[a]	0.47	199	228	5	13	10	21	34	47	59	69	79
0.29	0.94	398	456	10	27	20	41	54[b]	67	77	87	97
0.44[b]	1.4	597	684	15	40	30[c]	62	74[a]	84	94	104	114
0.7	2.4	996	1140	25	67	50[d]	99	109	119	129	139	149
1.5	4.7	1990	2280	51	133	100	184	194	204	214	222	225
2.9	9.4	3981	4560	102	266	200	281	284	286	288	291	293
4.4[e]	14	5971[f]	6840	152	400	300	330	333	335	337	340	342

[a]This row corresponds to the instantaneous benzene concentration measured at the Pentacrest (downtown Iowa City) on June 2 in a "not in plume / background" sample. Background $PM_{2.5}$ was ~10 μg/m^3 placing that hour in the "good" category. A background concentration of 0.05 ppb has been subtracted from the measured value.

[b]This row corresponds to the instantaneous benzene concentration measured in North Liberty on May 27, and at Dane Rd. on June 1. Background $PM_{2.5}$ was ~10 μg/m^3 placing those conditions in the "moderate" category. A background concentration of 0.05 ppb has been subtracted from the measured value.

[c]This row corresponds to the worst 1h datapoint from IA-AMS (based on measurements of $PM_{2.5}$). Background $PM_{2.5}$ was ~10 μg/m^3 placing those conditions in the "moderate" category.

[d]This row corresponds to the worst 1h datapoint from Hoover Elementary (based on measurements of $PM_{2.5}$). Background $PM_{2.5}$ was ~10 μg/m^3 placing those conditions in the "unhealthy for sensitive subpopulations" category.
[e]Both of the plume intercepts (May 28 and June 1) near the landfill (300 m from the landfill fire) had benzene in excess of 4.4 ppb, placing them in the "hazardous" category. The June 1 AQI is corroborated by acrolein and 1,3 butadiene (see h and i) while the May 28 has a much higher ratio of benzene to these other compounds (see g and h).
[f]This row corresponds to instantaneous CO measurements Kansas Ave. (1.0 km) from the plume under "very smoky" conditions on June 4. The CO concentration as a marker of the multipollutant mixture identifies the period as "hazardous" even though the health effect of CO itself is not considered in the AQI and the level of CO is below the TLV-TWA of 29,000 μg/m^3

1-h Average Pollutant in Tire Smoke							1-h Average Background $PM_{2.5}$ ($\mu g/m^3$)					
1,3 Butadiene (ppb)	1,3 Butadiene ($\mu g/m^3$)	Acrolein (ppt)	Acrolein (ng/m^3)	CO_2 (ppm)	CO_2 (mg/m^3 C)	$PM_{2.5}$ BaP (ng/m^3)	0	10	20	30	40	50
0	0	0	0	0	0	0	0	13	26	39	52	62
0.020	0.044	0.87	2	0.31	0.15	0.70	2	15	28	42	54	64
0.040	0.088	1.7	4	0.61	0.30	1.4	4	17	30	44	55	65
0.060	0.13	2.6	6	0.92	0.45	2.1	6	19	33	46	57	67
0.080	0.18	3.5	8	1.23	0.60	2.8	8	21	35	48	59	69
0.10	0.22	4.4	10	1.53	0.75	3.5	10	23	37	50	61	71
0.20	0.44	8.7	20	3.1	1.5	7.0	21	34	47	59	69	79
0.40	0.90	17	40	6.1	3.0	14	41	54[b]	67	77	87	97
0.60	1.3	26	60	9.2	4.5	21	62	74[a]	84	94	104	114
1.0[g]	2.2	44	100	15	7.5	35	99	109	119	129	139	149
2.0	4.4	87[h]	200	31	15	70	184	194	204	214	222	225
3.0	8.8	174	400	61	30	140	281	284	286	288	291	293
4.0[i]	13	262[j]	600	92	45	210	330	333	335	337	340	342

[g]This row corresponds to the instantaneous 1,3 butadiene measurement at the landfill edge on May 28, placing the sampling the "unhealthy for sensitive subpopulations" category. This conflicts with the benzene measurements (see note e).
[h]This row marks the acrolein MDL for the TO-15 sampling done during the Iowa City fire
[i]This row corresponds to the instantaneous 1,3 butadiene measurement at the landfill edge on June 1. This places the sample in the "hazardous category" and matches the determination based on benzene (note e) and acrolein (note j).
[j]The instantaneous acrolein at the landfill fire edge on June 1 exceeded this row's threshold by a factor of 6. This places the sample in the "hazardous category" and matches the determination based on benzene (note e) and 1,3 butadiene (note i).

8-h Average Pollutant in Tire Smoke							8-h Average Background $PM_{2.5}$ ($\mu g/m^3$)					
Benzene (ppb)	Benzene ($\mu g/m^3$)	CO (ppb)	CO ($\mu g/m^3$)	SO_2 (ppb)	SO_2 ($\mu g/m^3$)	$PM_{2.5}$ ($\mu g/m^3$)	0	10	20	30	40	50
0	0	0	0	0	0	0	0	23	45	64	82	100
0.015	0.047	20	23	0.5	1.3	1	3	26	48	67	85	102
0.029	0.094	40	46	1.0	2.7	2	6	29	52	69	87	105
0.044	0.14	60	68	1.5	4	3	9	32	54	72	90	107
0.06	0.19	80	91	2.0	5	4	12	35	57	74	92	110
0.07	0.24	100	114	2.5	7	5	15	38	59	77	95	112
0.15	0.47	199	228	5	13	10	30	53	72	90	108	125
0.29	0.94	398	456	10	27	20	61	79	97	115	132	150
0.44	1.4	597	684	15	40	30[k]	87	105[c]	123	140	157	173
0.7	2.4	996	1140	25	67	50	138	155	172	188	192	196
1.5	4.7	1990	2280	51	133	100	231	235	239	244	248	252
2.9	9.4	3981	4560	102	266	200	318	328	338	348	358	368
4.4	14	5971	6840	152	400	300	444	449	454	459	465	470

[k]This row corresponds to the worst 8-h period from Hoover Elementary (based on measurements of $PM_{2.5}$). Background $PM_{2.5}$ was ~10 $\mu g/m^3$ placing those conditions in the "unhealthy for sensitive subpopulations" category.

8-h Average Pollutant in Tire Smoke							8-h Average Background $PM_{2.5}$ ($\mu g/m^3$)					
1,3 Butadiene (ppb)	1,3 Butadiene ($\mu g/m^3$)	Acrolein (ppt)	Acrolein (ng/m^3)	CO_2 (ppm)	CO_2 (mg/m^3 C)	$PM_{2.5}$ BaP (ng/m^3)	0	10	20	30	40	50
0	0	0	0	0	0	0	0	23	45	64	82	100
0.020	0.044	0.87	2	0.31	0.15	0.70	3	26	48	67	85	102
0.040	0.088	1.7	4	0.61	0.30	1.4	6	29	52	69	87	105
0.060	0.13	2.6	6	0.92	0.45	2.1	9	32	54	72	90	107
0.080	0.18	3.5	8	1.23	0.60	2.8	12	35	57	74	92	110
0.10	0.22	4.4	10	1.53	0.75	3.5	15	38	59	77	95	112
0.20	0.44	8.7	20	3.1	1.5	7.0	30	53	72	90	108	125
0.40	0.90	17	40	6.1	3.0	14	61	79	97	115	132	150
0.60	1.3	26	60	9.2	4.5	21	87	105[c]	123	140	157	173
1.0	2.2	44	100	15	7.5	35	138	155	172	188	192	196
2.0	4.4	87	200	31	15	70	231	235	239	244	248	252
3.0	8.8	174	400	61	30	140	318	328	338	348	358	368
4.0	13	262	600	92	45	210	444	449	454	459	465	470

24-h Average Pollutant in Tire Smoke							24-h Average Background $PM_{2.5}$ ($\mu g/m^3$)					
Benzene (ppb)	Benzene ($\mu g/m^3$)	CO (ppb)	CO ($\mu g/m^3$)	SO_2 (ppb)	SO_2 ($\mu g/m^3$)	$PM_{2.5}$ ($\mu g/m^3$)	0	10	20	30	40	50
0	0	0	0	0	0	0	0	42	67	88	112	137
0.015	0.047	20	23	0.5	1.3	1	5	47	70	91	115	140
0.029	0.094	40	46	1.0	2.7	2[l]	10	52[e]	73	94	118	143
0.044	0.14	60	68	1.5	4	3	15	54	76	97	121	146
0.06	0.19	80	91	2.0	5	4	20	57	79	100	125	150
0.07	0.24	100	114	2.5	7	5	25	60	82	103	128	153
0.15	0.47	199	228	5	13	10[m]	49	75[d]	96	119	144	160
0.29	0.94	398	456	10	27	20	82	104	127	152	167	173
0.44	1.4	597	684	15	40	30	111	134	159	175	180	186
0.7	2.4	996	1140	25	67	50	174	190	195	201	206	211
1.5	4.7	1990	2280	51	133	100	246	251	257	262	267	272
2.9	9.4	3981	4560	102	266	200	368	378	388	398	408	418
4.4	14	5971	6840	152	400	300	494	504	514	524	534	544

[l]This row corresponds to the worst 24-h period from IA-AMS (based on dispersion model of $PM_{2.5}$). Background $PM_{2.5}$ was ~10 $\mu g/m^3$ placing the category as "good." This is corroborated by B[a]P measurements (see note n).
[m]This row corresponds to the worst 24-h period from Hoover Elementary (based on measurements of $PM_{2.5}$). Background $PM_{2.5}$ was ~10 $\mu g/m^3$ placing those conditions in the "moderate" category.

24-h Average Pollutant in Tire Smoke							24-h Average Background $PM_{2.5}$ ($\mu g/m^3$)					
1,3 Butadiene (ppb)	1,3 Butadiene ($\mu g/m^3$)	Acrolein (ppt)	Acrolein (ng/m^3)	CO_2 (ppm)	CO_2 (mg/m^3 C)	$PM_{2.5}$ BaP (ng/m^3)	0	10	20	30	40	50
0	0	0	0	0	0	0	0	42	67	88	112	137
0.020	0.044	0.87	2	0.31	0.15	0.70	5	47	70	91	115	140
0.040	0.088	1.7	4	0.61	0.30	1.4[n]	10	52[e]	73	94	118	143
0.060	0.13	2.6	6	0.92	0.45	2.1	15	54	76	97	121	146
0.080	0.18	3.5	8	1.23	0.60	2.8	20	57	79	100	125	150
0.10	0.22	4.4	10	1.53	0.75	3.5	25	60	82	103	128	153
0.20	0.44	8.7	20	3.1	1.5	7.0	49	75[d]	96	119	144	160
0.40	0.90	17	40	6.1	3.0	14	82	104	127	152	167	173
0.60	1.3	26	60	9.2	4.5	21	111	134	159	175	180	186
1.0	2.2	44	100	15	7.5	35	174	190	195	201	206	211
2.0	4.4	87	200	31	15	70	246	251	257	262	267	272
3.0	8.8	174	400	61	30	140	368	378	388	398	408	418
4.0	13	262	600	92	45	210	494	504	514	524	534	544

[n]This row corresponds to the worst 24-h period from IA-AMS (based on 24-h B[a]P measurements). Background $PM_{2.5}$ was ~10 $\mu g/m^3$ placing the category as "good." This is corroborated by dispersion modeling (see note k).

Section 9.4. After Action Review by Johnson County Department of Public Health

AFTER ACTION REVIEW
EVENT SUMMARY –
Incident Name: Landfill Fire of 2012
Dates of Assignment: May 26 – June 9, 2012
After Action Review – Air Quality
Monitoring Activities

At 6:38 pm on Saturday, May 26, the Fire Department responded to a call of a fire at the Iowa City Landfill, 3900 Hebl Ave., one mile west of Hwy 218 in Iowa City. The fire appears to have started at the working face of the landfill where garbage was dumped earlier in the day.

The fire then spread to the landfill liner system which includes a drainage layer of approximately 1.3 million shredded tires. Once the fire was in the drainage system, strong south winds spread it quickly along the west edge of the landfill cell.Landfill staff used bulldozers to cut a gap in the shredded tire layer to contain the fire, but the fire spread across the gap before it could be completed. Staff regrouped and cut two additional fire breaks to halt the rapidly moving fire.

Protecting the health and safety of the public and workers onsite remained the number one priority for the City and all cooperating agencies as the tire shreds continued to burn. Also of primary concern was keeping the fire from spreading to adjacent landfill cells and to a portion of the new cell that was successfully isolated in the days following the fire's ignition. On June 1, Iowa City Mayor Matt Hayek signed a Local Disaster Declaration document. The declaration facilitated access to state and federal resources, including advanced air quality monitoring and thermal imaging technology to assist with mitigating the incident.

The Johnson County Health Department partnered with the State Hygienic Laboratory, Iowa Department of Natural Resources and subject matter experts with the University of Iowa to monitor air quality throughout the region. Officials with the United States Environmental Protection Agency were actively partnering with local and state officials on those issues related to air quality. The following precautions were issued to the general public:

Persons in the path of the smoke plume should avoid exposure to the smoke as much as possible. Persons who have respiratory, heart or other conditions which may be

aggravated by smoke, pregnant women, and the young and elderly should shelter in places with outside sources of air shut off. Most home air conditioning units recirculate air from the interior and should be sufficient. Businesses and other structures which draw in outside air should close outside air sources if the smoke plume is present. Avoid outdoor activities such as exercising if the smoke plume is present. Nursing homes, day cares and other businesses which care for the elderly, very young, and persons with respiratory diseases should take special care to monitor the health of clients and to minimize exposure to the smoke plume.

On Tuesday, June 12, Environmental Restoration contactors completed a stir, burn, and cover strategy to finally contain the fire and stop the burning. Heavy equipment was in operation for a period of nine (9) days. Occasion flare-ups remain a possibility while overhaul operations are ongoing. After Action Review (AAR) Lessons Learned Incident Name: Landfill Fire of 2012

Dates of Assignment: May 26 – June 9, 2012

After Action Review – Air Quality

Monitoring Activities

The AAR is a tool that allows teams to learn from what they are doing and improve their performance. It is a structured discussion of specific events, inclusive of the entire team, and focused on learning from action to improve performance.

Lessons learned from the AAR discussion must be captured and put back into action and applied to performance quickly. The AAR is designed to help us understand why objectives were or were not accomplished, what really happened, what lessons can be learned, and how we can apply those lessons to improve performance.

AAR for Air Quality Activities:

June 27, 2012 1:00 – 3:00 pm

Johnson County Health and Human Services Building, Room 119D

Participants: Doug Beardsley and James Lacina, Johnson County Public Health; Scott Spak, U of I

Environmental Policy Program at the Public Policy Center; Dave Wilson, JC Emergency Management

Coordinator; Robert Bullard, U of I Dept. of Chemical & Biochemical Engineering; Betsy Stone and

Jared Downard, U of I Dept. of Chemistry; Pam Kostle and Wanda Reiter-Kintz, State Hygienic Laboratory; Josh Sobaski and Kurt Levetzow, IA Dept. of Natural Resources (by phone); Shane Dodge,
Linn County Public Health (by phone);

1. What was the most notable success at the incident that others may learn from? Please explain.

At the incident response level, use of the Incident Command System (ICS) was very instrumental in assuring that roles within the incident were understood and that information was shared and staff kept up-to-date on activities. Cooperation and willingness to help on the part of partner organizations was tremendous. Of particular note were the State Hygienic Laboratory and Linn County Public Health.
Staff from both agencies were on the phone with JCPH early on (and late night) with offers to assist with air monitoring. We had DNR involvement which led to participation by EPA as well to offer technical assistance.

The learning curve, while steep, was handled well by all parties involved. Again, the success was due to the large number of resources and the infrastructure (internet, search engines, access to subject matter experts, teleconferencing, etc.) to access them. Staff at JCPH made the response a priority and had to juggle very full schedules from other duties in order to conduct the monitoring activities (as did staff from other agencies and organizations). This prioritization in order to address an emergency was appreciated.

The early development of a health message related to the smoke and the consistency of the message in light of research and air monitoring seemed to lend to the success of Iowa City's efforts and public information. The City was very open with information and very proactive with making information accessible to the public.

2. What were some of the most difficult challenges faced and how were they overcome? Please explain.

Since this was a new area in which JCPH did not have expertise, we tried to locate some sort of standard approach for monitoring a smoke plume. There was ample research on the constituents of tire fire smoke and some enlightening case studies of other large fires, but we could not locate a "how to" approach on monitoring. We proceeded with what made sense and

shared that approach with local, state and federal partners for feedback. There was general consensus that our approach was good. We continued by sharing test results and continuously looked for feedback on monitoring strategies. It turns out that the strategy is fairly simple; drive in to the smoke at varying distances from the source and take samples. Most of our samples were "grab" samples. A better approach would be to take longer term samples to average out exposures. This challenge was overcome by doing what could be done and then being open with the public and being consistent and proactive with the message.

There was some initial confusion about who should be contacted and exact protocols to follow in order to access State and Federal resources. Early involvement of the County EMA was helpful, but sometimes there may have been parallel efforts aimed at the same resource. There was some confusion about "ownership" of SHL resources and how the DNR fit in to that. JCPH was not aware or did not understand the relationship of SHL capabilities and DNR funding of those services and whether or not SHL needed DNR acknowledgement to act. This may have been immaterial, however (no "need to know") as SHL secured whatever acknowledgements were needed. JC EMA was making requests but found that the feedback loop from State partners was inconsistent. This may have been complicated by too many people calling various duty officers (i.e. JCPH called the IDPH duty officer for assistance in contacting SHL and Linn CPH rather than directing all traffic via JC EOC.). Despite any confusion, there was no perceptible delay in deploying resources once we decided where we wanted to get samples.

EMA and SHL will follow up to review who has what authorities and how we can streamline or reaffirm the correct notification procedures to secure air monitoring assets in the future. While we would evaluate the air monitoring efforts as being successful, better coordination would have been welcome. JCPH was primarily coordinating the efforts and communicating with its partners who were providing testing services. Feedback during the AAR was that several strategy meetings with all air monitoring partners involved would have been helpful and may have changes how assets were deployed. Solution: in an incident of this magnitude in the future, staff up the air monitoring branch so a branch director is less involved in actual monitoring activities and has time to focus on coordination and strategy.

Additionally, there was some confusion or duplication when requesting Federal assets in the form of EPA assistance. When JCPH sent in a request for EPA assistance and then spoke with the EPA representative, other communication and/or requests had already been sent to EPA and they had

already received deployment orders before speaking with JCPH. We appreciated their prompt response but there were some moments of concern about deployment and "what are they planning to do" on the part of JCPH. It turned out well in this case, which is the bottom line, but it caused a bit of unnecessary worry.

Another challenge or lesson learned was not being aware of and using the full capabilities for air monitoring which exists on the Hazmat vehicles. The Hazmat testing equipment was eventually deployed as the incident got in to the "stir, burn, and cover" activities. EMA will review these capabilities and ensure that they are listed as a resource for similar future events.

3. What changes, additions or deletions are recommended to augment agency training curriculums and/or operating policies?

As mentioned above, we will review our procedures for requesting assistance outside of our jurisdiction. We will review if we should pursue individual agreements with Linn County Public Health and the SHL or if current procedures working through the EOC are adequate to meet liability, reimbursement and other issues associated with receiving assistance. We will continue to train staff in the ICS and role of the EOC.

4. What issues were not resolved to your satisfaction and need further review? Based on what was learned, what is your recommendation for resolution?

There were no major issues which had not been resolved during the course of the incident or have not already been addressed above.

5. What remedies will the organization pursue and who will champion each initiative? If possible, attach timelines for completion.